



HAL
open science

Characterization of biogenic volatile organic compounds (BVOCs) and their OH reactivity in various agro-ecosystems

Sandy Bsaibes

► **To cite this version:**

Sandy Bsaibes. Characterization of biogenic volatile organic compounds (BVOCs) and their OH reactivity in various agro-ecosystems. Global Changes. Université Paris Saclay (COMUE), 2019. English. NNT: 2019SACLV093 . tel-02614381

HAL Id: tel-02614381

<https://theses.hal.science/tel-02614381>

Submitted on 20 May 2020

HAL is a multi-disciplinary open access archive for the deposit and dissemination of scientific research documents, whether they are published or not. The documents may come from teaching and research institutions in France or abroad, or from public or private research centers.

L'archive ouverte pluridisciplinaire **HAL**, est destinée au dépôt et à la diffusion de documents scientifiques de niveau recherche, publiés ou non, émanant des établissements d'enseignement et de recherche français ou étrangers, des laboratoires publics ou privés.

Characterization of biogenic volatile organic compounds and their OH reactivity in various agro-ecosystems

Thèse de doctorat de l'Université Paris-Saclay
Préparée à l'Université de Versailles Saint-Quentin-en-Yvelines

Ecole doctorale n°129 Sciences de l'Environnement d'Île-de-France
(SEIF)
Spécialité de doctorat : chimie atmosphérique

Thèse présentée et soutenue à Gif-sur-Yvette, le 12 Décembre 2019 par

Sandy Bsaibes

Composition du Jury :

Didier Hauglustaine Directeur de Recherche, LSCE, CNRS	Président
Agnès Borbon Chargée de Recherche, LaMP, CNRS	Rapporteur
Jonathan Williams Senior Scientist, MPIC	Rapporteur
Corinne Jambert Maître de conférences, LA	Examineur
Benjamin Loubet Directeur de Recherche, Ecosys, INRA	Examineur
Valérie Gros Directeur de Recherche, LSCE, CNRS	Directeur de thèse

Contents

Acknowledgements	vii
Preface	x
Résumé	xii
Abstract	xiii
<i>1. Introduction to BVOCs and OH reactivity</i>	1
<i>Introduction Chapitre 1</i>	2
1.1. The troposphere	6
1.2. Volatile Organic Compounds	8
1.2.1. Context	8
1.2.2. BVOCs chemical diversity	8
1.2.3. Factors affecting BVOCs emissions	13
1.3. Reactivity and impacts in the atmosphere	17
1.3.1. Atmospheric oxidants: sources, levels and reaction mechanisms with VOCs	18
1.3.2. BVOCs lifetimes	22
1.3.3. Impact of BVOCs transformation in the atmosphere	24
1.4. Measurement methods	26
1.4.1. VOCs in ambient air	26
1.4.2. OH reactivity measurements techniques	29
1.5. OH reactivity in various environments	32
1.5.1. Forest areas	32
1.5.2. Rural and suburban areas	37
1.5.3. Missing OH Reactivity	38
1.6. Thesis objectives	38
<i>2. Experimental</i>	42
<i>Introduction Chapitre 2</i>	43
2.1. Proton Transfer Reaction-Mass Spectrometer (PTR- MS)	46
2.1.1. Instrumental set-up	46
2.1.2. Compounds sensitivity and volume mixing ratio	49
2.1.3. PTR-MS in atmospheric sciences	50
2.2. Fast Gas Chromatography/ Proton-Transfer-Reaction Mass Spectrometer	51
2.2.1. Instrument set-up and operational concept	51
2.2.2. System characterization	53
2.2.3. Field deployment of the FastGC/PTR-MS	57
2.3. The Comparative Reactivity Method (CRM)	58
2.3.1. General principle	58
2.3.2. Derivation of the basic equation for CRM	59

2.3.3.	Experimental set up	61
2.3.4.	Method calibration.....	62
2.3.5.	CRM artifacts and corrections.....	64
2.3.6.	LSCE-CRM.....	70
	<i>Conclusion Chapitre 2</i>	84
3.	<i>Variability of hydroxyl radical (OH) reactivity in the Landes maritime Pine forest: results from the LANDEX campaign 2017</i>	85
	<i>Introduction chapitre 3</i>	86
	Abstract	87
3.1.	Introduction	89
3.2.	Experimental	93
3.2.1.	Site description	93
3.2.2.	OH reactivity instruments.....	93
3.2.3.	Ancillary measurements and corresponding locations	100
3.2.4.	OH reactivity calculation.....	105
3.3.	Results	108
3.3.1.	Comparison between LSCE-CRM and UL-FAGE measurements.....	108
3.3.2.	Measured OH reactivity and meteorological parameters	112
3.3.3.	Measured and calculated R_{OH} within and above the canopy	116
3.3.4.	Contribution of VOCs (PTR-MS) to calculated OH reactivity within and above the canopy	117
3.3.5.	Description and investigation of potential missing OH reactivity during the LANDEX campaign	118
3.4.	Conclusion.....	127
	<i>Conclusion chapitre 3</i>	130
4.	<i>Characterization of total OH reactivity in a rapeseed field: Results from the COV³ER experiment in April 2017</i>	132
	<i>Introduction chapitre 4</i>	133
	Abstract	134
4.1.	Introduction	136
4.2.	Methodology	139
4.2.1.	Field site description.....	139
4.2.2.	Plant dynamic chamber and air sampling.....	140
4.2.3.	Meteorological measurements.....	140
4.2.4.	Instrumentation.....	141
4.2.5.	Calculation of OH reactivity	148
4.2.6.	Data availability.....	151
4.3.	Results and discussion.....	151
4.3.1.	Total OH reactivity.....	151
4.3.2.	Investigation of the missing OH reactivity.....	158
4.4.	Conclusion.....	165

<i>Conclusion chapitre 4</i>	168
5. <i>Monoterpenes chemical speciation with high time resolution using a FastGC/PTR-MS: Results from the experiment on Quercus ilex in Southern France, during summer 2018</i>	170
<i>Introduction Chapitre 5</i>	171
Abstract	172
5.1. Introduction	173
5.2. Materials and methods.....	176
5.2.1. Description of the measurement site	176
5.2.2. Branch enclosure	177
5.3. FastGC/PTR-MS system	178
5.3.1. Description of the FastGC system and mode of operation	178
5.3.2. Laboratory optimization phase	179
5.3.3. Operating conditions during the campaign.....	181
5.3.4. System calibration	182
5.3.5. FastGC/PTR-MS sampling system.....	183
5.3.6. Data analysis.....	184
5.3.7. Evaluation of the system efficiency in the separation of monoterpenes with a higher time resolution	185
5.4. Results	185
5.4.1. BVOCs concentrations for branch enclosures.....	185
5.4.2. BVOCs emission fluxes for branch enclosures	187
5.4.3. Monoterpenes chemical speciation.....	188
5.5. Conclusion.....	191
6. <i>Conclusion and Perspectives</i>	194
<i>Conclusion et Perspectives</i>	201
<i>Appendix</i>	205
<i>Supplement of chapter 3: Variability of hydroxyl radical (OH) reactivity in the Landes maritime Pine forest: results from the LANDEX campaign 2017</i>	206
<i>Supplement of chapter 4: Characterization of total OH reactivity in a rapeseed field: Results from the COV³ER experiment in April 2017</i>	219
<i>Characterization of particle and gaseous pollutant emissions from a French dairy and sheep farm</i>	231
List of Figures	263
List of Tables.....	267
References	268

*“We know only too well that what we are doing is nothing more than a drop in the ocean.
But if the drop were not there, the ocean would be missing something.”*

Mother Teresa

Acknowledgements

It is with a certain emotion and a lot of sincerity that I would like to thank all the people who supported me during the thesis and who made these three years an exceptional and memorable experience for life.

I would like to express my sincere thanks to the members of the jury who agreed to evaluate my work. To Dr. Agnès BORBON and Pr. Jonathan WILLIAMS, for agreeing to be the reviewers of my manuscript and for contributing to the improvement of it. I would also like to thank Dr. Corinne JAMBERT, Dr. Benjamin LOUBET and Dr. Didier HAUGLUSTAINE for the honor of being examiners of my thesis.

All my gratitude to my supervisor, Dr. Valérie GROS, for her patience, her availability and for all her wise advice. You're a great example of a leader, Valérie, and I allow myself to call you "super woman". Thank you for the trust you have placed in me, for all the support you have shown me as well as for your kindness, which has allowed me to grow as a researcher and to gain confidence in my work.

I wish to show my gratitude to Mr. François TRUONG, the engineer with whom I spent a large part of my thesis, either during laboratory experiments or those in the field. Thank you for your professionalism and your kindness, two qualities which made working with you a pleasant moment. Thank you for all the interesting discussions, in science and society, around a good coffee. I learned a lot from you François, and I am grateful for your generosity.

I would also like to thank Dr. Christophe BOISSARD, my office neighbor. It was a great pleasure to chat with you Christophe. Thank you for your generosity, your listening, your advice and your good humor. I learned from you how to be professional with a big heart. Thank you for the tasty teas, "chouquettes" and especially for the liquor chocolates.

I would also like to thank the former and present members of the CAE group. Nora ZANNONI, Sébastien SCHRAMM, Julien KAMMER and Jean-Eudes PETIT who impressed me with their professionalism and humor. Thank you for all the advice, discussions and great moments in the lab and in the field. Baptiste LANGUILLE, "the colleague" from day one. Thank you for your kindness, your help and for all the interesting discussions.

Many thanks go to the IMPACT project coordinator, Pr. Chris MAYHEW and to all my colleagues / friends from the project: Nijing, Felix, Ben, David, Michaela, Michal, Bartocz,

Giovanni and Renaud. For this unique and rewarding experience, for this small international family that we have formed and for the memories engraved for life, THANK YOU.

My deepest thanks go to my parents, to Eva my bit of sunshine and Assaad my idol. Throughout my studies, they were the soil that supported my ambitions and the water that watered them. They knew how to give me every chance to succeed. May they find, in this work, the culmination of their efforts as well as the expression of my most affectionate gratitude.

Thank you to my brothers Samer and Elie, the big hearts I can always count on. To my cousins Tamara, Toni, Maroun, Joe, Mike and Jimmy as well as to my big family, thank you for all the funny skypes and the affections crossing the globe.

From the bottom of my heart, thank you to people who are surely part of my heart and to whom I will always be grateful. Cynthia and Simon, a thank you will never be enough for everything you have done, especially during the last stretch. Ghady, thank you for being here along the way. I am grateful for your support and your encouragement. The Khourys, Hanane and Maroun, a sister and a brother that I won and who were a great support for me. Maria, Perla, Marie-José, Elie, Cyril, Marc, Rami, Rita, Estelle, thank you for your presence and your heart-warming messages. Thank you to all my friends from Lebanon, Rita, Monica, Mariam, Lama, Valérie, Marie-José, Yara and Dany for their unfailing support.

Finally, thank You. You for whom I am grateful for this fruitful opportunity and beautiful meetings. I saw you in the beauty of everything I experienced and everyone I met. I was and still confident of your unconditional love.

Preface

This thesis presents the work I have done during my PhD as an early stage researcher at Laboratoire des Sciences du Climat et de l'Environnement (LSCE).

The project aims to improve the Comparative Reactivity Method (CRM) and deploy it for total OH reactivity measurements in various ecosystems: forest and agricultural land. It also concerns the set-up, optimization and deployment of a Fast Gas Chromatography/ Proton-Transfer- Reaction Mass Spectrometer (GC/PTR-MS) system for monoterpenes rapid separation in a forest ecosystem.

The results presented herein include findings from laboratory tests as well as from three field campaigns: COV³ER (Biogenic volatile organic compounds (BVOC) emissions by managed ecosystems)-Grignon during April 2017, LANDEX (study of Secondary Organic Aerosols (SOAs) generated by the Landes forest) in June- July 2017 and COV³ER- Puéchabon in July 2018.

The project is part of the European Marie Skłodowska-Curie Innovative Training Network 'IMPACT' (Ion-Molecule Processes for Analytical Chemistry Technologies), which aims at developing molecular mass spectrometry techniques in different field in sciences, including environmental, food, medical sciences and homeland security. As part of the project, I had the opportunity to improve my technical skills on the PTR-MS (Ionicon, Kore), and to collaborate with other early stage researchers working on different topics (OH reactivity, VOCs measurements with PTR-MS, ammonia analysis, etc).

This thesis consists of five chapters. The first chapter is a general overview about VOCs, their sources, chemical diversity, and fate in the atmosphere. More particularly, their reaction with the hydroxyl radical making them an important sink of this powerful oxidant in the atmosphere. Total OH reactivity is defined, with a brief summary about the instruments used and a review on the studies performed since 2004 in forest and rural environments. The second chapter presents the main systems used during my PhD; the CRM and the FastGC with the PTR-MS as detector coupled to both of them. Tests and optimization results are also presented with an overview of the performance of both instruments on the field. A third chapter presents the findings on total OH reactivity in a maritime pine forest in the south of France, as part of the LANDEX project. These results are the subject of an accepted paper in ACP. The fourth chapter concerns findings on BVOCs and OH reactivity in the incoming and the outgoing air samples of a rapeseed crop, during the blooming season. This work, performed in the frame of the COV³ER- 2017 experiment is presented in the form of an article, submitted to a special issue on Atmospheric Volatile Organic Compounds in Atmosphere journal. Chapter 5 is a preliminary draft of an article describing results from the optimization and deployment of a FastGC/PTR-MS in a green oak forest, south of France, for monoterpenes chemical speciation with a fine time resolution, from different branch enclosures. Finally, chapter 6 is a summary of conclusions made of this PhD work, including suggestions for future research.

Caractérisation des composés organiques volatils biogéniques (COVBs) et leur réactivité OH dans divers agro-écosystèmes

Résumé

Le radical hydroxyle OH est le principal oxydant dans la troposphère, mais ses puits restent encore difficiles à quantifier. L'un de ses principaux puits, est l'oxydation des Composés Organiques Volatils (COVs), composés provenant principalement de sources naturelles, à l'échelle du globe. Ils comprennent une grande variété d'espèces chimiques avec des réactivités très variables vis-à-vis des radicaux OH. Mesurer la réactivité OH totale, permet d'évaluer la charge en espèces réactives et d'estimer l'importance des espèces non mesurées/ non connues. Dans ce contexte, ce travail de thèse a d'abord visé d'optimiser la CRM ou « Comparative Reactivity Method », pour la mesure de la réactivité OH. Une fois les performances vérifiées, la CRM a été déployée dans deux écosystèmes : forestier et agricole. Les mesures de réactivité OH dans une forêt de pins maritimes ont montré des maxima de nuit arrivant jusqu'à 99 s^{-1} dans la canopée ; des niveaux se situant dans la limite supérieure de ce qui a été précédemment vu en sites forestiers. Des réactivités plus faibles, ne dépassant pas les $20\text{-}30 \text{ s}^{-1}$ en milieu de journée, ont été observées dans un champ agricole, en sortie d'une chambre dynamique de colza, en milieu de floraison. Dans ces deux écosystèmes, une différence a été trouvée entre la réactivité mesurée et celle calculée à partir des composés gazeux mesurés individuellement. Elle indique la présence d'une fraction manquante de composés primaires et/ ou secondaires non mesurés/ non identifiés. Ces travaux ont également mis en évidence l'importance de déterminer la spéciation des monoterpènes. Ceci nous a motivé à optimiser et déployer un système de FastGC/ PTR-MS dans une forêt de chênes verts, ce qui nous a permis de suivre, avec une haute résolution temporelle, le cycle diurne des principaux monoterpènes, dont l'émission dépend du type de chêne ainsi que de la lumière.

Mots-clés : COVBs, Monoterpènes, Réactivité OH, FastGC/PTR-MS, Forêt, Agriculture

Characterization of biogenic volatile organic compounds (BVOCs) and their OH reactivity in various agro-ecosystems

Abstract

The hydroxyl radical OH is the most powerful oxidant in the troposphere, however, characterizing its sinks remains a challenge. One important OH sink, is the oxidation of volatile organic compounds (VOCs), mainly released from biogenic sources, on the global scale. VOCs include a wide variety of chemical species with different lifetimes towards OH. Measuring OH reactivity is a useful tool to evaluate the loading in reactive species and to estimate the amplitude of unmeasured/unidentified compounds. In this context, this PhD work aimed to build and optimize a CRM or Comparative Reactivity Method instrument for OH reactivity measurements. Afterwards, the CRM was deployed in a forest and an agricultural ecosystem. OH reactivity in a maritime pine forest showed maxima during night, reaching 99 s^{-1} inside the canopy, among the highest in forest environments. Relatively lower levels (max $20\text{-}30 \text{ s}^{-1}$ at mid-day), were recorded from a dynamic chamber, during the blooming season of a rapeseed field. In these ecosystems, a difference was obtained between measured and calculated OH reactivity from measured compounds. It highlights the presence of a missing fraction of unmeasured primary and/ or secondary compounds. These experiments demonstrate the importance of monoterpenes chemical speciation. In this perspective, a FastGC/PTR-MS system was optimized and deployed in a green oak forest. It allowed to monitor, with a fine time resolution, diurnal cycles of the main monoterpenes, which emissions are dependent on the tree type and on solar radiation.

Keywords : BVOCs, Monoterpenes, OH reactivity, FastGC/PTR-MS, Forest, Agriculture

*1. Introduction to BVOCs
and OH reactivity*

Introduction Chapitre 1

La troposphère représente la couche la plus basse de l'atmosphère terrestre. Elle comprend 85 - 90% de la masse atmosphérique avec les principaux constituants : N₂ (78%), O₂ (21%), Ar (0.9%), et une fraction inférieure à 1% comprenant le reste des composés, ce qui inclut les composés organiques volatils (COVs). Bien que présents à l'état de traces dans l'atmosphère (rapports de mélange de quelques ppbv au plus), les COVs jouent un rôle important dans les processus troposphériques, en particulier via leur implication dans les réactions d'oxydation. En effet, leur oxydation peut conduire à la formation d'ozone troposphérique, important gaz à effet de serre avec également des effets néfastes sur la santé et l'environnement. Les COVs sont également reconnus comme précurseurs d'aérosols organiques secondaires (AOS ou encore SOA en anglais), à impact radiatif direct par absorption et dispersion des rayonnements solaires et terrestres et à impact radiatif indirect en jouant le rôle de noyau de condensation induisant la formation des nuages.

Ces composés sont émis ou formés au niveau de la couche limite atmosphérique (1-2 km de la surface terrestre), dont l'état, dépendant de l'heure de la journée, peut induire leur dispersion ou leur accumulation dans la couche résiduelle. Caractérisés par une grande diversité chimique, les COVs sont émis par différentes sources anthropogéniques et biogéniques. Cependant, les COV biogéniques (COVBs) restent dominants à l'échelle du globe, avec une émission globale estimée à 760 – 1150 TgC / an (Guenther et al., 1995; Sindelarova et al., 2014). Les forêts tropicales ont été reportées comme principales sources de COVBs à l'échelle de la planète (≈ 50%), tandis que les surfaces agricoles et les bois contribuent à 10- 20% chacun. De même, une étude réalisée à l'échelle de l'Europe, montre des contributions de 55% et 27% au COVBs, par les forêts et l'agriculture, respectivement (Karl et al., 2009). Cependant, des changements au niveau des sols et de leurs couvertures végétales peuvent induire des changements dans les flux et la composition des COVBs.

Les COVBs peuvent être classés en différents groupes : Le groupe des terpénoids, comprenant, parmi d'autres, l'isoprène, les monoterpènes et les sesquiterpènes. L'isoprène reste le COVB le plus émis à l'échelle du globe et ainsi le plus étudié. Les monoterpènes constituent une grande famille de composés et représentent ≈ 11% des émissions globales de COVBs. Un intérêt de plus en plus important est accordé à l'étude de cette famille en terme d'émissions et de réactivité. D'une part, les monoterpènes sont émis par certains types de végétation et ces émissions sont dépendantes soit principalement de la température, soit à la fois de la lumière et

la température (similairement à l'isoprène). D'autre part, ils contribuent à la formation d'aérosols organiques secondaires avec des rendements pouvant être différents d'un monoterpène à l'autre. Les composés oxygénés forment un autre groupe, comprenant, parmi d'autres, le méthanol et l'acétone, parmi les plus abondants à l'échelle du globe. On trouve aussi les alcanes et les alcènes, les composés halogénés, les composés soufrés, ainsi que les composés benzéniques.

Les émissions de COVBs sont sujets à des variations dépendantes de plusieurs facteurs internes et externes. Pour les facteurs internes, il s'agit principalement de la génétique et des processus biochimiques. Pour les facteurs externes, on peut différencier les facteurs biotiques comme l'interaction avec d'autres plantes, microorganismes et insectes et les facteurs abiotiques, comme la température, la lumière et la disponibilité en eau. Des variations à plus grande échelle, comme le changement des niveaux en CO₂ et en O₃ dans l'atmosphère peuvent favoriser ou freiner les émissions de COVBs. Ceci reste lié à plusieurs facteurs comme le type de la plante, la saison, la nature chimique du COVB, etc. Des variations à plus long terme, comme le réchauffement climatique et le changement dans la couverture terrestre sont estimées influencer le niveau et la composition des COVBs dans l'atmosphère.

Une fois émis dans l'atmosphère, les COVs sont sujets à des processus physiques (dépôts sec et humide) et photochimiques (oxydation par OH, O₃ et radicaux nitrates), dominés par la photo-oxydation par le radical OH. Même si les sources de radicaux OH sont relativement bien connues, la quantification des puits reste associée à d'importantes incertitudes. Dans ce contexte, la réactivité OH, se présente comme un paramètre global, mesurable, permettant d'évaluer la charge en espèces réactives dans la troposphère et d'estimer la présence de composés inconnus/non mesurés, participant à la chimie de l'atmosphère. Elle est définie comme l'inverse du temps de vie du radical OH, exprimé en s⁻¹.

Plusieurs méthodes ont été adoptées pour la mesure des COVs en général et ceux des plantes en particulier. La chromatographie en phase gazeuse (GC) et la spectrométrie de masse par réaction de transfert de proton (PTR-MS) sont parmi les plus utilisées. La première est connue pour sa bonne sélectivité, bonne sensibilité et sa précision. Cependant, elle est limitée par sa résolution temporelle relativement faible (≥30 min). Le PTR-MS est apparu plus récemment. Il est largement déployé pour sa sélectivité et sa sensibilité élevées, ainsi que pour son temps de réponse très court (1- 10 s). Mais, vu qu'il mesure les concentrations des composés en fonction de la masse moléculaire, il ne permet pas une analyse détaillée des isomères. Des

premiers travaux ont été faits récemment pour combiner les avantages de ces deux instruments analytiques. Le résultat, connu comme FastGC/PTR-MS, s'est avéré prometteur pour la caractérisation des isomères en général et des monoterpènes en particulier, avec une résolution temporelle fine mais montrant encore certaines limitations. Pour les mesures de réactivité, deux approches existent : la mesure directe du taux de perte des radicaux OH suite à leur réaction avec les espèces réactives présentes dans l'échantillon, et une mesure indirecte appelée CRM pour « Comparative Reactivity Method », basée sur le suivi de la concentration d'une molécule de référence en absence et en présence d'espèces réactives.

Depuis une dizaine d'années, la réactivité OH a été mesurée dans divers environnements. Dans cette thèse, l'accent est mis sur les écosystèmes ruraux et forestiers. D'une façon générale, la réactivité OH a été largement étudiée dans des écosystèmes forestiers, où des niveaux relativement élevés ont été reportés. Parmi les plus importantes, les valeurs obtenues en forêts tropicales, avec des maximums arrivant jusqu'à 72 et 85 s⁻¹ durant la saison sèche (Nolscher et al., 2016; Sinha et al., 2008). Cependant des niveaux beaucoup moins élevés ont été mesurés sur le même site (Nolscher et al., 2016) pour la saison humide (6 -13 s⁻¹). Ces observations montrent clairement la variabilité saisonnière de la réactivité OH. Des mesures en forêt méditerranéenne (Zannoni et al., 2016) ont montré des niveaux aussi élevés (jusqu'à 70 s⁻¹) de réactivité OH, avec des moyennes similaires dans et au-dessus de la canopée. Alors qu'une autre étude (Hansen et al., 2014) a reporté des différences plus importantes entre les différents niveaux de mesures, ce qui met l'accent sur l'importance de caractériser la réactivité OH à différentes hauteurs de la canopée. Quant aux forêts boréales, des moyennes plus faibles ont été trouvées (Praplan et al., 2019) mais toujours avec une variabilité saisonnière marquée. Les forêts de conifères, ont été aussi étudiées montrant des niveaux relativement faibles (6 s⁻¹). Pour les sites ruraux, des niveaux faibles de réactivité ont été trouvés avec une variabilité diurne plus ou moins prononcée. Par contre, il n'existe pas de mesures de réactivité OH sur les cultures agricoles.

Toutes ces études ont mis en évidence la variabilité de la réactivité OH en fonction du site, de la végétation, de la proximité ou non des sources anthropogéniques, de la hauteur de mesure et des conditions météorologiques (incluant température, lumière, hauteur de la couche limite, la turbulence, ...). De plus, la mesure de la réactivité OH totale permet la comparaison avec la réactivité OH calculée à partir des espèces individuelles (à partir de leurs concentrations pondérées de leurs constantes cinétiques). Si la réactivité mesurée est significativement plus grande que la réactivité calculée, la différence est appelée réactivité manquante, ce qui a souvent

été le cas dans les études existantes. Cette fraction manquante est due à la présence de composés primaires ou produits d'oxydation secondaires non mesurés ou non identifiés.

Dans ce contexte, les objectifs de la thèse sont les suivants :

- Caractérisation des COVs biogéniques et leur réactivité OH dans et au-dessus de la canopée d'une forêt de pins maritimes, utilisant la CRM.
- Caractérisation des COVBs et leur réactivité OH en entrée et en sortie d'une chambre dynamique de colza, durant la saison de floraison, utilisant la CRM.
- Caractérisation des monoterpènes spéciés avec une résolution temporelle fine, dans une forêt de chênes verts, utilisant un système FastGC-PTRMS testé et optimisé au laboratoire.

1.1. The troposphere

The troposphere is the lowest layer of Earth's atmosphere and the layer to which changes can greatly influence the floral and faunal environments. It extends from Earth's surface to an average height of approximately 12 km, although this altitude actually varies depending on the latitude and time of the year (Speight, 2016). This layer contains approximately 85–90% of the atmospheric mass and almost all of the atmosphere's water vapor, which brings it to the central stage of all weather related phenomena, earth's climate controlling processes and atmospheric chemistry. The main constituents of the gas phase are N₂ (78%), O₂ (21%), Ar (0.9 %) and a fraction of less than 1% which contains all the remaining species, usually regarded as trace components. Trace gases include CO₂ (~379 ppmv), CH₄ (~1700 ppbv), O₃ (10- 100 ppbv), N₂O (~310 ppbv), halogenated compounds (3.8 ppbv), and non-methane volatile organic compounds VOCs (5- 20 ppbv) (Wallace and Hobbs, 2006). *Although they form less than 1% by volume of the total atmospheric constituents, VOCs play a major role in tropospheric processes since they can alter significantly the air quality, the weather and the climate.* There are also many small particles - solids and liquids – in suspension in the atmosphere. These particles, called "aerosols", include dust, spores and pollen, salt from sea spray, volcanic ash, and particles of anthropogenic origins.

The lowest part of the troposphere is known as the atmospheric boundary layer (ABL), that is directly influenced by the roughness (friction) and energy balance (heating or cooling) of the surface (Finnigan, 2014). The ABL is therefore generally characterized by turbulence and a diurnal cycle of temperature, wind, specific humidity, and other tracers in particular over land (Holtslag, 2015). Although the overland ABL is evolving continuously in response to the heating and cooling of the earth's surface, it does have distinct states (**Figure 1.1**), that can be described in simple terms. During daytime, due to the surface heating from shortwave radiation, turbulence is generated in the lower 1–2 km above the ground, which is called the mixed or the convective layer. A stable layer at the top of the mixed layer restrains the vertical extent of turbulence. This layer is called the entrainment zone because entrainment into the mixed layer occurs at this layer. After sunset, turbulence decays in the formerly mixed layer. The lower portion of the formerly mixed layer is transformed into a stable boundary layer, which is characterized by statically stable air with weaker, sporadic turbulence. After sunrise of the following day, the mixed layer starts to grow again (Hu, 2015; Stull, 1988).

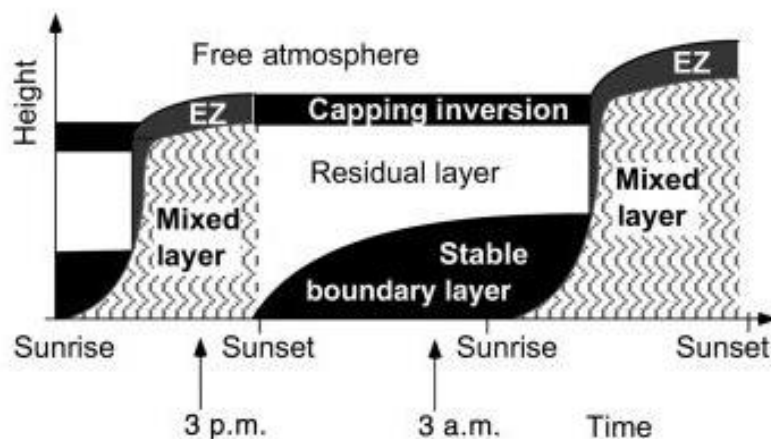


Figure 1.1: Idealized diurnal evolution of the atmospheric boundary layer over land in fair weather (after Stull, 1988).

It is important to note that, most chemical species are emitted or formed in the boundary layer. Therefore, the variation of the ABL plays a critical role for dictating their dispersion. Indeed, during day-time, the turbulence tends to mix heat, momentum, moisture and chemical compounds uniformly in the mixed layer, whereas, after sunset, the state variables and concentrations of chemical compounds remain mostly invariant in the residual layer.

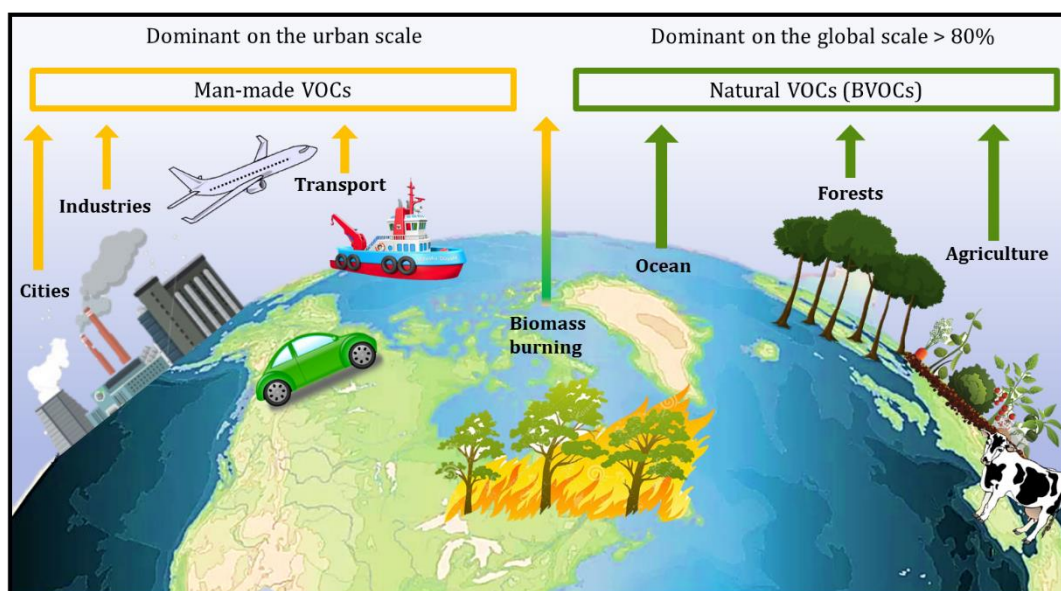


Figure 1.2: Schematic summarizing anthropogenic and biogenic sources of volatile organic compounds (VOCs) (de Gouw, 2006).

1.2. Volatile Organic Compounds

1.2.1. Context

Up to 10^4 - 10^5 of different organic species have been identified so far in the Earth's atmosphere. That may be only a small fraction of the number actually present (Goldstein and Galbally, 2007). Volatile organic compounds (VOCs), defined as organic species which have high vapor pressure in the earth's atmosphere ($>10^{-5}$ atm at ambient temperature), represent a key class of chemical species involved in global tropospheric chemistry and the global carbon cycle. Primarily, atmospheric VOCs arise from both biogenic and anthropogenic emissions (**Figure 1.2**). Anthropogenic sources, including motor-vehicle evaporative and exhaust emission, industries, biomass and biofuel burning and the use of chemical solvents, contribute with 60–140 TgC year⁻¹ to global emissions of VOCs. Biogenic VOCs (BVOCs), released by living organisms or biological processes necessary for the maintenance of life cycles, represent the largest contributor to global VOCs. With an estimated global emission of about 760-1150 TgC year⁻¹, they exceed those of their anthropogenic counterparts by about a factor of 10 (Guenther et al., 1995; Sahu, 2012; Sindelarova et al., 2014). These BVOCs are produced by a variety of sources in terrestrial ecosystems, including flowers, stems, trunks, roots, leaf litter, soil microbes, insects, and animals, but most of the global total emission is from foliage (Guenther, 2013). In terms of land cover, tropical woodlands (rain forest, seasonal, drought-deciduous, and savanna) contribute about half of all global natural VOC emissions, while croplands, shrub lands and other woodlands contribute 10-20% apiece (Guenther et al., 1995). More recently, similar contributions were reported by Karl et al. (2009) on the Pan-Europe scale, with 55% and 27% contribution to total BVOCs from forests and crops, respectively. However, changes in land cover/land use, can alter BVOCs emissions as well as their composition, that is detailed next.

1.2.2. BVOCs chemical diversity

As mentioned before, an enormously wide range of BVOCs are synthesized and emitted into the atmosphere. They are involved in plant growth, development, reproduction and defense. They also function as communication media within plant communities, between plants and

between plants and insects. They can be classified in several groups, as reported in the reviews of Fuentes et al. (2002); Guenther (2013) and Kesselmeier and Staudt (1999), including:

Terpenoid Compounds: Terpenoid compounds are considered to be the dominant BVOC on the global scale. This incredibly diverse group includes thousands of chemical species that can be classified as hemiterpenoids (C₅, e.g., isoprene), monoterpenoids (C₁₀, e.g., α -pinene), sesquiterpenoids (C₁₅, e.g., β -caryophyllene), homoterpenes (C₁₁ and C₁₆), diterpenoids (C₂₀, e.g., tocopherol and retinol), and larger compounds with low volatility that it is unlikely that they are emitted into the atmosphere in a gaseous form. Terpenoids also include oxygenated terpenes such as the hemiterpenoid methylbutenol (MBO), the monoterpenoid linalool, and the sesquiterpenoid cedrol. These oxygenated terpenoids represent a small fraction of the global total terpenoid emission but may be important in some regions.

- **Isoprene:** Isoprene is recognized as the dominant global biogenic compound emitted into the atmosphere, roughly equal to global emission of methane from all sources (Guenther et al., 2006). Guenther et al. (1995), reported a contribution of 44%, about half of the total global BVOC flux, when Sindelarova et al. (2014), estimated a higher contribution of about 70%. So it is not surprising that isoprene emission has been investigated more extensively than any other atmospheric BVOC. Isoprene is known to be rapidly lost by volatilization and is never stored in plants. The taxonomic distribution of isoprene emission is broad, with isoprene-emitting species being particularly common in the families *Salicaceae*, *Fagaceae*, and *Palmae* as well as in the genus *Picea* (spruces) and diverse ferns (Sharkey et al., 2007). However, isoprene emissions are less common among herbaceous and crop plants.
- **Monoterpenes (MTs):** The group of monoterpenes is the second largest contributor to global BVOCs emissions, after isoprene. This group, characterized by a wide variety of compounds (**Table 1.1**), represents around 11% of the estimated mean annual total BVOC emission based on MEGAN and MEGAN-MACC models (Guenther et al., 1995; Sindelarova et al., 2014). MTs include acyclic, and mono-, bi-, and tricyclic structures; they may exist with or without the inclusion of oxygen in compounds such as menthol, camphor, linalool and geraniol. They are known to constitute the main fraction of essential oils that are produced and stored in plant secretory organs like glandular trichomes and resin ducts. Their production has been found in 46 families of flowering plants and all conifers. The presence or absence of monoterpenes in plant tissues appears to vary at the familial level. Some families, such as *Pinaceae* (e.g., pine, fir, spruce) or *Lamiaceae* (e.g., mint, basil),

have high levels of monoterpenes in most of their members. Others such as *Fagaceae* (e.g., oak, beech, chestnut) have only a few species that show any significant levels of monoterpene emission. Indeed, this is the case of *Quercus ilex* which is characterized by high amounts of monoterpenes, but do not store them (Bertin et al., 1997).

- **Sesquiterpenes (SQTs):** SQTs include a broad range of biogenic volatile organic compounds made up of three isoprene units and having the general molecular formula $C_{15}H_{24}$. They are emitted from numerous plant species including conifer and broadleaf trees, shrubs, and agricultural crops. One of the largest uncertainties regarding SQTs is their emission rate from vegetation. They were reported to represent around 2.5% to the estimated mean annual total BVOC emission by Sindelarova et al. (2014) (Baker and Sinnott, 2009; Guenther, 2013).

Table 1.1: Chemical formulas, molecular weights, boiling points and chemical structures of selected biogenic VOCs (Fuentes et al., 2002).

Compound name	Chemical formula	Molecular weight (g mol ⁻¹)	Boiling point (K)	Chemical structure
Isoprene	C_5H_8	68.12	307	
Camphene	$C_{10}H_{16}$	136.24	320	
3-Carene	$C_{10}H_{16}$	136.24	441	
α -Pinene	$C_{10}H_{16}$	136.24	428	
β -Pinene	$C_{10}H_{16}$	136.24	436	
Limonene	$C_{10}H_{16}$	136.24	448	
Myrcene	$C_{10}H_{16}$	136.24	440	
Terpinolene	$C_{10}H_{16}$	136.24	459	
Sabinene	$C_{10}H_{16}$	136.24	437	
β -Caryophyllene	$C_{15}H_{24}$	204.35	396	
α -Humulene	$C_{15}H_{24}$	204.35	396	

Oxygenated compounds: Several oxygenated volatile organic compounds (OVOCs) are emitted by plants. Methanol and acetone are among the most abundant VOCs in the global atmosphere, representing 6% and 3 %, respectively, of the annual global emission of BVOCs. High rates of methanol emissions were reported from vegetation foliage, especially young expanding leaves. Terrestrial ecosystems are estimated to be responsible of 42- 78% of the global annual production of methanol (Jacob et al., 2005; Stavrou et al., 2011). Whereas, acetone from vegetation was reported to contribute between 22 and 35% to the global annual acetone emission (Fischer et al., 2012; Jacob et al., 2005). Other OVOCs, include carbonyl compounds and organic acids. A high number of carbonyl compounds can be produced by plants, including formaldehyde, acetaldehyde, propanal, acetone, butanal, i-butanal, butenal, i-butenal, 2-butanone, crotonaldehyde, 2-pentanone, 2-methyl-2-pentenal, hexanal, (E)-2-hexenal, (Z)-3-hexenal, benzaldehyde and methyl-vinyl-ketone (MVK). Direct emissions of carbonyl compounds were reported from forests, whereas for agricultural crops only, a small number of data exists. Regarding organic acids, the most prominent volatile organic acids emitted by the vegetation are formic and acetic acids. These compounds can be directly emitted by forest trees, whereas crops were found to act as a significant sink. It should be noted that, OVOCs, can have both natural and anthropogenic sources; they can be primarily emitted by plants or formed by secondary oxidation, and vegetation is both a source and a sink of these compounds.

Alkanes and Alkenes (including Oxygenated Alkanes and Alkenes): A variety of alkanes emission was reported from trees, crops, and grass- and marshland. Lichens, mosses and heather were also discussed as potentially relevant sources. However, according to Guenther et al. (1994), the global contribution of terrestrial vegetation to the atmospheric budget is low. Regarding alkenes, significant terrestrial biogenic sources are known for ethene, propene and butene from a forest. However, agriculturally used crops show a higher percentage of ethene and propene emissions than forest trees with emission of a large amount of isoprenoids.

Organic halides: Organic halides including methyl bromide, methyl chloride and methyl iodide, can be produced by vegetation. Even though methyl halide fluxes are small compared to terpenoid emissions, they represent an important source of halogens in the stratosphere where they play a role in stratospheric ozone depletion. Terrestrial ecosystems are both a source and a sink of these compounds.

Organic Sulfur Compounds: Biogenic organic sulfur emissions from marine and terrestrial ecosystems represent an important source of atmospheric sulfur compounds in clean environments. Soil microbes and plants are both sources of compounds that include methyl mercaptan, ethyl sulfide and dimethyl disulfide. A study done by Watts (2000), estimated the contribution of terrestrial ecosystems to be about 15% of the global dimethyl sulfide flux, with the remainder coming from oceans.

Benzenoid Compounds: It is widely recognized that there are several benzenoid compounds emitted as floral scents, such as benzaldehyde, anisole and benzyl alcohol, etc. These floral benzenoid emissions are thought to make a small contribution to annual regional BVOC emissions but can be a major emission at specific locations.

Table 1.2 : Annual global total averaged over the period of 1980–2010 for selected BVOC species (with standard deviation σ), their relative contribution to the global total of all BVOCs expressed as emission of carbon, maximal and minimal value within the modelled period. Note that the sum of monoterpenes already includes emissions of α -pinene and β -pinene (in italics). (Adopted from Sindelarova et al., 2014).

Global totals Species	mean Tg (species) yr ⁻¹	rel. contribution %	minimum Tg yr ⁻¹	maximum Tg yr ⁻¹
isoprene	594 ± 34	69.2	520	672
sum of monoterpenes	95 ± 3	10.9	89	103
<i>α-pinene</i>	32 ± 1	3.7	30	34
<i>β-pinene</i>	16.7 ± 0.6	1.9	15.6	17.9
sesquiterpenes	20 ± 1	2.4	18	23
methanol	130 ± 4	6.4	121	138
acetone	37 ± 1	3.0	35	40
ethanol	19 ± 1	1.3	17	21
acetaldehyde	19 ± 1	1.3	17	21
ethene	18.1 ± 0.5	2.0	17.1	19.2
propene	15.0 ± 0.4	1.7	14.1	15.9
formaldehyde	4.6 ± 0.2	0.2	4.3	5.1
formic acid	3.5 ± 0.2	0.1	3.2	3.8
acetic acid	3.5 ± 0.2	0.1	3.2	3.8
2-methyl-3-buten-2-ol	1.6 ± 0.1	0.1	1.4	1.8
toluene	1.5 ± 0.1	0.2	1.4	1.6
other VOC species	8.5 ± 0.3	0.8	7.9	9.0

Among the biogenic compounds, isoprene and monoterpenes are the most studied, with a number of publications covering their synthesis and emission factors (Laothawornkitkul et al., 2009), canopy fluxes (Karl et al., 2007), atmospheric mixing ratios (De Gouw and Warneke, 2007) and atmospheric role (Fuentes et al., 2002). This was confirmed by Guenther (2013), whose review showed that most studies worldwide focused on forests ecosystems, rich in isoprene and monoterpenes, and that there was little interest in BVOCs from agriculture, seen their low terpenoids emissions (**Figure 1.3**). However, 1990s investigations, highlighted the emission of substantial amounts of oxygenated VOCs from crops (König et al., 1995).

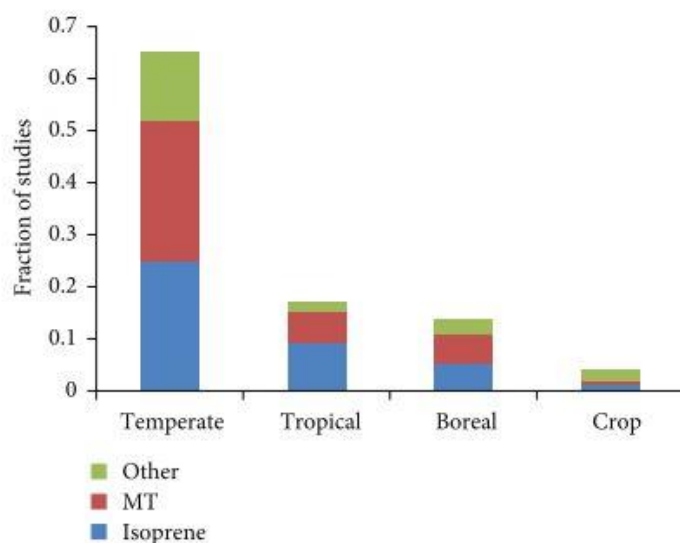


Figure 1.3: Comparison of the number of BVOCs emissions diversity studies (1957- 2011) for major biome types and compound categories (Guenther, 2013).

1.2.3. Factors affecting BVOCs emissions

Emissions essentially result from the diffusion of VOCs along a vapor pressure gradient from cellular compartments of relatively high concentrations to the air surrounding the leaf, where they are relatively found in low concentrations as a consequence of the short lifetime of most VOCs in the atmosphere. Emissions will thus be controlled by VOCs volatilities and those internal (genetic and biochemical) and external (biotic and abiotic) factors. Reviews by Kesselmeier and Staudt (1999); Laothawornkitkul et al. (2009) and Penuelas and Llusia (2001), summarize the main factors affecting BVOCs emissions.

- **Internal factors**

There is evidence to suggest that BVOC biosynthesis is largely controlled at the level of gene expression. Studies showed that changes in expression of the genes involved in BVOC synthesis positively correlate with their emission rates, and this control leads to spatial and temporal emission variabilities. Another internal factor is the enzymatic activity that regulates protein levels. Indeed, emissions of many BVOCs showed to be strongly correlated with enzyme activities. The availability of substrate for the final reaction leading to BVOC synthesis is also a crucial rate-limiting factor. In addition, the circadian regulation of substrate availability, transcription or enzyme activity can also influence the distinct diurnal and nocturnal patterns of some BVOCs emissions (Laothawornkitkul et al., 2009).

- **External factors**

Besides the genetically predetermined biodiversity in vegetation emissions, the release of VOCs by a given plant species exhibits important temporal and spatial variations, resulting from complex interactions between the organism and its environment.

- **Abiotic factors**

Temperature and light: Temperature exponentially increases the emission rates of most VOC, up to an optimum (**Figure 1.4**) by enhancing the synthesis enzymatic activities, raising the VOC vapor pressure and decreasing the resistance of emission pathway (Penuelas and Llusia, 2001). All studies on the emission of the major BVOCs (isoprene and monoterpenes) showed a clear temperature dependence, especially for monoterpenes that are generally stored in special organs. This exponential increase of emissions with temperature is usually described using the formula by Tingey et al. (1980):

$$E = E_S * \exp(\beta * (T - T_S)) \quad (1.1)$$

where E is the emission at temperature T, β is the slope $\frac{d \ln E}{dT}$ and E_S is the emission at a standard temperature. Slopes found in the literature range between 0.057 and 0.144 °C⁻¹. As a generally accepted mean value, 0.09 °C⁻¹ is used (Guenther et al., 1993).

Additionally, isoprene emissions have shown to be triggered by light (**Figure 1.4**), as a result of the link between isoprene emission and synthesis from photosynthetic products. Thus, solar radiation can influence on a short time scale of minutes and hours, the emissions of non-stored

VOCs such as isoprene. As no large pool exists, synthesis and hence isoprene emission will cease within minutes under dark conditions. Similarly, monoterpenes emissions respond to light from the leaves of the evergreen Mediterranean oak species that do not possess storage pools (Loreto et al., 1996; Staudt and Seufert, 1995). Indeed, all monoterpenes are synthesized from carbon, recently fixed by photosynthesis immediately prior to emission.

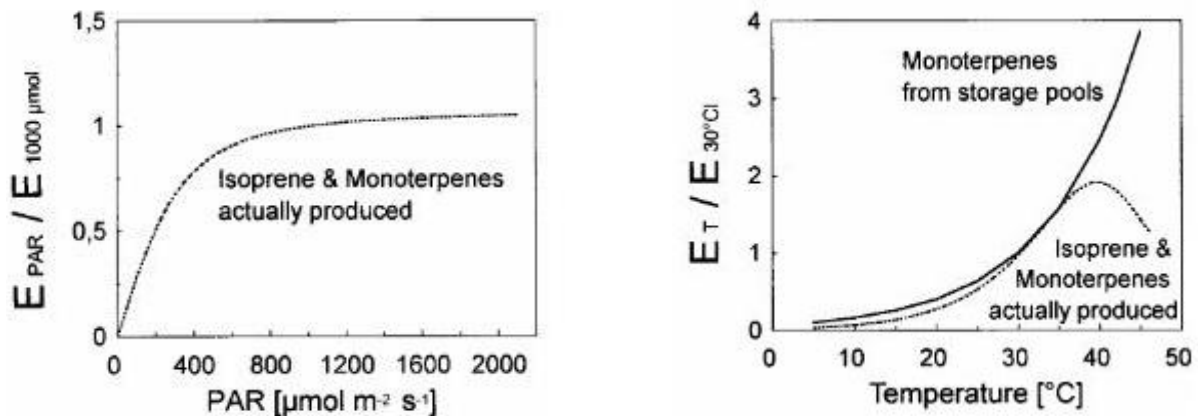


Figure 1.4: Generalized relative emission of isoprene and monoterpenes in relation to light (PAR) under constant temperature, and temperature under constant light as described by potential algorithms (Kesselmeier and Staudt, 1999).

Atmospheric relative humidity: It seems that relative humidity has a minor importance in controlling isoprene or monoterpene release by leaves. While some studies concluded that relative humidity does not affect monoterpene emissions like the one by Juuti (1990) on pine, others reported a slight or significant increase in monoterpene emissions (diverse conifers and aromatic shrubs) (Schade, 1999), although the exact mechanisms by which the apparent emission increase is triggered are not known.

CO₂ fluctuations in the atmosphere: The CO₂ concentration during growth may influence VOC emission rates. Experiments showed that elevated CO₂ concentrations can lead to an increase or a decrease in BVOC production and emission at the whole plant, shoot or leaf levels. Other studies suggested no significant effects. The mechanisms of these contrasting effects are unknown but of importance in the face of rising global atmospheric CO₂ concentration.

O₃ concentrations: Experimental evidence on the direct effects of O₃ on BVOC emissions is, as for other abiotic stresses, not clear cut, showing that elevated O₃ can increase, decrease or have no effect on BVOC emission rates. These differences depend on the plant species, the season and the BVOC species.

Drought and soil moisture: Soil moisture is the principal source of water for plants. Studies indicate that moderate drought can decrease, enhance or have no effect on isoprene and monoterpene emissions. However, severe, long-lasting water stress, can significantly reduce BVOC emissions.

Mechanical stresses: Mechanical stress, including injuries as well as herbivore and pathogen attacks can induce multiple impacts on VOC emissions from vegetation, on the short- and the long-term. Monoterpenes emission bursts were reported after slight mechanical stress, in plant storing monoterpenes (Staudt et al., 1997). Whereas, isoprene emission appeared to be either unaffected or inhibited by plant damages (Monson et al., 1994).

- **Biotic factors:**

BVOCs production and emission were also reported as a result of plant interactions with animals and other organisms. Many compounds act as chemical weapon presenting a defense capacity, whereas others are released to attract pollinators.

• **Long term factors**

Global warming: Various attempts have been made to estimate how an increase in temperature will enhance BVOC emission rates, since these emissions are strongly temperature dependent. Studies suggested that an increase in mean global temperatures by 2–3°C could enhance global BVOC emissions by 25–45%. Whereas, at a regional scale, very high temperatures ($\approx 40^\circ\text{C}$), could lead to a dramatic decline in isoprene emissions.

Land use changes: Because urbanization, agriculture and agro-industrialization, the Earth is experiencing massive land use and land cover changes. These pressures are altering plant species distributions and characteristics, and may dramatically influence BVOC emissions. A global increase in crop area of 455% was reported for the past 300 yr (1700–1990). Even though, grasses and cereals are not generally major isoprene emitters, they do emit oxygenated BVOCs, particularly during harvesting.

All different factors governing BVOCs emissions from terrestrial vegetation, are summarized in **Figure 1.5**.

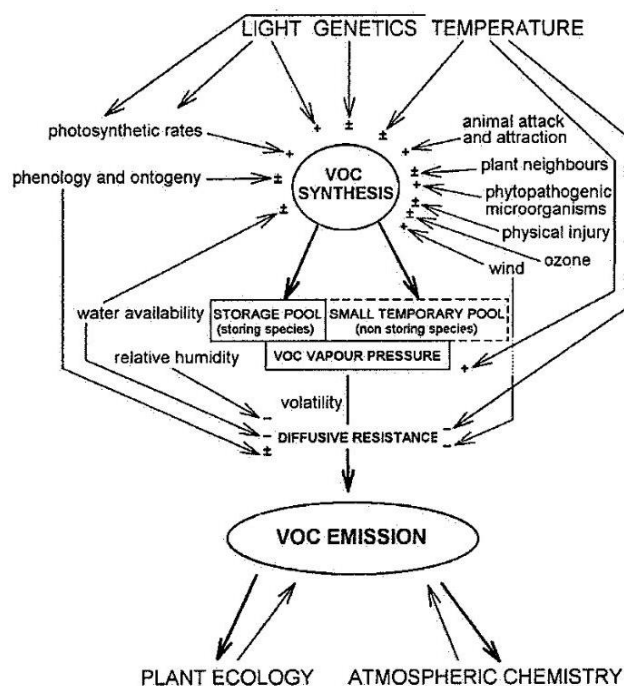


Figure 1.5: Factors controlling VOCs emissions (adopted from Penuelas & Llusia, 2001).

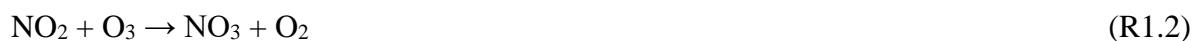
1.3. Reactivity and impacts in the atmosphere

When BVOCs are released into the atmosphere, they are subject to physical and photochemical processes, including wet and dry deposition, photolysis, reaction with the hydroxyl radical (OH), reaction with the nitrate radical (NO₃) and reaction with ozone (O₃). For most BVOCs, dry and wet deposition is probably of minor importance, though these physical removal processes could be important for the chemically long-lived methanol and for certain BVOC reaction products. Photolysis is expected to be potentially important for carbonyls and organic nitrates, and hence for many of the BVOC reaction products, since short-wavelength solar radiation is absorbed by O₂ and O₃ in the stratosphere, and the radiation reaching the troposphere is the one with wavelengths ≥ 290 nm. Regarding oxidation reactions, they are dominated by reactions with OH during day-time. These reactions potentially lead to the ultimate products of CO₂ and water. Sources of O₃, NO₃ radicals and OH radicals as well as their reaction mechanisms are discussed below.

1.3.1. Atmospheric oxidants: sources, levels and reaction mechanisms with VOCs

1.3.1.1. NO₃ radical reactivity

NO₃ radicals result from the oxidation of NO released in the troposphere from soils, natural fires and combustion processes, or formed in situ from lightening. Reactions are presented in equations (R1.1) and (R1.2), where NO is oxidized into NO₂, followed by the oxidation of NO₂ into NO₃:



Due to its rapid reaction with NO and its short lifetime (~5 s) in sunlight as a result of photolysis, NO₃ radical concentrations remain low during day-time. Its concentration increases substantially at night, making it important for nocturnal chemistry. Measurements showed that night-time NO₃ radical concentrations at or near ground level over continental areas can reach 1x 10¹⁰ molecule cm⁻³, corresponding to a mixing ratio of 430 pptv. Therefore, at night, when OH concentrations are effectively zero, VOC oxidation may be driven by reaction with the nitrate radical.

NO₃ reactions with alkanes and aldehydes proceeds via H-abstraction:



The alkyl radicals produced in reaction (R1.10) are transformed to peroxy radicals (RO₂) by reaction with O₂.

With alkenes, including isoprene and terpenes, NO₃ reacts by addition to a C = C double bond, with the abstraction of a hydrogen atom. Molecular oxygen adds to the resulting radical leading to a peroxy radical (RO₂). During night-time, RO₂ will isomerize or react with another RO₂, NO₃ or HO₂. Laboratory experiments showed that the NO₃ plus BVOC (NO₃+BVOC) reaction can be a source of night-time HO₂ and OH radicals (Monks et al., 2009; Ng et al., 2017).

1.3.1.2. O₃ reactivity

Stratosphere-to-troposphere transport is an important natural source of tropospheric ozone, which can occasionally influence ground-level ozone concentrations (Akritidis et al., 2016). Nevertheless, the dominant source of tropospheric O₃ is its photochemical formation from interactions of VOCs with nitrogen oxides (NO_x= NO+ NO₂), in the presence of light, as shown in equations (R1.11)- (R1.14). Organic peroxy (RO₂) radicals and HO₂ radicals formed during VOCs photo-oxidation, react with NO to form NO₂, whose photolysis leads to net O₃ formation through reactions (R1.11) and (R1.12).



Thus, tropospheric ozone is formed, as a result of these processes, with mixing ratios ranging between 10- 40 ppbv at ground level, in “clean” remote sites and levels often exceeding 100 ppbv in polluted peri-urban areas.

Ozone reacts with VOCs only by addition to C = C bonds. This reaction pathway consists of an initial O₃ addition to the C=C bond, to form a primary unstable ozonide which rapidly decomposes via two pathways leading to a carbonyl plus a “Criegee intermediate”. The initially energy-rich Criegee intermediates can further react, following a number of routes, with a potential formation of OH and RO₂ (Pinto et al., 2010).

1.3.1.3. OH radical's reactivity

The hydroxyl radical (OH) is the major chemical scavenger in the troposphere. It controls the atmospheric lifetime of most trace species of biogenic and anthropogenic origin. In the clean troposphere, the photolysis of ozone followed by the subsequent reaction of O(¹D) with water vapor is the main OH source during day-time (Stone et al., 2012).



In more polluted environments, the photo-dissociation of nitrous acid (HONO), the photo-oxidation of formaldehyde (CH₂O) and acetone (CH₃C(O)CH₃) can also be important OH sources. Besides these photolytic sources, other non-photolytic OH sources have been discovered. O₃ reactions with alkenes can produce a significant amount of OH. OH radicals could also result from night-time ozonolysis of alkenes, NO₃-facilitated decomposition of peroxyacyl nitrates (RC(O)O₂NO₂) and NO₃-initiated oxidation of alkenes (Ren et al., 2006).

Since OH is an extremely reactive radical, it reacts as soon as it is formed. It has a lifetime of less than a second. Therefore, OH radical concentration is extremely low, ranging between 1x10⁵ to 2x10⁷ molecules cm⁻³. Since OH formation depends on water vapor, the concentration of OH tends to decrease with altitude as the air becomes cooler and drier.

On a global scale, OH reacts primarily with carbon monoxide (40%) to form carbon dioxide. Around 30% of the OH produced is removed from the atmosphere in reactions with hydrocarbons (RH) and 15% reacts with methane (CH₄). The remaining 15% reacts with ozone (O₃), hydroperoxy radicals (HO₂) and hydrogen gas (H₂).

There are two general reaction mechanisms of OH with BVOCs: (1) addition to C = C bonds by OH radicals, that dominates (2) H-atom abstraction from C–H bonds by OH radicals, leading to the formation of hydroxy- substituted alkyl radicals.

The oxidation of a hydrocarbon (RH) proceeds via the following mechanism (**Figure 1.6**):





where R is an organic group and M is a third body reactant (O_2 or N_2).

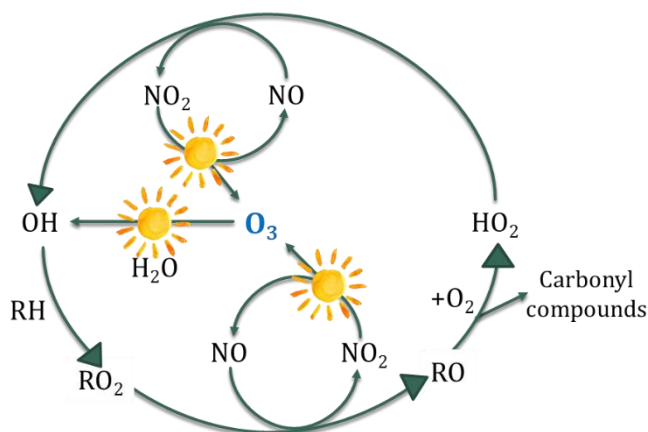


Figure 1.6: Scheme of VOCs oxidation with the hydroxyl radical OH.

Even though the main primary source for OH in the lower troposphere is the photolysis of ozone at short wavelengths, the OH production and loss processes are numerous and difficult to quantify. Such losses involve several hundreds of chemical species and as many reactions to consider. In this respect, a direct measurement of total OH reactivity (ROH) is of great interest as it provides a robust measure of the reactive species “loading” of an air mass, allowing a better understanding of the chemistry in the atmosphere and a better investigation of the budget of OH sinks in a particular environment. ROH is defined as the pseudo first-order loss rate (in s^{-1}) of OH radicals, equivalent to the inverse of the OH lifetime. It is the sum of the reaction frequencies of all chemical species reacting with OH, as shown in equation (1.2):

$$\text{ROH} = \sum k_{i-\text{OH}}.X_i \quad (1.2)$$

In this equation, a chemical reaction frequency for a species “i” with OH is the product of its rate-coefficient $k_{i-\text{OH}}$ with its concentration X_i . The measured total OH reactivity can be compared with calculated values based on the sum of reaction frequencies as shown in equation (1.2) and for which the concentration of “i” has been measured at the same location. Any significant discrepancy between measured and calculated OH reactivity explicitly demonstrates

missing OH sinks, commonly called missing OH reactivity, and points out that potentially important unmeasured reactive species and chemical processes associated with these species may affect our understanding of OH atmospheric chemistry.

1.3.2. BVOCs lifetimes

As mentioned before, the processes of removal of VOCs from the atmosphere include chemical and physical processes. The rate of efficiency of each process depends on the physico-chemical properties of the specific chemical compound. Hence, an organic compound can be simultaneously affected by the following removal processes: (i) oxidation reaction with any of the atmospheric major oxidants, (ii) photolysis by solar radiation, (iii) transport to the stratosphere, (iv) deposition onto surfaces, (v) partitioning into the particle phase, leading to a lifetime or a residence time (τ) expressed as shown in the following equation:

$$\tau = \frac{1}{k_c + k_{ph} + k_t + k_d + k_{pa}} \quad (1.3)$$

With k_c , k_{ph} , k_t , k_d , k_{pa} being the first order loss rate of the chemical compound due to chemical reactions, photolysis, transport, deposition and partitioning into the particle phase. Many factors influence the importance of one removal process compared to one another, including the physico-chemical properties of the considered species, such as its rate constant of reaction with one oxidant, its vapor pressure, its absorbance of UV and visible light as well as the environmental conditions (such as temperature, pressure, ...). Generally, oxidation reactions constitute the most important sink for VOCs, with well-established rate coefficients for the reaction of a wide variety of species with atmospheric oxidants. When combined with assumed ambient tropospheric concentrations of OH radicals, NO₃ radicals and O₃, these rate constants can be used to estimate a BVOC lifetime due to oxidation.

Atkinson and Arey (2003), calculated the lifetime of many BVOCs with all three atmospheric oxidants, assuming OH radical concentration to be around 2×10^6 molecules cm⁻³ (12-h day-time average), O₃ concentration to be around 7×10^{11} molecules cm⁻³ (24h average) and NO₃ radical concentration around 2.5×10^8 molecules cm⁻³ (12-h night-time average). Photolysis was also considered, with a calculated photolysis lifetime of ≈ 60 days in the lower troposphere.

The reported lifetimes (**Table 1.3**) are only indicative, in order to show a ranking of reactivity of the different BVOCs, hence, it is important to note that the instantaneous lifetimes of BVOCs

are function of the time of day, season, latitude, cloud cover and the chemical composition of the air mass containing the BVOC.

Table 1.3: Calculated atmospheric lifetimes of biogenic volatile organic compounds (Atkinson and Arey, 2003).

Biogenic VOC	Lifetime for reaction with		
	OH	O ₃	NO ₃
Isoprene	1.4 h	1.3 days	1.6 h
Monoterpenes			
Camphene	2.6 h	18 days	1.7 h
2-Carene	1.7 h	1.7 h	4 min
3-Carene	1.6 h	11h	7 min
Limonene	49 min	2.0 h	5 min
Myrcene	39 min	50 min	6 min
cis-/trans-Ocimene	33 min	44 min	3 min
α -Phellandrene	27 min	8 min	0.9 min
β - Phellandrene	50 min	8.4 h	8 min
α -Pinene	2.6 h	4.6 h	11 min
β -Pinene	1.8h	1.1 day	27 min
Sabinene	1.2 h	4.8 h	7 min
α -Terpinene	23 min	1 min	0.5 min
γ -Terpinene	47 min	2.8 h	2 min
Terpinolene	37 min	13 min	0.7 min
Sesquiterpenes			
β -Caryophyllene	42 min	2 min	3 min
α -Cedrene	2.1 h	14 h	8 min
α -Copaene	1.5 h	2.5 h	4 min
α -Humulene	28 min	2 min	2 min
Longifolene	2.9 h	> 33 days	1.6 h
Oxygenated			
Acetone	61 days	> 4.5 years	> 8 years
Camphore	2.5 days	> 235 days	> 300 days
1,8-Cineole	1.0 day	>110 day	1.5 year
cis-3-Hexen-1-ol	1.3 h	6.2 h	4.1 h
cis-3-Hexenyl acetate	1.8 h	7.3 h	4.5 h
Linalool	52 min	55 min	6 min
Methanol	12 days	> 4.5 years	2.0 years
2-Methyl-3-buten-2-ol	2.4 h	1.7 day	7.7 days
6-Methyl-5-hepten-2-one	53 min	1.0 h	9 min

As shown in (Table 1.3), terpenoids compounds are generally more reactive than most oxygenated species towards all three oxidants. While, for example, isoprene's lifetime towards OH is estimated to be around 1.4 hours only, that of methanol is much higher and is estimated to be around 12 days. Regarding monoterpenes, they represent a group of a large variety of chemical compounds, with variable lifetimes ranging between 0.5 min for α -terpinene lifetime towards NO_3 to 18 days for the lifetime of camphene towards O_3 . In terms of their reactivity with the hydroxyl radical, during day-time, α -terpinene is the most reactive with a lifetime of 23 min, whereas, the most abundant monoterpenes (α and β -pinene), have higher lifetime in the order of hours. α and β -pinene are less reactive towards O_3 and more reactive towards NO_3 , during the night, whereas, α -terpinene is more reactive with O_3 and even more reactive with NO_3 during dark hours. Hence, how strong is the reaction towards one specific oxidant compared to one other is again strictly species dependent, even for compounds belonging to the same family.

1.3.3. Impact of BVOCs transformation in the atmosphere

BVOCs play an important role in the chemistry of the planetary boundary layer. Once emitted in the atmosphere, VOCs compete for the OH radicals, which are the primary atmospheric sink of methane. This could result in a significant prolongation of CH_4 atmospheric lifetime, a very significant greenhouse gas. In high NO_x environments, VOCs contribute to the formation of tropospheric ozone. Ozone is known as a powerful greenhouse gas. It induces an extra radiative forcing of 0.35 W m^{-2} , about 20–25% of the human activity induced radiative forcing due to greenhouse gas changes. It is also at the center of tropospheric gas phase photochemistry, since it is the main source of hydroxyl radical, altering the oxidizing capacity of the atmosphere. Furthermore, tropospheric ozone was reported to have serious impact on human health and the environment. Due to its oxidative potential, O_3 can induce respiratory problems and is associated with premature human mortality. In addition, it produces tree damage, reduces photosynthesis and growth, and therefore crop yields (Ashmore, 2005; Felzer et al., 2007).

BVOCs were also reported to yield relatively non-volatile secondary oxidation products that form aerosols (Griffin et al., 1999; Hoffmann et al., 1997). The importance of BVOCs in tropospheric secondary organic aerosols (SOA) formation has shown to be variable depending on climate, the amount and nature of vegetation, the amount and chemical nature of emitted

compounds (as shown in **Figure 1.7** (Lee et al., 2006)), as well as on other environmental factors such as local meteorological parameters (Kammer et al., 2018). Bottom-up estimates give total biogenic SOA (BSOA) fluxes of 12–70 Tg yr⁻¹ (Kanakidou et al., 2005). This estimate has been revised by Hallquist et al. (2009) with a new best estimate for SOA of 88 Tg C yr⁻¹ (range 0–180), higher than the estimates (13–24 Tg yr⁻¹) presented previously for biogenically derived SOA by Griffin et al. (1999). Organic aerosols can exert a direct radiative effect by scattering and absorbing solar and terrestrial radiation but also indirect radiative effects, through their role as cloud condensation nuclei (CCN).

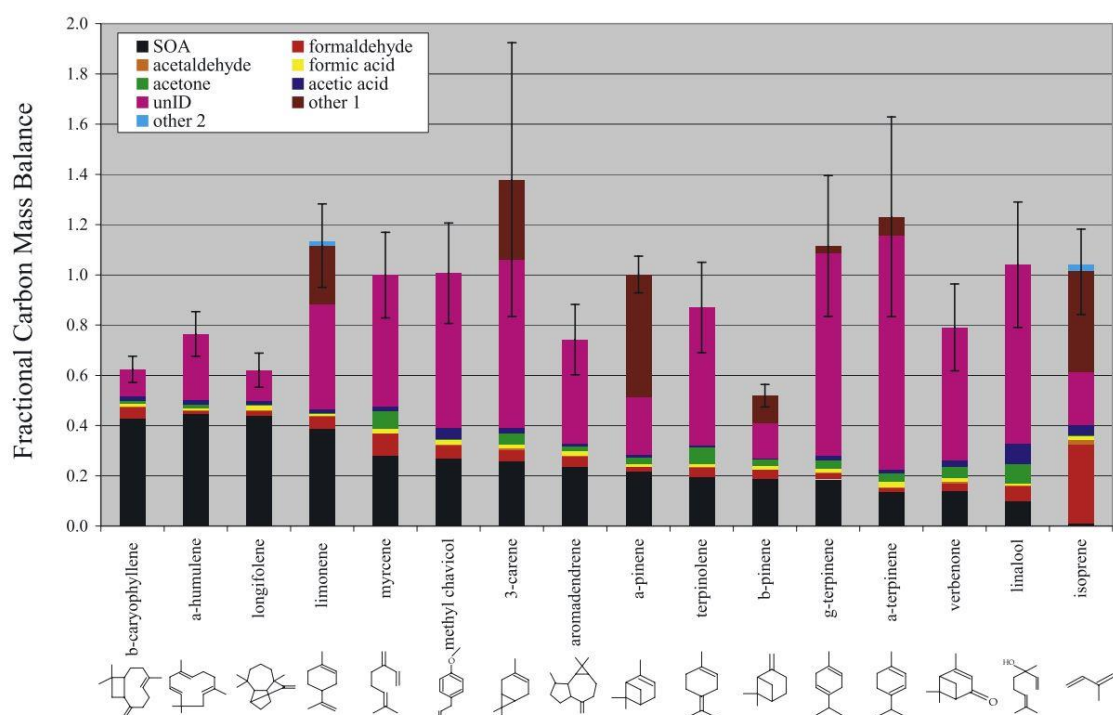


Figure 1.7: Carbon mass balance of SOA (assuming aerosol is 60% carbon) and gas-phase oxidation products resulting from the photooxidation of isoprene, eight monoterpenes, three oxygenated monoterpenes, and four sesquiterpenes, conducted individually at the Caltech Indoor Chamber Facility (Lee et al., 2006). The “other 1” category represents the calibrated products nopinone and MACR + MVK from b-pinene and isoprene, respectively, and the uncalibrated products limononaldehyde, caronaldehyde, pinonaldehyde, g-terpinaldehyde, and a-terpinaldehyde, from limonene, 3-carene, a-pinene, g-terpinene, and a-terpinene, respectively. The “other 2” category represents limonaketone from limonene and 3-methyl furan from isoprene. Aerosol molar yields (mg aerosol m⁻³/mg terpene m⁻³) were calculated assuming an aerosol density of 1.25 g cm⁻³.

The ability of the particles to serve as CCN depends on the water vapor supersaturation, particle-size distribution and also the chemical composition (Asmi et al., 2011; Roberts et al., 2010). Besides the processing of primary particles, other CCN sources were identified, such as regional new particle formation (NPF) events (Kerminen et al., 2012). NPF is a frequent

atmospheric phenomenon including the formation of small particles (nanometer-sized clusters) from gaseous precursors (very low volatile gases) and their subsequent growth to larger sizes (Kulmala and Kerminen, 2008; Rose et al., 2017). This secondary particle formation has been shown to be an important source of aerosols in the atmosphere.

1.4. Measurement methods

1.4.1. VOCs in ambient air

Several techniques have been used for online monitoring of VOCs in the atmosphere. Plant VOC research relies on analytical techniques for trace gas analysis, with the two most commonly used techniques for qualitative and quantitative analysis being: (1) gas chromatography (GC)–based techniques such as gas chromatography–mass spectrometry (GC-MS), GC with flame ionization detector (GC-FID), and thermal desorption–gas chromatography–mass spectrometry (TD-GC-MS); and (2) mass spectrometry based on soft chemical ionization, such as selected ion flow tube–mass spectrometry (SIFT-MS) and proton transfer reaction–mass spectrometry (PTR-MS).

It is quite challenging to detect and quantify BVOCs for a range of reasons, since:

- VOCs are very reactive to other compounds in the atmosphere;
- VOCs can react with monitoring equipment surfaces and some monitoring equipment materials can emit VOCs;
- Depending on the study, plants can be enclosed in a special chamber, which may stress the plant (e.g., change of light condition, wounding) and result in unrepresentative emissions;
- Measured concentrations are often very low—usually 1–100 ppbv (sometimes <1 ppbv)—thus challenging the detection limits of analytical instruments.

1.4.1.1. Gas chromatography- based methods (GC)

GC is a well-established method of continuous chemical separation of one or more individual compounds between two phases: a fixed phase called the stationary phase and a mobile phase which consists of a carrier gas flowing over the stationary phase. When injected via a heated inlet, components enter the stationary phase simultaneously but move along at different rates,

depending on each compound's vapor pressure and its solubility in the stationary phase. At the end of the column, compounds are detected and identified based on the retention time, knowing that a retention time is characteristic for a compound and the stationary phase at a given temperature. Temperature of the column is controlled in order to obtain a good separation and resolution of the analytes. Since the concentration of BVOCs emitted from plants can be quite low, online monitoring of VOCs with GC, generally requires sample pre-concentration in which the air sample passes through a cooled tube containing packing material. The most common gas chromatograph detectors for plant VOC research are flame ionization detectors (FID) and mass spectrometers. FIDs are simple, low-cost detectors for organic compounds (VOCs, such as hydrocarbons, which can be detected when burnt). When a mass spectrometer is used as a detector, analysis of the fragmentation patterns of the ions at each point in the total ion chromatogram enables compound identification. Detectors are specifically calibrated for each VOC compound present using known standards, to develop response factors and linear operating ranges for the method (Srivastava and Majumdar, 2011). GC was one of the first chromatographic separation techniques to be developed and has still today lost none of its importance, especially with the favorable combination of very high selectivity and resolution, good accuracy and precision, wide dynamic concentration range and high sensitivity (Driscoll, 2004; Sahu, 2012). However, the main disadvantage of GC-based instruments is that, usually due to the pre-concentration step, it has a poor temporal resolution (≥ 30 min), thus it is not suitable for research where high time resolution is needed.

1.4.1.2. Selected ion flow tube–mass spectrometry (SIFT-MS)

SIFT-MS is a soft chemical ionization technique that utilizes chemical ionization of the VOC with H_3O^+ , NO^+ , and O_2^+ as reagent ions. SIFT-MS is a sensitive instrument suitable for real-time monitoring of plant VOCs (Smith and Španěl, 2005). Precursor ions are generated via water and air in a microwave resonator, producing many different ions. A quadrupole mass filter allows the selection of the desired precursor ion (H_3O^+ , NO^+ , or O_2^+). Precursor ions enter the flow tube which consists of a metal cylinder, where helium is used as a carrier gas. The sample is introduced into the flow tube via a heated sampling capillary with a constant flow (usually 30 mL min^{-1}). Further down the flow tube, the precursor ions react with the sample VOCs and ionize them. The ionized VOCs are filtered by the detection quadrupole and detected by the ion detector. Based on the precursor ions count and a well-established kinetics library

for the flow tube, it is possible to calculate the concentrations of trace gases without further calibration of the instrument. SIFT-MS presents the advantage of providing real-time measurements, down to ppbv, with different available precursor ions which increases the selectivity and gases identification. In addition, this instrument does not require calibration against gas standards. However, SIFT-MS show some limitations. Indeed, using the H_3O^+ mode, Isoprene- H^+ , generated through the reaction of isoprene with the H_3O^+ precursor, has a mass-to-charge ratio (m/z) of 69, which overlaps with that of protonated methanol linked with two water molecules ($\text{CH}_3\text{OH}\text{-H}^+\text{-(H}_2\text{O)}_{x2}$). Thus, isoprene should be analyzed using the NO^+ precursor. Compared to GC-MS, SIFT-MS does not allow to differentiate isomers and compared to PTR-MS, SIFT-MS is less sensitive.

1.4.1.3. Proton transfer reaction–mass spectrometry (PTR-MS)

Proton transfer reaction-mass spectrometry (PTR-MS) is a relatively new on-line technique for the measurement and monitoring of a wide range of volatile organic compounds (VOCs) from widely different sources and processes, at low concentrations in gaseous samples. Utilizing low-energy chemical ionization, it combines the desirable attributes of high sensitivity (10- 100 pptv) and fast response time (1- 10 s) with good precision and accuracy (Lindinger et al., 1998). PTR-MS uses a hollow-cathode discharge source combined with a source drift region to generate hydronium ions with a purity of more than 99.5%. The air to be analyzed is continuously pumped through a drift tube reactor, and a fraction of the VOCs, those with a proton affinity higher than that of water ($\approx 697 \text{ kJ mol}^{-1}$), is ionized by proton transfer reactions from protonated water molecules (H_3O^+). Resulting ions are subsequently separated according to their mass/charge ratio (usually their molecular mass plus 1) either by a quadrupole (QUAD) or by a time-of-flight (TOF) mass spectrometer and detected quantitatively down- stream. The instrument gives raw data in counts per second (cps), which need to be converted to give concentrations in parts per billion (ppb). PTR-MS presents several advantages, including the highest sensitivity for real-time VOC research compared to the other available techniques. It can be equipped to have different precursor ions, which increase the analytical power of the instrument. Furthermore, the ion-molecule collision energy in a drift tube, known as E/N , can easily be changed by changing the electric field parameters on the electrodes, and hence improving the analytical power of the instrument (Blake et al., 2009; Ellis and Mayhew, 2014).

However, seen that PTR-MS gives the concentration of all compounds of the same molecular weight, it does not permit a qualitative analysis of isomers.

Thus, established measurement techniques for in situ BVOC monitoring typically offer a trade-off between sample frequency (PTR-MS) and speciation (GC-FID, GC-MS). In the attempt to combine these two complementary features in one instrument, fast-GC systems have been developed and coupled to PTR-TOF-MS instruments. These systems showed promising results since they allowed the separation of isomeric compounds in fast spectral runs. By using a rather short column coated with a low polar phase, and by applying a very fast temperature gradient, the analysis of VOC mixtures and the separation of isomers can be performed in less than a minute. However, the Fast-GC based methods retain the separation capability of conventional gas chromatography, yet offer significantly improved measurement frequency (Jones et al., 2014; Pallozzi et al., 2016; Romano et al., 2014).

1.4.2. OH reactivity measurements techniques

There are two general approaches that can be used to measure total OH reactivity, without the need to quantify individual sinks: direct measurement of the OH decay rate and the comparative reactivity method (CRM).

Several groups, have used laser-induced fluorescence (LIF) techniques with either discharge flow technique or the laser flash photolysis (LP) technique to directly detect the OH decay rate due to its reaction with trace species in a reaction tube (Hansen et al., 2015; Ingham et al., 2009; Kovacs and Brune, 2001; Lou et al., 2010; Sadanaga et al., 2004a). Similarly, chemical ionization mass spectrometry (CIMS) can be used to determine the variation of OH radicals.

Flow Tube- Laser Induced Fluorescence (FT- LIF): At the tip of a small diameter movable tube, OH radicals are generated in the FT-LIF technique, by the photolysis of water vapor with a 185 nm ultraviolet light, and injected in the center of a large flow tube to get mixed with ambient air flows. The detection technique is low-pressure laser induced fluorescence. By changing the position of the injector relatively to the detection point of OH, the contact time of OH with ambient species changes too, in fact as the movable tube is drawn further away from the detector, the observed OH signal decreases. The slope of the logarithm of the OH signal, as a function of the distance between the OH injector and detector divided by the velocity of the

air, determines the OH reactivity. However, this technique exhibits some disadvantages like the need of relatively high flow rates, leading to turbulent flows and thus, significant wall loss rates of OH in the flow tube. Another important limitation is the production of equal concentrations of OH and HO₂. In fact, HO₂ can react with NO to produce OH, which will reduce the observed decay rate of OH in the flow tube. Corrections should be made to overcome these interferences that are less significant in the LP-LIF method (Kovacs and Brune, 2001; Mao et al., 2009).

LP-LIF: The LP-LIF method consists on generating OH radicals by flash photolysis of ozone, using a pump laser pulse going through the flow tube at typically 266 nm, followed by the reaction of O(¹D) with ambient water vapor. OH radicals react with ambient reactive species in the reaction tube and the concentration of OH decreases with time after irradiating the laser pulse. The sampled air in the reaction tube is then introduced into a low-pressure detection cell where the OH decay is measured by laser-induced fluorescence with a high time resolution. Lower flow rates compared to FT-LIF result in lower OH losses to the walls and the use of O₃ photolysis instead of the photolysis of water vapor for OH generation, limits the recycling processes of OH due to the HO₂- NO reaction. In both cases, an instrument zero, due the wall losses reactions, has to be subtracted from all measurements, and a correction has to be applied for the recycling of OH radicals in the presence of NO (Sadanaga et al., 2004a and b; Stone et al., 2016). Since it is assumed that the reaction of OH with reactive trace compounds follows the pseudo-first order regime where the concentration of ambient species does not change significantly throughout the reaction zone, the loss of OH with time is represented by the following equations: $K_{OH} = -(\ln[OH]/[OH]_0)/t$ (Mao et al., 2009) in FT-LIF, where [OH]₀ represents the initial OH concentration, and [OH] represents the OH concentrations after a reaction time t between OH and its reactants in FT-LIF or the time after the pump laser irradiation in LP-LIF.

FT-CIMS: Another technique adopting the direct measurement approach of OH decay rate is the FT-CIMS which is based on using the flow-tube set-up with a chemical ionization mass spectrometer as a detector of OH concentrations. Briefly, this method consists on photolyzing ambient water vapor with a UV mercury lamp to produce a known concentration of OH radicals in front of a sample tube, before performing two sulfur dioxide injections. These latter injections lead to the conversion of the remaining OH into H₂SO₄, which occurs in the flow tube chemical reactor in front of the ionization region. H₂SO₄ is then ionized by charge transfer utilizing negative chemical ionization with NO₃⁻ reactant ions (Berresheim et al., 2000; Fuchs et al., 2017; Muller et al., 2018).

CRM: For indirect measurement of total OH reactivity, the Comparative Reactivity Method (CRM), used with a Proton Transfer Reaction Mass Spectrometer (PTR-MS) or Gas Chromatography- Photo Ionization Detector (GC-PID) monitors the concentration of a reference substance, generally pyrrole, that competes with ambient reactive species for the artificially generated OH radicals. In fact, ambient air, wet nitrogen and pyrrole are conducted into a glass reactor where OH radicals are produced by the photolysis of water vapor and where all analytical steps take place leading to the measurement of Total OH Reactivity. The CRM exhibits several advantages compared to direct measurements techniques, like the commercial availability of PTR-MS and the need of smaller sampling flows, which broadens the application of the technique to branch and plant enclosure studies for example. On the other hand, this method requires a raw data processing with careful corrections for measurements artifacts related to humidity changes, NO concentrations, pyrrole/OH ratios and the dilution of ambient air inside the reactor, which can lead to higher uncertainty.

Over the past two decades, many OH reactivity observations have been conducted in various field campaigns using the available techniques (Yang et al., 2016). However, only a few direct inter-comparison experiments were reported in the literature.

An inter-comparison exercise, involving two CRM systems from Laboratoire des Sciences du Climat et de l'Environnement and Mines Douai took place in a Mediterranean forest ecosystem (Zannoni et al., 2015). A correlation described by a linear least squares fit with a slope of 1 and an R^2 of 0.75 demonstrated the good agreement between both CRM systems and the robustness of the CRM in OH reactivity measurements. However, this study pointed out, as several previous studies using the CRM, the need of careful corrections which are, for now, specific to each CRM instrument. Another inter-comparison campaign between a CRM system from Mines Douai and a pump-probe technique from University of Lille was conducted in a high NO_x environment (Hansen et al., 2015). Results showed a good agreement between both techniques, after taking into account possible interferences and making appropriate corrections. In both systems, an underestimation of measured OH reactivity was concluded compared to the expected OH decay rate, calculated based on measured reactive species. This observed discrepancy was mainly due to potential photolysis of VOCs by the UV mercury lamp in the CRM method and from the difficulty to measure the instrumental zero, caused by impurities in humid zero air, in the pump-probe technique. A large number of OH reactivity instruments were deployed in a wider campaign conducted in the atmospheric simulation chamber SAPHIR in order to compare their performances (Fuchs et al., 2017). The results showed that OH reactivity

can be accurately measured for a wide range of atmospherically relevant chemical conditions by all instruments. However, CRM instruments exhibited larger discrepancies to reference measurements and to calculated OH reactivity compared to instruments directly measuring OH radicals, and these differences were more important in the presence of terpenes and oxygenated organic compounds. Therefore, technical improvements were made aiming to overcome this limitation and reduce the potential loss of reactive compounds in the sampling system.

1.5. OH reactivity in various environments

Since the development of the first measurement technique in the late 1990s, many total OH reactivity observations have been conducted globally, including ground-based ambient measurements, airborne measurements, branch enclosure/ plant cuvette and in flow tubes and environmental chambers. Ground-based measurements are the most common in the literature, they cover diverse environments, including urban, rural, forest and marine areas. All the reported studies have accumulated a great number of datasets, showing the various temporal and spatial patterns of measured OH reactivity. In this section, focus will be made on OH reactivity studies performed in forest and rural environments, two very different ecosystems, that showed different ranges of OH reactivity and they were further investigated during this PhD.

1.5.1. Forest areas

Forest areas are among the most studied in terms of total OH reactivity. Studies show the great variability depending on the forest type, the season, the most abundant VOC, meteorological parameters as well as the measurement height. The first characterization of OH reactivity in a forest ecosystem was the study made by Di Carlo et al. (2004) during the PROPHET 2000 intensive campaign. The experiment took place in a mixed, transition forest that consists of northern hardwood, aspen and white pine. Measured OH reactivity at $\approx 10\text{m}$ above the canopy height, varied between 1 and 12 s^{-1} . It was mainly dominated by isoprene (49%), followed by CO and NO_2 (21%), formaldehyde and acetaldehyde (12% each), anthropogenic VOCs (3%) and monoterpenes (2%), since both clean and polluted air were advected from the North and the South, respectively. The difference between measured and calculated OH reactivity was 2.6 s^{-1} (50%) on average and exhibited a temperature dependency.

At that time, analysis demonstrated that the OH missing reactivity observed during PROPHET 2000 was a result of unmeasured temperature-dependent BVOCs. However, later measurements of monoterpenes and sesquiterpenes at this site suggested that ~30% of the missing reactivity could be attributed to these primary VOCs (Kim et al., 2009). Additionally, Kim et al. (2011) found that measurements and calculations of OH reactivity in branch enclosures of isoprene-emitting trees at the same site were in good agreement. Using measurements taken at this site during 2009, Hansen et al. (2014) found that isoprene accounted for 60–70% of afternoon OH reactivity both within and above the forest canopy. Because in-canopy OH reactivity calculations and measurements were in good agreement, the authors concluded that there are unlikely to be unmeasured primary VOCs at this site. However, above-canopy comparisons showed a large missing fraction of reactivity, suggesting that unmeasured oxidation products may contribute at longer processing times. Later on, Zannoni et al. (2016) were also interested in OH reactivity characterization inside and above the canopy of an isoprene-dominated oak forest, and they provided the first set of OH reactivity data in a Mediterranean forest. In their study, and contrary to what was found by Hansen et al. (2014), measured OH reactivity was similar at both heights. It was amongst the highest measured (68–69 s⁻¹). No significant difference between measured and calculated OH reactivity was found for the majority of the time, except for two nights where the missing OH reactivity was up to 50%. This missing fraction was explained by locally produced unmeasured isoprene oxidation products. ***These observations highlight the importance of characterizing OH reactivity at different altitudes and different levels regarding forests canopies, taking into consideration the height of the canopy.***

Relatively high OH reactivity levels (mean= 53 s⁻¹, Max= 72 s⁻¹) were reported within the canopy (35m height) of a tropical rainforest in Suriname, as part of the GABRIEL campaign (Sinha et al., 2008). The field site was dominated by lowland evergreen broad leaf trees, semi-evergreen moist broadleaf trees and some sclerophyllus dry forest trees, and was mainly influenced by clean marine air during the dry season (October 2005). While isoprene, isoprene oxidation products, acetone and acetaldehyde made up only ~35% of the measured sink, a significant fraction of OH reactivity remained unexplained, highlighting similar observations as Di Carlo et al. (2004). It showed that important OH reactive compounds were likely missed by conventional measurements deployed at this forest site. Unfortunately, the limited data coverage of OH reactivity observations during this study meant that any conclusions about the potential identity of this missing OH sink were difficult to make. Later on, Edwards et al. (2013) published a study, part of the OP3 project, about OH reactivity observations during the wet

season, from a clearing atop a hill surrounded by pristine rainforest on Borneo. Despite close recorded maxima, the OP3 mean OH reactivity during the wet season was lower than that reported during the GABRIEL campaign during the dry season. ***These observations, highlight the seasonal variability of total OH reactivity***, that was also reported in the Amazon rainforest by Nolscher et al. (2016), during the ATTO campaign. Indeed, average OH reactivity inside canopy (24m height) was around 62.4 s^{-1} ($31\text{-}85 \text{ s}^{-1}$) and 9.9 s^{-1} ($6\text{-}13 \text{ s}^{-1}$), during the dry and the wet season, respectively, while averages were between 20 and 26 s^{-1} during wet-to-dry and dry-to-wet transition periods.

Interestingly, the day/night variability of OH reactivity at the Borneo site was, in part, attributed to local meteorological conditions. Indeed, the site was showed to be above the surrounding boundary-layer on many nights, leading to higher dilution and thus lower magnitude and variability of total OH reactivity. In contrast, during the day, the low winds experienced throughout the campaign allowed BVOCs emitted from the forest to be confined to the local boundary layer. ***This complex meteorology, combined with the temperature and light dependencies of many BVOC emission rates, results in higher and more variable OH reactivity during the day.*** However, the supporting measurements of OH sinks made during the field campaign did not close the reactivity budget, with the model suggesting that at least 50% of carbon-containing compounds which react with OH were not measured. Regarding potential candidates for missing OH reactivity, modelling demonstrated that this missing carbon is not only related to isoprene-like and isoprene oxidation products-like compounds. For the Borneo site, authors suggested that the missing fraction is most likely related to a large number of complex multifunctional organic compounds which monitoring remains a challenge to the community, whereas for the Amazon site, authors discussed potential, yet insufficient characterized source of OH reactivity released from the tropical forest floor (soil or litter emissions: hexane, methylfuran, 2-butene and ethyl mercaptan). Stress-released VOCs were also suggested as important contributors to the observed missing OH reactivity (Methyl salicylate, hexanal, linalool and many highly reactive sesquiterpenes).

Boreal forests were also subjected to many studies. They are known to be isoprene “poor” and monoterpene “rich” environments. First OH reactivity measurements from a boreal forest were conducted by Sinha et al. (2010), as part of the BFORM campaign at the SMEAR II measurement station during August 2008, in Hyytiälä, Finland. The forest vegetation consists mainly of coniferous trees, dominated by Scots pine and Norway spruce, with an average

canopy height of about 14m. Total OH reactivity measured inside canopy at 12 m, showed no diel cycle with an average of 9 s^{-1} both during day and night, which is in contrast with the pronounced diel cycle observed in tropical forest studies. This low variability was observed despite the differences in the diel emission profiles of individual VOCs and the higher night time mixing ratios of monoterpenes at this site, related to the formation of the shallow nocturnal boundary layer. *Interestingly, it seems that compensating effects of emissions and boundary layer evolution occurred, leading to a near constant OH reactivity regime at the site. Again, wind direction and air mass origin, also played a role on OH reactivity variability, bringing it to higher levels, up to 60 s^{-1} , during a pollution event.* Despite the monitoring of ~ 30 compounds, authors found missing OH sinks of between 25 and 75% of the total measured OH reactivity. These missing OH sinks were again attributed largely to unmeasured BVOCs. A one-dimensional model study of the same 2008 data set (Mogensen et al., 2011) also attributed the missing observed OH reactivity to an unmeasured primary emitted BVOC, as well as to uncertainties in the rate constants used in the chemical mechanism. Nölscher et al. (2012a), made observations of OH reactivity both within and above the canopy at the same site and found a 58% missing OH reactivity for “normal” boreal conditions. The presence of significant concentrations of unmeasured BVOCs in forested environments was also a conclusion of Holzinger et al. (2005), who reported emissions of highly reactive BVOCs in a ponderosa pine forest in California, inferred from the presence of large quantities of previously unreported oxidation products, measured by proton transfer mass spectrometry (PTR-MS). A more recent study, performed by Praplan et al. (2019), from April to June, 2016, highlighted that total OH reactivity at the SMEAR II station is not a simple function of a few variables. *They showed that it includes many complex processes involving sources and sinks that can change dramatically depending on the environmental conditions and the time of the year.* Indeed, the averaged experimental total OH reactivity increased from April to June (5.3 to 11.3 s^{-1}) before decreasing in July (8.8 s^{-1}) because of more humid nights and lower radiation during the measurement period. The total OH reactivity diurnal pattern from May to July followed the one of biogenic compounds with high values during the night due to the low mixing height, even though emissions are lower at night. These averages of OH reactivity in Hyyatiala boreal forest are in the same order of magnitude of those reported in the mixed deciduous forest, by Di Carlo et al., 2004, and lower than those reported for tropical rainforests. The missing fraction of the OH reactivity was higher during the night, possibly due to a larger fraction of non-measured oxidation products, compared to day-time, when the emissions are higher resulting in a larger fraction of known precursors.

Coniferous forests had also a part of total OH reactivity investigations in forest ecosystems. Average total OH reactivity was around 6.7 s^{-1} , during the BEACHON-SRM08 campaign, held at Manitou experimental temperate coniferous forest, in Colorado USA in August, 2008 (Nakashima et al., 2013). Lower values were recorded during the day and higher levels during night-time. *Interestingly, a large increase of OH reactivity was observed during a short period of this campaign, attributed to the strong wind that occurred, disturbing trees, damaging plants and resulting in a burst of BVOC.* From the calculation of OH reactivity based on the analysis of these trace species, including CO, NO, NO_y, O₃ and SO₂ and VOCs, 46.3% of OH reactivity for VOCs came from biogenic species that are dominated by 2-methyl-3-buten-2-ol (MBO), and monoterpenes. MBO was the most prominent contribution to OH reactivity of all trace species. The comparison between observed and calculated OH reactivity showed that the calculated OH reactivity is 29.5% less than the observed value, implying the existence of missing OH sinks, most likely linked to the oxidation products of biogenic species. Few years later (2014), Ramasamy et al. (2016) reported similar average OH reactivity in another coniferous forest located in Wakayama prefecture, Japan, during summer. Half of the forest consisted of coniferous trees, already known as strong monoterpene emitters, emitting especially high concentrations of α -pinene. Contrary to the BEACHON-SRM08 campaign, total OH reactivity varied diurnally with light and temperature and reached a maximum at noon-time, after which it decreased. Monoterpenes were the major contributors to total OH reactivity, accounting for 23.7% of the total OH reactivity, with α -pinene accounting the most. Average missing OH reactivity was similar to that reported in the US, with higher levels when the site was influenced by transported pollution events. Correlation of missing OH reactivity with temperature and light suggested that the missing fraction was linked to unmeasured primary and secondary species. However, reasonable correlations of missing OH reactivity with NO and O₃, suggested that anthropogenic sources and secondary products formed from oxidation of primary VOCs could also be responsible for the missing OH reactivity. **Figure 1.8** summarizes the studies conducted in forested areas between 2004 and 2016.

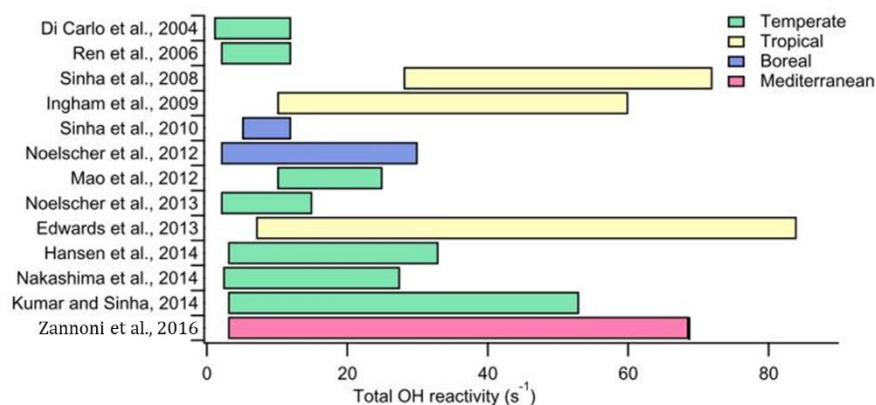


Figure 1.8: Total OH reactivity results from published experiments conducted worldwide at forested sites. Bars refer to the ranges observed between the minimum (often corresponding to the instrumental LOD) and the maximum values published (Adopted from Zannoni et al., 2016).

1.5.2. Rural and suburban areas

Unlike remote sites, suburban and surrounding areas are subjected to both anthropogenic and biogenic emissions, which should be of particular interest, seen the contribution of BVOCs in O₃ and SOA formation, as shown previously in paragraph 1.3.3. In these sites, OH reactivity can be extremely varying and dominated by anthropogenic or biogenic species, depending on the site location, surroundings, origins of air masses and on the time of the day. Indeed, OH reactivity showed a slight diurnal variation with higher values during daytime, lower values at night and an average of 5.6 s⁻¹, during the PMTACS–NY campaign. The experiment was conducted within the canopy of a deciduous forest (Ren et al., 2006), that is routinely in the path of regional air masses, influenced by urban emissions. This observation is in lower range of OH reactivity generally observed in forest ecosystems and is comparable to OH reactivity reported by Ren et al. (2005), in a site surrounded by agricultural lands and under the influence of anthropogenic pollutants. OH reactivity, with an average of 6.1 s⁻¹, showed little diurnal variation at this site and was dominated by CO, NO₂ and alkenes. However, during the PRIDE- PRD campaign (summer 2006), OH reactivity measured in a regional background site also surrounded by farmland (peanuts, lichees, trees), exhibited a diurnal variation with a minimum mean value of 20 s⁻¹ at local noon and a maximum mean value of 50 s⁻¹ at daybreak. The reactivity explained by measured trace gases was dominated by anthropogenic pollutants (e.g., CO, NO_x, light alkenes and aromatic hydrocarbons) at night,

while it was strongly influenced by local, biogenic emissions of isoprene during the day. While measured and calculated OH reactivity agreed well (within 10%) in the PMTACS–NY campaign, they revealed a missing reactivity of about a factor of 2 at day and night in the PRIDE-PRD campaign. The application of a Box model suggested that missing reactivity is due to unmeasured, secondary chemistry products (mainly aldehydes and ketones), photochemically formed by hydrocarbons oxidation.

1.5.3. Missing OH Reactivity

Most studied environments, especially forested areas, highlighted a missing fraction of OH reactivity, meaning that not all local OH relevant reactive species have been quantified. However, it is not possible to compare the missing fraction from site to another, since it is dependent on the amount of considered compounds in OH reactivity calculations. As mentioned before, the missing reactivity could be associated with unmeasured and unidentified primary emissions, as well as unmeasured or unknown secondary products.

Many approaches were adopted, aiming to investigate the origins of this missing fraction. Factor analysis is one approach, trying to correlate the missing OH reactivity to certain factors related to emissions or reactions. The exponential relationship between the missing OH reactivity and temperature can be investigated using: $E_{(T)} = E_{(293)} \exp[\beta(T-293)]$ (Di Carlo et al., 2004), generally used to describe monoterpenes emissions. Depending on the obtained β value, the missing fraction was linked to primary or secondary compounds. However, this factor should be interpreted carefully, seen that OH reactivity and the missing OH reactivity could be also affected by other parameters, like atmospheric turbulence. Some compounds were also used as tracers to elucidate the origin of missing OH reactivity (O_3 , HCHO, ...). Model simulation has showed to be a reasonable approach to diagnosing missing reactivity, especially with simultaneous high time- resolution HO_x and trace gas measurements (Yang et al., 2016).

1.6. Thesis objectives

In this chapter, biogenic VOCs with their various sources, different amounts, diverse chemical nature and multitude of factors influencing their emissions were introduced. This overview showed that the main studied ecosystems worldwide were forests and the main investigated compounds were isoprene, followed by monoterpenes. However, reviews and inventories highlighted the importance of croplands in land cover/ land use, especially on the

Europe scale, where BVOCs from agriculture can account for about 27%, with a significant contribution of OVOCs. Second, the reactivity of BVOCs with the different atmospheric oxidants was evoked. Indeed, once emitted in the atmosphere, VOCs are subject to physical and photochemical processes, that control their tropospheric lifetimes. These processes are dominated by the reaction with hydroxyl radical during day-time, which is considered the most powerful oxidant in the troposphere. In addition to their wide chemical diversity, BVOCs exhibit a wide range of reactivity towards OH, especially monoterpenes, which make their investigation and their speciation of great interest. In this part, total OH reactivity is introduced as a powerful tool to evaluate the loading in reactive species in the atmosphere and to estimate the presence or not of unidentified or undetected reactive species, that can play a more or less important role in tropospheric chemistry. The role of BVOCs in secondary pollutants formation was also presented, highlighting their direct or indirect impact on health, air quality and climate change. The next part, was dedicated to analytical techniques in BVOCs and OH reactivity measurements, with some recent improvements in monoterpenes chemical speciation with a relatively high time resolution, using Fast-GC/ PTR-MS systems. Finally, an overview on OH reactivity and respective missing fractions was presented. Results from different studies were compared. This overview, allowed us to see the variability of OH reactivity between ecosystems, with different hours of the day, different seasons, different canopy heights. The presented studies highlighted also the importance of air mass origins and the role played by the atmospheric boundary layer. A few studies were conducted near agricultural lands and two were found to be performed from dynamic chambers, among which one focused on measuring OH reactivity emission rates.

Thus, the scientific questions that this thesis addresses:

- **Characterization of BVOCs and their OH reactivity inside and above the canopy in a monoterpenes-dominated pine forest using the comparative reactivity method**

Temperate maritime pine forest in the Landes region is known as an important emitter of monoterpenes, especially during the hot season. Previous studies in this forest, studied the role played by monoterpenes in new particle formation episodes, highlighting a potential substantial chemistry on this site. In this context, OH reactivity was suggested to be part of the LANDEX campaign experiments, as a tool to help assessing, the loading of reactive compounds inside and above the forest; to evaluate whether the composition inside and above the forest is

completely determined and to better constrain atmospheric processes within a forest by using both the OH reactivity and missing reactivity.

- **Characterization of BVOCs and their OH reactivity from a rapeseed crop dynamic chamber, during the blooming season, using the comparative reactivity method**

Despite that agricultural lands can cover significant areas, we did not find a lot of studies investigating OH reactivity near croplands. However, the proximity of most croplands to urban sites and the predicted increase in croplands with the increase in human population, draws attention to the characterization of VOCs emissions and their OH reactivity from crops, especially that, BVOCs can react with abiotic compounds, leading to the formation of secondary pollutants (smog, ...). Therefore, it was chosen to conduct a study in a rapeseed field during the blooming season, to characterize the contribution of a single crop and a typical cropland to OH reactivity.

- **High-time resolution of monoterpenes chemical speciation using a FastGC/ PTR-QuadMS system, previously tested and optimized in the laboratory**

One of the limitations of current analytical techniques, which data is used to calculate an expected OH reactivity and compare it with the measured one in order to estimate the missing fraction, is the lack of monoterpenes chemical speciation with a high time resolution. In some ecosystems, like the one investigated during the LANDEX campaign, monoterpenes can represent the main emitted family of compounds. Individual monoterpenes concentrations can vary quickly and their reactivity towards atmospheric oxidants are pretty variable. In this context, a technical development was made, in collaboration with IONICON, to couple a PTR-QuadMS and a FastGC, in order to provide a low cost system (compared to the commercialized PTR-ToF-MS/ FastGC), allowing a relatively quick separation of monoterpenes from different compartments of a green oak forest. It allowed us to investigate the behavior of different monoterpenes in respect to more or less fast changes in abiotic external factors, such as temperature and light.

The thesis is therefore organized as followed:

Chapter 2 presents material and methods used during the thesis, focusing on the PTR-MS instrument and the two associated analytical systems (FastGC/PTR-MS and OH reactivity measurement by CRM).

Chapters 3, 4 and 5 include the results obtained on:

- Variability of hydroxyl radical (OH) reactivity in the Landes maritime pine forest: results from the LANDEX campaign 2017
- Characterization of total OH reactivity in a rapeseed field: Results from the COV³ER experiment in April 2017.
- Monoterpenes chemical speciation with high time resolution using a FastGC/PTR-MS: Results from the COV³ER experiment on *Quercus ilex* during summer 2018.

The manuscript ends with a conclusion and some perspectives about potential future research.

2. Experimental

Introduction Chapitre 2

Durant la thèse, trois systèmes analytiques ont été principalement utilisés : le spectromètre de masse à réaction de transfert de proton (Proton-Transfer- Reaction Mass Spectrometer), la chromatographie en phase gazeuse rapide (Fast Gas Chromatography « FastGC ») et la méthode de réactivité comparative (Comparative Reactivity Method « CRM »).

Dans ce chapitre, le PTR-MS est décrit en premier, comme étant le détecteur couplé à la FastGC et à la CRM. Ces deux systèmes sont ensuite présentés en terme de principe de fonctionnement, de conditions expérimentales et de déploiement au laboratoire et sur le terrain.

- Le PTR-MS

Le PTR-MS est une technique qui détecte les composés gazeux suite à leur ionisation chimique par des réactions de transfert de protons. Vu ses différents avantages, notamment les faibles taux de fragmentation, sa grande sensibilité (ordre du pptv) et sa sélectivité, le PTR-MS est largement déployé dans des études en chimie de l'atmosphère, chimie environnementale, émissions des plantes, sciences alimentaire et médicale.

Le système consiste en trois parties principales : (1) une source d'ions H_3O^+ , (2) une chambre de réaction et (3) un détecteur (dans notre cas un quadrupole). Brièvement, les ions primaires, le plus souvent H_3O^+ , sont produits dans une décharge cathodique creuse, et injectés dans la chambre de réaction. A ce niveau, ils entrent en collision avec les molécules gazeuses présentes dans l'échantillon injecté, ce qui induit des réactions de transfert de protons entre les ions primaires et les composés organiques ayant une affinité protonique supérieure à celle de l'eau (691 ± 3 kJ/mol). Les COVs protonés arrivent finalement au niveau du spectromètre de masse. Selon le ratio masse/ charge, les ions voyagent tout au long du quadrupole et gagnent le multiplicateur d'ions secondaires. A ce point, leur signal est transformé en électrons, puis amplifié sous forme de courant, connu comme « compte par seconde ».

Le PTR-MS est largement utilisé en sciences atmosphériques : pour les mesures des concentrations et des flux de COVs, comme détecteur couplé à la CRM et la FastGC, ainsi que pour la détermination de la fraction organique dans les particules atmosphériques.

- **FastGC/PTR-MS**

Dans le but d'effectuer la spéciation chimique des monoterpènes avec une résolution temporelle fine, une nouvelle version d'un prototype de FastGC (IONICON) a été couplée au PTR-QuadMS disponible dans notre laboratoire. En effet, la "Fast-GC" est une unité supplémentaire pouvant être ajoutée entre le système d'échantillonnage et la chambre de réaction d'un PTR-MS dans le but d'effectuer une pré-séparation des composés isomères et de réaliser par la suite une analyse structurale dans un temps rapide.

L'ensemble de la « FastGC » consiste en : (1) une colonne capillaire, apolaire de type MXT-1, de 10 m de longueur avec un D.I de 0.53 mm et une phase active de 0.25 µm d'épaisseur ; (2) un système de chauffage et de ventilation contrôlé automatiquement pour lancer la rampe de température, puis l'arrêter à un certain niveau en démarrant les ventilateurs ; (3) une vanne 10 voies pour effectuer des transitions rapides entre la mesure en mode PTR-MS et en mode FastGC/ PTR-MS. Au cours de la mesure directe par PTR-MS, une boucle est rincée en continu par l'échantillon alors que la colonne est rincée dans le sens inverse par le gaz vecteur pour la nettoyer ; (4) une bouteille d'Hélium (5.2) utilisé comme gaz vecteur ; (5) une bouteille d'azote (5.0) utilisé comme gaz de compensation. Les différences entre une « FastGC » et une GC classique sont : d'une part que la colonne capillaire est plus courte avec une phase active plus fine, d'autre part que la rampe de température est rapide ($>1^{\circ}\text{C/s}$). Par ailleurs l'injection de l'échantillon est également rapide, ce qui entraîne une moins bonne sensibilité du détecteur. Nous avons estimé la limite de détection (LOD) à approximativement 500 pptv. En revanche la résolution temporelle est meilleure qu'une GC classique, puisque nous pouvions descendre à 10 min.

- **La CRM/PTR-MS**

La CRM consiste à mesurer la réactivité OH (perte totale des radicaux OH suite à leur réaction avec les espèces réactives dans l'atmosphère) en suivant la concentration d'une molécule de référence, dans notre cas le pyrrole, dont la constante cinétique est connue avec le radical OH. Le choix de cette molécule est basé sur le fait, qu'elle est très peu présente en air ambiant et qu'elle peut être facilement détectée par PTR-MS sous la masse m/z 68. Ainsi, le système est principalement constitué (1) d'une cellule de réaction et (2) d'un détecteur, dans notre cas le PTR-MS.

La mesure par CRM consiste en quatre étapes analytiques : Dans un premier temps, le pyrrole est dilué dans l'air zéro et introduit dans la cellule de réaction avec l'azote sec. Sa concentration est détectée par le PTR-MS, elle est notée C0. Ensuite, la lampe UV est allumée, entraînant la photolyse d'une fraction du pyrrole. Ainsi, la concentration notée C1 représente la concentration initiale de pyrrole disponible dans le réacteur après photolyse. La troisième étape consiste à remplacer l'azote sec par l'azote humide et l'air zéro sec par l'air zéro humide permettant de générer synthétiquement des radicaux OH par photolyse de la vapeur d'eau. Suite à sa réaction avec les radicaux OH, la concentration du pyrrole mesurée diminue, elle est notée C2 et la différence entre C1 et C2 représente la quantité initiale de radicaux hydroxyles produits et complètement titrés dans le réacteur. Finalement, de l'air atmosphérique, chargé en espèces réactives est introduit dans la cellule. Ces espèces entrent en compétition avec le pyrrole pour les radicaux OH disponibles dans le réacteur, et comme la quantité de radicaux OH disponibles pour réagir avec le pyrrole, diminue, la concentration restante de pyrrole augmente et elle est notée C3. En comparant la concentration du pyrrole en sortie du réacteur *avec* (C3) et *sans* l'air ambiant (C2), on peut déterminer la réactivité à travers la relation suivante, dans laquelle k_{py} est la constante de réaction du pyrrole avec OH :

$$R_{air} = \frac{C3 - C2}{C1 - C3} \cdot k_{py} \cdot C1 \quad (\text{Sinha et al., 2008})$$

Le dispositif expérimental consiste en (1) un petit réacteur en verre dans lequel le pyrrole et l'air ambiant (ou les standards se mélangent) et réagissent avec les radicaux OH, (2) un PTR-MS (Proton Transfer Reaction – Mass Spectrometer) qui détecte le pyrrole dans l'air sortant du réacteur, (3) des contrôleurs de débit massique, et (4) deux bouteilles de gaz (azote et air synthétique).

Il est important de noter que les mesures par CRM peuvent être sujettes à des interférences pour lesquelles les corrections suivantes doivent être bien caractérisées et appliquées aux données brutes : (1) correction pour la différence d'humidité entre C2 et C3 ; (2) correction pour la déviation du pseudo-premier ordre ($[pyr] \gg [OH]$) ; (3) correction pour le recyclage des radicaux OH suite à la réaction entre HO₂ et NO en présence de fortes concentrations ambiantes de NO ; (4) correction pour la dilution de l'échantillon dans le réacteur.

In this chapter, the three main instruments deployed during this PhD are presented. The first part is about the Proton Transfer Reaction- Mass Spectrometer (PTR-MS), the detector used for VOCs and OH reactivity measurements. The second part presents the FastGC add-on for isomers pre-separation. And the last part is about the Comparative Reactivity Method (CRM), for OH reactivity measurements. Each sub-section includes a general description of the instrument, its operational principle as well as its implementation in laboratory and field work.

2.1. Proton Transfer Reaction-Mass Spectrometer (PTR- MS)

2.1.1. Instrumental set-up

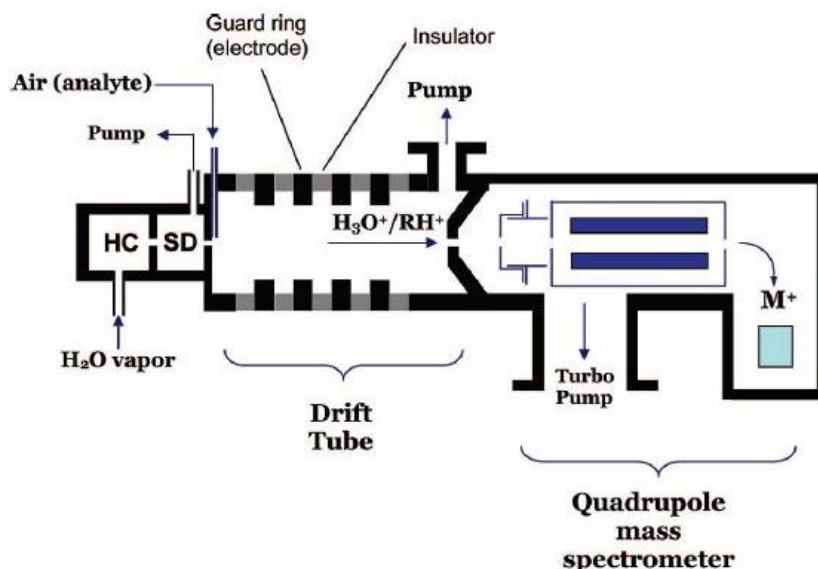


Figure 2.1: Simplified representation of a proton-transfer reaction mass spectrometer utilizing a quadrupole mass filter: HC = hollow cathode discharge source and SD = source drift region (Blake et al. 2009).

Proton-transfer-reaction mass spectrometry (PTR-MS) was developed by Professor Werner Lindinger and co-workers at the University of Innsbruck in Austria (Lindinger et al., 1998). The system works on the basic idea of using proton transfer reactions to induce chemical ionization of the vapors to be analyzed and monitored. Following its development and commercialization (Ionicon GmbH, Innsbruck, Austria), there has been considerable growth and exploitation of PTR-MS for trace gas monitoring in various chemical and physical environments and in particular for the detection of volatile organic compounds (VOCs). Areas

of application include atmospheric chemistry, environmental chemistry, plant and tree emissions and food and medical sciences. The main advantage of proton transfer chemical ionization is that in most cases it does not induce any significant fragmentation, and when it does only few fragments are produced. Together with the fast response times and high sensitivities, the PTR-MS allows very efficient analysis and monitoring of mixtures of VOCs. **Figure 2.1** gives a schematic drawing of the PTR-MS instrument. The set-up consists of (1) a discharge ion source to produce H_3O^+ ions, (2) a drift-tube reactor, in which the proton-transfer reactions between H_3O^+ and VOCs take place, and (3) a quadrupole mass spectrometer for the detection of reagent and product ions.

- (1) The ion source consists of a hollow-cathode discharge source where water vapor generates H^{2+} , H^+ and O^+ ions which further react with water molecules to form H_3O^+ with high efficiency (> 99.5%). Other reagent gases can be used for such scope, O_2 or O_2 together with N_2 for instance, can produce O^{2+} and NO^+ ions with slight less efficiency (90-95% and 95-99%, respectively). Typical count rates for H_3O^+ are 10^6 cps.
- (2) After production, the reagent ions enter via a transfer section the adjacent drift tube. The drift tube consists of a number of stainless steel rings that are separated by Teflon rings, which seal the vacuum and isolate the drift rings electrically. The sample to be analyzed is continuously injected in the drift tube via a sample line system with an adjustable flow between 50 and 1000 sccm and adjustable temperature between 40–150 °C. The pressures in the drift tube are maintained between 2.2 and 2.4 mbar. In the drift-tube, the reagent ions undergo many collisions with the molecules of the sample and proton- transfer- reactions occur between hydronium ions and VOCs or chemical ionization reactions of NO^+ and O^{2+} with VOCs, in the following way:



Proton affinities are commonly used to assess whether or not a proton transfer reaction is likely to be spontaneous. When H_3O^+ is used as reagent ion, molecules with a proton affinity larger than water (691 ± 3 kJ/mol) undergo exothermic hence spontaneous reactions. Due to their low proton affinities, the major components of air (i.e. O_2 , N_2 , CO_2 , O_3 , H_2O) and methane do not react with the primary ions in the drift tube. However, most VOCs, possessing a proton affinity higher than that of water are ionized in proton transfer reactions.

Many features of the PTR-MS drift-tube make it advantageous for trace gas analysis: (a) the short reaction time due to the use of a short drift tube with no need to dilute the sample, (b) the ability of measuring only trace molecules, (c) the soft ionization character of proton transfer reactions avoiding extensive fragmentation of ions, (d) the application of a homogeneously increased voltage to the rings of the drift tube generating a homogeneous electric field, responsible for the transport of ions along the tube and eliminating the need of a large pump. All these characteristics make PTR-MS a unique instrument with a high detection sensitivity in a relatively compact size. Standard electric field applied, expressed as E/N are 120-140 Td (1 Td= 10^{-17} V cm²). Changing E/N and thus the mean collision energy in the drift tube allows to distinguish between product ions based on different fragmentation pathways (for instance between methacrolein and methyl vinyl ketone, the main oxidation products of isoprene which are usually measured together at the protonated mass m/z 71). Finally, the outgoing product VOCs ions enter, via a specially designed transfer lens system, the mass spectrometer.

- (3) The ion detection system can be either a quadrupole (QMS) or a time of flight mass spectrometer (TOF-MS). Our PTR-MS is equipped with a commercial quadrupole mass filter (Balzers QMG 421) and a SEM (secondary electron multiplier) for ion pulse counting detection. The ions exiting the drift tube are extracted into the quadrupole through a sampling orifice while the buffer is pumped away. A quadrupole is composed of four parallel metallic rods between which is applied a tension generating an electron field that forces the ions to run under a different oscillating trajectory according to their mass-to-charge (m/z) ratio. Ions with a selected m/z will travel along the quadrupole and reach the SEM where their signal will be converted into electrons and amplified in a current expressed as counts per seconds. In a TOF-MS, ions are accelerated to the same kinetic energy by an applied electric field. The detection is based on the time that molecules take in flying a known distance. In this manner, molecules of different molecular masses hit the detector at different times. Thus, it is possible to distinguish different peaks within multiplets and take into account the decimals of the molecular masses to identify compounds. A full spectrum can be measured at once, every 0.1 s, corresponding to 400 mass peaks and 400 empirical formulas (Blake et al., 2009; de Gouw & Warneke, 2007; Portillo-estrada, 2014).

2.1.2. Compounds sensitivity and volume mixing ratio

A Calibration of the PTR-MS for different molecules is conducted by measuring the response in normalized counts per second (ncps) of a standard gas molecule with a certified concentration. For VOCs measurements, the calibration is usually performed at different steps with variable concentrations (typical range for calibrations is 0-20 ppbv) and repeated for different relative humidity values. For one-month field campaigns, two calibrations, one at the beginning and one at the end of the campaign, are usually sufficient. Linear least squares fits of the ncps measured versus the ppbv injected for a specific molecule are used to determine the detector sensitivity to such molecule. Normalized sensitivities ($Snorm$) and count rates ($I(RH_i^+)$) are expressed as follows:

$$Snorm = \frac{I(RH_i^+)norm}{VMR_{standar}} \quad (2.1)$$

$$I(RH_i^+)norm = 10^6 \times \left(\frac{I(RH_i^+)norm}{\frac{m}{z}21 \times 500 + \frac{m}{z}37} - \frac{I(RH_i^+)zero}{\frac{m}{z}21 zero \times 500 + \frac{m}{z}37zero} \right) \quad (2.2)$$

where m/z 21 and m/z 37 represent, the reagent ion (H_3O^+) and the first water cluster ($H_3O^+(H_2O)$).

Volume mixing ratios can be alternatively calculated through the transmission coefficients approach, in particular when the calibration for a specific molecule is not achievable:

$$VMR = \frac{I(RH_i^+)norm}{Snorm} \quad (2.3)$$

$$I(RH_i^+)norm = 10^6 \times \left(\frac{I(RH_i^+)norm}{\frac{m}{z}21 \times 500 + \frac{m}{z}37} - \frac{I(RH_i^+)zero}{\frac{m}{z}21 zero \times 500 + \frac{m}{z}37zero} \right) \quad (2.4)$$

The accuracy of the results is lower compared to the calibration with a gas standard, due to uncertainty in the reactions rate coefficients and relative transmission curve (de Gouw & Warneke, 2007; Taipale et al., 2008). A measure of the concentration of molecules when only zero air is introduced inside the PTR-MS is useful to derive the background level for each species, which is therefore subtracted from the measured concentration to obtain the actual concentration level. The limit of detection (LOD) for each compound is usually calculated as 3σ its background value.

2.1.3. PTR-MS in atmospheric sciences

A major application of PTR-MS technology has been in the area of atmospheric sciences. As a relatively compact and robust instrumental technique, PTR-MS has been deployed on a range of atmospheric measurement platforms including ground-based measurement stations, vehicles, ships, research aircraft and operational aircraft. Seen its advantageous features, in terms of sensitivity and selectivity, PTR-MS is widely used to measure atmospheric mixing ratio of VOCs. These datasets are then integrated to constrain chemical transport models and climate models as well as to predict air pollution and climate effects. Furthermore, VOCs are subject to many physical and chemical processes affecting their atmospheric mixing ratios. The direct measure of the flux of a reactive species helps to unravel surface exchange from other processes. Eddy covariance is the most direct method to measure surface fluxes. This technique relies on atmospheric turbulence measurements, which require sampling at high temporal frequency, 10 Hz. PTR-MS is the suitable technique since its higher temporal resolution permits to conduct real-time eddy covariance fluxes.

PTR-MS is often deployed as a detector in OH reactivity measurements using the Comparative Reactivity Method. In this method, one reference molecule (pyrrole) is monitored unambiguously during all the experimental steps. Its robustness over time and its high sensitivity makes PTR-MS favorable for OH reactivity measurements. Additionally, the same instrument can be used to conduct both ambient mixing ratios and OH reactivity measurements (Kumar and Sinha, 2014).

PTR-MS was combined to thermal desorption units in order to speciate the organic fraction in atmospheric particles (Holzinger et al., 2010). It was also coupled to a stripping cell allowing to determine the liquid–gas partition coefficients (HLC) of volatile organic compounds (VOCs) in water–air systems (Karl et al., 2003).

Finally, PTR-MS was used with a gas chromatography (GC-PTR-MS). The system showed to be a useful approach in identifying VOCs contributing to different masses. However, adding the GC, slowed the measurement speed to that of GC, allowing only to get snapshots, aiding in species identification. Therefore, a FastGC module was recently introduced by Ionicon Analytik. However, the detection limit was relatively high (1.2 ppbv for monoterpenes experiments). No application in ambient environments has been reported (Yuan et al., 2017).

2.2. Fast Gas Chromatography/ Proton-Transfer-Reaction Mass Spectrometer

Aiming to execute a rapid chromatographic separation of monoterpenes in a green oak forest, with fast spectral runs (tens of seconds), a FastGC add-on (a prototype version, IONICON, Analytik, Innsbruck, Austria), which is a modification of the setup used by Romano et al. (2014) and Ruzsanyi et al. (2013), was coupled to a PTR-QuadMS (IONICON, Analytik, Innsbruck, Austria). This work was done in collaboration with Felix Piel (early stage researcher at Ionicon), in the frame of the IMPACT network. The FastGC was available for two months, prior to the planned field experiment in order to: (i) combine the FastGC to the PTR-QuadMS and (ii) optimize the operational parameters for a rapid and satisfying separation of the main monoterpenes. A description of the system, its operational principle as well as results from laboratory experiments are presented in this section.

2.2.1. Instrument set-up and operational concept

The deployed set-up (**Figure 2.2**) consists of a 10 m, nonpolar MXT-1 column (Restek, USA) with an I.D. of 0.53 mm and an active phase of 0.25 μm (dimethyl polysiloxane). It also includes a 10-port passivated valve (VICI AG, Switzerland), a magnetic gas valve, two flow controllers for the carrier gas and the makeup gas and a heating/ cooling controller. All parts of the inlet system are installed within the oven that houses the drift tube to prevent cold spots. This revised set-up enabled constant filling of the sample loop and constant back-flushing of the capillary column with the carrier gas. The pre-separation using the FastGC is achieved by resistive heating of the column, which allows for fast heating rates (up to 30 K/s). This resistive heating was done via a laboratory power supply (PSI 5000 A, EPS Stromversorgung GmbH, Germany), that was controlled by a microcontroller (Arduino UNO ref3, Arduino, USA). In addition, since the current is run directly through the column, cooling rates are also very high, seen the low thermal mass of the heating module. The FastGC mode can be activated when required, without affecting the normal PTR-MS operation.

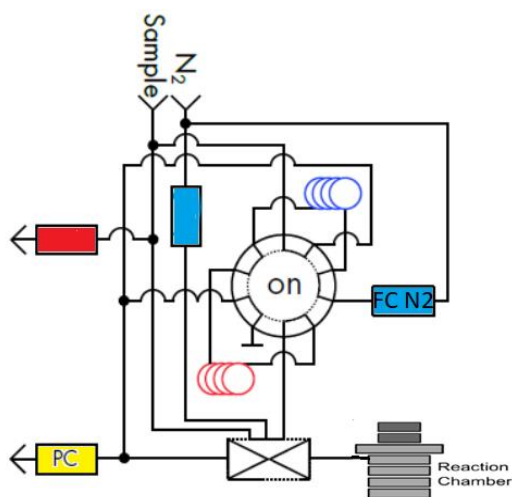


Figure 2.2: Set-up of the fastGC add-on, including the capillary column, the sample loop, the 10-port valve and the PTR-MS drift-tube.

During real-time measurements, the sample loop is constantly flushed. At this time, the sampling unit of the FastGC is isolated from the column which is continuously back flushed with the carrier gas. When switching to FastGC mode, it goes as follows: a first step consists of filling the sample loop with the air sample. Second, the valve is switched so the sample loop is connected in series with the GC column, allowing the injection of the air sample that is pushed through the column by a constant flow of the carrier gas. Finally, compounds are separated in the column and they elute at different times, heading to the PTR-MS to be analyzed. The efficiency of the separation and the quality of the resulting chromatograms can be influenced by operational parameters, such as temperature and carrier gas flow rates, which can play a role on the retention times as well as on the peaks shapes. For this reason, extensive laboratory experiments were performed, in order to optimize the operational parameters, more specifically for monoterpenes separation. Indeed, these experiments aimed to characterize the system prior to its deployment in a forest ecosystem to monitor the variability of individual monoterpenes from different compartments of a monoterpenes- dominated forest.

2.2.2. System characterization

2.2.2.1. Effect of temperature

A first set of experiments aimed to study the effect of the temperature parameter on the peak shape as well as on each compound's retention time. Samples were injected from the headspace of individual monoterpenes solutions. N₂ was used as carrier and makeup gas at this stage, with a flow of 10 sccm and 25 sccm, respectively. *m/z* 21, *m/z* 32 and *m/z* 137, corresponding to H₃O⁺, O₂ and monoterpenes (C₁₀H₁₆) were monitored during FastGC runs, with the O₂ peak indicating the sample injection time (*t*₀).

First, α -pinene, myrcene, Δ -3-carene, limonene and terpinene samples were injected individually. Each injection was repeated several times with the application of a temperature ramp (Tramp I), obtained by applying a gradient voltage, or in isothermal conditions. In this case, one voltage was applied ranging between 35 and 60V. Results showed that it is better to work with a temperature ramp, seen the better peak resolution. Whereas, isothermal conditions resulted in faster GC runs at the expenses of the peak quality. Indeed, and as shown for α -pinene (**Figure 2.3**), working under a constant voltage of 60V, led to a larger and less intense peak. This was the case for some other monoterpenes too. These tests allowed us also to get a first idea about each compound's retention time, that changed as function of the temperature conditions.

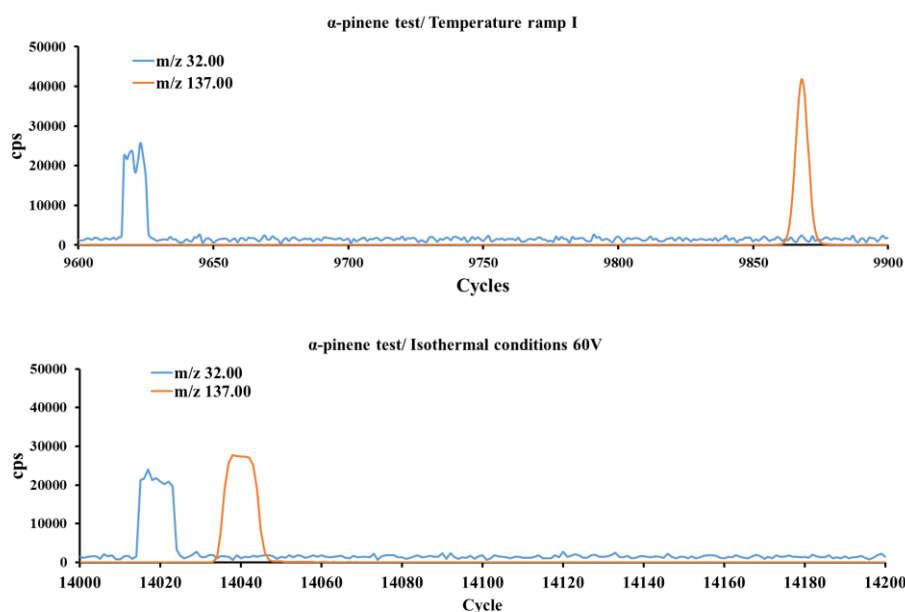


Figure 2.3: FastGC/ PTR-MS chromatograms after the injection of an α -pinene sample. *m/z* 32 and *m/z* 137 refer to O₂ and α -pinene, respectively.

Afterwards, a mixture of all mentioned monoterpenes was prepared and tests were also done under a constant or a varying temperature (**Table 2.1**). Satisfying peak resolution and separation were obtained with Tramp I with a total GC run of ≈ 100 s. Under isothermal conditions (35 V), the GC run duration was close to the one seen with Tramp I, however terpinene exhibited a larger peak. Therefore, it was chosen to work with a temperature program.

Table 2.1: Retention times of 5 monoterpenes resulting from operating the FastGC/PTR-MS system with a temperature program (TrampI) or under a constant temperature (constant voltage of 35 V).

Mixture (headspace)	Heating Conditions	tr (s)
a-pinene	Temp ramp I (2 tests)	Peak 1: 79- 81s
Myrcene		Peak 2: 87- 88s
Δ -3-carene		Peak 3: 90- 92s
Limonene		Peak 4: 92- 94s
Terpinene		Peak 5: 97- 99s
a-pinene	Isothermal (1 test)	Peak 1: 51s
Myrcene		Peak 2: 66s
Δ -3-carene		Peak 3: 70s
Limonene		Peak 4: 80s
Terpinene		Peak 5: 90s

2.2.2.2. Effect of the carrier gas flow rate

In a second set of experiments, the effect of different carrier gas flows was tested. For the same PTR-MS operational conditions, several N₂ flows were injected ranging between 5 and 15 sccm. At this stage another ramp (Tramp 2) was adopted. **Figure 2.4**, shows two chromatograms obtained when the same gas mixture of the five monoterpenes was injected. With the same sample dilution flows, we noticed a decrease in the signal intensity, so these flows were changed between the first (**Figure 2.4.a**) and the final experiment (**Figure 2.4.b**), which explains the different signal intensities. It is clear from the presented results, that a better separation is obtained when operating with relatively lower carrier gas flow rates, however, this means that the total GC run duration is longer. Thus, it is important to make a compromise between a good separation, a good peak resolution and a fast GC run, to be able at the end to characterize individual isomers variability with a fine time resolution. Setting the carrier gas to 5 sccm resulted in a total duration of 133 s, which was still satisfying in terms of higher frequency of measurements, compared to classical GC techniques.

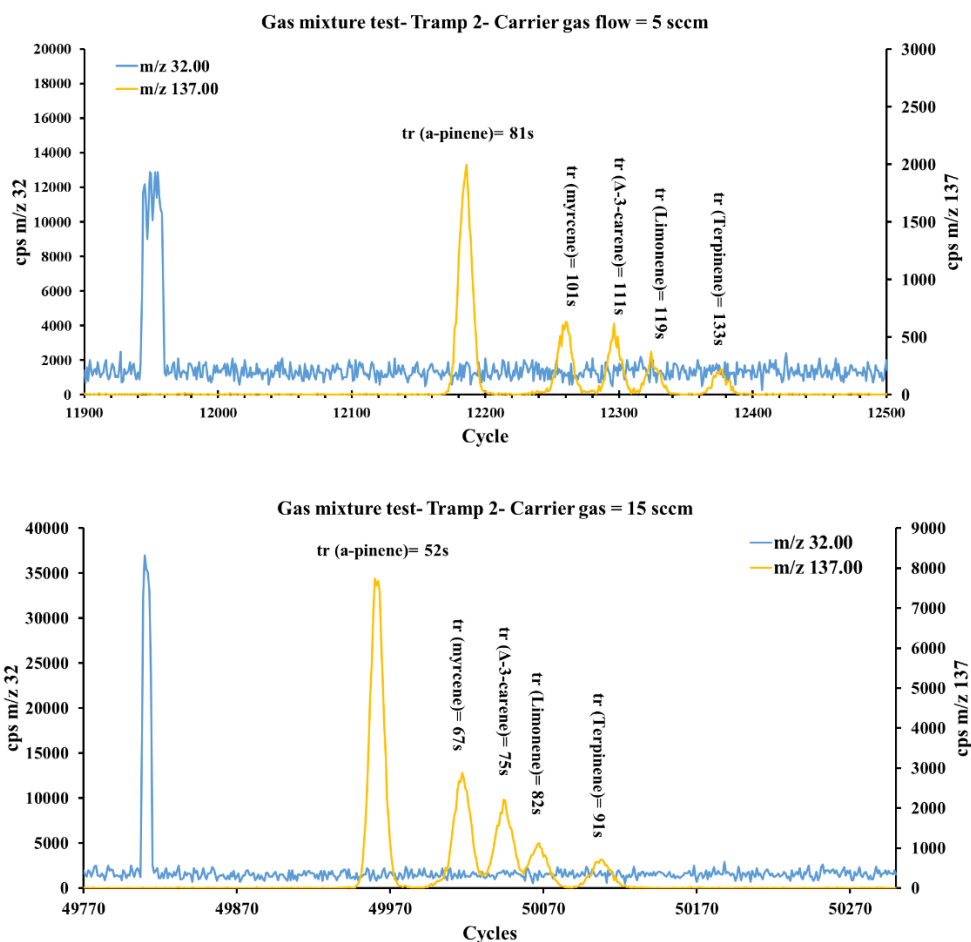


Figure 2.4: Comparison between two chromatograms of the same monoterpenes gas mixture, injected in the same conditions but with two different carrier gas flow rates: the upper graph (a) corresponds to the experiment with a flow rate of 5 sccm and the lower graph (b), to the experiment with a carrier gas flow rate of 15 sccm.

2.2.2.3. Different combinations of temperature programs and carrier gas flow rates

Since temperature and carrier gas flows were the main operational parameters that could be tuned for a better separation and a short analysis time, several combinations of these two parameters were tested. All temperature ramps/ carrier gas flow rates (N_2) tested combinations are summarized in **Table 2.2**. It should be noted that, meanwhile, monoterpenes were monitored under m/z 81 (fragment of monoterpenes) instead of m/z 137, seen the PTR-MS higher sensitivity on this m/z . Among tested combinations, Tramp 2.6 with a N_2 flow rate of 3 sccm exhibited a satisfying peak resolution and an acceptable analysis duration of 157s, as shown in **Figure 2.5.a**.

Table 2.2: Summary of all the temperature conditions (T °C) and carrier gas (N₂) flow rates.

	Test num	T conditions	Ti (°C)	Carrier gas flow (mL min ⁻¹)	
Serie 1	1	T ramp 1	35	10	
	3	T ramp 2	50	10	
	4	T ramp 2	48	8	
	5	T ramp 2	—	5	
	6	T ramp 2	48	5	
	7	T ramp 2	48	15	
	8	T ramp 3	63	5	
	9	T ramp I		5	
Serie 2	2	T ramp I	30	5	
	3	T ramp I	28	15 than 5	
	4	T ramp I	30	15	
	5	T ramp I	32	15 than 5	
	6	T ramp 4		5	
	7	T ramp 2	41	5	
	8	T ramp 5	41.6	5	
	9	T ramp 5	44.3	8	
	10	T ramp 6	44.4	8	
	11	T ramp 7	41.6	8	
	Serie 3	1	T ramp 2	37.7	8
2		T ramp 2	38.8	5	
3		T ramp 2	40.6	10	
4		T ramp 2	41	3	
5		T ramp 6	45	3	
6		T ramp 6	45.5	2	
7		T ramp 6	45.4	5	
8		T ramp 7	46.4	5	
9		T ramp 7	47.1	3	
Serie 4	2	T ramp 8	39.1	3	
	3	T ramp 9	42	3	
	4	T ramp 9	43.5	15 than 3	
	5	T ramp 10	47.7	3	
	6	T ramp 10	51.3	5	
	7	Isothermal 45V	53.8	3	
	8	Isothermal 45V	49.2	5	
	9	T ramp 9'	47.5	5	
	10	T ramp 9'	46.2	3	
	12	T ramp 2.1	40.6	3	
	13	T ramp 2.2	42.7	3	
	14	T ramp 2.3	44.7	3	
	15	T ramp 2.4	34.1	3	
	16	T ramp 2.5	34.1	3	
		17	T ramp 2.6	31	3

2.2.2.4. Effect of the carrier gas

For capillary gas chromatographic analyses, nitrogen, helium and hydrogen are the most commonly used carrier gases. The selection and linear velocity of the carrier gas are known to affect the resolution as well as retention times. Helium is generally used since it provides good separations, is inert, and is safe to use. However, it remains more expensive than the other two options. This said, a test was performed introducing α -pinene from a commercial standard (10

ppmv). The standard was diluted with zero air prior to injection. Similar conditions were adopted as the experiment of **Figure 2.5.a** with N₂ as carrier gas. Comparing both chromatographs, the α -pinene peak appears earlier when using He as carrier gas. This is expected seen helium's higher velocity in the temperature range of 0- 300°C, compared to N₂.

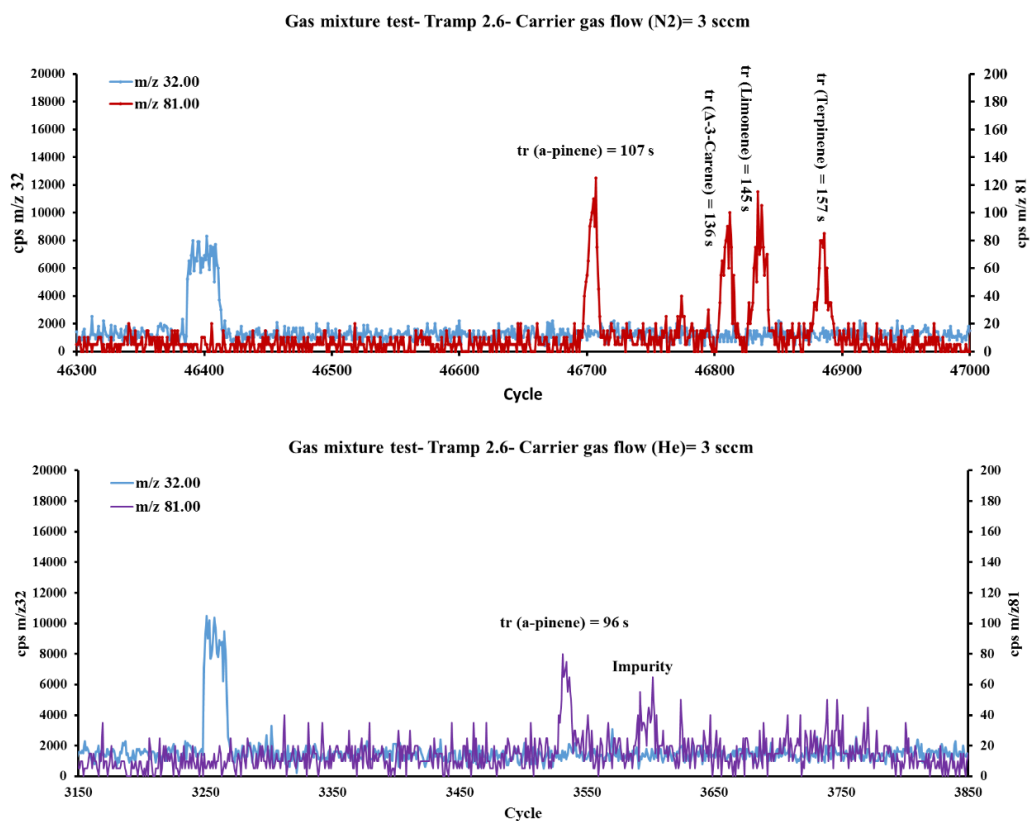


Figure 2.5: Chromatograms of a) in-house made mixture of monoterpenes under optimized Tramp and carrier gas flow rate, using N₂ as carrier gas and b) an α -pinene standard injected under the same optimized conditions with He as carrier gas.

Based on these tests, He was chosen as carrier gas with a flow rate of 3 sccm and T ramp 2.6 was adopted for field measurements with some slight changes.

2.2.3. Field deployment of the FastGC/PTR-MS

The FastGC/PTR-MS system was deployed during a three-weeks field campaign, within the ADEME- COV³ER project. The experiment site was a forest dominated by green oak trees, known for their important emissions of monoterpenes. Therefore, participating in this work was an opportunity to test the feasibility of the system in ambient and dynamic chamber

measurements, of a real environment. Indeed, and as mentioned before (Yuan et al., 2017), no FastGC/PTR-MS deployment was reported for ambient measurements.

Operational parameters during the campaign, were set as follows:

- He as carrier gas with a flow rate of 3 sccm
- N₂ as makeup gas with a flow rate of 15 sccm
- Temperature program “2.6”, selected after laboratory experiments, with slight modifications. More details about the experimental conditions on site can be found in chapter 5.
- The time resolution was about 10 min and the LOD around 500 pptv/monoterpene.

Measurements were performed in the incoming (10 min/1h) and the outgoing chambers air (50 min/1h), of four different branches, on four different oak trees. The main emitted monoterpenes in this ecosystem were detected and quantified: α -pinene, sabinene, β -pinene, myrcene and limonene(+ocimene), allowing to monitor their variability as function of the tree type and the external parameters (light and temperature).

2.3. The Comparative Reactivity Method (CRM)

2.3.1. General principle

The Comparative Reactivity Method (CRM) is an indirect method for measuring total OH reactivity in ambient air, by producing a competition between a reference molecule and reactive molecules in ambient air to react with synthetically generated OH radicals. It was first developed and described by Sinha et al. (2008). The system mainly consists of a glass reactor, equipped with a UV mercury lamp and connected to a detector which is generally a proton-transfer- reaction mass spectrometer (PTR-MS). Pyrrole (C₄H₅N), has often been used as the reference reagent molecule since it is not usually found in ambient air, it has a well-established reaction rate with OH radicals and it can be easily detected through the PTR-MS at protonated m/z 68 (C₄H₅NH⁺), without any major interferences.

The overall experiment is based on four main analytical steps, summarized in **Figure 2.6**:

- 1- Pyrrole is introduced into the glass reactor with dry nitrogen and dry air. Its concentration is monitored as C₀.

- 2- The UV mercury lamp is switched on. Pyrrole absorbs UV light and undergoes photolysis, its concentration decreases and is monitored as C1. C1 corresponds to the initial concentration of pyrrole inside the reactor after potential photolysis.
- 3- Dry nitrogen is replaced by wet nitrogen by passing the dry nitrogen flow through a bubbler containing milliQ water. With the UV mercury lamp on, hydroxyl radicals are artificially produced inside the reactor from the photolysis of water vapor. Pyrrole reacts with OH, its concentration decreases and it is monitored as C2.
- 4- Once C2 is acquired, zero air is replaced by ambient air and competitive OH reactions occur between pyrrole and ambient trace gases. This competition leads to an increase of the pyrrole concentration to C3.

Alternate switches between C2 and C3 make an accurate determination of the OH reactivity in ambient air possible. The higher the concentration and number of reactive species in ambient air, the broader is the difference between C2 and C3.

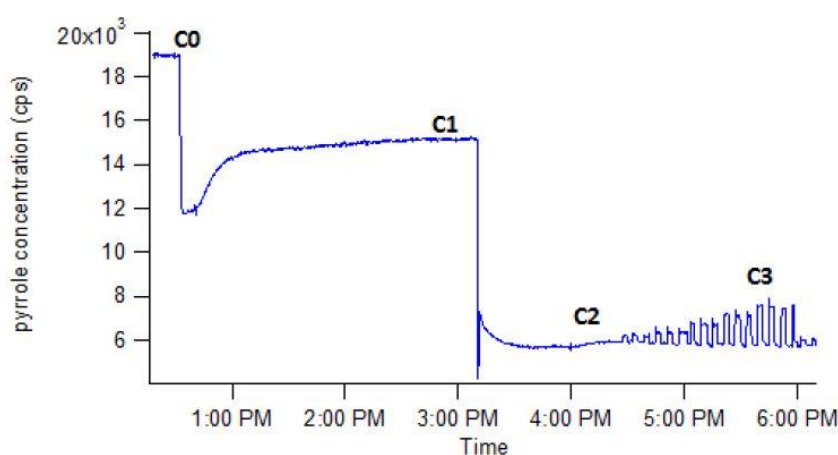


Figure 2.6: Pyrrole concentration monitored with the PTR-MS during a typical OH reactivity measurement with the CRM. C0, C1, C2 and C3 are the mixing ratios at the different stages of the experiment (Zannoni et al., 2015).

2.3.2. Derivation of the basic equation for CRM

An expression derived in terms of C1, corresponding to pyrrole initial concentration, C2 representing pyrrole's background concentration and C3 which is the concentration of pyrrole after competition with air reactants for the available OH, is used to determine OH reactivity from the experiment of **Figure 2.6**.

Considering that the hydroxyl radical is lost in a two component mixture, that consists of pyrrole and air, the equations describing the loss of OH are the following:



Thus, the rate expression is:

$$-\delta[\text{OH}]/dt = k_{\text{pyrrole}+\text{OH}} [\text{OH}][\text{pyrrole}] + k_{\text{OH}+\text{air}} [\text{OH}][\text{air}] \quad (2.5)$$

Where $k_{\text{pyrrole}+\text{OH}}$ is the rate coefficient of the reaction of pyrrole with OH, $k_{\text{air}+\text{OH}}$ is the rate coefficient of the reaction of all reactive components in air with OH and [air] is the summed concentration of all air components.

Seen that pyrrole concentration is higher than that of OH, it is assumed that pyrrole reacts with OH following pseudo-first order reaction kinetics. Hence, the reaction of OH with pyrrole is given by:

$$R_{\text{pyrrole}} = k_{\text{pyrrole}+\text{OH}} [\text{pyrrole}] \quad (2.6)$$

and the reaction of OH with air components is given by:

$$R_{\text{air}} = k_{\text{air}+\text{OH}} [\text{air}] \quad (2.7)$$

with $R_{\text{pyrrole}} + R_{\text{air}}$ being the total loss rate of OH.

Considering that all OH is lost in reaction with pyrrole and air, the change in pyrrole concentration ($C1 - C3$) is expressed as:

$$(C1 - C3) = \frac{R_{\text{pyrrole}}}{R_{\text{pyrrole}} + R_{\text{air}}} \cdot [\text{OH}] \quad (2.8)$$

Seen that $[\text{OH}] = (C1 - C2)$ and $[\text{pyrrole}] = C1$, equation 2.8 is equivalent to:

$$k_{\text{OH}} = \frac{C3 - C2}{C1 - C3} \cdot k_{\text{pyrrole}+\text{OH}} \cdot C1 \quad (2.9)$$

With k_{OH} being the reactivity in ambient air (R_{air}), and $C1$, $C2$, $C3$, the concentrations of pyrrole at different stages of the experiments. $k_{\text{pyrrole}+\text{OH}}$ rate constant of the reaction between pyrrole and OH = $(1.20 \pm 0.16) \times 10^{-10} \text{ cm}^3 \text{ molecule}^{-1} \text{ s}^{-1}$ (Atkinson, 1985). Since concentrations

have unit of molecules cm^{-3} and the rate constant of reaction of $\text{cm}^3 \text{ molecules}^{-1} \text{ s}^{-1}$, k_{OH} has the unit s^{-1} , corresponding to the inverse of the lifetime of the OH radicals.

2.3.3. Experimental set up

2.3.3.1. The glass reactor

Figure 2.7 represents a schematic of the glass flow reactor used in CRM experiments, along with all the inlets (arms A, B and C) and the outlets (arms D and E). The length and volume of the glass reactor are approximately 14 cm and 94 cm^3 , respectively. The typical flow rate achieved inside the reactor is around 300- 350 sccm.

Gas phase pyrrole, mixed with zero/ambient air, enters the reactor through arm A, at a constant flow. Its concentration is monitored in the air existing the reactor (arm E) with the PTR-MS. Dry or humidified N_2 enters the reactor from arm B, leaving the other two arms to the UV lamp (arm C) and to an exhaust pump (arm D).

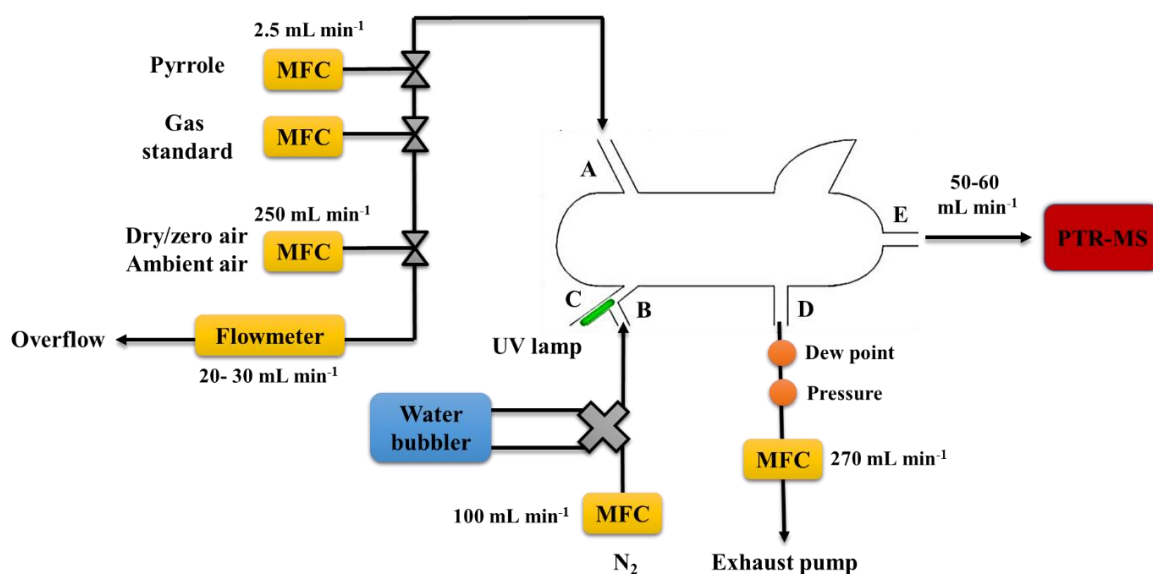


Figure 2.7: Schematic of the CRM instrument built at LSCE. Flow rates of the injected and the extracted gases are shown.

As mentioned before, during the first stages of CRM experiments (C0 and C1), dry nitrogen is introduced, when dry conditions are required in order to avoid OH radical's generation inside the reactor. Humidification of nitrogen is accomplished by passing gaseous nitrogen through a bubbler where ultrapure water is kept at room temperature. The lamp is a Pen ray spectral Hg

vapor lamp (LOT Oriel, France) which emits at 184.9 nm, 253.6 nm, 312.5 nm, 365 nm and 435.8 nm; water vapor absorbs at 184.9 nm and dissociates to form OH radicals.

The glass reactor design includes a "wood's horn" shape opposite to the arm where the lamp is placed. It aims to minimize reflection of the lamp and photochemical reactions along the length of the reactor. The total incoming flow rate is driven by the pump at the exhaust arm and the incoming flow at the detector. All the incoming flows (pyrrole+ air+ N₂), are set in a way that the total incoming flow is slightly higher (\approx 20- 30 sccm) than the total flow exiting the reactor (exhaust pump + detector). Mass flow controllers are used to set the flows, except for the flow entering the detector, it is regulated through an inlet valve. The overflow is continuously monitored with a flowmeter, through a T-shaped joint placed in line with the zero air gas line, before the mixing with pyrrole. Such opening is useful to monitor any change in flows occurring in the system and to prevent over-pressure building within the reactor, ensuring atmospheric pressure all times. Alternate measures of C2 and C3 (mixing pyrrole with zero air or ambient air, respectively) are achieved through a 4-way valve where zero air or ambient air is alternatively driven inside the reactor.

2.3.3.2. The detector: PTR-MS

In most cases, the proton transfer reaction mass spectrometer is deployed to monitor pyrrole's mixing ratio during the different stages of CRM experiments. PTR-MS has been extensively used in environmental sciences and atmospheric chemistry to monitor volatile organic compounds and it is described in details in section 2.1.

With a proton affinity (209.2 kcal mol⁻¹) higher than that of water (165.2 kcal mol⁻¹), pyrrole is detected, unambiguously, at mass 68 (C₄H₅NH⁺), without any fragment. This instrument offers also the advantage of tracking humidity changes in the air exiting the reactor, by monitoring masses 37 (first water cluster ion H₃O⁺. H₂O) and 55 (second water cluster ion H₃O⁺. (H₂O)₂). Other compounds can also be measured with the PTR-MS, such as methanol (*m/z* 33), acetaldehyde (*m/z* 45) and acetone (*m/z* 59), which can be useful to identify leakage or impurities- related issues within the instrument.

2.3.4. Method calibration

In order to verify that the CRM is reliably quantifying samples of known OH reactivity, tests with single and mixed hydrocarbons standards are performed. These tests consist of introducing

a gas standard at different concentrations, through the same line used to introduce ambient air inside the reactor. Hence, test gases are mixed with zero air before entering the system, then the mixture test gas and zero air mixes with pyrrole and enters the reactor (Arm A). Mixing can be achieved by using a simple tee-piece or a mixing vessel.

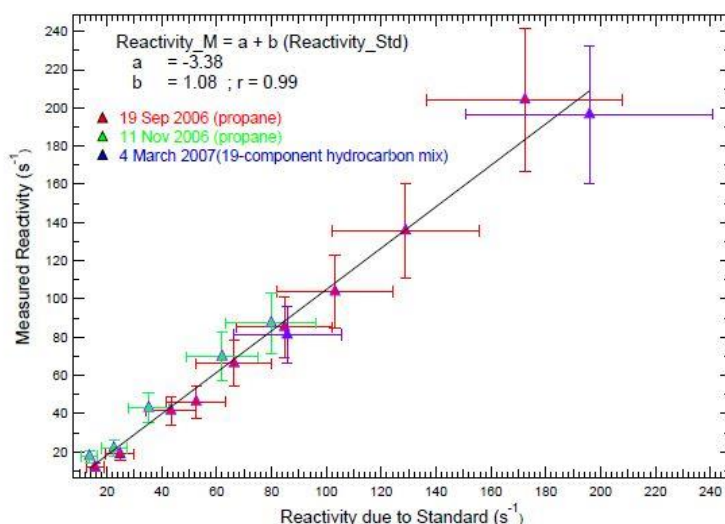


Figure 2.8: A method validation and calibration using different standards showing a good reproducibility, with error bars representing the total calculated uncertainty (Sinha et al., 2008).

In the absence of the standard, pyrrole’s signal is at its baseline value (C2 level). Once the standard is introduced, a competition takes place between pyrrole and the gas standard, for the available OH radicals. Pyrrole’s signal increases to C3 and this C2-C3 modulation depends on the nature of the gas standard and its concentration. Knowing the rate coefficient of the reaction of the standard with OH (k_{i-OH}) and its concentration inside the reactor (X_i), an expected OH reactivity can be calculated based on the following equation:

$$ROH_{(i)\text{expected}} = k_{i-OH} \cdot X_i \quad (2.10)$$

The measured reactivity is then plotted versus the theoretical one, as shown in **Figure 2.8**. Several standards have been used with a wide range of rate coefficients for the reaction with OH. This includes propane ($1.1 \times 10^{-12} \text{ cm}^3 \text{ molecules}^{-1} \text{ s}^{-1}$), ethane ($2.4 \times 10^{-13} \text{ cm}^3 \text{ molecules}^{-1} \text{ s}^{-1}$), isoprene ($1 \times 10^{-10} \text{ cm}^3 \text{ molecules}^{-1} \text{ s}^{-1}$) and mixtures of hydrocarbons. Such molecules are chosen as proxies for atmospheric reactive gases. An excellent linearity and good accountability (slope of the linear regression of the measured vs. the injected reactivity) are usually found. Depending on the chosen test gas and concentration, different range of reactivity

can be investigated. So far, an excellent linearity for the method has been reported until 1200 s⁻¹ (Kim et al., 2011).

2.3.5. CRM artifacts and corrections

The CRM suffers from several measurement artifacts for which the measured OH reactivity values need to be corrected.

First, and as mentioned before, total OH reactivity is derived in terms of C1, C2 and C3. The use of C1 in the calculation of OH reactivity permits to exclude potential interference due to pyrrole's photolysis. Indeed, pyrrole can absorb at some of the wavelengths emitted by the UV mercury lamp used to generate OH radicals via the photolysis of water vapor. And since pyrrole's concentration is measured before (C0) and after (C1) photolysis, it is possible to assess its photolytic loss.

Corrections, in the order of their application in the data processing, are as follows:

- Correction in C2 for relative humidity variations between C2 and C3
- Correction in C3 for the spurious production of OH from the reaction between HO₂, formed from HO₂ photolysis and ambient NO
- Correction in OH reactivity values for not operating the instrument under pseudo-first order kinetics
- Correction in OH reactivity values for dilution

2.3.5.1. Humidity difference between zero air and ambient air

Since the concentration of OH inside the reactor is driven by water photolysis, a small difference in RH can lead to a significant difference in OH levels between the background level of pyrrole (C2) and the concentration of pyrrole after the injection of ambient air (C3). This is considered as one of the principal interferences identified for the CRM. These differences observed between C2 and C3, often lead to an under or over estimation of the value of reactivity in ambient air.

To track relative humidity changes during CRM experiments, the m/z 37/ m/z 19 ratio (first water cluster divided by the number of protons) in the PTR-MS is monitored. Experiments are performed in order to assess the correction factor to be applied on the raw data of reactivity. These experiments consist of varying the humidity level and follow C2 sensitivity and thus pyrrole dependency to RH variations (Michoud et al., 2015; Zannoni et al., 2015). Practically,

humid zero air is diluted by introducing various flow rates of dry zero air, providing different levels of RH inside the reactor.

A linear least squares fit describes the dependency of C2 on $m/z37/m/z19$ (**Figure 2.9**). The slope of the fit (coefficient p in eq. (2.11)) obtained from the experimental tests is then used to correct the C2 value during ambient measurements in the following way:

$$C2_{\text{corrected}} = C2 + p[(m/z37/m/z19)_{\text{duringC3}} - (m/z37/m/z19)_{\text{duringC2}}] \quad (2.11)$$

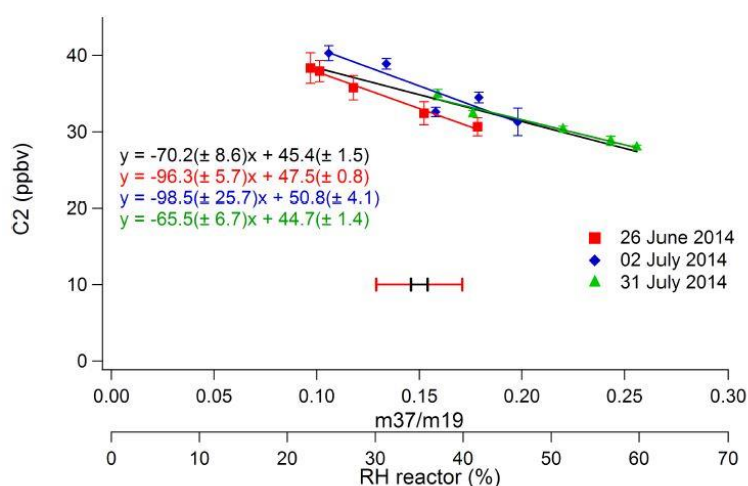


Figure 2.9: Changes in C2 (ppbv) depending on changes in $m/z37/m/z19$ and RH changes during four different humidity tests performed in the frame of the Dunkirk field campaign by Michoud et al. (2015).

2.3.5.2. Recycling of OH due to $\text{HO}_2 + \text{NO}$ reaction

One drawback of using water vapor photolysis for OH radical's generation (R2.4), is the formation of similar amount of HO_2 radicals (R2.5).



When NO is present in the sampled air, HO_2 radicals can be rapidly converted into OH radicals:



This secondary formation of OH leads to differences in OH levels between C2 and C3, and therefore to an artifact in the C3 measurement. In order to assess this interference, tests are done

by introducing different concentrations of NO in the presence and in the absence of reactive test gases.

To assess the required correction for C3 values, different amounts of NO were introduced inside the reactor while sampling zero air, to examine the effect of NO on 0 s^{-1} OH reactivity, or while measuring C3. In this case, a gas standard is introduced inside the reactor to reach higher values of reactivity. When NO is added into the system, reactions R2, R3 and R4 occur, and OH recycling is evident seen the decrease of pyrrole concentration measured by the detector. Hence, the variation of C3 ($\Delta C3$) is computed as the difference between an expected C3 and the measured C3. The expected C3 is calculated using measured levels of C1 and C2, as well as an expected OH reactivity due to NO, based on Eq. (2.9). $\Delta C3$ (ppbv) is plotted as function of the introduced NO (ppbv). The difference between C3 measured and expected is higher for higher concentrations of NO introduced into the system. A quadratic regression forced through the origin was applied by Michoud et al., (2015) (**Figure 2.10**). They also reported a variability in the quadratic regression parameters for different pyrrole-to-OH ratios. Indeed, for 100 ppbv of NO inside the reactor, they found an absolute change in reactivity of 80 s^{-1} at pyrrole/OH equal to 3.9, which is the double observed for the same concentration of NO under pyrrole/OH of 1.6. Therefore, they derived the following expressions to correct for NO interferences:

$$C3_{\text{corrected}} = C3_{\text{measured}} + \Delta C3 \quad (2.12)$$

$$\text{With } \Delta C3 = a[\text{NO}]^2 + b[\text{NO}] \quad (2.13)$$

$$\text{With } a = a_1 \frac{\text{pyrrole}}{\text{OH}} + a_2 \text{ and } b = b_1 \frac{\text{pyrrole}}{\text{OH}} + b_2 \quad (2.14)$$

$$\text{So } \Delta C3 = (a_1 \frac{\text{pyrrole}}{\text{OH}} + a_2)[\text{NO}]^2 + (b_1 \frac{\text{pyrrole}}{\text{OH}} + b_2)[\text{NO}] \quad (2.15)$$

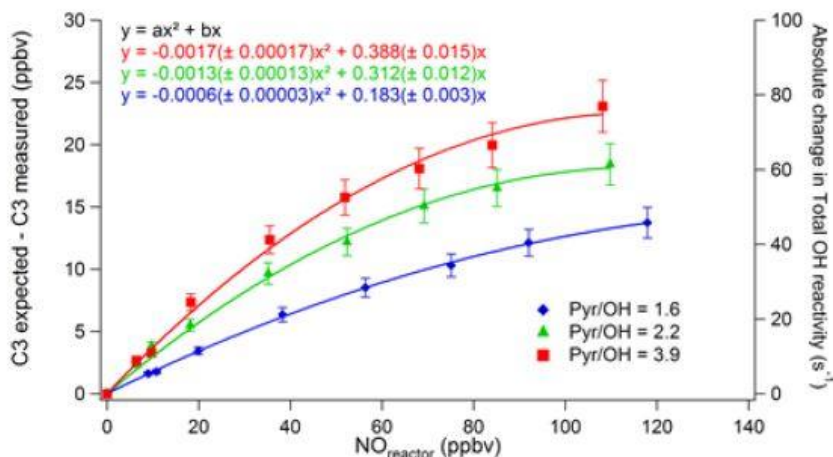


Figure 2.10 : Changes in C3 as function of NO in the reactor. Three experiments conducted at different pyrrole-to-OH ratios (1.6, 2.2 and 3.9) are presented. The right axis corresponds to the absolute change in OH reactivity for the experiment conducted at pyrrole-to-OH 2.2 (Michoud et al., 2015).

2.3.5.3. Deviation from pseudo-first-order kinetics

In equation (2.9), pseudo-first-order conditions are assumed for pyrrole ($[\text{pyrrole}] \gg [\text{OH}]$). However, the CRM is often operated in conditions that do not comply with this assumption. Therefore, the calculated OH reactivity values from equation (2.9), should be corrected.

Two approaches have been developed so far to correct the data: a theoretical approach, as reported by Sinha et al. (2008), and an experimental approach, as reported by Michoud et al. (2015) and Zannoni et al. (2015). The theoretical correction consists on using FACSIMILE, which is a model built on simple numerical simulations where an initial concentration of OH is reacting first with pyrrole, and then with pyrrole and a hydrocarbon chosen as a proxy for ambient air (rate coefficient with OH $\approx 2 \times 10^{-13}$) at different concentrations, for an OH reactivity in ambient air between 8 and 300 s^{-1} . However, this approach is based on simple simulations, where only one competition reaction is computed and other reactions, as radicals-radicals are not considered.

The experimental approach consists on introducing gas standards, with well-established reaction rate with OH, inside the CRM reactor at different concentrations. Hence, an injected OH reactivity could be expected using the concentration of the test gas in the reactor and its rate coefficient with OH (eq. (2.7)). The comparison of measured OH reactivity with the calculated one allows to derive a correction factor (the inverse of the obtained slope) that can vary as function of the test gas and the operational pyrrole-to-OH ratio. Therefore, these

experiments are conducted with several test gases to cover a broad range of OH reactivity and under different pyrrole-to-OH ratios, especially that the latter parameter can be subject to variations due to flows fluctuations affecting the dilution of pyrrole inside the instrument, humidity affecting the production of OH radicals in the system and lamp efficiency.

Figure 2.11 shows an example of two plots, corresponding to two CRM instruments, where a correction factor is represented versus the pyrrole-to-OH ratio. The empirical determination of the correction to apply for the kinetics regime strictly depends on the reactor itself and on operational settings deployed during the experiments, which are specific to each CRM instrument.

However, similar trends are always observed: the correction factor decreases for higher pyrrole-to-OH ratios, since the regime becomes closer to pseudo-first-order conditions; larger differences among tests are usually seen for lower correction factors, when the regime is further away from pseudo-first-order conditions.

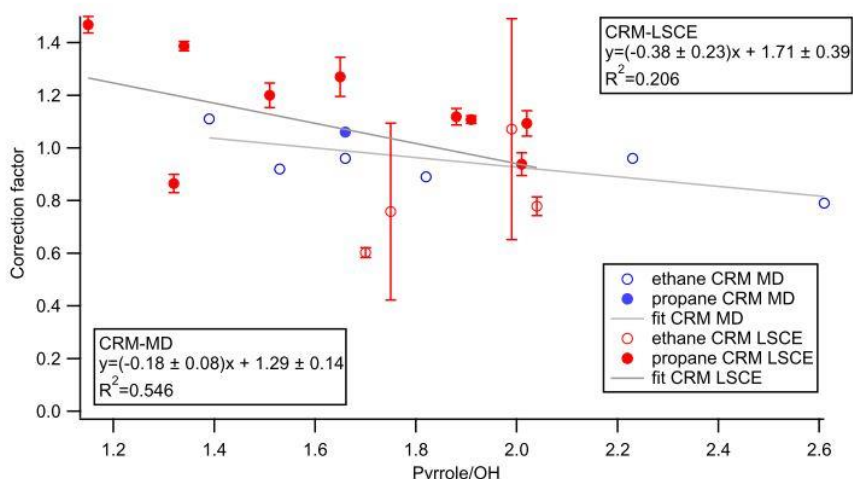


Figure 2.11 : Correction factor of reactivity for the kinetics regime reported vs. pyrrole-to-OH ratio in the reactors of two CRM (LSCE and Mines de Douai) instruments during an intercomparison. Correction for CRM- LSCE is represented in red while correction for CRM-MD is represented in blue. Full circles refer to the experiments conducted with propane while hollow circles refer to the experiments with ethane as gas standard. Linear fits include coefficient values $\pm 1\sigma$ (Zannoni et al., 2015).

Since small differences among reactors (as lengths of the arms, pointing of the arms) can lead to slight different behaviors, it is important that each reactor gets qualified experimentally in order to take such differences into account. The correction factor is then multiplied by the measured OH reactivity to obtain the corrected OH reactivity.

It is worth noting that Michoud et al. (2015) compared the trends of correction factors (F) derived from experiments with those obtained from model simulations (**Figure 2.12**). The simulated correction factors were higher for ethane and even higher for isoprene. Interestingly, both experiments and simulations exhibited a similar trend: a decrease of the correction factors with increasing pyrrole-to-OH ratios, and showed that the dependency of F on the reactivity of added gas standards is reduced at higher pyrrole-to-OH ratios. Seen the disagreement between the experimental and the model approaches, authors preferred to consider experimentally derived factors for their corrections. Indeed, they suggested that the simulations are not really representative of the secondary chemistry of pyrrole and they do not account for the flow dynamic inside the reactor.

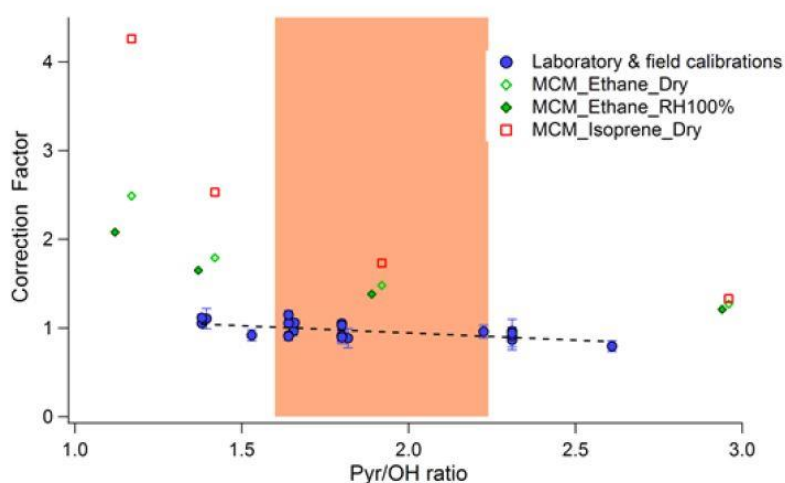


Figure 2.12: Comparison of the trends of the simulated and measured correction factors with the pyrrole-to-OH ratio. The measured correction factors are presented in blues circles. The simulated correction factors stem from simulations conducted using MCM and constrained with ethane under dry conditions (green open diamonds) and wet conditions (green filled diamonds), or constrained with isoprene under dry conditions (red open squares). The colored area corresponds to the range of pyrrole-to-OH ratios observed during the Dunkirk field campaign (1.6–2.2) (Michoud et al., 2015).

2.3.5.4. Dilution inside the flow reactor

The dilution factor is calculated as the ratio between the sampling flow rate and the total flow rate inside the reactor (sum of flow rates of N₂, pyrrole and ambient air). The corrected OH reactivity is multiplied by this values to obtain the reactivity in ambient air.

2.3.5.5. Other artifacts

- In some CRM instruments, an interference due to O₃ in the reactor was observed and had to be assessed for an adequate correction. OH could be reformed in the reaction of HO₂ with O₃ in the reaction volume of the CRM, where O₃ is present in sampled ambient air but is also produced in the photolysis of oxygen by the 185 nm radiation of the Pen-Ray lamp.



The assumption is that the effect of OH reformation on the measurement is typically insensitive to the exact concentration of ambient ozone, which is not present in all modes of the measurement cycle. If this assumption is not true, the OH reactivity is underestimated depending on the ambient ozone concentration.

- While NO₂ is not expected to lead to the formation of secondary OH inside the reactor (like NO), its conversion into NO through photolysis or other chemical processes can cause an artifact. Indeed, experiments showed that NO₂ can result in a similar effect as NO. Michoud et al. (2015) speculated that heterogeneous chemical processes on stainless steel pieces of the system might be the real cause of such conversion. In their study, an average conversion of NO₂ into NO of 24% was reported. Using a similar approach as the one described for NO, the correction for NO₂ interference affects the C3 level, using a quadratic regression from experimental calibrations with gradual additions of NO₂ into the reactor. Experiments demonstrated that the correction is independent on the pyrrole-to-OH ratio and the magnitude for NO₂ correction is lower than the one applied for NO.

2.3.6. LSCE-CRM

2.3.6.1. Historical overview

Since 2011, the comparative reactivity method exists in our laboratory. The first set-up was built, optimized and successfully deployed in the MEGAPOLI field campaign to characterize OH reactivity in Paris (Dolgorouky et al., 2012). Afterwards, the system was

subject to important technical and operational upgrades, aiming to improve the performance of the system and to minimize possible interferences (Zannoni, 2015). Indeed, the instrument sensitivity was increased, by modulating the flows regime, reducing the pyrrole flow (to 2 sccm) to reduce its initial concentration and by increasing the dwell time of acquisition of pyrrole in the PTR-MS (20s). This allowed to measure down to 3 s^{-1} OH reactivity (LOD), which can be observed in remote sites. In addition, and in order to reduce the temperature dependency, the reactor was enclosed in a temperature regulated box ($\approx 25^\circ\text{C}$). This was also advantageous in terms of reducing pyrrole polymerization in the lines. Furthermore, zero air overflow was checked periodically for flow fluctuations and a 4-port valve, controlled via the PTR-MS control software, was added in order to do automatic switches between C2 and C3 during ambient measurements. Pyrrole photolysis rate was also reduced by reducing pyrrole concentration, reducing the UV mercury lamp intensity and by acting on the lamp position. This said, pyrrole photolysis rate was reduced to be between 5- 10% compared to 18- 20% in the previous set-up. Finally, it was decided to use a catalytic converter to generate zero air at ambient humidity which allowed to reduce humidity differences between C2 and C3. However, small differences were still observed and a correction factor has to be applied on OH reactivity raw data.

LSCE-CRM was part of two intercomparison exercises. The first intercomparison was conducted during July 2013 at the Mediterranean site of Ersa, Cape Corsica, France and included another CRM instrument (MD-CRM) that of Mines de Douai. Correction for humidity differences between C2 and C3 had an average impact of 12% for CRM-LSCE, whereas it was lower (4%) for MD-CRM. An experimental approach was used by both groups to assess the correction factor needed to account for the deviation from pseudo-first-order kinetics. Several standards were introduced before, during and after the campaign, with these standards being representative for the range of reactivity of ambient trace gases with OH (10^{-13} - $10^{-10} \text{ cm}^3 \text{ molecule}^{-1} \text{ s}^{-1}$). The range of pyrrole-to-OH ratio investigated was between 1.2 and 2.6, in respect to the ratios observed during the field campaign. A linear dependency was obtained for both instruments when plotting the correction factor F with the pyrrole-to-OH ratios, and the correction factor decreased for higher pyrrole-to-OH. However, this linear dependency was fairly significant only for MD-CRM (with an $R^2 = 0.546$). For this reason, the choice was made to apply a mean correction factor derived from the experiments performed on site, for LSCE-CRM. Using the linear regression by MD-CRM or a mean factor for LSCE-CRM, close corrections were obtained on average for both instruments (mean corrections of 0.97 and 0.98). An important point was noticed during this exercise, is the variability of correction factors

obtained from LSCE-CRM experiments compared to those from MD-CRM experiments. This was attributed to possible small differences in the reactors designs, leading to a potential difference in the mixing efficiency inside the reactor. Therefore, it is important that each CRM instrument undergoes its own characterization experiments, especially regarding the correction for the deviation from pseudo-first-order regime. When all the corrections were applied, they resulted in an average impact of 20% and 49%, on MD-CRM and LSCE-CRM, respectively. Finally, linear least squares fits of total OH reactivity measured by LSCE-CRM versus total OH reactivity measured by MD-CRM, showed a correlation with a slope of 1 and a coefficient R^2 of 0.75. Thus, the two sets of data showed a good agreement, within instrumental uncertainties.

The second intercomparison exercise took place in the atmospheric simulation chamber SAPHIR at Forschungszentrum Jülich in Octobre 2015, including all types of instruments currently used for OH reactivity measurements: Flow tube- laser-induced fluorescence “FT-LIF” (Penn State University(PSU)), Flow tube- chemical ionization mass spectrometer “FT-CIMS” (German Meteorological Service (DWD)), Laser photolysis- laser-induced fluorescence “LP-LIF” (University of Lille, University of Leeds, Forschungszentrum Julich (FZJ)) and the Comparative Reactivity Method “CRM” (Mines de Douai (MD), Laboratoire des Sciences du Climat et de l’Environnement (LSCE) and the Max-Planck Institute (MPI)). The performance of all instruments was tested by stepwise increasing the concentrations of different gas standards inside the chamber: CO, CH₄, NO, isoprene, acetaldehyde, monoterpenes, sesquiterpenes.

Regarding LSCE-CRM, a Teflon pump was added to the sampling system for the first time, since pressure differences were seen between two measurements mode. Hence, the sample was not directly injected in the reactor, but had to pass through the pump, which could have affected the performance of the instrument. In the presence of CO and CH₄, all instruments showed a good agreement with the expected OH reactivity, with LSCE-CRM measuring higher reactivity than expected. Whereas, in the presence of isoprene in an urban environment (CO and NO₂), LSCE-CRM had a better performance, however measurements were lower than expected. These two different observations were attributed to the correction factor for the deviation from pseud-first-order kinetics, that was derived from experiments with propane and isoprene, more representative of the experimental conditions during the isoprene injection than those in the presence of only CO and CH₄. This showed the importance of a more intensive characterization of this correction for different atmospheric chemical conditions. Monoterpenes and sesquiterpenes were also injected in the chamber. In these conditions, the level of agreement

between CRM instruments and reference measurements tended to be significantly smaller compared to the other techniques. Since sampling was done through unheated PFA tubing for LSCE-CRM, with a Teflon pump prior to the reactor, observations suggested that the underestimation of monoterpenes and sesquiterpenes OH reactivity is probably due to low-volatility OH reactants in the sampling system. However, this cannot exclude the impact of monoterpenes and sesquiterpenes chemistry on CRM measurements. In the presence of up to 120 ppbv of NO, agreement with calculated reactivity within the accuracy of measurements and calculations was observed for LSCE-CRM. Finally, during this intercomparison exercise LSCE-CRM showed no dependence on O₃ concentrations inside the reactor, while another CRM instrument suffered from the O₃ artifact, despite that O₃ concentration in all CRM instruments was the same. The exact reason is not clear but might be related to different HO₂ concentrations in the instruments. The insensitivity to the ozone interference, indicates that operating conditions exist for which the interference is negligible. Further investigations should be performed to characterize these conditions.

This campaign showed that OH reactivity can be accurately measured for a wide range of atmospherically relevant chemical conditions by all instruments. The variability in the accuracy of the correction emphasizes the need for a careful characterization of instrument-specific operational-conditions.

2.3.6.2. Current set-up

When I started my PhD, the first stage was to build a new CRM system, similar to the previous one and qualify it, based on all the classical tests. Many optimized parameters were kept the same, specially that the new system consisted of the same glass reactor and the same PTR-MS.

Brand new Teflon lines and Teflon joints made the connections between the reactor and all the inlets and the outlets. A stainless steel 4-way valve allowed manual switches between dry and wet nitrogen. The walls of the box, where the reactor is inhouse, were equipped with an isolation material in order to reduce the system's sensitivity to temperature variations. However, attempts to regulate the temperature inside the box, were not to successful. In fact, whenever the temperature controller was on, periodic fluctuations were observed on the pyrrole signal. Therefore, it was decided to operate the CRM without a temperature control, and temperature sensors were added at different levels inside the box (near the reactor, the water reservoir and

in the middle), to monitor the temperature continuously. This action was taken after noticing the formation of water droplets in the line connecting the reactor to the water reservoir. So it was important to check for temperature differences inside the system which can lead to water vapor condensation in the lines. Furthermore, and in order to minimize the chances for water to condensate, which is paralyzing for OH reactivity tests and measurements, this line was heated and isolated. Finally, the stainless steel 4-way valve was replaced with a Teflon one, since it can represent a cold point favorable for water vapor condensation. Pressure and humidity were also monitored in the flow out of the reactor using adequate sensors. One of the major improvements done in this version of LSCE-CRM is the creation of an online platform (**Figure 2.13**), allowing to control all the flows, to monitor continuously the air overflow, the pressure, the temperatures and the humidity inside the reactor and to program measurement sequences depending on the constraints of each field campaign.

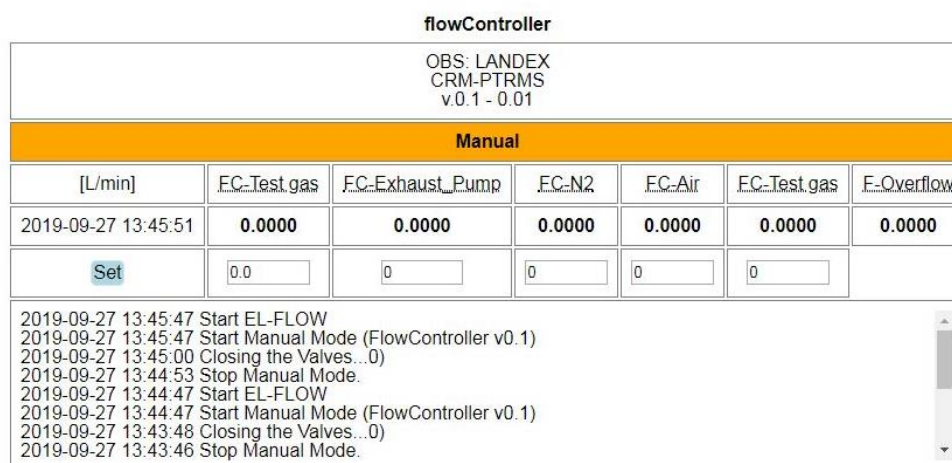


Figure 2.13: Photo of the online page allowing an automatic control of the gas flows and a continuous monitoring of the overflows, the pressure and the relative humidity in the exhaust flow and the temperatures at different location inside the box.

Regarding the operational parameters, the inlet and the outlet flow rates were set as follows:

Inlets: pyrrole: 2.5 mL min⁻¹, N₂: 100 mL min⁻¹, air: 250 mL min⁻¹

Outlets: exhaust pump: 270 mL min⁻¹, PTR-MS: 50- 60 mL min⁻¹, and the air overflow was around 20- 30 mL min⁻¹. The pressure inside the reactor was around atmospheric pressure all the time and the temperature around 25°C in the laboratory.

It is worth noting that between the first (COV³ER, rapeseed, agricultural ecosystem) and the second field campaign (LANDEX, pine, forest ecosystem), the Teflon tubing making the inlets and the outlet to the PTR-MS was replaced by sulfinert lines. Indeed, based on the intercomparison in the SAPHIR chamber, all CRM instruments, including LSCE-CRM,

underestimated the reactivity of monoterpenes. This was explained by the possible loss of monoterpenes in unheated teflon lines. Since the second field work was planned in monoterpenes-rich forest environment, these changes were made in the CRM instrument as well as in its sampling system, in order to make them more suitable to the environment constraints.



Figure 2.14: LSCE-CRM new set-up. On the left the first version with a stainless-steel 4-way valve for switching between dry and wet N₂, with no heating of the line between the water reservoir and the reactor. On the right, the second version with a Teflon 4-way valve and a heated/covered line conducting nitrogen to the reactor, with several temperature sensors.

2.3.6.3. LSCE-CRM performance

- Calibration of pyrrole inside the CRM for dry and wet conditions

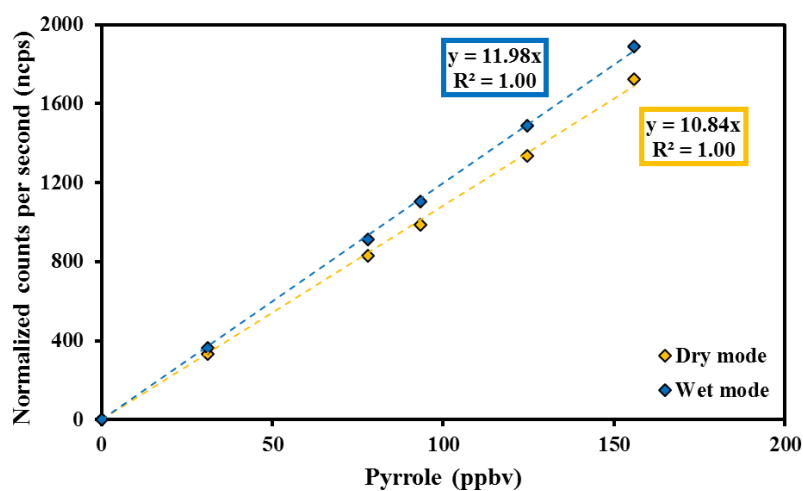


Figure 2.15 : Example of a calibration performed in dry and humid conditions, introducing different levels of pyrrole.

A sensitivity around 10 to 17 ncps ppbv⁻¹ is found with the system being generally more sensitive for wet pyrrole than for dry pyrrole. This was also reported by Sinha et al. (2009). The results of one of the calibrations performed during my PhD is presented in **Figure 2.15**.

- **Photolysis rate**

The photolysis rate is determined from the difference between C0 and C1. As mentioned before, operational parameters including lamp intensity, the dilution of pyrrole and nitrogen flow rate were set to have a low enough photolysis rate. In this version of LSCE-CRM, the photolysis of pyrrole was around 5- 6%.

- **Assessment of the humidity correction**

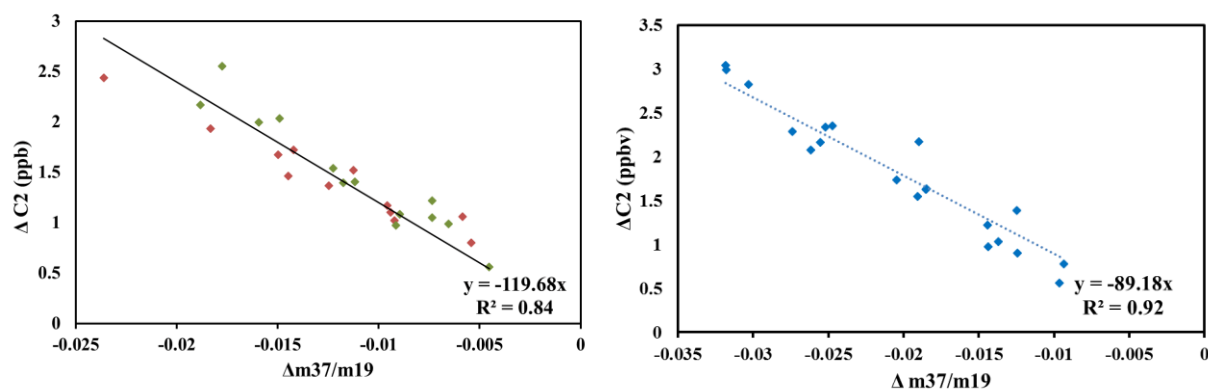


Figure 2.16: Linear least square fit of $\Delta C2$ (ppb) vs. $\Delta(m37/m19)$ for the tests conducted during field experiments to assess the correction for humidity differences between C2 and C3. The left graph corresponds to the COV³ER field campaign with green dots and red dots resulting from tests performed with ambient air and outgoing chamber air, respectively. The right graph corresponds to the LANDEX field campaign.

Figure 2.16 shows the variation of C2 according to different humidity changes in the sampled air. The slope of linear fit between $\Delta C2$ and $\Delta m/z_{37/m/z_{19}}$ is used in eq. (2.11) as the value p to correct for humidity changes.

- **Assessment of the correction for the NO interference**

Figure 2.17 shows experiments conducted to quantify the C3 dependence on NO due to spurious formation of OH from HO₂ + NO. As expected, a decrease of the pyrrole mixing ratio is observed when NO is introduced inside the reactor. A quadratic regression ($y= ax^2 + b$) is

obtained when plotting the variation of C3 versus NO concentration. The presented tests were performed during the COV³ER field campaign, since the site could be under the influence of anthropogenic sources, with corresponding high levels of NO. They were conducted under a pyrrole-to-OH ratio of 1.8- 1.9, close to the ratio of 2.2, observed when a maximum NO level was recorded on the morning of the 21st, April.

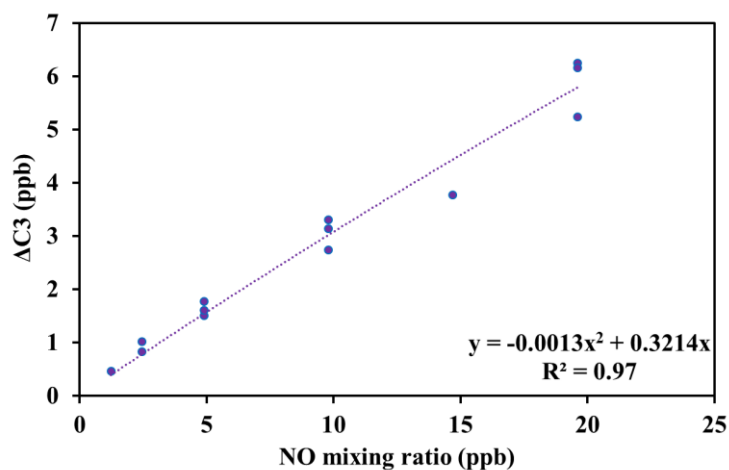


Figure 2.17 : Changes in C3 ($\Delta C3 = C3_{\text{expected}} - C3_{\text{measured}}$) as function of NO concentration introduced inside the reactor during the COV³ER field work.

- LSCE-CRM calibration and assessment of the deviation from pseudo-first order kinetics

One of the main points investigated during my PhD, was the variation of the correction factor for the deviation from pseudo-first order regime as function of the pyrrole-to-OH ratio. **Figure 2.18** displays experimental observations of the measurement bias caused by not operating the instrument under pseudo-first order conditions. In this figure, OH reactivity measured values by LSCE-CRM instrument are plotted against OH reactivity values calculated from the addition of a gas standard.

Figure 2.18.a shows results from the addition of propane at different pyrrole-to-OH ratios ranging between 1.4 and 2.4. A linear relationship exists between the measured and the calculated OH reactivity for propane standard, with a slope close to 1 and a correction factor of 1. However, for isoprene, which is relatively highly reactive with OH, the slope and thus the correction factor is clearly dependent on the pyrrole-to-OH ratio. As shown in **Figure 2.18.b** the lowest slope (the largest correction) is when pyrrole-to-OH ratio is around 1.8. The slope increases and the correction decreases for higher pyrrole-to-OH ratios, being close to 1 for a ratio close to 3.4. This observation is consistent with a kinetic regime getting closer to pseudo-first-order conditions ($[OH] \ll [\text{pyrrole}]$) and therefore to correction factors closer to 1.

Considering the same pyrrole-to-OH ratio, higher correction factors are found for isoprene, more reactive towards OH than propane. However, the difference observed between propane and isoprene is lower for higher pyrrole-to-OH ratio (i.e. 2.3-2.4 compared to 1.8 as shown in **Figure 2.18.c and d**).

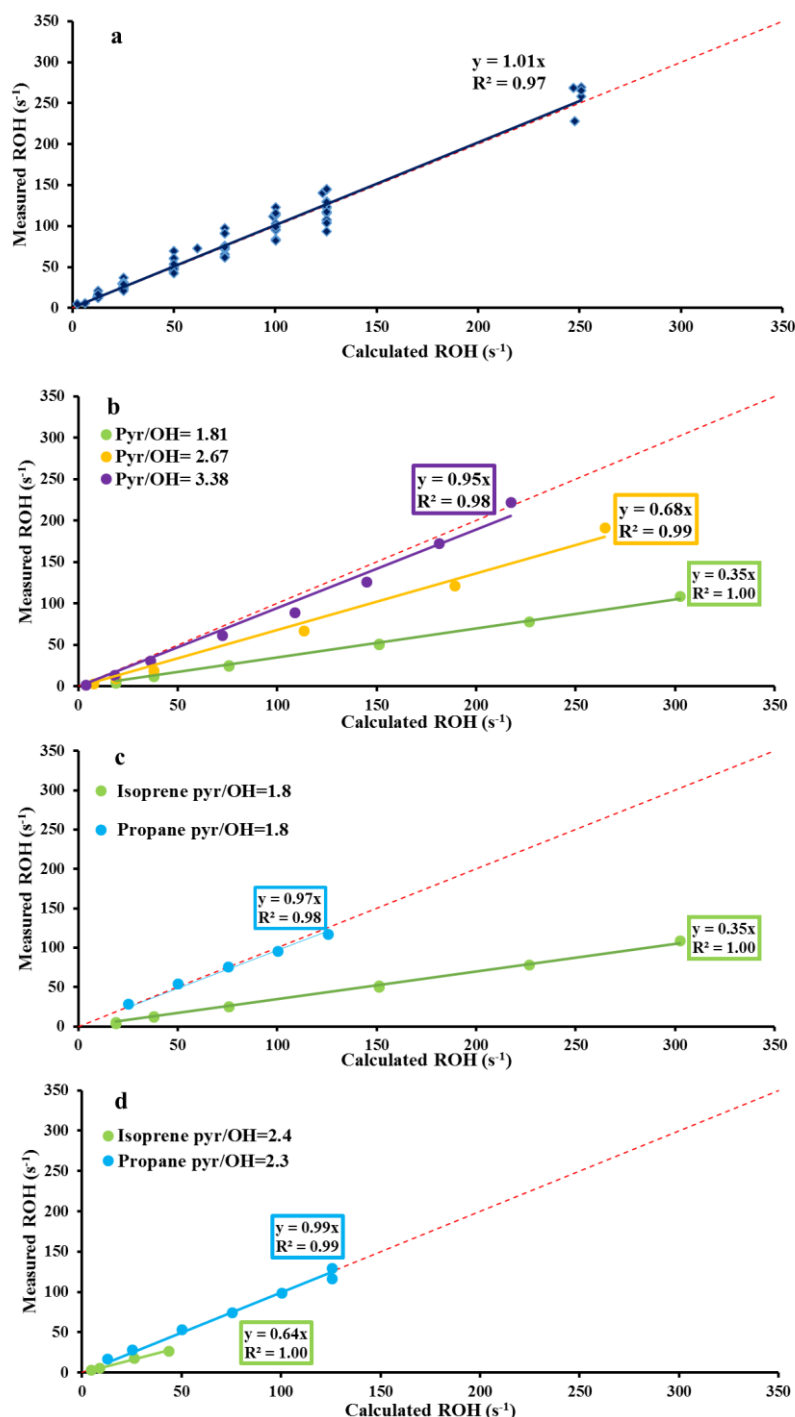


Figure 2.18: Comparison of measured OH reactivity with the calculated one from the addition of gas standards at various pyrrole-to-OH ratios. Graph a) corresponds to propane tests and graph b) to isoprene tests. Graphs c and d, show isoprene and propane tests at pyrrole-to-OH ratios of 1.8 and 2.3-2.4, respectively.

Since ambient air is a mixture of a large number of compounds with reaction rate constants ranging between those of propane and isoprene, the correction factor should consider an averaged correction factor determined using a VOC with a slow rate constant with OH (as propane) and a VOC exhibiting a fast constant with OH (as isoprene). However, in an environment dominated by slow reactive compounds or highly reactive compounds, the average could also induce a bias. In this context, and in order to correct for the deviation from pseudo-first-order kinetics on OH reactivity measurements, performed in a monoterpenes-dominated forest, this correction was also characterized using an α -pinene standard. These experiments were done in collaboration with Nijing Wang from ORSUM research group at the Max-Planck Institute for Chemistry in Mainz, Germany. The idea was, to perform OH reactivity tests on two CRM systems, under different pyrrole-to-OH ratios and compare the results afterwards.

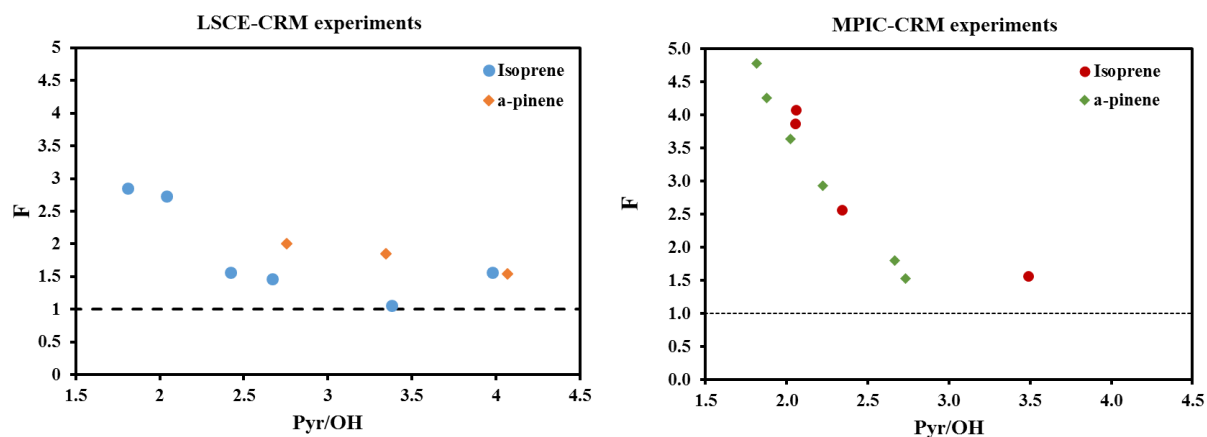


Figure 2.19: Variation of correction factors derived from laboratory experiments, introducing isoprene and α -pinene standards. Under different pyrrole-to-OH ratios. The left graph corresponds to LSCE-CRM correction factors and the right graph corresponds to MPIC-CRM correction factors.

Figure 2.19 shows the variation of the correction factor for the deviation from pseudo-first-order kinetics, derived from isoprene and α -pinene tests, performed under different pyrrole-to-OH ratios, by LSCE-CRM and MPIC-CRM instruments. As shown in the graphs of both instruments, and similarly to what has been reported in the literature, higher the pyrrole-to-OH ratio, lower is the correction factor. Interestingly, the trend of the correction factor F as function of pyrrole-to-OH, follows a polynomial relationship, that is more pronounced in the MPIC-CRM experiments. This trend is though similar to what resulted from model derived correction factors, as reported by Michoud et al., (2015) (**Figure 2.12**) and Praplan et al., (2019). For LSCE-CRM, isoprene exhibited generally lower correction factors than α -pinene, whereas in

MPIC-CRM experiments, both standards showed close correction factors. However, in the CRM characterization paper of Michoud et al., 2015, higher correction factors were reported for standards characterized by a faster reaction with OH, which is in this case for isoprene. For pyrrole-to-OH ratios lower than 2.5, MPIC-CRM showed higher correction factors, reaching 4.8 for α -pinene at a pyrrole-to-OH =1.8, when LSCE-CRM exhibited a factor of 2.9 for isoprene. For higher pyrrole-to-OH ratios (> 2.5), the correction factor was around 1.5- 2 for both instruments. In the investigated pyrrole-to-OH range (1.8 - 4), neither LSCE-CRM nor MPIC-CRM correction factors were down to unity. Meaning that, a wider range should be studied, in order to get closer to pseudo-first-order conditions.

From all these experiments, it appears essential to:

- 1) Do tests with different gas standards with different reactivity with OH
- 2) Perform tests with each standard at different pyrrole-to-OH ratios, wider the range, better it is.
- 3) Take into account the pyrrole-to-OH ratio in the corrections to be applied to measured OH reactivity.
- 4) Perform a whole set of characterization tests, specific for each instrument, seen the inter-instrument variability, most probably due to small differences in the reactor design and differences in operational parameters.

2.3.6.4. Field deployment of the CRM/PTR-MS

We deployed the CRM/PTR-MS in two ecosystems: a rapeseed field representing a typical agricultural ecosystem and in a forest.

The first field campaign was conducted in a rapeseed field during the blooming season. It aimed to characterize BVOCs and their OH reactivity in the incoming and the outgoing air of a dynamic chamber, installed on a healthy rapeseed crop. OH reactivity measurements were performed during one month, in April 2017, in parallel with VOCs and inorganic compounds measurements. In this context, the first stage of my PhD, focused on building and optimizing the CRM system, starting with operational parameters already chosen from previous work on the system, allowing to detect small differences between C2 and C3 and to minimize humidity differences between these two analytical steps. To reduce the sensibility of the system to temperature fluctuations, the set-up was isolated in a box. Some technical improvements were

made, including the automation of flows control and continuous monitoring of the pressure, the temperature, the relative humidity and the overflow. A 4-port valve was used for automatic switches between the incoming and the outgoing air samples and the sampling lines were heated ($\approx 50^\circ\text{C}$) with a flow rate of about 1 L min^{-1} , in order to minimize compounds losses in the lines. The CRM/PTR-MS measured between the 7th and the 25th, April 2017, however only data from the 20th to the 23rd, were subject to a complete analysis and interpretation. In fact, data gaps among our results due to instrumental controls, as well as data gaps among other instruments used for OH reactivity calculation, limited our analysis to few days, when all instruments were measuring simultaneously.

The second field campaign, took place in the maritime pine forest in the Landes region, south of France. It is a forested site influenced by biogenic VOCs (mainly monoterpenes) directly emitted by trees and their higher oxidation products, with relatively poor anthropogenic influence. In this site, we deployed the CRM during one month in July 2017, shortly after the COV³ER rapeseed field experiment. The main constraints on this site: (i) the high level of OH reactivity, since monoterpenes are among the most reactive compounds towards OH, (ii) measurements at two different levels, inside and above the canopy, (ii) instrumental accuracy for an environment dominated by highly reactive species (monoterpenes and isoprene); (iii) elevated ambient temperature. Following the outcome of the OH reactivity intercomparison exercise (Fuchs et al. 2017) which had suggested that the loss of monoterpenes in the Teflon lines could have been the reason of the underestimation of OH reactivity measured by the CRM systems, we have replaced the Teflon sampling lines by sulfinert lines. The choice of sulfinert has been made following tests performed by colleagues at Institut Mines Douai (S. Sauvage, personal communication). Those sulfinert lines were heated, with a flow of $1\text{-}1.2 \text{ L min}^{-1}$, trying to minimize the losses of reactive compounds in the sampling system. We developed a sampling sequence to carry out alternatively measures of OH reactivity at two heights in the forest in order to better elucidate the intra and inter-canopy variability. The sampling lines of OH reactivity and other instruments (PTR-ToF-MS, GCs) were located close to each other to perform collocated observations.

Table 2.3 reports a comparison of the performance of our CRM between the two field works. We can see that the system exhibited similar performances during both field campaigns. No correction for the OH recycling due to the reaction of $\text{NO} + \text{HO}_2$ was applied on data from the forest, seen the relatively low levels of NO and larger correction factors for the deviation from pseudo-first order kinetics were applied for the LANDEX field campaign dataset, since the site

is dominated by relatively highly reactive compounds with OH (isoprene and α -pinene), which were chosen for system's calibration.

Table 2.3: Summary of the CRM operational conditions during the COV3ER and LANDEX field campaigns.

	ADEME- COV ³ ER Grignon, France, between the 7 th and the 25 th , April 2017	ADEME- LANDEX The Landes, France, between the 3 rd and the 19 th , July 2017
Limit of detection (LOD, 3σ)	3 s ⁻¹	3 s ⁻¹
Total systematic uncertainty	35%	35%
Detector sensitivity to pyrrole	Dry calibration: 17.04 ncps ppbv ⁻¹ Wet calibration: 16.68 ncps ppbv ⁻¹	Dry calibration: 15.45 ncps ppbv ⁻¹ Wet calibration: 15.51 ncps ppbv ⁻¹
C1	70.5 \pm 0.3 ppbv	70.7 \pm 4 ppbv
Photolysis rate	6 %	5 %
Humidity correction test	Linear correction, slope= -119.68 (R2= 0.84)	Linear correction, slope= - 89.18 (R2= 0.92)
NO correction	Quadratic regression, a=-0.0013 and b=0.3214	No NO correction
Test with external test gases	Linear response in the range: 3- 300 s ⁻¹	Linear response in the range: 3- 300 s ⁻¹
	F = 1.59x ² - 7.22x + 9.46 with x = pyrrole/OH, Tests with propane and isoprene	F = -0.52 x +3.38, with x = pyrrole/OH, Tests with isoprene and α -pinene

In summary, I have worked on two different systems during my PhD, with the PTR-MS as the detector.

1- For OH reactivity measurements, I used the Comparative Reactivity Method. In a first phase, I participated in building a new version of the system with the introduction of several technical improvements. I did several tests in order to evaluate the performance of the system and to determine the different correction factors. After, I deployed the system in two field campaigns: the first one was conducted in a rapeseed field, during the blooming season, in April 2017 and the second one took place in a maritime pine forest, in June- July 2017. For these campaigns, I prepared the system, set it up on the field. I participated in the whole measurement campaign, performing control tests and dealing with some technical problems when occurred (including electrical power cuts, PTR-MS shut down due to pump membrane issue...). Finally, I have handled the CRM-OH reactivity dataset treatment which involves all the corrections which have to be taken into account (which were not detailed in this chapter but were time consuming).

2- For monoterpenes chemical speciation, I deployed the FastGC/PTR-MS system. A first phase consisted on installing the FastGC on the PTR-QuadMS available in our laboratory. I did several tests, in collaboration with Felix Piel, to test the performance of the instrument and optimize the operational parameters for a fast and satisfying separation of monoterpenes. After, I set the system in the field, for a three-weeks field campaign, and I had to replace a 6-port-valve with a 10-port valve within the drift-tube chamber. Daily calibrations and control tests were done as well as a close monitoring of the system, since it is the first time that it was deployed in continuous real measurements. Finally, I took care of the data analysis (with the help of an intern student) using the Matlab script developed by Felix Piel.

Conclusion Chapitre 2

Durant la thèse, deux systèmes ont été déployés avec le PTR-MS comme détecteur :

Pour la FastGC, le système a été sujet d'une série de tests de laboratoire, visant à optimiser les paramètres opérationnels pour une meilleure séparation en un temps rapide. Plusieurs combinaisons de rampes de température et de débits de gaz vecteur ont été testés. L'hélium a montré une meilleure séparation en un temps plus court, comparé à l'azote, et les analyses quantitatives ont permis de déterminer la limite de détection, qui est de 500 pptv/monoterpène. Comme il permettait de séparer les principaux monoterpènes avec un point de mesure tous les 10 min, le système s'est avéré prometteur pour une application sur le terrain. Il était possible de séparer et de quantifier les principaux monoterpènes en temps relativement court. Cependant, des améliorations peuvent être apportées afin de pouvoir séparer des espèces qui co-eluent (limonene+ ocimene), et détecter des niveaux de concentrations inférieures à 500 pptv.

Pour la CRM, une première phase consistait à construire et tester une nouvelle version du système. Plusieurs améliorations techniques ont été apportées par rapport à la version précédente. En particulier : (1) le système a été rendu plus compact et plus automatisé, (2) le suivi en continu des conditions de température, pression et humidité relative a été intégré au sein du système d'acquisition, (3) ainsi qu'un meilleur contrôle des flux de gaz a été intégré. Une série de tests a été conduite au laboratoire ainsi qu'au début, au milieu et la fin de chaque campagne de mesure, afin de tester la performance du système et de déterminer les facteurs de corrections. La correction pour la déviation du pseudo-premier ordre s'est montrée dépendante de l'espèce injectée et du rapport pyrrole/OH (C1/OH). En effet, les expériences ont montré que : (1) la correction est plus faible pour les composés relativement moins réactifs (propane) avec OH, (2) plus le rapport est élevé, plus la correction est faible pour tous les composés testés et plus la différence dans le facteur de correction entre un composé peu réactif et un autre plus réactif est faible, (3) chaque système réagit différemment concernant ces corrections, ce qui met l'accent sur l'importance d'une caractérisation complète, spécifique à chaque système CRM.

3. Variability of hydroxyl radical (OH) reactivity in the Landes maritime Pine forest: results from the LANDEX campaign 2017

Introduction chapitre 3

En juillet 2017, la CRM a été déployée durant la campagne de mesure ADEME-LANDEX (LANDEX : study of Secondary Organic Aerosols (SOAs) generated by the Landes forest), réalisée sur un site faisant partie des forêts de pin maritime des Landes, au Sud de la France. Ce projet impliquait plusieurs équipes de recherche, déployant divers techniques analytiques pour la mesure de la phase gazeuse et particulaire. Entre le 3 et le 19 juillet, la réactivité OH, ainsi que les COVs ont été mesurés dans (6 m) et au-dessus de la canopée (12 m), afin de caractériser leur variabilité inter et intra-canopée et évaluer la présence potentielle d'une réactivité manquante, comme c'est le cas dans nombreuses études en milieux forestiers. Durant cette campagne, un instrument FAGE (Fluorescence Assay by Gas Expansion) déployé par le laboratoire « Physicochimie des processus de combustion et de l'atmosphère » (PC2A), mesurait également la réactivité OH, pour une partie de la campagne (entre le 13 et la 19 juillet), ce qui constituait une opportunité de comparer les mesures des deux instruments, dans un environnement forestier réel. Mesurant au même endroit dans la canopée, les mesures par CRM et par FAGE montraient un accord satisfaisant, en prenant en compte les incertitudes sur les mesures. La comparaison des mesures à deux endroits différents dans la canopée, a révélé aussi un bon accord ainsi qu'une possible hétérogénéité dans la composition atmosphérique à l'échelle horizontale.

Variability of hydroxyl radical (OH) reactivity in the Landes maritime Pine forest: results from the LANDEX campaign 2017

Sandy Bsaibes¹, Mohamad Al Ajami², Kenneth Mermet^{3,4,5}, François Truong¹, Sébastien Batut², Christophe Hecquet², Sébastien Dusanter³, Thierry Léornadis³, Stéphane Sauvage³, Julien Kammer^{1,4}, Pierre-Marie Flaud^{4,5}, Emilie Perraudin^{4,5}, Eric Villenave^{4,5}, Nadine Locoge³, Valérie Gros¹, Coralie Schoemaeker²

¹ Laboratoire des Sciences du Climat et de l'Environnement, LSCE, UMR CNRS-CEA-UVSQ, 91191 Gif-sur-Yvette, France

² Laboratoire PhysicoChimie des Processus de Combustion et de l'Atmosphère, PC2A, UMR 8522, 59655 Villeneuve d'Ascq, France

³ IMT Lille Douai, Univ. Lille – SAGE - Département Sciences de l'Atmosphère et Génie de l'Environnement, F-59000 Lille, France

⁴ Univ. Bordeaux, EPOC, UMR 5805, F-33405 Talence Cedex, France

⁵ CNRS, EPOC, UMR 5805, F-33405 Talence Cedex, France

Correspondence to: Sandy Bsaibes (sandy.bsaibes@gmail.com)

Valérie Gros (valerie.gros@lsce.ipsl.fr)

Abstract

Total OH reactivity measurements were conducted during the LANDEX intensive field campaign in a coniferous temperate forest located in the Landes area, south-western France, during July 2017. In order to investigate inter-canopy and intra-canopy variability, measurements were performed inside (6 m) and above the canopy level (12 m), as well as at two different locations within the canopy, using a Comparative Reactivity Method (CRM) and a Laser Photolysis-Laser Induced Fluorescence (LP-LIF) instrument. The two techniques were intercompared at the end of the campaign by performing measurements at the same location. Volatile organic compounds were also monitored at both levels with a proton transfer-time of flight mass spectrometer and online gas Chromatography instruments to evaluate their contribution to total OH reactivity, with monoterpenes being the main reactive species emitted in this *Pinus pinaster* Aiton dominated forest. Total OH reactivity varied diurnally, following the trend of BVOCs of which emissions and concentrations were dependent on meteorological parameters. Average OH reactivity was around 19.2 s^{-1} and 16.5 s^{-1} , inside and above the canopy, respectively. Highest levels of total OH reactivity were observed during nights with a low turbulence ($u^* \leq 0.2 \text{ m s}^{-1}$) leading to lower mixing of emitted species within the canopy

and thus an important vertical stratification, characterized by a strong concentration gradient. Comparing the measured and the calculated OH reactivity highlighted an average missing OH reactivity of 22 % and 33 %, inside and above the canopy, respectively. A day/night variability was observed on missing OH reactivity at both heights. Investigations showed that during day-time, missing OH sinks could be due to primary emissions and secondary products linked to a temperature-enhanced photochemistry. Regarding night-time missing OH reactivity, higher levels were seen for the stable and warm night of the 4th-5th, July, showing that these conditions could have been favorable for the accumulation of long-lived species (primary and secondary species) during the transport of the air mass from nearby forests.

3.1. Introduction

The hydroxyl radical OH is considered as the most important initiator of photochemical processes in the troposphere during day-time, and the prevailing “detergent” from local to global scales. It controls the lifetime of most trace gases and contributes to the self-cleansing power or so-called “oxidation capacity” of the atmosphere.

Even though the main primary source for OH in the lower troposphere is the photolysis of ozone at short wavelengths, the OH production and loss processes are numerous and difficult to quantify. Such losses involve several hundreds of chemical species and as many reactions to consider. In this respect, a direct measurement of total OH reactivity (R_{OH}) is of great interest to better understand the OH chemistry in the atmosphere and to investigate the budget of OH sinks in a particular environment. R_{OH} is defined as the pseudo first-order loss rate (in s^{-1}) of OH radicals, equivalent to the inverse of the OH lifetime. It is the sum of the reaction frequencies of all chemical species reacting with OH, as shown in Eq. (3.1):

$$R_{OH} = \sum_{i=1}^n k_{OH+X_i} \cdot [X_i] \quad (3.1)$$

In this equation, a chemical reaction frequency for a species X_i with OH (R_{OH+X_i}) is the product of its rate-coefficient k_{OH} with its concentration $[X_i]$. The measured total OH reactivity can be compared with calculated values based on the sum of reaction frequencies as shown in Eq. (3.1) and for which the concentration of X_i has been measured at the same location. Any significant discrepancy between measured and calculated OH reactivity explicitly demonstrates missing OH sinks, commonly called missing OH reactivity, and points out that potentially important unmeasured reactive species and chemical processes associated with these species may affect our understanding of OH atmospheric chemistry.

Two approaches have been used to measure the total OH reactivity. The first approach derives OH reactivity from direct measurements of OH decay rates due to its reaction with trace species present in ambient air introduced in a reaction tube. OH can be generated and detected differently according to 3 types of techniques: The Flow Tube-Laser Induced Fluorescence (FT-LIF, (Hansen et al., 2014; Ingham et al., 2009; Kovacs and Brune, 2001)), the Laser Photolysis-Laser Induced Fluorescence (LP-LIF, (Sadanaga et al., 2004; Parker et al., 2011; Amédro, 2012; Stone et al., 2016; Fuchs et al., 2017)) and the Flow Tube-Chemical Ionization Mass Spectrometry (FT-CIMS, (Muller et al., 2018)). The second approach is called the Comparative Reactivity Method (CRM) and it consists in an indirect quantification of OH losses from the

concentration change of a reference molecule that competes with ambient reactive species to react with artificially produced OH. The reference substance, pyrrole, is measured with a Proton Transfer Reaction - Mass Spectrometer (PTR-MS, (Sinha et al., 2008; Dolgorouky et al., 2012; Michoud et al., 2015)) or with a Gas Chromatograph-Photo Ionization Detector (GC-PID, (Nölscher et al., 2012b)) or chemical ionization mass spectrometry (CIMS, (Sanchez et al., 2018)).

Both LP-LIF and CRM techniques were deployed in a Pine forest for this study, the instruments deployed are presented in more details below and a general description is provided here. In the LP-LIF method, OH is generated by laser pulsed photolysis of ozone in a reaction tube, at typically 266 nm, followed by the rapid reaction of O(¹D) with ambient water vapor. OH radicals react with ambient reactive species in the reaction tube and the concentration of OH decreases after the laser pulse. The air from the reaction tube is continuously pumped into a low-pressure detection cell where the OH decay is monitored by laser-induced fluorescence at a high time resolution (range of hundreds of μs) (Sadanaga et al., 2004a). Compared to flow-tube set-ups, lower flow rates of ambient air are needed in the LP-LIF technique (less than 10 L min^{-1} compared to several tens of L min^{-1}). In addition, the use of O₃ laser photolysis instead of continuous water photolysis by lamps at 185 nm for OH generation, the latter being commonly used in FT-LIF or CRM, limits the spurious formation of OH from the reaction of HO₂ with ambient NO. However, in order to quantify wall loss reactions, an instrument zero has to be subtracted from all measurements, and a correction may have to be applied for the recycling of OH radicals in the presence of high NO levels (Stone et al., 2016; Fuchs et al., 2017).

In the Comparative Reactivity Method (CRM), ambient air, wet nitrogen and pyrrole are introduced into a glass reactor where OH radicals are produced by the photolysis of water vapor. The mathematical expression used to determine the OH reactivity of the analyzed sample is derived in terms of the initial concentration of pyrrole (C1), the background concentration of pyrrole reacting alone with OH (C2) and the concentration of pyrrole after competition with air reactants (C3). The CRM exhibits several advantages compared to direct measurements techniques, like the commercial availability of PTR-MS and the need of a smaller sampling flow rate of ambient air (few hundreds of mL min^{-1}), which broadens the application of the technique to branch and plant enclosure studies. On the other hand, this indirect method requires a raw data processing with careful corrections for measurement artifacts related to humidity

changes and secondary chemistry that can impact the pyrrole concentration (Sinha et al., 2008; Michoud et al., 2015).

A few inter-comparisons were reported in the literature for urban and remote areas (Hansen et al., 2015; Zannoni et al., 2015; Sanchez et al., 2018) and chamber experiments (Fuchs et al., 2017) aiming at reproducing ambient conditions observed in various environments. The latter, including a large number of OH reactivity instruments (FT-LIF, LP-LIF, CRM) and conducted in the SAPHIR atmospheric simulation chamber, allowed to compare the performances of each technique. Results showed that OH reactivity can be accurately measured for a wide range of atmospherically relevant chemical conditions by all instruments. However, CRM instruments exhibited larger discrepancies to calculated OH reactivity compared to instruments directly probing OH radicals, and these differences were more important in the presence of terpenes and oxygenated organic compounds.

Over the past two decades, OH reactivity measurements were conducted in various environments at the ground level using the available techniques: urban and suburban areas, forest areas, marine areas (Yang et al., 2016; Dusanter and Stevens, 2017). A few aircraft measurements have also been carried out to complete ground-based observations (Mao et al., 2009). Many studies highlighted the interest of investigating OH reactivity in forest areas exhibiting large concentrations of biogenic VOCs (BVOCs) since BVOC emissions exceed anthropogenic VOCs by a factor of 10 at the global scale (Guenther et al., 1995). Results showed that our understanding of OH sinks in these environments was incomplete with observations of large missing OH reactivity ranging between 25 % and 80 %. Total OH reactivity appeared to be impacted by several factors such as the forest type and the dominant emitted species, the seasonality, the canopy level as well as specific atmospheric conditions (Hansen et al., 2014; Nölscher et al., 2013; Praplan et al., 2019; Sanchez et al., 2018; Zannoni et al., 2017).

Among these biogenic hydrocarbons, monoterpenes represent a large class of $C_{10}H_{16}$ compounds, which are mainly emitted by conifers as well as broad-leaves trees. They can be oxidized by OH, ozone and the nitrate radical, leading to atmospheric lifetimes ranging between minutes and days (Atkinson and Arey, 2003). The oxidation of primary BVOCs can therefore contribute to the formation of tropospheric ozone and secondary organic aerosols from the local to the regional scales, with oxidation products of BVOCs having a potential impact at a larger scale. Regarding coniferous forests, an averaged OH reactivity of 6.7 s^{-1} was observed over a temperate Pine forest located in the southern part of the Rocky Mountains in the USA during

summer 2008 (Nakashima et al., 2013). Measured OH reactivity exhibited a diurnal variation with minima during day-time when MBO (2-methyl-3-buten-2-ol) was the main contributor, and maxima during night-time when the OH reactivity was dominated by monoterpenes. Approximately 30% of the measured OH reactivity remained unexplained and could be related to unmeasured or unknown oxidation products of primary emitted biogenic compounds. Another campaign also carried out in a temperate coniferous forest, located in the Wakayama Forest Research Station in Japan during summer 2014 (Ramasamy et al., 2016), showed comparable results with an average total OH reactivity of 7.1 s^{-1} . OH reactivity varied diurnally with temperature and light, reaching a maximum at noon-time. Monoterpenes were the main drivers of the total OH reactivity in the considered ecosystem, accounting for 23.7 %, followed by isoprene (17.0 %) and acetaldehyde (14.5 %). The missing OH reactivity (29.5 % on average) was found to be linked to light and temperature dependent unmeasured primary and secondary species.

In the present study, we report on the measurement of total OH reactivity from a field experiment conducted in the Landes temperate forest, southwestern France. This work was part of the LANDEX project (LANDEX, i.e. the Landes Experiment: Formation and fate of secondary organic aerosols generated in the Landes forest) that aimed at characterizing secondary organic aerosol formation observed in this monoterpene-rich environment. The dominant tree species at the site is maritime pine, *Pinus pinaster* Aiton, which is known to be a strong emitter of α and β -pinene, leading to a diurnal concentration profile of monoterpenes characterized by maximum values at night and minimum values during day-time (Simon et al., 1994). Nocturnal new particle formation episodes (NPFs) were reported in this ecosystem, suggesting the contribution of BVOC oxidation to the nucleation and growth stages of particles (Kammer et al., 2018).

Measurements of OH reactivity and trace gases were performed at two heights to cover the inside and above canopy, and at two different locations inside the canopy to investigate the intra-canopy variability. Two different instruments were deployed: the CRM from LSCE (Laboratoire des Sciences du Climat et de l'Environnement) that measured inside and above the canopy and the LP-LIF from PC2A (PhysicoChimie des Processus de Combustion et de l'Atmosphère) that performed measurements inside the canopy. The deployment of two different instruments was a good opportunity to (i) compare measurements made with both methods in a real biogenic environment after the inter-comparison experiment performed in the SAPHIR chamber and recent improvement of the CRM instrument, (ii) investigate the levels

and diurnal variability of OH reactivity at two different heights, and (iii) investigate both the OH reactivity budget and the missing reactivity pattern using a large panel of concomitant trace gas measurements.

3.2. Experimental

3.2.1. Site description

The LANDEX intensive field campaign was conducted from the 3rd to the 19th of July 2017 at the Bilos field site in the Landes forest, south-western France. The vegetation on the site was dominated by maritime pines (*Pinus pinaster* Aiton) presenting an average height of 10 m. The climate is temperate with a maritime influence due to the proximity of the Atlantic Ocean. This site is part of the European ICOS (Integrated Carbon Observation System) Ecosystem infrastructure. A more detailed description of the site is available in Moreaux et al. (2011) and Kammer et al. (2018).

3.2.2. OH reactivity instruments

The LP-LIF instrument, referred here as UL (University of Lille)-FAGE (Fluorescence Assay by Gas Expansion), measured the OH reactivity in the canopy, whereas the CRM instrument, referred as LSCE-CRM, alternatively measured the OH reactivity at two heights (see **Fig. 3.1.b**). **Table 3.1** summarizes the performance of both instruments. The LP-LIF technique has a 3-fold better limit of detection than the CRM, however the CRM has a larger dynamic range since it can measure the OH reactivity up to 300 s⁻¹ without sample dilution. The overall systematic uncertainty (1σ) is around 15 % and 35 % for the LP-LIF and the CRM, respectively. The LSCE-CRM and UL-FAGE characteristics are given in the following paragraphs.

Table 3.1: Performance of the two OH reactivity instruments deployed during the LANDEX campaign.

Instrument	LOD*(s⁻¹) (3 σ)	ROH max (s⁻¹)	Time resolution (s)	Uncertainty (1 σ)
LSCE-CRM	3	300	600	35 %
UL-FAGE	0.9	150**	30-120	15 %

* LOD: Limit of Detection; ** Without dilution

3.2.2.1. The Comparative Reactivity Method (CRM) and instrument performance

The total OH reactivity was measured during the whole campaign, inside and above the canopy, by the LSCE-CRM instrument. This technique, first described by Sinha et al. (2008), is based on measuring the concentration of a reagent compound (pyrrole) that reacts with OH under different operating conditions (i.e. steps) at the output of the sampling reactor by a PTR-MS instrument. The first step consists in introducing pyrrole with dry nitrogen and dry zero air to measure the C1 level, which corresponds to the pyrrole concentration in absence of OH. C1 accounts for potential photolysis due to photons emitted by the mercury lamp used to produce OH. During the second step, dry nitrogen and zero air are replaced by humid gases and a pyrrole concentration C2 is measured. C2 is lower than C1 because pyrrole reacts with OH. In the last step, zero air is replaced by ambient air, which leads to a competition between the reactions of OH with pyrrole and ambient trace gases. A C3 concentration, higher than C2, is measured. The difference between C3 and C2 depends on the amount and reactivity of reactive species present in ambient air and is used to determine the total OH reactivity from Eq. (3.2), where it is assumed that pyrrole reacts with OH following pseudo-first order reaction kinetics, i.e. [pyrrole] \gg [OH]:

$$R_{OH} = \frac{(C3 - C2)}{(C1 - C3)} \cdot k_p \cdot C1 \quad (3.2)$$

Where k_p is the reaction rate constant of pyrrole with OH ($1.2 \times 10^{-10} \text{ cm}^3 \text{ molecule}^{-1} \text{ s}^{-1}$ (Atkinson, 1985)).

This technique requires multiple corrections to derive reliable measurements of total OH reactivity due to: (1) potential differences in relative humidity between C2 and C3, leading to different OH levels, (2) the spurious formation of OH in the sampling reactor when

hydroperoxy radicals (HO_2) react with nitrogen monoxide (NO), (3) not operating the instrument under pseudo-first order conditions, and (4) dilution of ambient air inside the reactor by the addition of N_2 and pyrrole (Sinha et al., 2008; Michoud et al., 2015). In some CRM systems, corrections for potential NO_2 and/or O_3 artifacts are also considered (Michoud et al., 2015; Praplan et al., 2017). On one hand, NO_2 is subject to photolysis leading to NO , which can subsequently react with HO_2 yielding OH . On the other hand, O_3 can also be photolyzed in the reactor, producing $\text{O}(^1\text{D})$, which reacts further with H_2O , yielding two OH radicals.

Intensive laboratory experiments as well as tests during the LANDEX field campaign were performed to characterize these corrections and assess the performances of the instrument over time. During the LANDEX field campaign, a slightly modified version of the CRM-LSCE instrument was used compared to the instrument previously deployed during the intercomparison experiment at the SAPHIR chamber (Fuchs et al., 2017). Indeed, this last study showed that the OH reactivity measured by all CRM instruments was significantly lower than the reactivity measured by the other instruments in the presence of monoterpenes and sesquiterpenes. A potential reason discussed for this discrepancy was the loss of terpenes in the inlet of the CRM instruments. The LSCE-CRM sampling system was built with 1/4" OD non-heated PFA tubing and was relying on a Teflon pump to introduce the sample into the reactor. In order to measure the total OH reactivity in a monoterpene-rich environment, several technical improvements were made on the previous version of the instrument described by Zannoni et al. (2015). First, all the PFA sampling lines were replaced by 1/8" OD sulfinert lines, continuously heated to around 50°C to prevent condensation and minimize sorption processes. Second, temperature sensors were placed at several locations inside the system to monitor potential variations; the dew point was measured in the flow out through the pump to monitor humidity fluctuations, and the pressure was also monitored to make sure that measurements were performed at atmospheric pressure. All the flows going in and out of the reactor, the temperature at various places, the humidity and the pressure in the reactor were recorded continuously to track potential variations.

Ambient air sampling

Ambient air was sampled through two 1/8" OD sulfinert lines collocated on a mast close to the trailer (see **Fig. 3.1.a**). The lines lengths were 8 m for the measurements performed inside the canopy and 12 m for those performed above. These lines were heated up to 50 °C as it was

shown that losses of highly reactive molecules (i.e. β -caryophyllene) were negligible for temperatures above 20 °C (Kim et al., 2009).

During sampling, the air flow was driven through one line by two pumps. The first one was a Teflon pump located upstream of the reactor and the other one was that from the Gas Calibration Unit (GCU) used to generate humid zero air from ambient air. Together, the two pumps allowed air sampling between 1 – 1.2 L min⁻¹, with the excess going to an exhaust.

CRM-LSCE system characterization

Several tests were performed before, during and after the campaign to assess the performance of the instrument operated during the whole campaign. The PTR-MS was calibrated at the beginning and at the end of the field campaign showing a good stability under dry and wet conditions (slope of 15.5 ± 0.9 (1 σ)). Regular C1 measurements were made to check the stability of the initial pyrrole concentration all along the campaign. C1 was 70.7 ± 4.0 (1 σ) ppbv.

Small differences in humidity observed between C2 and C3 were considered while processing the raw data. In order to assess this correction, experiments were performed to assess the variability of C2 on humidity by contrasting the change in C2 ($\Delta C2$) for various changes in the m/z 37-to- m/z 19 ratio ($\Delta [m/z$ 37-to- m/z 19 ratios]), m/z 37 and m/z 19 being representative of $H_3O^+(H_2O)$ and H_3O^+ , respectively, and their ratio being proportional to humidity. During this campaign, three humidity tests were performed by varying the humidity in ambient air samples. These tests were in good agreement and showed a linear relationship between $\Delta C2$ (ppbv) and $\Delta (m/z$ 37-to- m/z 19 ratio) with a slope of -89.18. The correction was applied as discussed in Michoud et al. (2015).

An important assumption to derive R_{OH} from Eq. (3.2) is to operate the instrument under pseudo-first-order conditions (i.e. [pyrrole] \gg [OH]), which is not the case with current CRM instruments. To determine the correction factor for the deviation from pseudo-first order kinetics, injections of known concentrations of isoprene ($k_{\text{Isoprene}+OH} = 1 \times 10^{-10}$ cm³ molecule⁻¹ s⁻¹, 1- 120 ppbv) and α -pinene ($k_{\alpha\text{-pinene}+OH} = 5.33 \times 10^{-11}$ cm³ molecule⁻¹ s⁻¹, 3 -190 ppbv) (Atkinson, 1985) were performed before and after the field campaign since they represent the dominant species in this forest ecosystem.

The measured OH reactivity obtained from these tests were then compared to the expected OH reactivity, leading to a correction factor that is dependent on the pyrrole-to-OH ratio. Therefore, standard OH reactivity experiments were conducted at different pyrrole-to-OH ratios ranging from 1.7 to 4.0, which encompass the ratio observed most of the time during the campaign. These tests led to a correction factor $(F) = -0.52 \times (\text{pyrrole-to-OH}) + 3.38$.

NO mixing ratios were lower than 0.5 ppbv (corresponding to the detection limit of the NO_x monitor deployed during LANDEX) most of the time for the measurement time periods used in this study, and no correction was applied for the spurious formation of OH from the HO₂+NO reaction. Similarly, for NO₂, no correction was applied due to the low ambient mixing ratio of 1.1 ± 0.8 ppbv. Regarding O₃, no dependency was seen for LSCE-CRM, based on previous experiments (Fuchs et al., 2017). Therefore, no correction was applied. The correction (D) on the reactivity values due to the dilution was around 1.46 during the campaign. Thus, the total OH reactivity may be expressed as:

$$R_{\text{OH final}} = \left[\frac{C_3 - C_2(\text{corrected})}{C_1 - C_3} \cdot kp \cdot C_1 \right] \cdot F \cdot D \quad (3.3)$$

Finally, overall uncertainties were estimated at 35 % (1σ) for the measured OH reactivity by the CRM (Zannoni et al., 2015).

Table 3.2 reports a summary of the corrections resulting from our tests and their impact on measurements. As shown in **Table 3.2**, the application of (F), for the deviation from pseudo-first order kinetics, induces the largest correction, with an absolute increase of 10.4 s^{-1} on average. Furthermore, this factor (F) has the largest relative uncertainty, with $\pm 36 \%$, against $\pm 2 \%$ for the humidity correction factor.

Table 3.2: Summary of corrections applied to raw reactivity data for LSCE-CRM. Correction coefficients are obtained from experiments performed before, during and after the field campaign.

Correction	Correction factor	Mean absolute change in OH reactivity (s ⁻¹)
Humidity changes between C2 and C3	-89.18±2.16	+ 2.2
Not operating the CRM under pseudo first order conditions	$F = (-0.52 \pm 0.20) \times (\text{pyrrole-to-OH}) + (3.38 \pm 0.60)$	+ 10.4
Dilution	D = 1.46	+ 2.6

3.2.2.2. UL-FAGE reactivity instrument

Total OH reactivity was measured at a different location inside canopy, from the 13th to the 19th of July, using LP-LIF instrument of the PC2A laboratory (UL-FAGE reactivity) which has already been used in several intercomparisons and field campaigns (Hansen et al., 2015; Fuchs et al., 2017). The reactivity instrument comprises three parts: the photolysis laser, the photolysis cell (reaction tube) and the LIF cell based on FAGE technique. The photolysis laser is used to generate OH radicals within the photolysis cell by the photolysis of O₃ in the presence of water vapor. The photolysis laser is a YAG laser (Brilliant EaZy, QUANTEL) with a doubling and a quadrupling stage providing a radiation at 266 nm with a repetition rate of 1 Hz. The photolysis beam is aligned at the center of the photolysis cell and is expanded (diameter of 4 cm reaching the entrance of the cell) by two lenses (a concave one f=-25 mm and a convex with f=150 mm) in order to increase the photolysis volume and to limit the diffusion effect in the photolysis cell.

This photolysis cell is a stainless steel cylinder with an internal diameter of 5 cm and a length of 48 cm. It presents two openings on the opposite sides, one as an entrance for the air samples and the second connected to a pressure monitor (Keller PAA-41) to measure the pressure inside the cell. Ambient or humid clean air (which is produced by passing a fraction of dry synthetic air, purity of 99.8 %, through a water bubbler, called zero air and used to determine the OH

reactivity in the absence of reacting species) are injected through the first opening with a small flow of synthetic air (about 20 mL min⁻¹) passing through an ozone generator (Scientech) to generate an ozone concentration of about 50 ppbv in the total flow. The ozone concentration is chosen to produce enough OH to have a good signal/noise ratio, but kept low enough to minimize the reactions involving O₃.

The sampled mixture is continuously pumped into the FAGE cell (pressure=2.3 Torr) by a dry pump (Edwards, GX 600L) and the LIF signal is collected by a CPM (Perkin Elmer MP1982), an acquisition card and a LabView program. The detection of the fluorescence is synchronized with the photolysis laser pulses by delay generators. The OH reactivity time resolution was at the minimum set to be 30 s, meaning that each OH decay was accumulated over 30 photolysis laser shots and fitted by a mono-exponential decay. The number of sets of 30 photolysis laser shots accumulated is determined according to the signal to noise ratio (S/N) obtained (typically 4). When the S/N is lower, a set of 30 OH decays is added to the previous one and so on until reaching the criteria. As the reactivity and the humidity vary along the day, S/N varies as a function of the ambient species concentrations. In order to check the consistency of the OH reactivity measurements, the well-known (CO + OH) reaction rate constant was measured. Different CO concentrations, from 4 × 10¹³ to 3.7 × 10¹⁴ cm⁻³ in humid zero air are injected in the photolysis cell, allowing to measure reactivities ranging from 10 to 90 s⁻¹ and to determine (using a linear regression: R² = 0.97) a rate constant of k_{CO + OH} = (2.45 ± 0.11) × 10⁻¹³ cm³ molecule⁻¹ s⁻¹, in good agreement with the reference value of 2.31 × 10⁻¹³ cm³ molecule⁻¹ s⁻¹ (Atkinson et al., 2006) at room temperature. Under these conditions (absence of NO), HO₂ formed by the reaction of CO+OH is not recycled in OH and does not interfere with the measurements of OH.

Ambient air sampling

Ambient air was sampled in the canopy at about 5 m through a PFA line (diameter = 1/2 inches), a PFA filter being installed at the entrance of the tube to minimize particle or dust sampling. In the photolysis cell, the gas flow was sampled at 7.5 L min⁻¹ and the pressure was approximately 740 Torr, i.e. lower than the atmospheric pressure due to the restriction of the flow through the Teflon sampling line. For the reactivity measurements in zero air, synthetic air from a cylinder was used and a part of the flow (2 L min⁻¹) passed through a bubbler filled with Milli-Q water to reach a water vapor concentration of about 3000 ppmv.

R_{OH, zero} analysis

In order to determine the OH reactivity in ambient air $R_{OH,ambient}$, it is necessary to subtract the reactivity measured using "zero air" $R_{OH,zero}$, which represents the OH losses not related to the gas phase reactions with the species of interest, present in the ambient air, but due to wall losses, diffusion, etc., to the reactivity measured.

$$R_{OH,ambient} = R_{OH,measured} - R_{OH,zero} \quad (3.4)$$

Zero air tests were conducted twice a day (in the morning and at night) when the reactivity measurements took place. The average of all experiments performed with zero air leads to a mean value of $R_{OH,zero} = (4.0 \pm 0.5) \text{ s}^{-1}$. This value was therefore chosen as k_{zero} for the whole campaign.

3.2.3. Ancillary measurements and corresponding locations

Measurements of VOCs (**Table 3.3**) were performed at different locations (**Fig. 3.1**) by a proton transfer reaction-mass spectrometer (PTR-MS) and four on-line gas chromatographic (GC) instruments. Ozone scrubbers (Copper tube impregnated with KI) and particle filters were added to the inlets of all GC sampling lines. Losses of BVOCs in these ozone scrubbers were investigated under similar sampling conditions in the absence and presence of O_3 (Mermet et al., 2019). The scrubbers exhibited less than 5 % losses for most non-oxygenated BVOCs, whereas in the presence of ozone, losses were relatively higher for some BVOCs, but remained lower than 15 % (lower than 5 % for α - and β -pinene). High flow rates were applied in the sampling lines: 1 L min^{-1} for GC instruments and 10 L min^{-1} for the PTR-MS, therefore, the contact time between ambient BVOCs and the particle filters was extremely short and no significant losses are expected.

GC-BVOC1 is a gas chromatograph coupled to a flame ionization detector (airmoVOC C6-C12, Chromatotec), used by LSCE to monitor high-carbon VOCs (C6- C12) at 12 m height with a time resolution of 30 min. Sampling was undertaken for 10 min. The instrument sampled ambient air with a flow rate of 60 mL min^{-1} . Once injected, the sample passed through a capture tube containing the adsorbent Carbotrap C, for VOCs preconcentration at room temperature; the capture tube is then heated up to $380 \text{ }^\circ\text{C}$ and the sample is introduced into the separating column (MXT30CE, id = 0.28 mm, length = 30 m, film thickness = $1 \text{ }\mu\text{m}$), with hydrogen as

the carrier gas. During the campaign, calibrations were performed with a certified standard containing a mixture of 16 VOCs (including 8 terpenes) at a concentration level of 2 ppbv (National Physical Laboratory, Teddington, Middlesex, UK). Three calibrations were performed 3 times (at the beginning, in the middle and at the end of the campaign). As they were showing reproducible results (within 5 % for all the terpenes except cineole), a mean response factor per VOC was used to calibrate the measurements. Note that limonene and cymene had close retention times which lead to overlapping peaks and for this reason, only the sum of both compounds has been reported. For further details, refer to Gros et al. (2011). The sampling was done using a 13-m long sulfinert heated line (1/8") connected to an external pump for continuous flushing.

GC-BVOC2 is an online thermodesorber system (Markes Unity 1) coupled to a GC-FID (Agilent). It was used to monitor 20 C₅-C₁₅ BVOCs, including isoprene, α - and β -pinene, carenes and β -caryophyllene at the 6 m height with a time resolution of 90 min. Ambient air was sampled at a flow rate of 20 mL min⁻¹ for 60 min through a sorbent trap (Carbotrap B) held at 20 °C by a Peltier cooling system. The sample was thermally desorbed at 325 °C and injected into a BPX5 columns (60 m \times 0.25 mm \times 1 μ m) using helium as carrier gas (30 min). Calibrations were performed at the beginning, in the middle and at the end of the campaign with a certified standard mixture (NPL, Teddington, Middlesex, UK, 2014) containing 33 VOCs (including 4 BVOCs: α - pinene, β -pinene, limonene and isoprene) at a concentration of 4 ppbv each. The sampling was done using a 10 m long sulfinert line (1/4") heated at 55 °C and connected to an external pump to adjust the sampling flow rate at 1 L min⁻¹. The method has been optimized in terms of temperature of the thermodesorption, the column, the sampling volume and sampling line including a scrubber. Tests showed a low response for some compounds (i.e. sabinene, terpinolene, ...), however, the most abundant compounds, were well measured. More details about the optimization and the tests performed can be found in Mermet et al. (2019).

GC-NMHC is an online GC equipped with two columns and a dual FID system (Perkin Elmer[®]) that was described in detail elsewhere (Badol et al., 2004). It was used to monitor 65 C₂-C₁₄ non-methane hydrocarbons (NMHC), including alkanes, alkenes, alkynes and aromatics, at the 12 m height with a time resolution of 90 min. Ambient air was sampled at a flow of 15 mL min⁻¹ for 40 min through a Nafion membrane and through a sorbent trap (Carbotrap B and Carbosieve III) held at -30°C by a Peltier cooling system. The trap was thermodesorbed at 300°C and the sample was introduced in the GC system. The chromatographic separation was

performed using two capillary columns with a switching facility. The first column used to separate C₆-C₁₄ compounds was a CP-Sil 5 CB (50 m × 0.25 mm × 1 μm), while the second column for C₂-C₅ compounds was a plot Al₂O₃/Na₂SO₄ (50 m × 0.32 mm × 5 μm). Helium was used as carrier gas. Calibrations were performed at the beginning, middle and end of the campaign with a certified standard mixture (National Physical Laboratory (NPL), Teddington, Middlesex, UK, 2016) containing 30 VOCs at a concentration level of 4 ppbv each. The sampling was done using a 13 m long sulfinert line (1/4") heated at 55 °C and connected to an external pump for continuous flushing at 2 L min⁻¹.

GC-OVOC is an online GC-FID (Perkin Elmer[®]) used to monitor 16 C₃-C₇ oxygenated VOCs (OVOCs), including aldehydes, ketones, alcohols, ethers, esters and six NMHCs (BVOCs and aromatics). A detailed description can be found in Roukos et al. (2009). The measurements were performed at the 12 m height with a time resolution of 90 min. Ambient air was sampled at a flow rate of 15 mL min⁻¹ for 40 min through a water trap (cold finger, -30 °C) and a quartz tube filled with Carbopack B and Carbopack X held at 12.5 °C. VOCs were thermally desorbed at 280 °C and injected into a CP-Lowox columns (30 m × 0.53 mm × 10 μm) using helium as carrier gas. Calibrations were performed 3 times during the campaign using a standard mixture (Apel Riemeer, 2016) containing 15 compounds. This mixture was diluted with humidified zero air (RH = 50 %) to reach VOC levels of 3-4 ppbv. The sampling was done with the same sampling system than the GC-NMHC. Sulfinert material chosen for all GCs sampling lines and used in LSCE-CRM sampling system, is recommended by ACTRIS, 2014. High flows were set in the lines (residence time of less than 8 s), that were heated up to 50 °C to minimize the losses of potential reactive species. Filters and scrubbers were changed twice for the GC-BVOC1 and one time for the other GC instruments.

The PTR-MS (PTR-QiToFMS, IONICON Analytic GmbH) sequentially measured trace gases at 4 levels (L1=12 m, L2=10 m, L3=8 m, L4=6 m) with a cycle of 30 minutes (6 min at each level and 6 min of zero air). The drift tube was operated at a pressure of 3.8 mbar, a temperature of 70 °C and a E/N ratio of 131 Td. Four identical sampling lines of 15 meters were used to sample ambient air at each height. The lines (PFA, 1/4" OD) were heated at 50 °C and were constantly flushed at 10 L min⁻¹ using an additional pump and rotameters. Indeed, Kim et al. (2009) tested losses of β-caryophyllene in similar operating conditions. Authors varied the temperature from zero to 40 °C showing that losses of β -caryophyllene are negligible above 20 °C. The residence time was lower than 2 s.

Teflon filters were used to filter particles at the entrance of the sampling lines. The PTR-MS drawn ambient air at a flow rate of 300 mL min^{-1} from the different lines using Teflon solenoid valves and a 1.5-meter-long inlet (PEEK, 1/16" OD) heated at $60 \text{ }^{\circ}\text{C}$. Zero air was generated using a Gas Calibration Unit (GCU, IONICON Analytic GmbH) containing a catalytic oven and connected to L1. Ion transmissions were calibrated over the 21-147 Da mass range every 3 days using the GCU unit and a certified calibration mixture provided by IONICON (15 compounds at approximately 1 ppmv, including methanol, acetaldehyde, acetone, aromatic compounds, chlorobenzenes, etc.). Measurements of methanol, acetonitrile, acetaldehyde, acetone, isoprene, methacrolein + methylvinylketone + fragment ISOPOOH, methylethylketone, sum of monoterpenes, sum of sesquiterpenes, acetic acid, nopinone and pinonaldehyde, obtained from levels 1 and 4 corresponding to the levels where OH reactivity measurements were performed, are discussed in this article. Sesquiterpenes, acetic acid, nopinone and pinonaldehyde measurements were not corrected for fragmentation in the drift tube and we cannot rule out the detection of other isomers at these masses such as glycolaldehyde for acetic acid measurements.

Inorganic traces gases (O_3 and NO_x) were measured by commercial analyzers deployed by IMT-Lille-Douai (L1 to L4 for O_3) and EPOC (L4 for NO_x). The nitrate radical (NO_3) was measured using an IBB-CEAS instrument (Incoherent Broad Band Cavity Absorption Spectroscopy) developed by the LISA (Laboratoire Interdisciplinaire des Systèmes Atmosphériques) research group and deployed for the first time on site during the LANDEX field campaign. Meteorological parameters such as temperature, relative humidity, global radiation, vertical turbulence, wind speed and wind direction were monitored using sensors already available at the ICOS measurement site. More details can be found in Kammer et al. (2018).

Table 3.3: Summary of supporting measurements performed inside and/or above the canopy.

Instrument	Resolution time (min)	Measured species
GC-BVOC1	30	α -pinene, β -pinene, myrcene, Δ -carene, p-cimene, limonene + cymene, cineol
GC-BVOC2	90	α -pinene, β -pinene, myrcene, limonene, camphene, sabinene, α -phellandrene, 3-carene, p-cymene, ocimene, 1,8-cineol(=eucalyptol), α -terpinene, γ -terpinene, terpinolene, isoprene [§] , nopinone [§] , linalool [§] , β -caryophyllene [§]
		<i>§ These compounds were not considered in the calculation of the weighted k rate constant for the reaction of monoterpenes with OH. Nopinone, linalool and β-caryophyllene had relatively low contributions to OH reactivity, that were around 0.02, 0.37 and 0.18 s⁻¹ on average, respectively. Maximum contributions did not exceed 2.2 s⁻¹ for linalool and 1.5 s⁻¹ for β-caryophyllene.</i>
GC-NMHC	90	ethane, ethylene, propane, propene, isobutane, butane, acetylene, trans-2-butene, cis-2-butene, isopentane, pentane, 1,3-butadiene, 2-methyl-butene + 1-pentene, cyclopentene or terpene, hexene, hexane, 2,4-dimethylpentane, benzene, 3,3-dimethylpentane, 2-methylhexane, isooctane, heptane, toluene, octane, ethylbenzene, m+p-xylenes, styrene, o-xylene, nonane, 4-ethyltoluene, 2-ethyltoluene, 1,2,4-trimethylbenzene, 1,3-dichlorobenzene, undecane, isopropylbenzene, n-propylbenzene
GC-OVOC	90	furan, tert-amylmethylether, 2-butanone, ethanol, isopropanol, butanol+2-hexanone, benzaldehyde
PTR- MS	6 min every 30 min at each level	methanol, acetonitrile, acetaldehyde, acetone, isoprene, methacrolein+methylvinylketone+fragment ISOPOOH, methylethylketone, sum of monoterpenes, sum of sesquiterpenes*, acetic acid*, [#] nopinone*, pinonaldehyde*
		<i>*Fragmentation was not corrected for and reported concentrations are likely lower limits,</i>
		<i>[#]potential interferences from isomeric compounds such as glycolaldehyde</i>

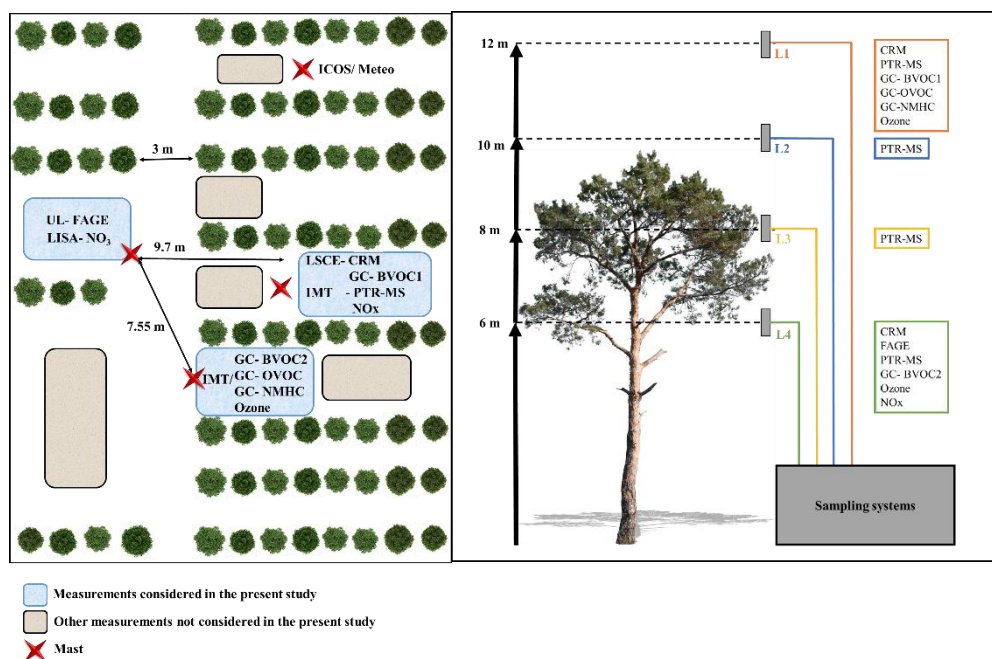


Figure 3.1: Deployment of instruments at the measurement site. Left side (a) corresponds to the horizontal deployment, the right side (b) represents the different sampling levels with respect to the average trees' height.

3.2.4. OH reactivity calculation

As different instruments were available to quantify VOCs at different locations (**Fig. 3.1** and **Table 3.3**), a selection of the data used to calculate the OH reactivity (Eq. (3.1)) was made, based on data availability for the different instruments (**Table S3.1**). Since measurements from the PTR-MS instrument covers the whole campaign and were performed at the same heights than OH reactivity measurements, these measurements, including methanol, acetonitrile, acetaldehyde, acetone, isoprene, methacrolein+methylvinylketone+fragment ISOPOOH, methylethylketone and the sum of monoterpenes, were selected to calculate the OH reactivity and to evaluate the potential missing OH reactivity at both levels. However, using only this set of data presents some limitations:

- 1) The PTR-MS only measures the sum of monoterpenes (m/z 137+ m/z 81), while the detected monoterpenes are speciated by the GCs.
- 2) It was observed that isoprene measurements at m/z 69 were disturbed by the fragmentation of some terpenic species (Kari et al., 2018; Tani, 2013), which led to a significant impact on the night-time measurements when isoprene was low.

- 3) Some NMHCs and OVOCs measured by GC at the 12 m height were not measured by the PTR-MS. This requires to assess the contribution of these additional species to the total OH reactivity for both heights.

To overcome these limitations, several tests were made to evaluate the reliability of the PTR-MS data to calculate the OH reactivity.

- 1) In order to use the sum of monoterpenes measured by the PTR-MS to calculate the total OH reactivity, it was necessary to determine a weighted rate constant for the reaction of monoterpenes with OH. After checking the consistency between the two GCs (BVOC1 and BVOC2, see supplementary material S3.2) and comparing the sum of monoterpenes measured by each GC to the PTR-MS measurements (simultaneous measurements at the same height - **Fig. S3.2.b** and **c**), the weighted rate constant was calculated as the sum of the rate constants of each OH + monoterpene reaction multiplied by the average contribution of each specific monoterpene to the sum. The contribution of each monoterpene was calculated by dividing the concentration of the 8 speciated monoterpenes that were measured by both GCs (α -pinene, β -pinene, myrcene, Δ -carene, p-cimene, limonene + cymene, cineol), by their total concentration (Fig. S3(a)). The weighted rate constant is defined as:

$$k_{OH,weighted} = \sum_i k_{OH+X_i} F_i \quad (3.5)$$

Where F_i represents the contribution of each individual species to the total concentration of monoterpenes, and k_{OH+X_i} the corresponding rate constant with OH. The reaction rate constant of the different trace species quantified in the field were taken from the literature (Atkinson et al., 2006). The OH reactivity of monoterpenes measured by PTR-MS was calculated according to the following equation:

$$R_{OH-monoterpenes} = k_{OH,weighted} \times [MT] \quad (3.6)$$

where [MT] represents the sum of monoterpenes measured by PTR-MS.

The calculated OH reactivity inside and above the canopy (**Fig. S3.3.b** and **e**) from (i) the use of the weighted OH reaction rate constant and the total concentration of monoterpenes measured by GC and (ii) the use of individual species and their associated rate constants are in

relatively good agreement as shown by the scatter plots. A slope of 0.95, $R^2=0.99$ has been obtained using the monoterpenes measured with the GC-BVOC1 at 12 m (**Fig. S3.3.c**); a slope of 0.94, $R^2=1.0$ using the same 8 compounds commonly monitored with GC-BVOC1 but measured at 6 m with GC-BVOC2 (**Fig. S3.3.f**). When replacing the total concentration of monoterpenes measured by GCs by the PTR-MS measurements, slopes of 1.22 and 1.19 were obtained at 12 and 6 m heights, respectively (**Fig. S3.3.d** and **S3.3.g**). This increase in the slope values is likely due to an underestimation of the total monoterpene concentration by the GC instruments since these instruments only measured the most abundant monoterpenes present at the site. We cannot rule out a small overestimation of monoterpenes by the PTR-MS since fragments from other species such as sesquiterpenes could be detected at the monoterpene m/z . However, this interference should be negligible due to the low concentration of ambient sesquiterpenes. These results are in agreement with the scatter plots comparing the sum of monoterpenes measured by GC and by PTR-MS (slopes of 1.29 and 1.10 at the 12 and 6 m heights, respectively, see **Fig. S3.2.b** and **S3.2.c**). Thus, the PTR-MS data was used to calculate the OH reactivity from monoterpenes for both heights, with a weighted reaction rate constant of $76 \times 10^{-12} \text{ cm}^3 \text{ molecule}^{-1} \text{ s}^{-1}$ at the 12 m height and $77.9 \times 10^{-12} \text{ cm}^3 \text{ molecule}^{-1} \text{ s}^{-1}$ at the 6 m height.

- 2) As mentioned above, some monoterpenes have been observed to fragment at m/z 69.0704, which would result in an interference for isoprene measurements. In order to use the PTR-MS data for this species (only instrument measuring isoprene at 12 m), the contribution of monoterpenes to m/z 69 has been estimated by comparing the GC-BVOC2 and PTR-MS measurements of isoprene performed at 6 m. This comparison showed that approximately 4 % of the monoterpene concentration measured by PTR-MS had to be subtracted to that measured at m/z 69.0704 to get a good agreement between the PTR-MS and GC-BVOC2 measurements of isoprene as shown in **Fig. S3.4.a**.
- 3) A large range of NMHCs and OVOCs were measured at the 12 m height only by GC-NMHC and GC-OVOC (**Table 3.3**). Butanol (from SMPS exhausts) was also checked and found to be negligible at 12 m and highly and rapidly variable at 6 m (short peaks). NO and NO₂ were only measured at the 6 m height. Mean NO mixing ratio was below the LOD for the measurement period and NO₂ was around 1.1 ± 0.8 ppbv on average. Thus, it was chosen not to take these species into account in the OH reactivity calculations. However, sensitivity tests were performed, in order to compute their relative contribution to OH reactivity (See sect. 3.3.5 and **Fig. S3.5** and **S3.6**). Regarding methane and carbon monoxide, an estimation

was made seen their relatively low k reaction rate coefficient with OH, taking mean concentration values of 2000 ppbv and 150 ppbv, respectively.

The above limitations are summarized in **Table S3.7** (supplementary material). Data used to calculate the OH reactivity has been resampled to 1 min, based on a linear interpolation (see **Table 3.3** for the respective time resolution of the different instruments). This time base was chosen to be comparable to the time resolution of the UL-FAGE reactivity instrument, in order to keep the dynamics in OH reactivity variability.

3.3. Results

Measurements performed by both instruments at the same location were first compared to evaluate the agreement between the two techniques. The horizontal variability of total OH reactivity (same height) is also discussed. A second part of the result section is dedicated to a description of the total OH reactivity variability on the vertical scale with some meteorological parameters. A comparison between measured and calculated OH reactivity for both the 6 and 12 m heights as well as a description of the BVOC contributions to the measured OH reactivity are then presented. Finally, we discuss the missing OH reactivity observed during this campaign and its possible origin.

3.3.1. Comparison between LSCE-CRM and UL-FAGE measurements

3.3.1.1. Inter-comparison of LSCE-CRM and UL-FAGE OH reactivity measurements at the same location

The direct comparison between LSCE-CRM and UL-FAGE reactivity instruments was done during the last two days of the campaign (**Fig. 3.2**). The sampling line of LSCE-CRM was moved to be collocated to the sampling line of UL-FAGE. Both instruments were measuring at the same location inside the canopy level, above the UL container at 5 m height. In this way the comparison between both instruments was made possible while minimizing the variabilities which could be related to the heterogeneity in ambient air. During this period, similar values were measured by both instruments, as shown in **Fig. 3.2**, with total OH reactivity ranging between 5 and 69 s^{-1} . The lowest values were observed during day-time.

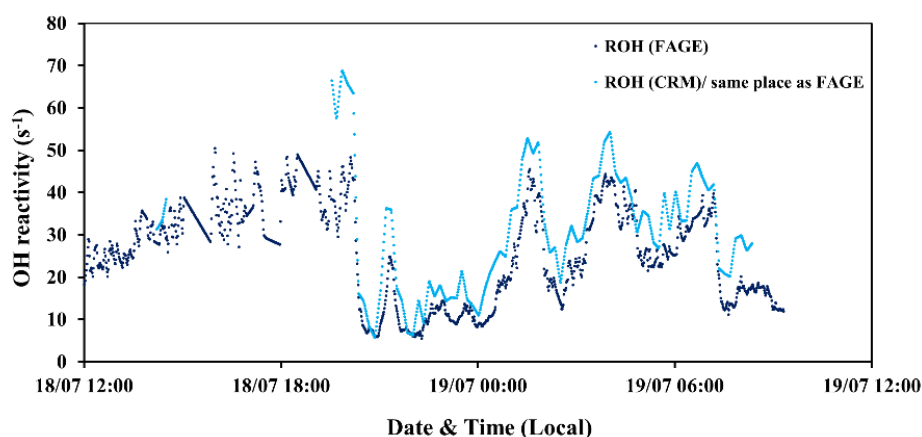


Figure 3.2: Time series of total OH reactivity measured by UL-FAGE (dark blue) and LSCE-CRM (light blue) instruments from the 18th to 19th of July 2017, at the same location inside canopy.

When OH reactivity measurements from LSCE-CRM are plotted versus OH reactivity measurements from UL-FAGE (**Fig. 3.3**), the linear regression exhibits an R^2 of 0.87. Applying the orthogonal distance regression technique, which takes into account the uncertainties on LSCE-CRM and UL-FAGE measurements, a slope of 1.28 ± 0.02 and an intercept of $0.96 \pm 0.23 \text{ s}^{-1}$ are obtained. These results indicate that both instruments respond similarly (within 30 %) to changes in OH reactivity with a relatively low intercept. This intercept can be due to an overestimation of LSCE-CRM measurements or an underestimation of the UL-FAGE measurements or both. Nevertheless, it stays within the range of uncertainties. It is worth noting that the higher points of OH reactivity observed in **Fig. 3.3** correspond to the period from 19h30 to 20h (local time) of the 18th, July when the ambient relative humidity increased quickly by 20 % which was not seen on previous days and may have interfered with LSCE-CRM OH reactivity measurements.

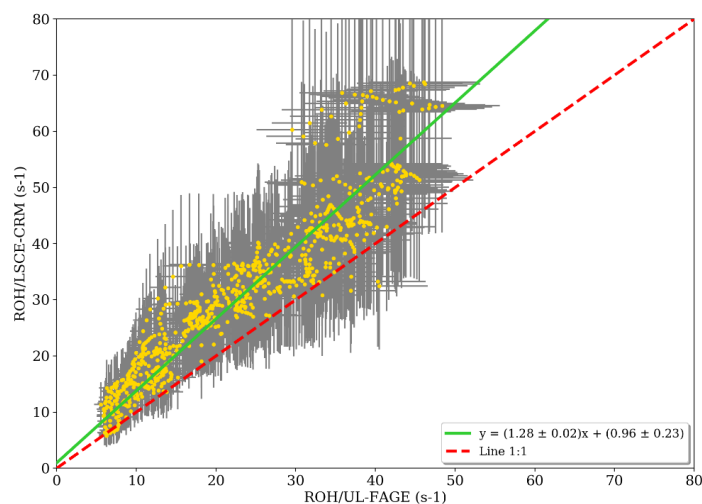


Figure 3.3: Measured reactivity by LSCE- CRM instrument as function of the measured reactivity by UL- FAGE when both instruments were measuring at the same location within the canopy (data resampled with a time resolution of 1 min). Errors bars represent the overall systematic uncertainty (1σ) that is around 15 % and 35 % for LP- LIF and the CRM, respectively.

3.3.1.2. LSCE-CRM and UL-FAGE OH reactivity measurements at two different locations inside the canopy

From the 13th to 15th midday of July (1st period) and from the 17th midday to 18th midday (2nd period), the two instruments were sampling at the same height but from different horizontal locations within the canopy (with sequential within/above canopy measurements for CRM during the second period). The horizontal distance between the two inlets was around 10 m as shown in **Fig. 3.1**. Similar trends in OH reactivity are seen between the two datasets, even if the first period was associated with a clear vertical stratification (**Fig. 3.4**, green frame), leading to higher concentrations of monoterpenes within the canopy, whereas the second period was characterized by a higher vertical mixing (mean $u^* \approx 0.3 \text{ m s}^{-1}$), leading to similar concentrations of monoterpenes at the two heights (**Fig. 3.4**, dashed green-yellow frame). These observations are linked to the vertical turbulence which influences BVOC levels inside and above the canopy, resulting in a more or less important vertical stratification, as discussed in section 3.3.2.

At the same height but different horizontal locations, the linear regression of LSCE- CRM data plotted against UL-FAGE data (not shown) indicates a good correlation with an R^2 of 0.87. Using the orthogonal distance regression technique, both data sets show a good agreement with a slope of 1.28 ± 0.02 and an intercept of -2.63 ± 0.15 (1st and 2nd period). Compared to the

results at the same location (vertical and horizontal), the slopes and the correlation coefficients are the same. Only the intercept differs slightly (-2.63 ± 0.15 compared to 0.96 ± 0.23). This change could be related to air mass inhomogeneities which could be systematically less reactive at one location compared to the other one. From these observations, we can conclude that reactivity measurements performed at different horizontal locations are consistent and that inhomogeneities in ambient air can lead to differences on the order of several s^{-1} .

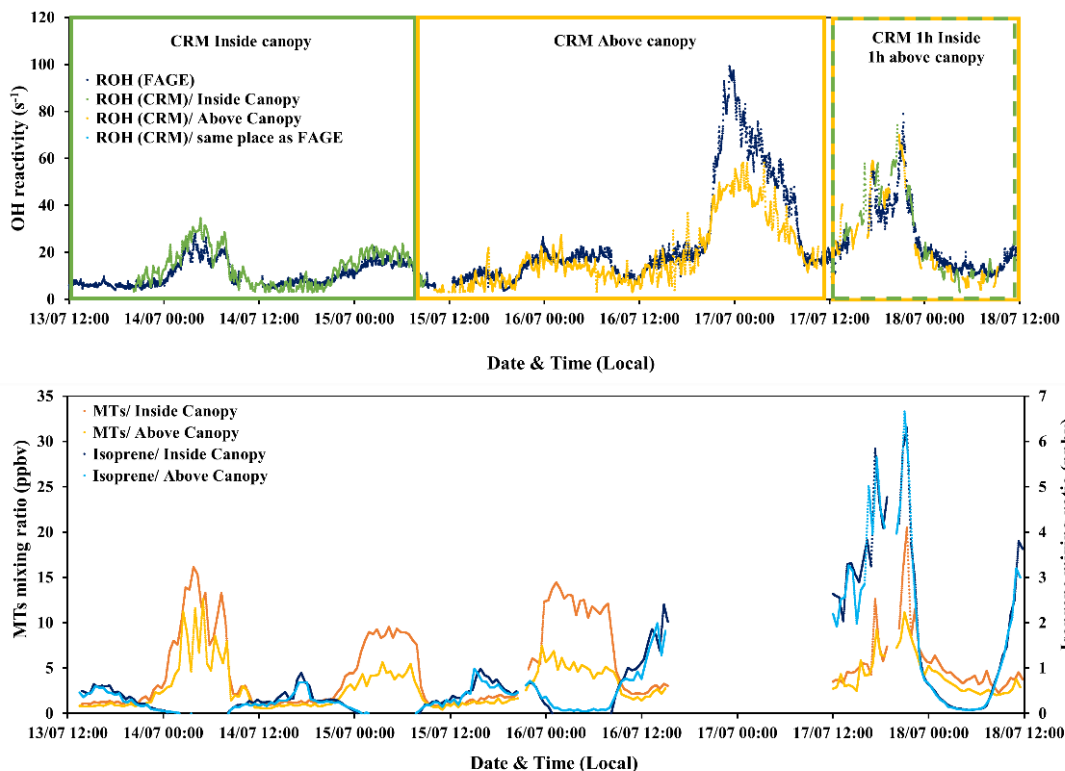


Figure 3.4: (a) Time series of total OH reactivity measured by UL-FAGE and LSCE-CRM instruments from the 13th to 18th of July 2017 (upper graph). Dark blue symbols represent the measured reactivity by UL-FAGE, green and yellow symbols represent the measured reactivity by LSCE-CRM inside and above the canopy, respectively. The lower graph (b) shows the sum of monoterpenes (MTs) and isoprene measured with the PTR-MS, in the field for the same period. Dark blue and light blue dots correspond to isoprene concentrations at 6 and 12 m height, respectively. Orange and yellow dots represent monoterpenes concentrations at 6 and 12 m height, respectively.

3.3.2. Measured OH reactivity and meteorological parameters

Figures 3.5.a and **3.5.b** show the variability of total OH reactivity measured inside and above the canopy by LSCE-CRM and UL-FAGE, together with global radiation, temperature and friction velocity. Considering the whole campaign, the measured OH reactivity at both heights shows a diurnal trend ranging between LOD (3 s^{-1}) and 99 s^{-1} inside canopy and between LOD and 70 s^{-1} above canopy, with maximum values of OH reactivity mostly recorded during nights. These OH reactivity levels are larger than other measurements performed in forested environments (Dusanter and Stevens, 2017; Yang et al., 2016), with maximum values of approximately 80 s^{-1} reported for the tropical forest (Edwards et al., 2013).

The predominant meteorological parameter that had a role on OH reactivity levels was the friction velocity. It traduces the vertical turbulence intensity that was high during the day (mean day-time $u^* \geq 0.4 \text{ m s}^{-1}$) and lower during most nights (mean night-time $u^* \leq 0.2 \text{ m s}^{-1}$). Based on this parameter, night-time OH reactivity (between 21:00 and 06:00 local time of the next day) was separated in 3 classes:

- Class S: Stable atmospheric conditions (mean $u^* \leq 0.2 \text{ m s}^{-1}$)
- Class U: Unstable atmospheric conditions (mean $u^* \geq 0.4 \text{ m s}^{-1}$)
- Class SU: Stable and unstable conditions during the same night.

The lower vertical turbulence intensity, observed for “S” nights as well as for some hours of “SU” nights, led to a lower boundary layer (Saraiva and Krusche, 2013) and a significant nocturnal stratification within the canopy, with higher concentrations of primary compounds within the canopy (**Fig. 3.5.c**). These stable atmospheric conditions, together with no photochemical oxidation of BVOCs, resulted in higher total OH reactivity during these nights due to higher BVOCs concentration even though their emissions are lower compared to day-time (Simon et al., 1994).

Another important parameter to consider is ambient temperature, which is known to enhance BVOCs emissions during the day when stomata are open, and which also plays a role for night-time emissions due to permeation, even though stomata are closed in the dark (Simon et al., 1994). Considering temperature, 2 sub-classes can be added to night-time OH reactivity classification: the sub-class “Wn” corresponding to warm nights (nights with mean $T \geq 18.9 \text{ }^\circ\text{C}$ which is the mean night-time temperature over the whole campaign) and the sub-class “Cn”

that includes cooler nights (nights with mean $T < 18.9\text{ }^{\circ}\text{C}$). Thus, comparing “S/Wn” nights and “S/Cn” nights, it can be seen that, for similar turbulent conditions, the magnitude of the measured OH reactivity was temperature dependent. Indeed, higher OH reactivity values were linked to higher ambient temperatures: nights of the 4th-5th, 6th-7th and 16th-17th of July (S/Wn) were characterized by an average temperature of $21\text{ }^{\circ}\text{C}$ compared to $16.6\text{ }^{\circ}\text{C}$ for the nights with lower OH reactivity (S/Cn).

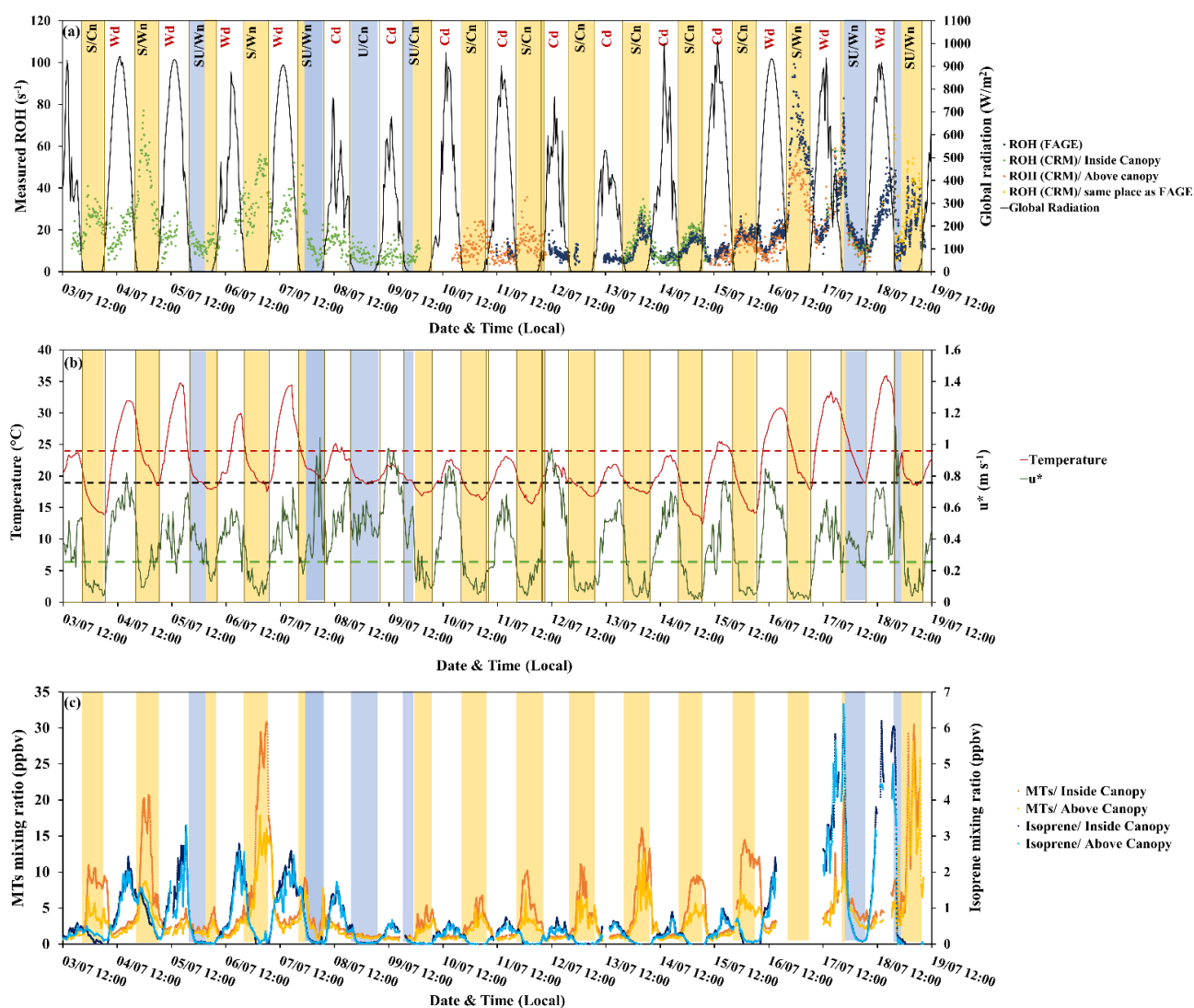


Figure 3.5: Variability of measured OH reactivity by LSCE-CRM and UL-FAGE, inside and above the canopy with (a) global radiation (black), (b) temperature (red), friction velocity (green) and with (c) monoterpenes and isoprene concentrations. Yellow stripes indicate stable night-time atmospheric conditions (S nights with mean $u^* \leq 0.2\text{ m s}^{-1}$) and blue stripes indicate unstable night-time conditions (U nights with mean $u^* \geq 0.4\text{ m s}^{-1}$). Class SU includes nights with stable and unstable atmospheric conditions (blue + yellow stripes). Wn and Wd stand for warm nights and warm days respectively. Cn and Cd stand for cooler nights and cooler days respectively. Red dashes and black dashes indicate the temperature thresholds to distinguish warm and cool days and nights, respectively. Green dashes indicate the friction velocity threshold to distinguish stable and unstable nights.

Regarding the period when measurements were done simultaneously at both heights (15th to 18th of July, LSCE-CRM above canopy and UL-FAGE within canopy), we can analyze the effect of turbulence on the above-within canopy differences. For the night of the 16th-17th of July (S/Wn) when the vertical turbulence was relatively low, total OH reactivity measured above the canopy (LSCE-CRM) was lower than the one measured inside the canopy by a mean factor of 1.6 (UL-FAGE reactivity) despite similar general trends. For the night of the 17th-18th of July (SU/Wn), stable atmospheric conditions started to settle at the beginning of the night (20h30 local time) inducing a similar stratification to that observed on the previous nights. However, this situation did not last the whole night since these stable conditions were disturbed by higher turbulences around 21h00. This led to a decrease in OH reactivity values going to similar levels inside and above the canopy. A similar event occurred during the night of the 18th-19th of July, where three OH reactivity peaks showed up, not correlated neither with variation of turbulence intensity nor with temperature changes. However, it is worth noting that during this night, an intense wind, rain and thunders occurred, which could have led to the observed bursts of BVOCs (Nakashima et al., 2013), leading to distinct peaks of BVOCs and total OH reactivity and thus relatively high total OH reactivity compared to other nights from the same class.

Total OH reactivity also increased during the day, although on a lower extent than during night-time, and reached a day-time maximum of up to 74.2 s⁻¹ inside the canopy and 69.9 s⁻¹ above the canopy, following the same trends than temperature and solar radiation. Temperature appeared to be an important driving factor of total OH reactivity during day-time hours, therefore, day-time OH reactivity was divided into 2 classes: Class “Wd” with warm conditions (mean day-time T ≥ 24 °C) and class “Cd” with cooler temperatures (mean day-time T < 24 °C) indicated on **Fig. 3.5**. The solar radiation also played a role on day-time OH reactivity since it is responsible of initiating the emission of some compounds like isoprene, that is light and temperature dependent. Thus with the first rays of sunlight, the emission and the concentration of isoprene increased leading to an increase in total OH reactivity.

Examining BVOC profiles (**Fig. 3.5.c**), we can see how the variability of primary BVOC concentrations can explain the day/night variability of total OH reactivity. Indeed, monoterpenes, which are the main emitted compounds in this ecosystem, were influenced by vertical turbulence and night-time temperature, exhibiting a diurnal profile with maxima during stable nights and minima during day-time. Under stable atmospheric conditions (class S), monoterpenes concentration started to increase at the beginning of the night (between 20h and

21h local time) corresponding to the time of the day when the turbulence intensity started to drop and the nocturnal boundary layer started to build up. Maximum mixing ratios were reached in the middle of the night, corresponding to a lower dilution in the atmosphere and a lower oxidation rate (low OH concentrations, nitrate radical mixing ratios lower than the LOD (3ppt/min) most of the time, and BVOC's chemistry with ozone generally slower than during day-time (Fuentes et al., 2002)). Finally, the monoterpenes concentration dropped as soon as the first sunlight radiations broke the stable nocturnal boundary layer inducing lower levels of OH reactivity. Under these conditions, the concentration of monoterpenes inside the canopy was higher than above the canopy, showing a clear stratification, consistent with differences seen on total OH reactivity at the different heights. On the contrary, during turbulent night hours (Class U and SU), the concentration of monoterpenes was lower inside the canopy and similar to that observed above, leading to lower and closer night-time OH reactivity at both measurements heights.

At the end, even though BVOC emissions are more intense during the day (Simon et al., 1994), the higher turbulence observed compared to night-time led to a faster mixing within the canopy and thus similar levels of isoprene and monoterpenes inside and above the canopy. These day-time levels were lower than those observed at night for monoterpenes and higher for isoprene, the latter being light and temperature dependent.

To conclude, these observations show that on one hand, lower turbulence inducing stable atmospheric conditions during the night explains the observed stratification in terms of monoterpenes levels and thus in terms of OH reactivity levels within the canopy, when on the other hand, higher turbulence during day-time leads to higher mixing within the canopy and a vertical homogeneity, with similar BVOCs concentrations and OH reactivity levels at both heights. Diurnal average values of total OH reactivity, for inside and above canopy measurements are given in **Table S3.9**.

3.3.3. Measured and calculated R_{OH} within and above the canopy

Figure 3.6 shows that there is a good co-variation of the measured total OH reactivity by the CRM instrument with the values calculated from the PTR-MS data (22- 24 % (2σ)). However, a certain fraction of the measured total OH reactivity remains unexplained by the considered compounds (**Table 3.3**). Diurnal variations of OH reactivity were observed within the canopy, during the major part of the campaign, with maximum values recorded during most nights and averages of $19.2 \pm 12.8 \text{ s}^{-1}$ and $19.3 \pm 16.3 \text{ s}^{-1}$ measured by the LSCE-CRM and UL-FAGE instruments, respectively. This diurnal cycle was also observed above canopy where the average total OH reactivity was $16.5 \pm 12.3 \text{ s}^{-1}$, which is higher than observations made in other temperate coniferous forests (Ramasamy et al., 2016) where the reported OH reactivity ranges from 4-13 s^{-1} (campaign average).

During the first part of the campaign (3rd – 10th of July), when the LSCE-CRM was measuring alone inside the canopy, total OH reactivity varied between LOD (3 s^{-1} at 3σ) and 76.9 s^{-1} , while the calculated reactivity ranged between 1.4 and 60 s^{-1} . During the second period (13th – 15th and 17th – 18th of July), similar maxima were recorded by the LSCE- CRM (74.2 s^{-1}) and the UL- FAGE instruments (78.9 s^{-1}), when both were measuring at two different locations within the canopy. Regarding the calculated OH reactivity, it varied between 2.6 and 59.3 s^{-1} . During this same period, the FAGE instrument measured alone within the canopy from the 15th to the 17th of July and recorded total OH reactivity values ranging between 3.6 and 99.2 s^{-1} , however the PTR-MS data were not taken into account for the period going from the 16th 15:00 to the 17th 12:00 due to an electrical failure. Finally, during the last two days (18th- 19th of July), total OH reactivity showed a particular behavior as mentioned in section 3.3.2. It started to increase in the afternoon, reached a maximum at the beginning of the night that was suddenly broken by turbulences and showed three peaks during the night corresponding to more stable conditions observed for both the measured and calculated reactivity.

Regarding above canopy measurements, the measured OH reactivity varied between LOD and 35.7 s^{-1} between the 10th and the 12th of July, whereas the calculated reactivity varied between 1.2 and 14.5 s^{-1} . A similar trend was observed for the second period of measurements performed above the canopy (15th - 18th of July) during which higher OH reactivity was recorded with a maximum of 69.9 s^{-1} , which is 1.7 times higher than the calculated OH reactivity (40.8 s^{-1}).

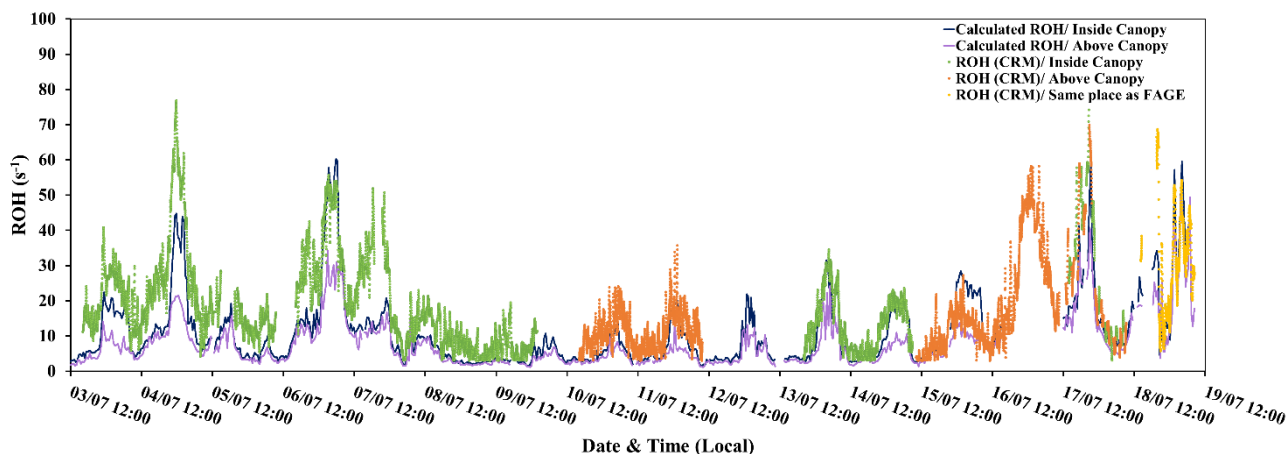


Figure 3.6: Variability of measured ROH (LSCE-CRM) and calculated ROH (PTR-MS) at 6 and 12 m height.

3.3.4. Contribution of VOCs (PTR-MS) to calculated OH reactivity within and above the canopy

Figure 3.7 shows the breakdown of trace gases to the calculated OH reactivity during day-time and night-time at the two heights, taking into account the whole measurement period (campaign average). We note that primary BVOCs (monoterpenes, isoprene) are by far the main contributors to the calculated OH reactivity, representing 92- 96 % of the calculated OH reactivity on average.

Monoterpenes exhibited the most prominent contribution to the calculated OH reactivity. These species had a similar contribution within and above the canopy, but significant differences between day-time (68- 65 %) and night-time (92- 89 %). Next to monoterpenes, isoprene had a maximum contribution during day-time and represented on average 25- 27 % of the calculated OH reactivity, followed by acetaldehyde (3 %) and MACR + MVK + ISOPOOH (2- 3 %) at both measurements heights. However, during night-time, isoprene accounted for only 4- 6 % of the OH reactivity measured within and above the canopy, acetaldehyde contributing for approximately 2 % and MACR + MVK + ISOPOOH around 1 %.

Thus, we can conclude that no substantial difference in the atmospheric chemical composition existed between the two sampling heights, even when we only consider stable nights (monoterpenes relative contribution is around 92 % inside and above the canopy).

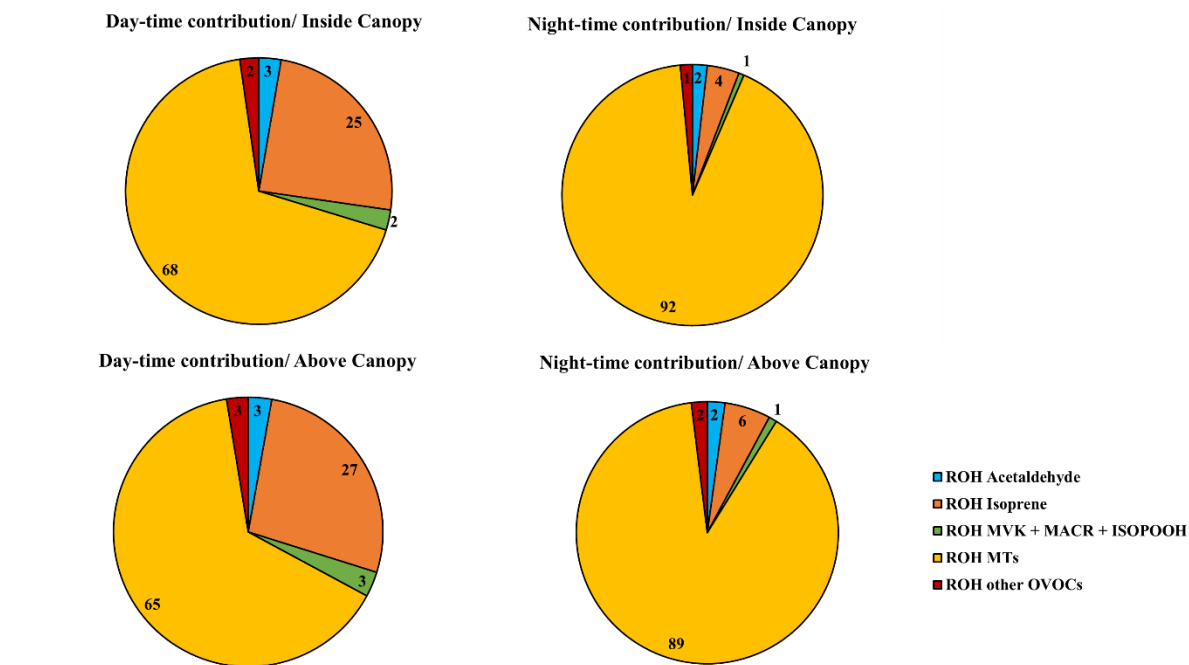


Figure 3.7: The components of calculated OH reactivity within and above the canopy during day-time and night-time. The compounds measured by the PTR-MS (Table 3.3) were used to calculate their relative contributions.

3.3.5. Description and investigation of potential missing OH reactivity during the LANDEX campaign

The missing OH reactivity was calculated as a difference between the total OH reactivity measured by LSCE-CRM, since it was operated over the whole campaign and at both heights, and the OH reactivity calculated from PTR-MS data. It is worth noting that a scatter plot of the LSCE-CRM and UL-FAGE data led to a slope of 1.28 and an intercept of 0.96 s^{-1} (section 3.3.1), indicating higher OH reactivity values measured by the CRM instrument. Considering OH reactivity values measured by the CRM instrument may therefore maximize the missing OH reactivity. In the following, the analysis on the missing OH reactivity was performed when it was higher than both the LOD of 3 s^{-1} (3σ) and 35% of the measured OH reactivity (uncertainty on the CRM measurements, see section 3.2.2).

Figure 3.8 shows a) the variability of the missing OH reactivity within and above the canopy, together with ambient temperature, b) friction velocity (red), and ozone mixing ratios within (yellow) and above (blue) the canopy. The ozone variability is discussed below as ozone chemistry can dominate night-time chemistry of BVOCs observed at this site (α -pinene, β -pinene) (Fuentes et al., 2002; Kammer et al., 2018).

The concentration of OH was 4.2×10^6 molecules cm^{-3} on average during day-time with a maximum of 4.3×10^7 molecules cm^{-3} and around 1.5×10^6 molecules cm^{-3} on average during night-time (data available between the 13th and the 19th, July). However, a potential artifact on OH radical's measurements leading to a possible overestimation of OH radical's concentrations, could not be ruled out. Regarding ozone, its mixing ratio showed a diurnal cycle with maximum values during the day (max ≈ 60 ppbv, mean ≈ 29 ppbv), that were similar within and above the canopy due to efficient mixing, and lower levels during nights, with an average of 18 ppbv inside canopy, while levels higher by 1 - 10 ppbv on average, above the canopy. Considering OH and O₃ average mixing ratios, the α -pinene lifetime was estimated to be 1.2 hours and 4 hours, respectively, during the day, and 3.6 hours and 5.8 hours, respectively, during the night. At maximum OH and O₃ mixing ratios during day-time, the α -pinene lifetime was reduced to 7.4 min and 2 hours, respectively. Thus, OH chemistry remained dominant compared to ozonolysis of main emitted compounds on this site (i.e. α -pinene). An article on the reactivity of monoterpenes with OH, ozone and nitrate for this campaign is in preparation (Kenneth Mermet, personal communication).

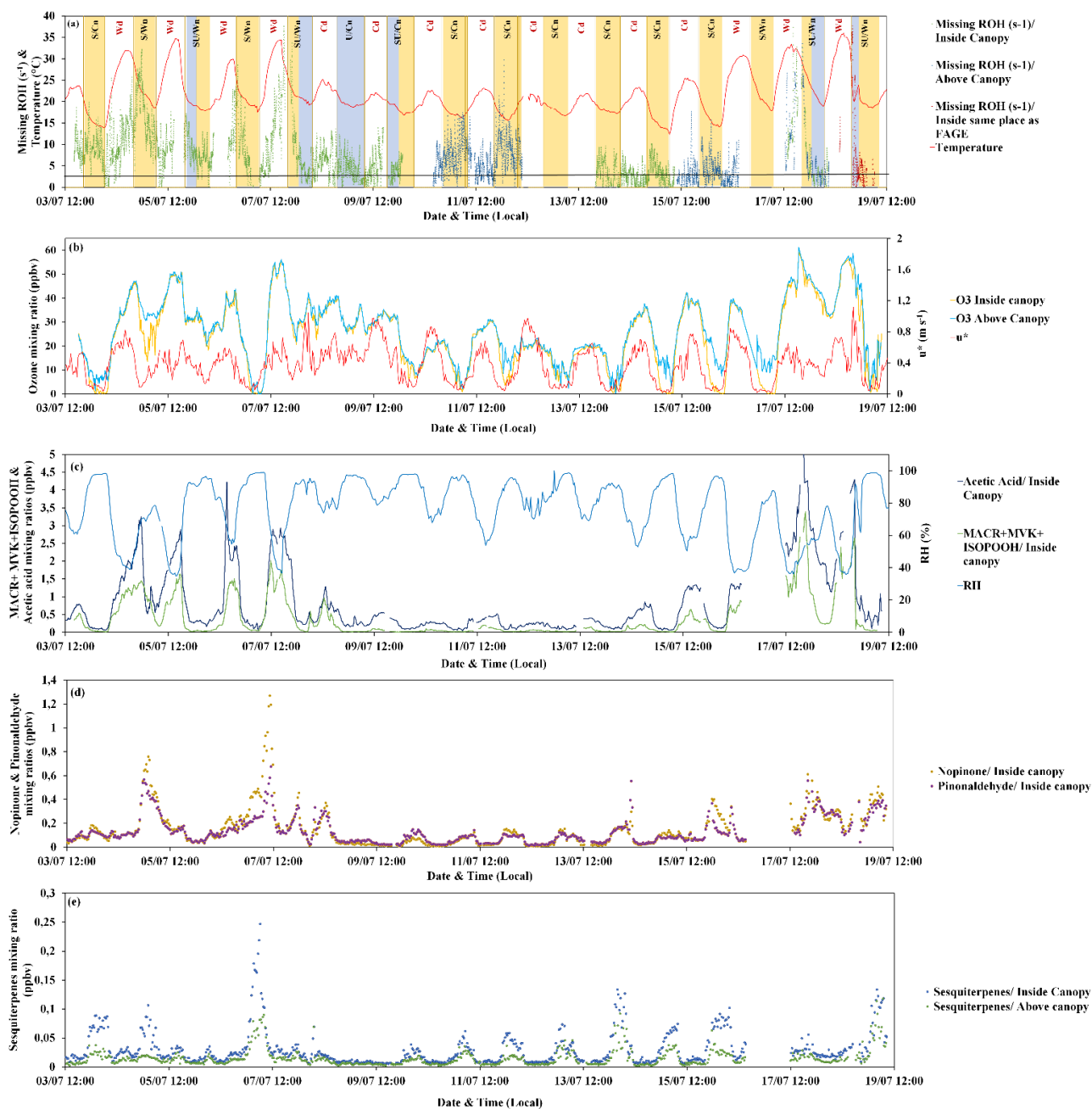


Figure 3.8: Missing OH reactivity inside and above the canopy together with (a) temperature, (b) friction velocity (red), ozone mixing ratios inside (yellow) and above (blue) the canopy, (c) relative humidity (clear blue), MACR+ MVK+ ISOPOOH (dark blue) and acetic acid (green) inside the canopy, (d) Nopinone (yellow) and pinonaldehyde (purple) inside the canopy and (e) sesquiterpenes inside (blue) and above (green) the canopy.

When comparing measurements of OH reactivity with calculations based on PTR-MS data (see **Table 3.3**), an average of 38 % (7.2 s^{-1}) and 48 % (6.1 s^{-1}), remained unexplained inside and above the canopy, respectively.

Considering other measurements performed inside the canopy (6 m) and not included in the OH reactivity calculations, such as NO, NO₂, ozone and butanol (leakage from SMPS), and assuming constant concentrations of CO (150 ppbv) and methane (2000 ppbv), their contribution can reach 3.0 s⁻¹ on average (maximum around 7 s⁻¹) at this level. This said, the mean missing OH reactivity was finally around 4.2 s⁻¹ (22 %) inside canopy for the whole measurement period.

Regarding other measurements performed above canopy, online chromatographic instruments (**Table 3.3**) provided information on other oxygenated VOCs (7 compounds) and non-methane hydrocarbons (36 compounds). These compounds could explain 0.48 s⁻¹ on average (0.43 s⁻¹ from NMHC and 0.05 s⁻¹ from OVOC measured by GC) of the missing OH reactivity between the 10th and the 12th of July. However, after the 14th of July, the GC measuring OVOC stopped working, but NMHCs alone could account for 0.5 s⁻¹ of missing OH reactivity on average. While O₃ was measured at 12 m, no NO_x measurement were performed at this height, however, their contribution at the 6 m height was 0.3 s⁻¹ on average, suggesting only a small contribution to the missing OH reactivity. Methane and CO were also considered, assuming the same mixing ratios as inside. Finally, looking at butanol measured by the PTR-MS at the 12 m height, a maximum mean contribution of 0.3 s⁻¹ was assessed for the nights of 10th-11th of July. Hence, considering OVOCs, NMHC, O₃, CO, CH₄ and butanol, the mean missing OH reactivity above the canopy level was around 4.3 s⁻¹ (33 %). However, this missing fraction exhibited a diurnal variability at both heights, that is worth discussing in details. A summary of mean missing OH reactivity values at both heights, is presented in **Table 3.4**.

Table 3.4: Summary of the measured OH reactivity and the missing OH reactivity inside and above the canopy, during the day and the night, taking into account only PTR-MS data or all the data available at each height for OH reactivity calculations. These averages are calculated for the periods when CRM, PTR-MS and others instruments data are available.

	Mean Measured ROH (s^{-1})	Mean Missing ROH considering PTRQi-ToFMS data (s^{-1})	Mean Missing ROH considering PTRQi- ToFMS data + other measurements (s^{-1})
Inside	19.1	7.2	4.2
Day	16.8	7.3	4.7
Night	22.0	7.1	3.6
Stable cool nights	20.5	5.5	< LOD
Stable warm nights	41.6	10.7	6.7
Unstable cool nights	7.9	4.5	< LOD
Unstable warm nights	13.5	6.8	3.6
Above	12.8	6.1	4.3
Day	10.7	5.1	3.3
Night	15.5	7.5	5.6
Stable cool nights	14.8	7.5	5.7
Stable warm nights	—	—	—
Unstable cool nights	—	—	—
Unstable warm nights	20.5	7.1	5.2

- Day-time missing OH reactivity

Analyzing the behavior of missing OH reactivity during day-time for inside canopy measurements, **Fig. 3.9** shows that it increases exponentially with temperature. Indeed, the average missing OH reactivity was around $7.5 s^{-1}$ for “Wd” days, after taking into account other available measurements at this height (NO, NO₂, O₃, butanol and estimated CO and CH₄), whereas no missing reactivity was seen for cooler days (< LOD). As reported in Di Carlo et al. (2004), the missing OH reactivity was fitted with an equation usually used to describe

temperature-dependent emissions of monoterpenes (Guenther et al., 1993): $E(T) = E(293) \exp(\beta(T-293))$, where $E(T)$ and $E(293)$ represent the emission rate at a given temperature T and at 293K, respectively. In this equation, $E(T)$ was substituted to $MROH(T)$ and $E(293)$ by $MROH(293)$ with $MROH$ representing the missing OH reactivity (Hansen et al., 2014). The value of β determined from the fit of the data for the 6 m height (day-time), is around 0.17, higher than the values attributed to monoterpenes emissions from vegetation (0.057 to 0.144 K^{-1}). Higher β -values were also obtained by Mao et al. (2012), Hansen et al. (2014) and Kaiser et al. (2016), where they suggested that day-time missing reactivity is mostly linked to secondary oxidation products. However, the use of β factor must be made with caution, as the missing OH reactivity can be influenced by processes that do not affect BVOCs emissions (i.e. the boundary layer height and the vertical mixing). Furthermore, we cannot exclude the possibility of light and temperature dependent emissions. Indeed, Kaiser et al. (2016) also investigated the temperature dependency of day-time missing OH reactivity in an isoprene-dominated forest, reporting that part of the missing emissions could be characterized by a light and temperature dependence, knowing that temperature increases with increasing solar radiation. Regarding above canopy, most measurements were performed during cool days. Thus, it was not possible to analyze the temperature dependence of above canopy day-time missing OH reactivity.

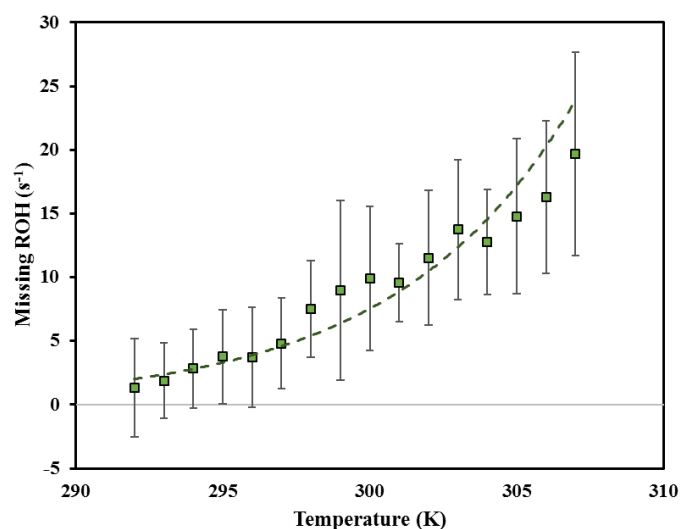


Figure 3.9: Day-time missing OH reactivity binned by ambient temperature for the 6 m height for temperatures ranging from 292 and 308 K. Error bars represent the standard deviation on missing OH reactivity calculated for each temperature bin.

Another way to investigate the origin of missing OH reactivity is by examining its co-variability with compounds such as acetic acid as well as MACR+MVK+ISOPOOH, knowing that MACR and MVK are oxidation products of isoprene. First, for higher day-time missing OH reactivity observed for Wd days (within and above the canopy), **Fig. 3.8.c** shows that the missing reactivity increases with acetic acid (mixing ratio up to 5 ppbv). Acetic acid can be directly emitted by the trees and the soil (Kesselmeier and Staudt, 1999) and could also be an oxidation product of BVOCs, including isoprene (Paulot et al., 2011). This compound showed a diurnal cycle similar to that of isoprene (**Fig. 3.5.c**), and was not used to calculate the OH reactivity. Despite its relatively low reactivity with OH, this compound showed a maximum calculated OH reactivity during Wd days that was, on average (0.07 s^{-1}), 4 times higher than that of Cd days. Thus it could explain, with other compounds exhibiting a similar temporal behavior, part of the missing OH reactivity seen during warm days. MACR+ MVK + ISOPOOH showed a general trend with higher values during the day and lower values during the night, suggesting that oxidation products of isoprene could be responsible of the day-time missing OH reactivity. These levels were generally higher for Wd days than for Cd reflecting a higher yield of secondary products and a more intense photochemistry during warm days.

- **Night-time missing OH reactivity**

On average the highest night-time missing OH reactivity inside canopy (13.1 s^{-1}) was observed on the stable/ warm night of the 4th- 5th, July. Whereas, during stable/cool and unstable/warm nights, no significant missing OH reactivity was found ($< \text{LOD}$). Interestingly, the stable/warm night of the 6th-7th, July, did not show a significant missing OH reactivity, meaning that the missing fraction inside canopy during night, was not only influenced by meteorological parameters, even if, as shown before, BVOCs concentrations and total OH reactivity were. So what was the difference between these two nights with similar meteorological conditions?

Checking monoterpenes' oxidation products variabilities (nopinone and pinonaldehyde), both nights exhibited higher concentration levels of these species, however their contribution to OH reactivity remained relatively low, and did not exceed 1 s^{-1} , on average for both nights, keeping in mind that this is a lower limit of their contribution (since the reported measurements do not account for potential fragmentation in the PTR-MS). Thus, only a small fraction of the missing fraction can be explained by these species. Interestingly, isoprene, acetic acid and MVK+ MACR+ISOPOOH exhibited higher concentration levels during the night of the 4th- 5th, July,

which was not the case for the 6th-7th, July night. Indeed, these species marked relatively high nocturnal/ inside canopy levels. When looking at air masses backward trajectories (Fig. 3.10), the 4th-5th night was characterized by an air mass originally coming from the ocean, which spent at least 48 hours above the continent before reaching the site. This could have led to the enrichment of the air mass with species emitted by the widely spread Landes forests and their oxidation products. Thus, the significant missing OH reactivity observed during the mentioned night is likely related to unconsidered compounds of biogenic origin characterized by a similar behavior to that of isoprene, acetic acid and MVK+MACR+ISOPROOH, which accumulated in the stable nocturnal boundary layer. In contrast, air masses spent approximately 12-18 hours above the continent during the 6th-7th of July, with more time above the ocean. Marine air masses are generally known to be clean, with relatively low levels of reactive species. Even though, the night of the 5th-6th, July shows similar air mass backward trajectories to the night of the 4th-5th, the higher turbulence during this night prevents the accumulation of reactive species (including long-lived oxidation products) due to a higher boundary layer height, lowering the reactivity and the missing OH reactivity (Fig. 3.10).

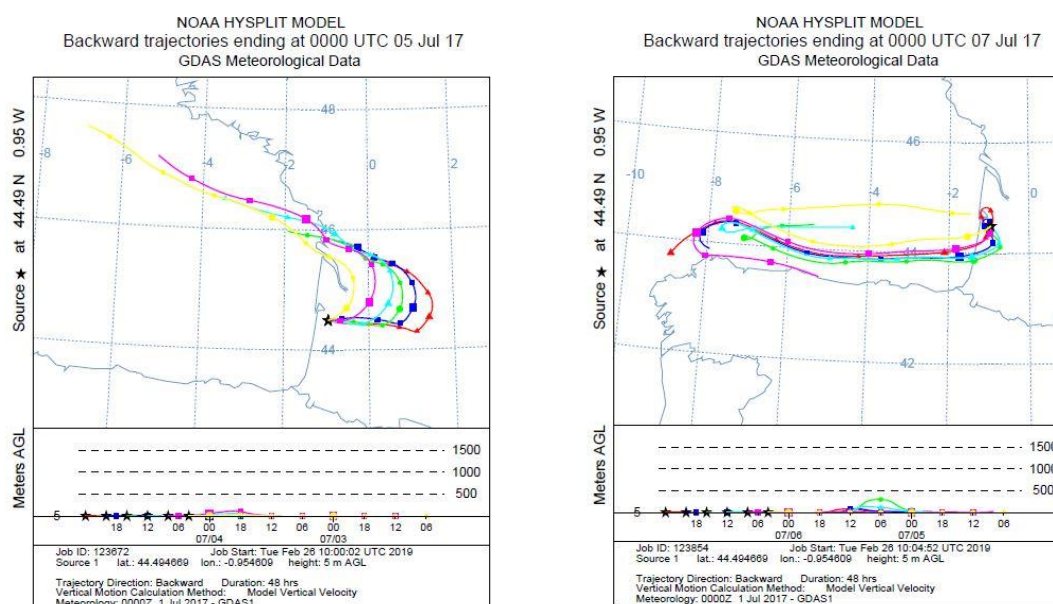


Figure 3.10: Air masses backward trajectories for the 4th-5th and the 6th- 7th, July nights. Red lines represent air masses arriving around mid-night UTC (around 02:00 local time), to the site. The time difference between 2 points is 6 hours.

Regarding above canopy measurements (10th- 12th and 15th- 18th, July), the night-time average missing OH reactivity was 5.6 s⁻¹ (all the nights were characterized by stable/ cool atmospheric conditions). Monoterpenes oxidation products had similar concentration levels above and inside canopy. Their maximum contribution was around 0.4 s⁻¹ on average for the SU/W night of the 17th-18th, July. Therefore, these monoterpenes night-time oxidation products are only responsible for a small fraction of the missing OH reactivity observed above canopy during the night. Sesquiterpenes (SQT) exhibited a similar temporal trend than monoterpenes, showing higher mixing ratios during night-time. Interestingly, sesquiterpenes mixing ratios were higher inside the canopy compared to above and the difference was significant during stable nights. O₃ mixing ratios during these nights decreased to very low levels. Plotting the ratio SQT(above)/MTs(above) with the ratio SQT(inside)/MTs(inside) shows a good linear correlation with a slope of 0.73 and an R² of 0.6. Knowing that sesquiterpenes are highly reactive with ozone (Ciccioli et al., 1999), which can dominate the chemistry during dark hours, this observation suggests that a larger fraction of these species ($\approx 30\%$) could be consumed by ozonolysis above canopy, leading to the formation of unidentified secondary compounds. However, sesquiterpenes were present at relatively low concentrations (max of 0.25 ppbv and 0.11 ppbv, inside and above canopy, respectively). Assuming that all sesquiterpenes are β -caryophyllene and considering that 30 % are transformed into first generation oxidation products through ozonolysis reactions, the maximum mixing ratio of these products would be around 0.07 ppbv each assuming a yield of 1. However, it was reported by Winterhalter et al. (2009) that oxidation products of β -caryophyllene were much less reactive (100 times) than their precursor. Thus, the contribution of sesquiterpenes night-time oxidation products to the missing OH reactivity is likely negligible.

Finally, it is worth noting that Holzinger et al. (2005) reported the emission of highly reactive BVOCs in a coniferous forest, which is 6-30 times the emission of monoterpenes in the studied Ponderosa pine forest. This large fraction of BVOCs is subject to oxidation by ozone and OH leading to unidentified, non-accounted for secondary molecules. These oxidation products can participate to the growth of new particles. Indeed, new particle formation episodes were recently reported on this site (Kammer et al., 2018).

To summarize, higher day-time missing OH reactivity was observed for warm days (Wd), inside and above the canopy, exhibiting a dependency on temperature profiles and showing that trace gases leading to the missing OH reactivity could be linked to an enhancement of primary species as well as secondary products formation. Regarding night-time missing OH reactivity,

higher levels were seen for the stable and warm night of the 4th-5th, July, showing that these conditions could have been favorable for the accumulation of long-lived species (primary and secondary species) during the transport of the air mass from nearby forests.

3.4. Conclusion

During summer 2017, total OH reactivity measurements were conducted as part of the LANDEX field campaign, in the Landes maritime pine forest (France). During this campaign, two instruments (LSCE-CRM and UL-FAGE) were deployed to measure total OH reactivity inside and above the canopy as well as at two different locations inside the canopy level. The comparison between both instruments, based on measurements done at the same location at the end of the campaign, showed a good agreement within instruments uncertainties (slope of 1.28 on a linear correlation plot). Measuring at two different locations demonstrated a good horizontal homogeneity inside the canopy, even during episodes of vertical stratification that was observed during some nights.

Total OH reactivity recorded an average of 19.2 s⁻¹ at 6 m height, 1.2 times higher than that observed above the canopy level at 12 m height. It varied similarly at both heights, following a diurnal cycle with two maxima, one during day-time following isoprene's profile and a higher one during night-time when monoterpenes concentrations reached their maxima. The later were the main emitted compounds in this forest ecosystem.

The variability of BVOC concentrations and OH reactivity were strongly dependant on meteorological parameters. Day-time OH reactivity was linked to ambient temperatures and light, two parameters governing the emissions of temperature and/ or light dependent compounds (like isoprene), whereas night-time OH reactivity was influenced by night-time temperatures and vertical turbulence intensity. Indeed, low turbulence, high temperature and lower oxidation rates than during day-time, led to higher concentrations of monoterpenes and thus higher OH reactivity during stable and warm nights. In addition, higher differences in BVOCs levels and total OH reactivity were observed between the two studied heights particularly during stable nights.

Furthermore, monoterpenes showed to be the main contributors to total OH reactivity during both day-time and night-time. These species accounted for more than 60 % of the OH reactivity during day-time, followed by isoprene (25- 27 %), acetaldehyde (3%) and MACR+ MVK+

ISOPOOH (2- 3 %). However, the contributions of isoprene and OVOCs were much lower at both levels during the night, leading to a higher contribution of monoterpenes, which was slightly more important inside the canopy level due to the stratified conditions.

An investigation of the missing OH reactivity indicated averages of 22 % and 33 %, inside and above the canopy, respectively, over the whole campaign, when comparing the measured OH reactivity to the calculated one from PTR-MS and other available measurements. However, it showed some diurnal variability at both heights. During day-time, higher missing OH reactivity was observed on warmer days inside and above the canopy. Plotted against temperature, inside canopy missing OH reactivity showed a dependency on temperature. The analysis suggested that the missing OH reactivity may be due to unmeasured primary emitted compounds and oxidation products. In this context, OH reactivity measurements from a *Pinus pinaster* Aiton branch enclosure, could be of great interest to verify the contribution of unaccounted/unmeasured BVOCs emissions to OH reactivity as done by Kim et al. (2011), for red oak and white pine branch enclosures. Furthermore, higher levels of isoprene oxidation products on warmer days also suggest that the missing reactivity could be due to the formation of unmeasured oxidation products. Regarding the night-time period, the highest missing OH reactivity was found inside canopy for the 4th-5th, July night. This night was characterized by higher levels of isoprene and its oxidation products, compared to the night of the 6th-7th, July with similar atmospheric conditions. Air masses backward trajectories showed a continental origin for this night, suggesting that species, emitted by the largely spread Landes forest, could have been imported to the site and accumulated due to the stable nocturnal boundary layer. These species, unmeasured by the deployed analytical instruments and hence not considered in OH reactivity calculations, could explain the higher missing OH fraction for the 4th-5th, July night. The investigation of sesquiterpenes and monoterpenes oxidation products (nopinone and pinonaldehyde) measured by PTR-MS highlighted their small contribution in terms of OH reactivity. They only explained a small fraction of the observed missing OH reactivity inside and above canopy during night. Finally, seen the time needed and the data required, no modeling study was performed, however, it would be interesting to run a box model in order to get more insights into the origin of the missing OH reactivity.

Data availability: Data is available upon request to the corresponding author.

Authors contribution: S. Bsaibes and F. Truong set up and carried out OH reactivity measurements with the LSCE-CRM. M. Al Ajami, C. Schoemaeker, S. Batut and C. Hecquet set up and carried out OH reactivity measurements with the UL-FAGE instrument. K. Mermet, T. Léornadis, S. Sauvage and N. Locoge carried out GC-BVOC2, GC-OVOCs and GC-NMHCs measurements and provided analyzed data. V. Gros provided GC-BVOC1 analyzed data. S. Dusanter carried out PTR-MS measurements and provided the corresponding data. J. Kammer and P.-M. Flaud provided NO_x data and meteorological parameters. E. Villenave, E. Perraudin and P.-M. Flaud have coordinated the LANDEX project and field campaign. S. Bsaibes prepared the manuscript with the co-authors contribution, mainly M. Al Ajami, C. Schoemaeker, D. Dusanter, and V. Gros.

Acknowledgements: This study was supported by the European Union's Horizon 2020 research and innovation program under the Marie-Sklodowska-Curie grant agreement No 674911-IMPACT, ADEME- LANDEX and the CNRS. The authors want to acknowledge the Bilos ICOS team for meteorological data and site availability and Ineris for sharing their mobile laboratory. We would like to thank S. Schramm, D. Baisnée and R. Sarda-Esteve for their help during the installation of the PTR-Quad-MS and the GC-FID. We are also thankful to J.-Y. Peterschmitt for his help in the Orthogonal Distance regression technique using Python. The PC2A and SAGE participation was supported by the French ANR agency under contract no. ANR-11-LabX-0005-01 CaPPA (Chemical and Physical Properties of the Atmosphere), the Région Hauts-de-France, the Ministère de l'Enseignement Supérieur et de la Recherche (CPER Climibio) and the European Fund for Regional Economic Development.

Competing interest: The authors declare that they have no conflict of interest

Conclusion chapitre 3

Les mesures réalisées dans une forêt de pins maritimes au sud de la France, montrent une variabilité diurne de la réactivité OH, sur les deux niveaux de mesure, avec des maxima de nuit arrivant jusqu'à 99 s^{-1} dans la canopée et 70 s^{-1} au-dessus de la canopée, des niveaux parmi les plus élevés en milieux forestiers. Cette variabilité diurne s'est révélée similaire à celle des composés majoritairement émis dans cet écosystème : les monoterpènes. En effet, et sous l'influence de la couche limite plus basse durant les nuits stables, où la turbulence verticale est relativement faible (moyenne $u^* \leq 0.2 \text{ m s}^{-1}$), les monoterpènes se trouvaient plus concentrés, même s'ils présentent de moindres émissions par rapport au jour, conduisant à une réactivité OH plus élevée la nuit. Ils sont les principaux contributeurs à la réactivité OH avec des niveaux similaires durant le jour ou la nuit, dans et au-dessus de la canopée. Pas de différence significative, en terme de composition chimique, a été trouvée dans et au-dessus de la canopée. La comparaison de la réactivité mesurée à celle calculée, en se basant sur les composés individuellement mesurés aux deux niveaux, révèle une réactivité manquante de 22% et 33% en moyenne, dans et au-dessus de la canopée, respectivement. Cependant, cette réactivité manquante montre aussi une certaine variabilité diurne intéressante à discuter : durant le jour, une réactivité manquante plus importante a été trouvée pour les jours les plus chauds, ce qui suggère que la fraction qui manque est apparemment due à des composés dont la présence est favorisée par des températures plus hautes. La corrélation entre réactivité manquante et température, a révélé qu'elle est due, non seulement à des émissions primaires renforcées par la chaleur, mais aussi, à la présence de produits d'oxydation secondaires, dont la formation est accentuée par les hautes températures. Durant la nuit, la réactivité manquante la plus importante, été obtenue pour la nuit du 4-5 juillet, une nuit stable et chaude. Cependant, une autre nuit montre des conditions météorologiques similaires sans observer une différence significative entre la réactivité mesurée et celle calculée. L'origine des masses d'air pour cette nuit du 4-5 juillet, calculée à partir des rétro-trajectoires, révèle des masses d'air continentales, ayant passé 48 h au moins au-dessus des forêts environnantes, transportant avec elles des émissions primaires et leurs produits secondaires de longue durée de vie. Apparemment, les conditions stables de la nuit du 4-5 juillet s'avèrent favorables à l'accumulation de ces composés dans la basse couche limite nocturne. Dans ce contexte, des mesures de réactivité OH en sortie d'une chambre dynamique d'une branche de pin maritime, aiderait certainement à avoir une idée plus claire sur l'origine de la réactivité manquante. L'utilisation d'un modèle de chimie atmosphérique serait aussi une approche complémentaire, pour ce type d'étude, afin de

mieux comprendre les processus prenant lieu dans et au-dessus de la canopée ainsi que les origines potentielles de la fraction manquante.

4. Characterization of total OH reactivity in a rapeseed field: Results from the COV³ER experiment in April 2017

Introduction chapitre 4

Suite au développement technique au laboratoire, la CRM a été déployée dans une première campagne de mesures, dont les conditions expérimentales et les résultats sont présentés dans ce chapitre.

Organisée dans le cadre du projet ADEME-COV³ER, une collaboration entre l'INRA-ECOSYS et le LSCE, une campagne de mesures a eu lieu dans un champ de Colza, à Grignon, Sud-Ouest de Paris, durant la période de floraison (Avril 2017). L'objectif principal était de caractériser les composés organiques volatils (COVs) et leur réactivité OH à l'échelle de la culture comme étant une source agricole, ainsi qu'en air ambiant. Dans ce contexte, un jeune brin de colza, non fleuri, a été sélectionné pour installer une chambre dynamique, pendant à peu près un mois. Des mesures de réactivité OH ont été effectuées par CRM, en entrée et en sortie de la chambre. Des mesures complémentaires de composés organiques volatils (COVs, méthane) ainsi que d'autres espèces inorganiques (NOx, CO) ont été réalisées, afin de calculer une réactivité attendue, en se basant sur les concentrations de ces espèces et leurs constantes cinétiques de réaction avec le radical OH.

Characterization of total OH reactivity in a rapeseed field: Results from the COV³ER experiment in April 2017

Sandy Bsaibes¹, Valérie Gros¹, François Truong¹, Christophe Boissard^{1,2}, Dominique Baisnée¹, Roland Sarda-Esteve¹, Nora Zannoni^{1,3}, Florence Lafouge⁴, Raluca Ciuraru⁴, Pauline Buysse⁴, Julien Kammer^{1,5}, Lais Gonzaga Gomez⁴, Benjamin Loubet⁴

¹ Laboratoire des Sciences du Climat et de l'Environnement, LSCE, UMR CNRS-CEA-UVSQ, IPSL, Gif-sur-Yvette, Île-de-France, 91191, France

² Université de Paris, 75013, France

³ Now: Max-Planck Institute for Chemistry, Hahn-Meitner-Weg 1, 55128 Mainz, Germany

⁴ Institut national de recherche pour l'agriculture, l'alimentation et l'environnement, INRAe, UMR INRAe-AgroPariTech, Université Paris Saclay, Route de la Ferme, 78850 Thiverval-Grignon, France

⁵ Now: Department of Chemistry and Environmental Research Institute, University College Cork, Cork, Ireland

Correspondence to: Sandy Bsaibes (sandy.bsaibes@gmail.com)

Valérie Gros (valerie.gros@lsce.ipsl.fr)

Abstract

Croplands remain poorly studied ecosystems in terms of total hydroxyl radical (OH) reactivity, compared to forests. As part of the COV³ER project, total OH reactivity (ROH), defined as the total loss rate of OH due to its reaction with reactive species in the atmosphere, was characterized in a rapeseed field (Grignon- France) during the blooming season in April 2017. Measurements were performed in a dynamic chamber as well as in ambient air using the Comparative Reactivity Method (CRM). Complementary measurements of organic (including a proton transfer reaction – time of flight – quadrupole ion - mass spectrometry, PTRQI-ToFMS) and inorganic compounds were also performed in order to calculate the expected OH reactivity and evaluate the missing fraction. Measured ROH varied diurnally in the dynamic chamber ($mROH_{\text{chamber}}$) with maxima around 20 to 30 s^{-1} at mid-day and minima during dark hours, following the variability of the enclosed branch VOC_{rapeseed} , which is light and temperature-dependent. Oxygenated VOCs were the major compounds emitted by the rapeseed crop. However, in terms of contribution to OH reactivity, isoprene accounted for 40 % during day-time, followed by acetaldehyde (21 %) and monoterpenes (18 %). The comparison between $mROH_{\text{chamber}}$ and calculated ROH ($cROH_{\text{chamber}}$) exhibited little or no difference during dark hours, whereas a maximum difference appeared around mid-day, highlighting a significant

missing fraction (46 % on average during day-time) mainly related to biogenic temperature and/or light dependent emissions.

Keywords: OH reactivity, Biogenic VOCs, CRM-PTRMS, PTRQi-ToFMS, crops

4.1. Introduction

Up to 10^4 - 10^5 of different organic species have been identified so far in the Earth's atmosphere and this figure may only represent a small fraction of the number actually present (Goldstein and Galbally, 2007). They arise from anthropogenic and natural sources; the latter emissions being dominant (90%) on the global scale (Guenther, 1995). Once emitted in the atmosphere, volatile organic compounds (VOCs) are transformed by photochemical processes, leading to the formation of harmful secondary pollutants such as ozone (O_3) and secondary organic aerosols (SOAs), which have serious impact on human health and the environment. The major depletion route of atmospheric VOCs is via reaction with OH radicals, representing the main tropospheric oxidant during day-time (Helmig et al., 2009).

Natural sources of VOCs include forests, agricultural lands, grasslands, shrubs, biomass burning and oceans (De Gouw and Warneke, 2007). They are involved in growth, reproduction and defense mechanisms of the plant and they play an important role in the allelopathic interactions (Laothawornkitkul et al., 2009). It has been reported that biogenic VOCs (BVOCs) chemical composition and emission rates are linked to internal factors to the plant like genetics and biochemical processes. They can be affected by abiotic and biotic external factors such as temperature, radiation, water availability and interactions with other living species (Kesselmeier and Staudt, 1999; Penuelas and Llusia, 2001). Biogenic VOCs exhibit a large chemical diversity. They include terpenoids, which are dominant in the global atmosphere (isoprene, monoterpenes, sesquiterpenes, ...), oxygenated VOCs (OVOCs such as methanol, acetone, acetaldehyde, formaldehyde, ...) and other classes such as sulfur and nitrogen containing compounds, organic halides, alkanes and alkenes (Guenther, 2013). All these compounds represent a strong potential sink for atmospheric oxidants and hence to the hydroxyl radical.

One way to characterize the overall sink of OH in a given environment and to evaluate the importance of atmospheric photochemistry is to measure total OH reactivity. Total OH reactivity is defined as the total loss rate of OH, which is the inverse of OH lifetime (s^{-1}). It represents the sum of the reaction frequencies with OH of all chemicals, calculated as the product of each compound concentration by the compound coefficient rate of reaction with OH (Williams and Brune, 2015). Measurements of total OH reactivity have been performed using Laser Induced Fluorescence systems (pump-and-probe or flow reactor) and the Comparative Reactivity Method (CRM) using a Proton-Transfer-Reaction Mass Spectrometer (PTR-MS) as

a detector or a fast Gas-Chromatographic/ Photo-Ionization Detector, each system exhibiting advantages and limitations (Fuchs et al., 2017). Total OH reactivity proved to be an effective parameter for quantifying the contribution of VOCs to atmospheric chemistry in various environments. However, the comparison between the measured and the calculated OH reactivity from measured species often revealed differences, showing that there are still some unidentified or unquantified OH sinks (Yang et al., 2016).

Since the 1960s, focus was mainly made on BVOCs emissions from forests, and little interest was shown for BVOC emissions from agriculture (Guenther, 2013). Karl et al. (2009) introduced a new plant-specific emission inventory where they showed that, on the Pan-Europe scale, agriculture contributes up to 27% to total BVOC emissions. These emissions are dominated by OVOCs (65%), followed by monoterpenes (26%) and isoprene (7%). However, they also reported a lack of experimental data on terpenes, sesquiterpenes and oxygenated VOCs, especially from crops, leading to higher uncertainties on BVOCs emission estimates from agriculture included in inventories. Similarly, in terms of OH reactivity, most of the studies conducted in natural ecosystems were in forested areas. Only two took place in suburban areas, near agricultural lands (Lou et al., 2010; Ren et al., 2005) where different observations were reported. Ren et al. (2005) found a mean OH reactivity of 6.1 s^{-1} , with little diurnal variation, in an agricultural research farm in Pennsylvania, US, between May and June. Whereas, Lou et al. (2010), described a diurnal cycle of OH reactivity in a regional background site surrounded by farmlands in the Pearl River Delta- China, during summer, with a mean maximum of 50 s^{-1} at dawn dominated by anthropogenic emissions and a mean minimum of 20 s^{-1} at noon more influenced by local biogenic emissions. These differences highlighted the need to better characterize the OH reactivity in rural environments, in which BVOC emissions can add a significant contribution of photochemical pollution due to the surrounding abiotic VOC emissions (Chameides, 1988). In particular, assessment of the OH reactivity at the branch scale, using dynamic chambers, would be a relevant approach to improve our understanding of the photochemical impacts of agriculture. So far, two studies were found to investigate the OH reactivity, using dynamic branch enclosures (Kim et al., 2011; Nölscher et al., 2013). The first one, conducted by Kim et al. (2011) on four different tree species (red oak, white pine, beech, and red maple) and the second by Nölscher et al., (2013) on Norway spruce trees studying total OH reactivity emission rates (TOHRE). No study was found on OH reactivity from a crop dynamic chamber.

Agricultural lands occupy around 37% of land use, worldwide (FAOSTAT, 2016). With the increase in global human population (10.2 billion by year 2100), the increased demand for food and nutrition would require an additional \approx 2 billion hectares of cropland (Tilman et al., 2011). Furthermore, in order to meet the increasing need of energy in the modern society, biofuels from plants appeared to be an important mitigation strategy for the impact of fossil fuels on the environment (Rodionova et al., 2017). Thus, a new era of agriculture is encouraging the cultivation of biofuel producing crops such as soybean, corn, rapeseed, etc. Oilseed rape or rapeseed (*Brassica napus*) is one of the main oil and protein producing plants grown in Europe (De Bouille et al., 1989; McEwan and Macfarlane Smith, 1998). It represents up to 69% of oleaginous crops and 13% of total agricultural area of cereals, oil and protein producing crops in France (Agreste, 2017). Rapeseed flowering period is considered as a period of high photochemical activity, especially on clear days, where the light yellow surface of the crop reflects the sunlight, increasing the radiation density and leading to the emission of various amounts of BVOCs (Müller et al., 2002). Some studies have reported that oilseed growing can also be responsible of allergic effects especially at the mid-flowering stage of development (McEwan and Macfarlane Smith, 1998; Parratt, D., Macfarlane Smith, W.H., Thomson, G., Cameron, L.A. and Butcher, 1995). Previous studies investigated the variety and amount of BVOCs emitted by the spring rapeseed, showing that OVOCs and monoterpenes were the main emitted compounds. Gonzaga Gomez et al., (2019), found methanol to be the most emitted compound, whereas McEwan and Macfarlane Smith, (1998), reported high levels of monoterpenes from spring rapeseed, with limonene exhibiting the highest concentration, followed by β -myrcene and sabinene. In the light of all these observations, a better characterization of BVOCs and their contribution to OH reactivity in croplands, among which rapeseed fields, is of great importance.

This study aims to investigate BVOCs and their total OH reactivity on a rapeseed crop level in a typical agricultural ecosystem, based on the CRM/ PTR-MS. A dynamic chamber was installed in April 2017 on a healthy, initially non-flowered rapeseed plant to perform measurements during the blooming period. In parallel, VOCs were also sampled in the incoming and the outgoing chamber air using a proton transfer reaction – time of flight – quadrupole ion - mass spectrometry (PTRQi-ToFMS). An expected OH reactivity was calculated from PTRQi-ToFMS data and other complementary measurements of organic and inorganic compounds. Thereby, it was possible to estimate the amount of a potential missing OH reactivity and to discuss its possible sources on diel basis.

4.2. Methodology

4.2.1. Field site description

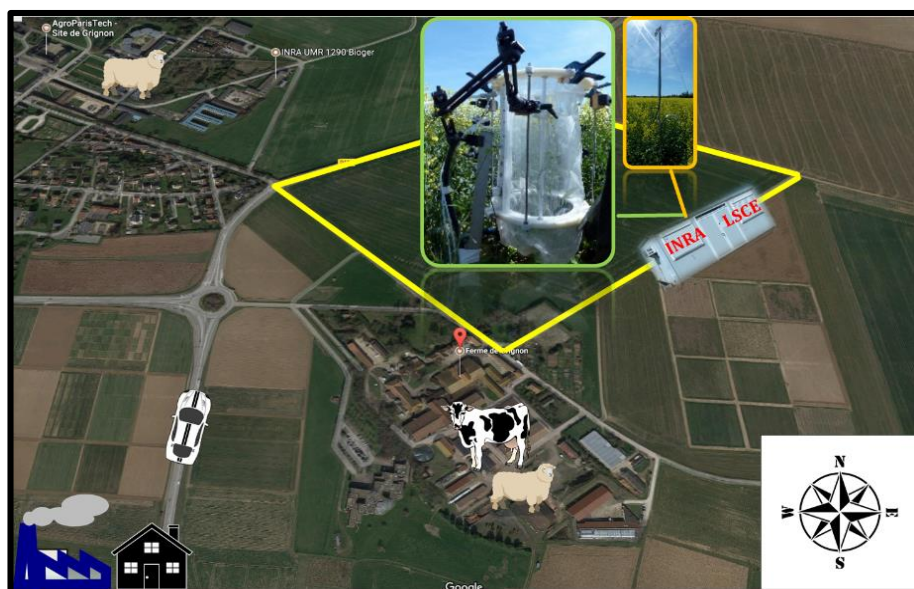


Figure 4.1: Satellite image of Grignon farm, the surrounding area and the chamber used for this study.

As part of the ADEME- COV³ER project (Biogenic Volatile Organic Compounds: Emissions by managed ecosystems), a field campaign was conducted from the 7th to the 25th of April 2017. The ICOS FR-Gri measurement site (**Figure 4.1**) is a 19 ha field belonging to the AgroParisTech experimental farm of Grignon (48°51'N, 1°58'E) and located about 30 km West from Paris, France. The usual crop rotation at the field site is winter wheat – silage maize – winter barley, with only one former occasional occurrence of rapeseed in 2013. From the South, the East, the North-West and the South-West, the site is surrounded by roads with substantial traffic (5000 to 15000 vehicles per day, 2010 counts, “Statistiques du département des Yvelines pour 2010”). From the North, the South and the East, other agricultural lands surround the site. The small (1100 inhabitants, Insee 2015) village of Grignon is located around 700 m West of the measurement site, and an animal farm (more than 200 cows and 1000 sheep) is situated 400 m to the South-West. The main wind directions are North-West during clear days and South-West during cloudy and rainy days (Laufs et al., 2017; Loubet et al., 2012;

Vuolo et al., 2017). Rapeseed was sown on the 16th, August 2016, with a density of 460 000 plants/ ha. The canopy height was around 134 cm.

4.2.2. Plant dynamic chamber and air sampling

In order to determine the chemical nature and the concentration of BVOCs emitted from a rapeseed plant as well as their OH reactivity, a young, healthy, non-flowered rapeseed plant (*Brassica napus*), was selected for the installation of an enclosure system (a dynamic chamber) from which the measurements were made. The enclosure system was a 60 L polytetrafluoroethylene (PTFE) cylindrical frame closed by a sealed 50 μm thick PTFE film to which ambient air was introduced at 15 L min^{-1} using a PTFE pump, leading to a residence time of about 4 min. A rapid mixing of the chamber air and a slight overpressure were ensured using a PTFE fan. Temperature (T $^{\circ}\text{C}$), photosynthetic active radiation (PAR $\mu\text{mol m}^{-2} \text{s}^{-1}$), relative humidity (RH %), carbon dioxide (CO_2 $\mu\text{mol mol}^{-1}$) and water vapor (H_2O mmol mol^{-1}) were continuously monitored inside the chamber. For more details about the enclosure system refer to Genard-Zielinski et al. (2015).

4.2.3. Meteorological measurements

Measurements of meteorological variables were carried out at the FR-Gri ICOS site, according to the ICOS standard protocols (<http://www.icos-etc.eu/icos/documents/>). They include two profiles of air temperature and relative humidity (measurement heights at 1, 2.7 and 5 m) and wind speed/direction (measurement heights at 0.5, 1, 2, 3 and 5 m), radiation measurements (short- and long-wave incoming and reflected radiation, photosynthetically active radiation, albedo), soil temperature and humidity profiles from the surface down to 90 cm, and soil surface heat flux. The data were acquired continuously with dataloggers (Campbell Inc., USA) at rates from 20 s to 1 min, quality-checked and post-processed to get half-hourly averages. All sensors were regularly maintained and calibrated to ensure good quality data.

4.2.4. Instrumentation

4.2.4.1. Comparative reactivity method (CRM) and instrument performance

Total OH reactivity measurements were performed using the CRM, first developed and described by Sinha et al. (2008). This technique relies on quantifying the competition between a reference molecule (pyrrole C₄H₅N) and ambient reactive species to react with in-situ generated OH radicals. The whole experiment can be summarized in three main analytical steps: pyrrole, which is not normally present in ambient air, is introduced with dry zero air and dry nitrogen, in a glass reactor. The latter is equipped with a UV mercury lamp and connected to a detector which in our case is a proton transfer reaction – quadrupole - mass spectrometer (PTR-MS). During this first step, no OH radicals are generated due to dry conditions in the system. The pyrrole concentration is monitored at the protonated m/z 68 as C1 which corresponds to the initial concentration of pyrrole available in the reactor after potential photolysis. Then, dry N₂ is humidified in order to generate OH radicals by H₂O photolysis under the 184.9 nm wavelength emitted by the lamp. Pyrrole concentration at this stage is C2, lower than C1, due to its reaction with OH. The third and final step consists in introducing ambient air instead of zero air. The various species present in ambient air compete with pyrrole for the available OH, leading to an increase in pyrrole concentration measured as C3. Measurements of C1, C2 and C3 allow determining the OH reactivity of the sampled air in a quantitative manner where the difference between C2 and C3 is dependent on the amount and reactivity of VOC present in the sampled air. Total OH reactivity is derived from equation (4.1), where it is assumed that pyrrole reacts with OH following the pseudo –first order kinetical regime i.e. [Pyrrole] >> [OH]:

$$R_{OH} = \frac{(C3 - C2)}{(C1 - C3)} \cdot k_p \cdot C1 \quad (4.1)$$

With k_p the reaction rate of pyrrole with OH ($1.2 \times 10^{-10} \text{ cm}^3 \text{ molecule}^{-1} \text{ s}^{-1}$ (Atkinson, 1985)). However, three main measurement artifacts can occur while operating the CRM, for which corrections should be applied on OH reactivity raw values: (1) changes in the relative humidity within the set-up between zero air (C2) and ambient air (C3), leading to different OH levels, (2) recycling of OH in the presence of nitrogen oxide (NO) due to the NO + HO₂ reaction and (3) deviation from pseudo-first order kinetics. An additional correction is applied due to the dilution of ambient air inside the reactor by N₂ and pyrrole flows.

- CRM/PTR-MS system characterization

In order to assess the performance of the instrument and to apply adequate corrections on OH reactivity raw data, a set of tests have been performed throughout the field campaign (see **S4.1**). The PTR-MS was calibrated at the beginning and the end of the campaign showing a good stability in dry and wet conditions. The photolysis rate $((C_0 - C_1))/C_0$ was determined to be around 6 % since pyrrole can absorb at some of the wavelengths emitted by the UV mercury lamp. And C_1 was 70.5 ± 0.3 ppbv on average for the measurement period presented herein.

Even though a catalytic converter was used to generate zero air from ambient air, small differences in humidity are still observed between ambient and zero air. These changes can influence the level of OH radicals between C_2 and C_3 , leading to an artifact in the C_2 measurement. Therefore, six humidity tests were done, measuring the change in C_2 (ΔC_2) with the change of RH, tracked using the variation in the m/z 37-to- m/z 19 ratio (Δ [m/z 37-to- m/z 19 ratios]) (with m/z 37 being $H_3O^+ \cdot H_2O$ the first water cluster and m/z 19 being H_3O^+ , the number of primary ions and their ratio being proportional to the absolute humidity inside the reactor). These tests, performed on incoming and outgoing chamber air were in good agreement, showing a linear relationship between ΔC_2 (ppbv) and Δ (m/z 37-to- m/z 19 ratio) with a slope (mean humidity correction factor) of -119.68 ± 3.2 and $R^2 = 0.84$. The application of this factor on C_2 (Equation (4.1)) gives a corrected C_2 (C_2^*).

As mentioned before, OH radicals are artificially generated inside the reactor using the photolysis of water vapor. This reaction also results in hydrogen atoms that can be associated to oxygen molecules present in air leading to the formation of HO_2 . In the presence of high levels of NO in sampled air, HO_2 radicals can be rapidly converted into OH radicals resulting in different levels of OH between C_2 and C_3 and leading to an artifact on C_3 measurements. Therefore, tests were performed by introducing different levels of NO (1.2 to 19.6 ppbv) inside the reactor while sampling humid zero air. When the NO level in the system increases, the pyrrole mixing ratio in C_3 decreases. The variation of C_3 (ΔC_3) was thus monitored as the difference between an expected C_3 and the measured C_3 , where the expected C_3 is calculated using C_1 , C_2 and an expected OH reactivity due to NO. The relationship between ΔC_3 and NO mixing ratio is not linear. It follows a quadratic regression (**S1.b**), $\Delta C_3 = a [NO]^2 + b[NO]$, where [NO] is in ppbv with the following parameters fitted during this pre-experimental test $a = -0.0013$ and $b = 0.3214$ (see also Michoud et al., 2015). This correction leads to corrected C_3 (C_3^*). We note that this correction was minor most of the time as the NO mixing ratio was low during the campaign (0.7 ± 0.5 ppbv on average during the considered period except for one

peak recorded on the morning of the 21st April, 2017 when the NO mixing ratio reached 46 ppbv around 06:00 UTC (Local time= UTC + 2).

Regarding nitrogen dioxide (NO₂), no tests have been performed on site, since NO₂ is not expected to lead to the formation of secondary OH inside the reactor. However, its conversion into NO showed that it can cause an artifact (Michoud et al., 2015). During the intercomparison of OH reactivity instruments over the SAPHIR chamber (Fuchs et al., 2017), our CRM/PTR-MS suffered from an artifact from high (≥ 10 ppbv) NO₂ concentration, even if this effect was on a lower extent compared to other CRM instruments. The absolute change in OH reactivity values was about + 1.9 s⁻¹ in the presence of 10 ppbv of NO₂. This correction was only considered in order to estimate the weight of the NO₂ interference on OH reactivity measurements. As NO₂ was on average 12 ppbv during the campaign, this could have led to an underestimation of about 2 s⁻¹ of the corresponding OH reactivity.

OH reactivity values are determined based on equation (4.1). This equation assumes that the instrument is operated under pseudo-first order conditions (i.e. [Pyrrole] \gg [OH]), which is not the case with current CRM instruments. To assess this correction, injections of known concentrations of propane and isoprene were performed during the field campaign. These two gas standards represent extreme cases since propane is a medium reactive VOCs in the atmosphere ($k_{(\text{propane-OH})} = 1.09 \times 10^{-12} \text{ cm}^3 \text{ molecules}^{-1} \text{ s}^{-1}$), while isoprene is one of the most reactive ($k_{(\text{isoprene-OH})} = 1.0 \times 10^{-10} \text{ cm}^3 \text{ molecules}^{-1} \text{ s}^{-1}$). The measured OH reactivity obtained from these tests is then compared with the expected OH reactivity, which allows extracting a correction factor that depends on pyrrole-to-OH ratio [34]. Therefore, standard OH reactivity experiments were conducted at various pyrrole-to-OH ratios ranging between 1.7 and 2.7, which is the range observed most of the time during the COV³ER campaign, leading to a correction factor $F = 1.59x^2 - 7.22x + 9.46$ with $x = \text{pyrrole/OH}$. Finally, correction on reactivity values due to dilution was around 1.44 during the campaign (D).

Taking all mentioned corrections into account, final OH reactivity was determined following equation (4.2):

$$R_{\text{OH}} = \frac{(C3^* - C2^*)}{(C1 - C3^*)} \cdot kp \cdot C1 \cdot F \cdot D \quad (4.2)$$

The limit of detection was about 3 s⁻¹ (3 σ) and overall uncertainties have been estimated at 35 % (1 σ) for the measured OH reactivity by our CRM/PTR-MS (Zannoni, 2015).

- **Ambient air sampling**

The sampling lines were shared with the PTRQi-ToFMS. In total 8 ¼' internal diameter PFA 20 m lines were sampled at a flow rate of $\sim 7 \text{ L min}^{-1}$. Among these 8 lines, the line from the rapeseed enclosure and the line sampling ambient air at 270 cm height were subsampled to the 4 port-valve of the CRM system, with a flow rate around 1 L min^{-1} , through a 1/8' internal diameter PFA line, using two pumps: the first one is a PTFE coated pump located upstream of the reactor and the other one is from the Gas Calibration Unit (GCU) used to generate humid zero air from ambient air (**Figure S4.2**). All Teflon lines were heated to 50°C .

Since the PTRQi-ToFMS was used during this campaign to measure gradients, eddy covariance fluxes and the air out of the dynamic chambers, the measurement sequence was programmed as following: 20 min of eddy covariance measurements followed by 5 min of gradient measurement, 3 min in the chamber out and 2 min of background.

4.2.4.2. Proton transfer reaction Quadrupole ion-Time of Flight Mass Spectrometer (PTRQi-ToFMS)

- **Instrument setup**

A PTRQi-ToFMS (Ionicon Analytik GmbH, Innsbruck, Austria) was used for continuous online measurements of VOC mixing ratios at 10 Hz. The analyzer was described in details before (Abis et al., 2018; Gonzaga Gomez et al., 2019; Sulzer et al., 2014) and the set up used in this study is detailed in Gonzaga Gomez et al. (2019). VOCs are protonated inside a reaction tube, then injected into a quadrupole ion guide and electromagnetic lenses that focuses the ions into the time-of-flight mass spectrometer (ToF, TofWerk, Switzerland) which separates the ions by inertia prior to their detection on a multi-channel-plate (MCP) coupled to a time-to-digital converter (Burle Industries Inc., Lancaster, PA, USA). The drift tube pressure was tuned to $4 \pm 0.0001 \text{ mbar}$, drift temperature was $80 \pm 0.06 \text{ }^\circ\text{C}$, and drift voltage E was $995 \pm 0.03 \text{ V}$. These conditions ensured an E/N ratio (where E is the electric field strength and N the gas density) of $132 \pm 0.03 \text{ Td}$ ($1 \text{ townsend} = 10^{-17} \text{ V cm}^2$), which was chosen as a good compromise to avoid fragmentation and limit clustering (Pang, 2015; Tani et al., 2003). The number of detection channels was set to 240 000 and the mass spectrum spanned 15 to 530 m/z . The extraction rate of ions in the ToF was set to $40 \text{ } \mu\text{s}$ (25 kHz). 2500 extracted spectra were averaged prior to

recording at 10 Hz. The proton transfer reaction is effective for compounds having a proton affinity higher than that of water ($691.7 \text{ kJ mol}^{-1}$), which means that the major atmospheric compounds are not protonated (N_2 , O_2 , CO_2 , CH_4 , N_2O) allowing for detection of trace compounds.

- **Acquisition and pre-processing of PTRQi-ToFMS data**

Data acquisition was performed with home-made Labview® software which logged a list of ion peaks integrated online by the TOFDAQ software (TOFWERK, SW). The desired ion peak list was set up at the start of the experiment based on measured air sampled at the site, analyzed by a home-made Labview peak analyzer. Every 5 min, the data were stored on the hard drive, and a mass calibration was performed with the automatic TOFDAQ software feature using ions m/z 21.0221 ($\text{H}_3^{18}\text{O}^+$) and m/z 59.049 (acetone $\text{C}_3\text{H}_6\text{OH}^+$), and a 2-seconds moving average. Mass calibration was quality checked online by computing the peak mass of m/z 21.022 and m/z 59.049 after calibration and was found to be stable throughout most of the experiment. Unstable mass calibration periods were discarded at the computation stage. The channels number of the 16-way valve embedded in the PTRQi-TOFMS was also recorded. The synchronized data were pre-processed with another Labview program that computed the mean and standard deviation of the cps at the entry and exit of the chamber as well as at reference level (2.7 m) and in the canopy at 1.34 m. In this pre-processing step, the first 15 seconds and the last 5 seconds of a record were removed prior to computing cps statistics to avoid unstable drift pressures that occurred after each valve switching.

- **PTRQi-ToFMS calibration**

In order to account for the sensitivity changes the PTRQi-ToFMS was regularly calibrated. We used a standard cylinder containing 102 ppbv of benzene, 104 ppbv of toluene, 130 ppbv of ethylbenzene and 336 ppbv of xylene (122 ppbv Ortho, 121 ppbv Meta, 123 ppbv Para; BTEX, Messer). Gas from this cylinder was diluted with synthetic air (alphagaz 1, Air Liquide, FR) using two fluorinert coated mass flow controllers (Bronkhorst), to generate concentrations from 0 to 50 ppbv of BTEX. The calibration was done almost every week. The zero check was performed every 30 minutes by passing through a hydrocarbon filter (Supelco ref 22445-12 ou Restek ref 21991) for 2 minutes and keeping the last 30 seconds. The zero was withdrawn from

the normalized cps every 30 min as shown in equation (S4.3.1). The sensitivity S_i was calculated as the slope with zero intercept of the regression between mixing ratio in equation (S4.3.1) assuming $S_i = 1$ and the known mixing ratio. The procedure was applied for the three compounds cited above for the calibration. We found that the sensitivity was 2 ± 0.15 . Based on an inter-comparison between our PTRQi-ToFMS and a PTR-MS inter-compared within the ACTRIS network (Holzinger et al., 2019) we adjusted methanol sensitivity to $S_{methanol} = 14$ as explained in Gonzaga Gomez et al. (2019). Except for methanol, a single sensitivity value was applied for all masses, since the protonation reaction constant was assumed equal for all masses.

4.2.4.3. Gas chromatography- flame ionization detector (GC- FID)

A gas chromatograph equipped with a Flame Ionization Detector (airmoVOC C₂- C₆, Chromatotec, Saint Antoine, France) was used to measure hydrocarbons in the C₂- C₆ fraction. The sampling was done for 10 min with a flow rate of 11 sccm via a stainless steel inlet, followed by a 20 min analysis. After going through a Nafion dryer, ambient air arrives to a preconcentration unit cooled down to -8°C, filled with Carboxen, Carbopack B and Carbotrap C. A thermodesorption at 220 °C follows and the sample is injected into a metal capillary column (Porous Layer Open Tubular Column PLOT, Al₂O₃/ KCL; 0.53 mm inner diameter and 25 m length, Varian Inc, USA). Calibrations were performed frequently using a certified standard VOC mixture (National Physical Laboratory, UK). The overall uncertainty was estimated to be 15 % (1 σ) (Gros et al., 2011).

4.2.4.4. NO_x concentration measurements

Nitrogen oxides (NO_x) concentrations in ambient air were measured with a NO-NO₂-NO_x chemiluminescence analyzer (Model 42-CTL, Thermo Environnement, Météatec, France). Data were acquired continuously at 1 Hz using a datalogger (Model CR10, Campbell Inc., USA). The NO-NO₂-NO_x instrument was calibrated in the laboratory before being installed on the field, and the span was regularly checked during the campaign (about once every two weeks). The inlet was placed at a height of 2.5 m, on the side of the FR-Gri field.

4.2.4.5. CO and CH₄ measurements

A 48i-TL, thermo-Environnement was used to measure carbon monoxide (CO), by the absorption of light in the infrared range. A zero was done every 4 h, and the calibration was checked several times through the campaign, by the injection of a pre-calibrated air bottle (\approx 200 ppbv).

Regarding methane (CH₄), a G2201-i Picarro based on Cavity Ring Down Spectroscopy (CRDS), was deployed. CRDS uses a single frequency laser diode to measure specific gas-phase molecules which scatter and absorb light in the near infrared absorption spectrum. By measuring the height of absorption peaks, the concentrations can be determined. More details on the instrument and setup used in this campaign can be found in Assan, et al. (2017).

All deployed instruments are summarized in **Table 4.1** and **Figure 4.2**.

Table 4.1: Instruments deployed in the campaign and used for data analysis.

Technique	Measurement	Time resolution
CRM	Total OH Reactivity (ROH)	10 min
PTRQi-ToFMS	VOCs Formaldehyde, Methanol, Acetaldehyde, Butanol, Acetone, Acetic acid, Isoprene, MethylEthylKetone (MEK), Hexadiene/ GLV, Styrene, Monoterpenes	0.1 sec
GC-FID	C ₂ - C ₆ HCs Alkanes: Ethane, Propane, I-butane, N-butane, I-Pentane, N-Pentane, 2-MethylPentane, N-hexane Alkenes: Ethene, Propene, Trans-2-butene, 1-butene, I-butene, Cis-2-butene, 1,3-butadiene, Trans-2-pentene, 1-pentene Alkynes: Acetylene	30 min
NO-NO ₂ -NO _x chemiluminescence analyzer	NO, NO ₂	1 min
G2201-i Picarro	CH ₄	1 min
48i-TL, thermo-Environnement	CO	1 min

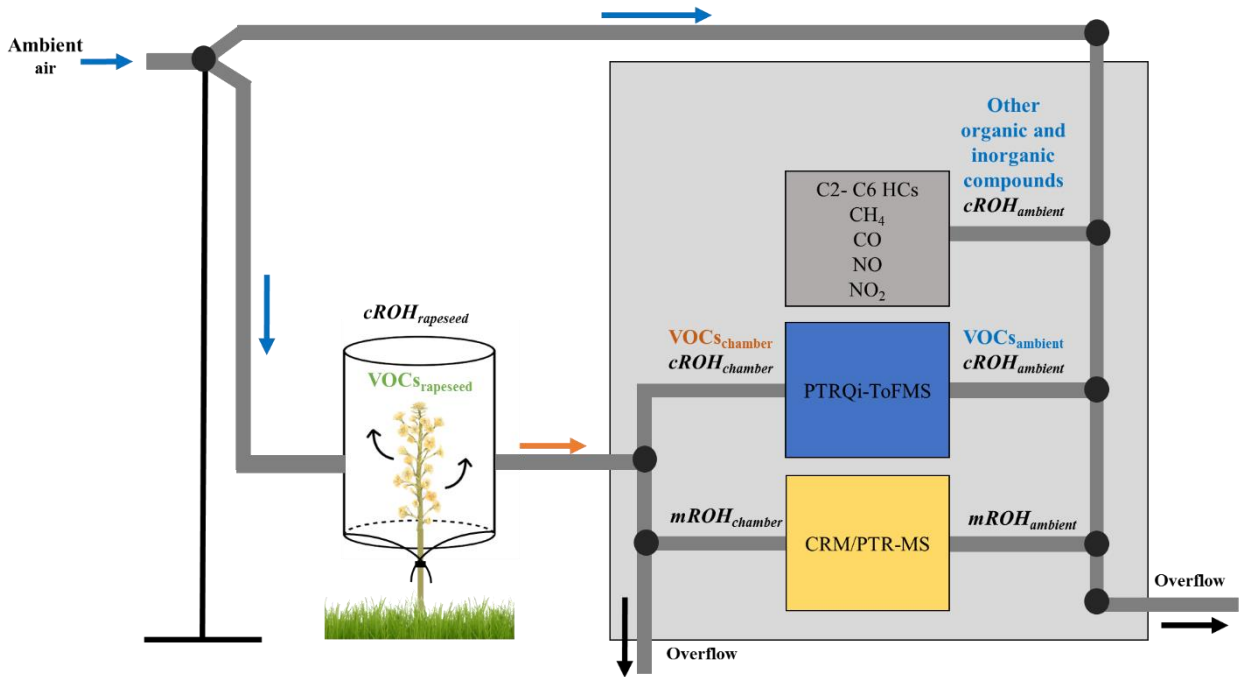


Figure 4.2: Schematic representation of the system used for the measurements in the incoming and the outgoing chamber air. $mROH_{ambient}$ and $mROH_{chamber}$ stand for measured OH reactivity in the incoming and the outgoing air, respectively. $cROH_{ambient}$ and $cROH_{chamber}$ represent the calculated OH reactivity in the incoming and the outgoing chamber air, respectively. $cROH_{rapeseed}$ is calculated using $VOCs_{rapeseed}$, determined from $VOCs_{chamber} - VOCs_{ambient}$ (both measured with the PTRQI-ToFMS).

4.2.5. Calculation of OH reactivity

Based on the available trace gases observations, mentioned in section 4.2.3, an expected OH reactivity (calculated OH reactivity, $cROH$) could be determined using the following equation:

$$cROH = \sum cROH_i = \sum k_{i-OH} \cdot X_i \quad (4.3)$$

where $cROH_i$ is the calculated OH reactivity of a compound i , X_i its concentration and k_{i-OH} its respective rate coefficient of the reaction with the hydroxyl radical OH.

While $cROH_{ambient}$ was calculated considering $VOCs_{ambient}$ (PTRQI-ToFMS), light (C_2 - C_6) hydrocarbons, NO_x , CO and CH_4 , measured in ambient air (**Figure 4.2**), $cROH_{chamber}$ was determined using $VOCs_{chamber}$ (PTRQI-ToFMS) measured in the outgoing chamber air and the

organic and inorganic species measured in ambient air, assuming that inorganic compounds and light hydrocarbons were not emitted nor deposited in the rapeseed chamber.

As reported in Gonzaga Gomez et al. (2019), the PTRQi-ToFMS deployed during the COV³ER campaign, detected 1078 ions (fragments and isotopes included) with a mass-to-charge ratio (m/z) ranging from 31 to 500. For rapeseed, around 420 ions exceeded the set threshold (signal/ noise ratio > 3), from which 24 masses were selected as the main contributors to rapeseed BVOCs emission fluxes, based on their mean net flux. This list of 24 masses was considered first, including m/z 31.018, m/z 33.034, m/z 41.038, m/z 43.018, m/z 45.033, m/z 57.069, m/z 59.048, m/z 61.028, m/z 69.070, m/z 79.063, m/z 81.069, m/z 83.084, m/z 90.946, m/z 91.053, m/z 93.035, m/z 105.069, m/z 108.956, m/z 125.957, m/z 137.131, m/z 153.052, m/z 190.962, m/z 192.960, m/z 223.061, m/z 225.043. However, when it came to consider $\text{VOC}_{\text{Sambient}}$ and $\text{VOC}_{\text{Schamber}}$ in $\text{cROH}_{\text{ambient}}$ and $\text{cROH}_{\text{chamber}}$, respectively, this list was shortened to 12 masses, with known chemical nature and established rate coefficients for the reaction with OH. It is important to note that, in our case, total monoterpenes are represented by the sum of m/z 81.068 and m/z 137.129, since m/z 81.068 was mainly a monoterpene fragment. Isoprene, detected at m/z 69.070 also exhibited a fragment at m/z 41.038, therefore, the corresponding signal was corrected for the potential fragmentation with a factor of 1.3. Formaldehyde could be detected and quantified at m/z 31.018. Indeed, Warneke et al. (2011) reported that PTR-MS can be used for formaldehyde measurements, even though HCHO detection by PTR-MS can be strongly dependent on humidity and can be less sensitive than for other compounds. The 12 selected PTRQi-ToFMS masses as well as the other organic and inorganic measured trace gases are listed in **Table 4.2**, together with their respective rate coefficients for the reaction with OH used for calculations. It is worth noting that, the OH reactivity of monoterpenes was calculated as the product of the concentration of total monoterpenes (m/z 137 and m/z 81) and the rate constant of the reaction of limonene with OH. This assumption was based on previous studies, where limonene was reported to be the dominant monoterpene emitted by *Brassica napus* (McEwan and Macfarlane Smith, 1998).

Finally, this list of compounds mentioned in **Table 4.2**, contains species known to be biogenic compounds (isoprene, monoterpenes) as well as several OVOCs (formaldehyde, methanol, acetaldehyde, acetone, ...). OVOCs can be of anthropogenic or biogenic origins and can be primary emitted by plants or generated from secondary reactions (acetaldehyde, acetic acid, ...). Therefore, it is important to distinguish between rapeseed BVOCs emissions and

background air emissions. In this context, we determined the concentration of VOCs related to the enclosed plant emissions as $\text{VOCs}_{\text{rapeseed}} = \text{VOCs}_{\text{chamber}} - \text{VOCs}_{\text{ambient}}$ (Figure 4.2).

Table 4.2: List of selected compounds used for OH reactivity calculations with their respective $k_{i\text{-OH}}$ at 298 K and pressure 1 atm.

	Protonated theoretical mass	Chemical compound	Name	Rate constant ($\times 10^{-12}$ $\text{cm}^3 \text{ molecule}^{-1} \text{ s}^{-1}$)	Ref
PTR-ToF-MS protonated masses	m31.018	(CH ₂ O)H+	Formaldehyde	8.5	(Atkinson et al., 2006)
	m33.033	(CH ₃ OH)H+	Methanol	0.9	(Atkinson et al., 2006)
	m45.033	(CH ₃ CHO)H+	Acetaldehyde	15	(Atkinson et al., 2006)
	m57.069	(C ₄ H ₈)H+	Butanol fragment	8.5	(Atkinson et al., 2006)
	m59.049	(C ₃ H ₆ O)H+	Acetone	0.18	(Atkinson et al., 2006)
	m61.029	(C ₄ H ₄ O ₂)H+	Acetic Acid	0.74	(Atkinson et al., 2006)
	m69.070	(C ₅ H ₈)H+	Isoprene	100	(Atkinson et al., 2006)
	m73.064	(C ₄ H ₈ O)H+	Butanone/ MEK	1.2	(Atkinson et al., 2006)
	m81.068	(C ₆ H ₈)H+	MTs fragment	165	(Atkinson et al., 2003)
	m83.084	(C ₆ H ₁₀)H+	Hexadiene/ C ₆ GLV	69.1	(Peeters et al., 2007)
	m105.066	(C ₈ H ₈)H+	Styrene	53	(Bignozzi et al., 1981)
m137.129	(C ₁₀ H ₁₆)H+	Monoterpenes (MTs)	165	(Atkinson et al., 2003)	
GC-FID		C ₂ H ₆	Ethane	0.24	(Atkinson et al., 2006)
		C ₂ H ₄	Ethene	7.9	(Atkinson et al., 2006)
		C ₃ H ₈	Propane	1.1	(Atkinson et al., 2006)
		C ₃ H ₆	Propene	29	(Atkinson et al., 2006)
		C ₄ H ₁₀	I-butane	2.35	(Atkinson et al., 2003)
		C ₄ H ₁₀	N-butane	2.35	(Atkinson et al., 2003)
		C ₂ H ₂	Acetylene	0.75	(Atkinson et al., 2003)
		(E)-2-C ₄ H ₈	Trans-2-butene	63.7	(Atkinson, 1985)
		1- C ₄ H ₈	1-butene	31.5	(Atkinson, 1985)
		I- C ₄ H ₈	I-butene	51.5	(Atkinson, 1985)
		(Z)-2-C ₄ H ₈	Cis-2-butene	56	(Atkinson, 1985)
		iso-C ₅ H ₁₂	I-pentane	3.65	(Wilson et al., 2006)
		n-C ₅ H ₁₂	N-pentane	3.92	(Sivaramakrishnan and Michael, 2009)
		CH ₂ =CH-CH=CH ₂	1,3-butadiene	58	(Grosjean and Williams, 1992)
		2- (E)- C ₅ H ₁₀	Trans-2-pentene	57.1	(Grosjean and Williams, 1992)
		1-C ₅ H ₁₀	1-pentene	35	(Grosjean and Williams, 1992)
	(CH ₃) ₂ CH(CH ₂) ₂ CH ₃	2-Me-pentane	5.2	(Atkinson and Arey, 2003)	
	C ₆ H ₁₄	N-hexane	5.38	(Sivaramakrishnan and Michael, 2009)	
Other compounds		CO	Carbon monoxide	0.228	(Atkinson et al., 2003)
		CH ₄	Methane	0.0064	(Atkinson et al., 2003)
		NO	Nitrogen oxide	9.7	(Atkinson et al., 2003)
		NO ₂	Nitrogen dioxide	11.3	(Atkinson et al., 2003)

4.2.6. Data availability

The CRM/PTR-MS system operated from the 7th to the 25th, April 2017. However, final experimental conditions, including heating the sampling lines and sampling ambient air from a mast at ≈ 2.7 m height, were only set starting from the 10th, April 2017. All other instruments were operational between the 10th and the 25th, April except for the NO_x analyzer due to technical problems between the 14th and the 19th, April. Since NO data is important to correct for the CRM artifact due to the recycling of OH radicals (NO + HO₂), only OH reactivity data corrected for the NO interference are presented. It should be noted that one to two days were dedicated at the beginning, the middle and the end of the campaign, to perform some tests aiming to check the stability of the CRM system. In addition, enclosure measurements were interrupted for 2 days during the campaign (between the 15th and the 17th, April 2017), since a fungicide application was planned for this period. Therefore, taking into account the CRM/PTR-MS availability as well as the availability of the other deployed instruments, only the results from the 20th to the 23rd of April, representing the later stage of the blooming period, are presented and further discussed.

4.3. Results and discussion

In the first part of the result section, the variability of measured total OH reactivity in the outgoing chamber air ($mROH_{\text{chamber}}$) as well as in the incoming ambient air ($mROH_{\text{ambient}}$) is described, linked to some meteorological parameters. In a second part, calculated OH reactivity is determined in ambient air ($cROH_{\text{ambient}}$) as well as from the rapeseed branch ($cROH_{\text{rapeseed}}$), with a description of the individual contribution of biogenic and abiotic compounds to $mROH_{\text{chamber}}$. The final part is dedicated to discuss the possible origins of missing OH reactivity, based on the investigation of further masses measured with the PTRQi-ToFMS.

4.3.1. Total OH reactivity

Figures 4.3.b and **c** report the variability of measured total OH reactivity from the rapeseed dynamic chamber ($mROH_{\text{chamber}}$) with temperature, PAR and RH, from the 20th to the 23rd of April, 2017. $mROH_{\text{chamber}}$ varied diurnally between the limit of detection and 47.6 s^{-1} , with an average of $12.0 \pm 6.7 \text{ s}^{-1}$. Higher values were measured during day-time and minimum values

during night-time, following PAR and temperature profiles. The average day and night $mROH_{\text{chamber}}$ was 14.9 ± 7.1 and $8.1 \pm 3.1 \text{ s}^{-1}$, respectively. The night-time $mROH_{\text{chamber}}$ was in the same order of magnitude of the mean total OH reactivity measured in the incoming chamber air (mean $mROH_{\text{ambient}} = 7.5 \pm 2.4 \text{ s}^{-1}$). However, the latter did not show a clear diurnal cycle as in the chamber reactivity. Such findings were similar to the observations made by Ren et al. (2005) during a field experiment conducted in an agricultural research farm, where averaged ambient OH reactivity was 6.1 s^{-1} with little diurnal variation. However, our results are lower than the mean values (20 s^{-1} at noon and 50 s^{-1} at day-break) recorded in ambient air by Lou et al. (2010) during the PRIDE-PRD2006 campaign at a rural site which was dominated by anthropogenic pollutants (CO, NO_x, ...) at night and strongly influenced by local biogenic emissions of isoprene during the day (Lou et al., 2010). Our results were also lower than the 25 s^{-1} OH reactivity reported by (Nölscher et al., 2013) from a dynamic branch cuvette enclosure system mounted on a Norway spruce and much lower than the OH reactivity recorded by Kim et al. (2011) from red oak, white pine, beech, and red maple branch enclosures and which ranged between tens and hundreds of s^{-1} (Kim et al., 2011). Thus, recorded levels of OH reactivity in ambient air and in dynamic chamber, were in the lower range of total OH reactivity, compared to various forest ecosystems, where OH reactivity reached maximum levels between 30 and 100 s^{-1} ((Bsaibes et al., 2019; Edwards et al., 2013; Kim et al., 2011; Nölscher et al., 2013; Ramasamy et al., 2016; Sinha et al., 2010; Zannoni et al., 2017).

During this period of the campaign (20th- 23rd, April 2017), the crop growth was relatively stable as shown by the stem length, the leaves total length and the fraction of open flowers evolution (see **S4.4**). $mROH_{\text{chamber}}$ showed to be clearly correlated to environmental abiotic factors rather than changes in plant physiology. As mentioned before, $mROH_{\text{chamber}}$ minima recorded during nights were close to the levels measured in ambient air. It means that at night there was no or little contribution from the plant emissions to OH reactivity. This observation is confirmed by $\Delta mROH = mROH_{\text{chamber}} - mROH_{\text{ambient}}$ (**Figure 4.3.a**), with relatively low values during the night. Whereas, during the day, $\Delta mROH$ reached a maximum of 10 s^{-1} on average at mid-day (between 11h and 14h UTC). This difference appeared around 05:00 (UTC) when the sun rose ($PAR > 0 \mu\text{mol m}^{-2} \text{ s}^{-1}$), peaked around noon in parallel with maximal solar radiations and temperatures, and decreased in the late afternoon down to a minimum around 19:00 (UTC). Mid-day difference was the highest on the 21st of April ($\Delta mROH = 14.3 \text{ s}^{-1}$), when a higher day-time temperature and a more intense solar radiation were recorded inside the enclosure. These observations show that the contribution of plant emissions to OH reactivity

were temperature and/ or light dependent. It is worth noting that a higher temperature was recorded inside the chamber compared to ambient air (mean difference = 8.5°C, see S4.5), this should be kept in mind when analyzing $\Delta mROH$.

It is worth noting that an extra day-time peak of $mROH_{\text{chamber}}$ (Figure 4.3.b) was recorded in the morning of the 21st of April (05:00 – 07:30 UTC), that did not appear on the other days and was also seen on $\Delta mROH$ (Figure 4.3.a). This peak of $\Delta mROH$ is likely due to the subtraction of a $mROH_{\text{ambient}}$ (an average of 7.5 s⁻¹) not representative of the atmospheric conditions at that hour of the day; indeed, we remind that $mROH_{\text{ambient}}$ was only recorded 1 hour each 4 hours, and that the ambient air composition can change quickly. In addition, higher night-time levels were observed during the nights of 21st and the 22nd, April (around 01:00 UTC). These events are further discussed in section 4.3.2 while investigating the contribution of measured compounds to total measured OH reactivity.

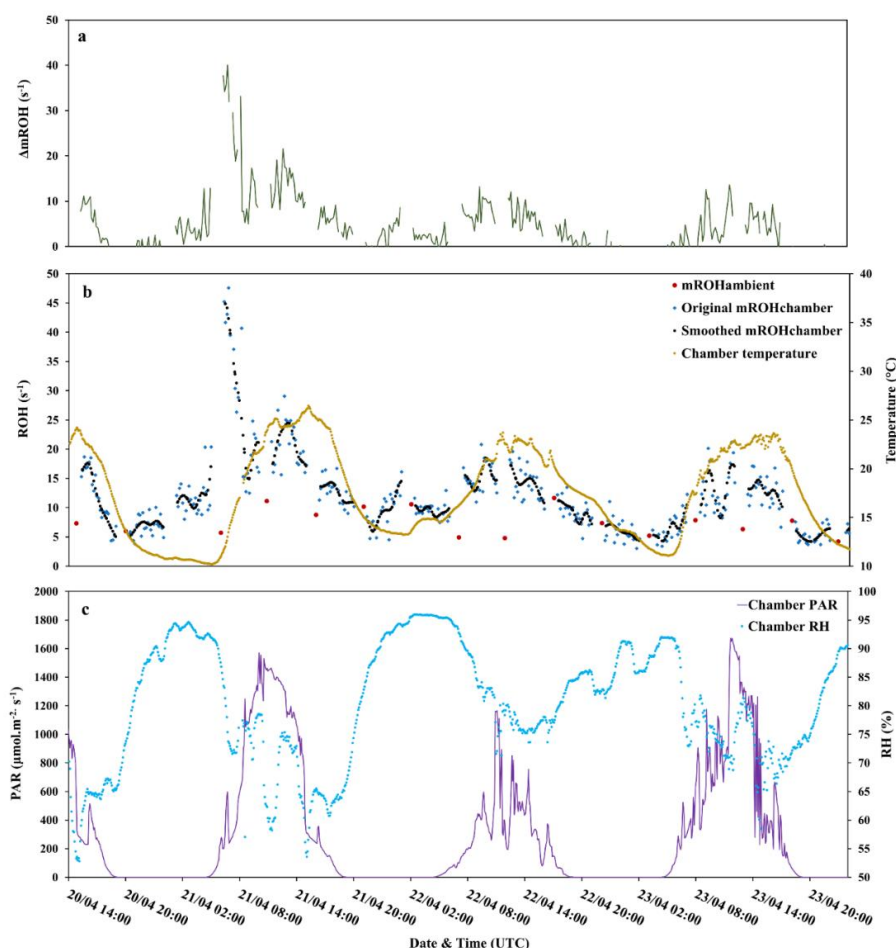


Figure 4.3 : Variability of a) $\Delta mROH = mROH_{\text{chamber}} - mROH_{\text{ambient}}$ and b) total $mROH_{\text{chamber}}$ (blue dots represent the original OH reactivity data and black dots represent the trend obtained after smoothing the original data) and total $mROH_{\text{ambient}}$ (red dots) from the 20th to the 23rd, April 2017 with temperature (T°C- yellow), c) photosynthetic active radiation (PAR $\mu\text{mol m}^{-2} \text{s}^{-1}$ - purple) and relative humidity (RH%- blue), all three parameters measured inside the chamber.

4.3.1.1. Ambient air measurements and their calculated OH reactivity ($cROH_{\text{ambient}}$)

Measurements in ambient air included NO, NO₂, CO, CH₄, C₂-C₆ hydrocarbons and other VOCs (**Figure S4.6.a**). As already stated, NO was around 0.7 ± 0.5 ppbv on average for the considered period, except for one peak recorded on the morning of the 21st April, 2017 when the NO mixing ratio reached 46 ppbv around 06:00 UTC. NO₂ showed higher mixing ratios than NO and was around 12 ppbv on average. CO was on average 151 ± 21 ppbv with a higher mixing ratio on the morning of the 21st April, occurring at the same time as the NO peak and reaching 243 ppbv around 07:00 UTC. These high peaks of NO and CO, observed on the morning of the 21st, April correspond to the hours of the day when the wind was mainly coming from the east of the site (wind direction $\approx 50^\circ$) and had a low speed, which means little mixing in the surface layer. These peaks lasted for 2-3 hours and they are most probably related to traffic from the road nearby and advection from Paris and its suburbs. In terms of calculated OH reactivity, these two inorganic compounds, accounted for 4.6 s^{-1} on average to the ambient measured OH reactivity, with a maximum of 14.3 s^{-1} on the morning of the 21st, April 2017 (**S4.6.b**).

Regarding VOCs, CH₄ presented an average of 2100 ppbv, with a higher level on the night between the 20th and the 21st, April and a high/ sharp peak around 01:00 UTC of the 22nd. The same observation was made on the sum of C₂-C₆ hydrocarbons (GC-FID) and the oxygenated VOC_{Sambient} (PTRQi-ToFMS). In terms of OH reactivity, CH₄, non-methane hydrocarbons in the C₂-C₆ fraction and OVOCs accounted, each, for $0.3 - 0.4 \text{ s}^{-1}$ on average, with a maximum of 0.7, 1 and 1.2 s^{-1} , respectively around midnight on the 22nd. Monoterpenes accounted for 0.7 s^{-1} on average and isoprene had a negligible contribution, around 0.1 s^{-1} , both showing surprisingly the same midnight peak reaching 3.2 and 0.7 s^{-1} , respectively. This peak coincides with a wind mainly coming from the north of the site and highlights possible emissions from a nearby waste treatment plant (Font et al., 2011).

All the mentioned compounds, accounted for 6.5 s^{-1} on average of $mROH_{\text{ambient}}$, representing a relative mean contribution of 87 %.

It should be reminded that, assuming that the inorganic compounds and light hydrocarbons were not emitted nor deposited in the rapeseed chamber, all the compounds present in the incoming chamber air (ambient air) contribute to $mROH_{\text{chamber}}$. This contribution was around 89 % and 41 % during night-time and day-time, respectively.

4.3.1.2. BVOCs from the rapeseed plant ($\text{VOC}_{\text{rapeseed}}$) and their calculated OH reactivity ($\text{cROH}_{\text{rapeseed}}$)

As mentioned before, the PTRQI-ToFMS was the only instrument measuring VOCs from the dynamic chamber ($\text{VOC}_{\text{chamber}}$) as well as in ambient air ($\text{VOC}_{\text{sambient}}$). Thereby, it was possible to characterize VOCs originating directly from the enclosed plant ($\text{VOC}_{\text{rapeseed}} = \text{VOC}_{\text{chamber}} - \text{VOC}_{\text{sambient}}$), on which we focus in the following part.

The summed mean mixing ratios of the 11 $\text{VOC}_{\text{rapeseed}}$, is presented in **Figure 4.4.a**. It exhibits a diel variability with a maximum of 11 ppbv on average around mid-day (11h-14h UTC) and a minimum during the night (\approx LOD), similar to temperature and light profiles. This observation confirms that BVOCs emissions from rapeseed and their concentrations in the enclosure are generally light and/or temperature dependent. It also highlights that these compounds are the main drivers of the day/ night variability seen on $\text{mROH}_{\text{chamber}}$.

Between the 20th and the 23rd, April, biogenic OVOCs (listed in **Table 4.2**) accounted for the major (92 %) part of $\text{VOC}_{\text{rapeseed}}$. Among the measured biogenic OVOCs, methanol was dominant with 1.4 ppbv on average, representing 38 % of the oxygenated compounds emitted, followed by acetaldehyde and acetone, with 0.8 ppbv each, accounting for 21- 22 %. Acetic acid (0.4 ppbv) presented around 11 %, whereas the others (formaldehyde, butanol and MEK) did not exceed 8 % together. Regarding isoprene and monoterpenes, they had relatively low contributions to the total $\text{VOC}_{\text{rapeseed}}$, with 0.2 and 0.01 ppbv on average, amounting to 5.2 % and 0.2 %, respectively. These observations during the blooming period are in agreement with other studies on rapeseed. König et al. (1995) classified rapeseed as OVOCs- emitter with other crop species. Müller et al. (2002), reported an important emission and/or rapid formation of carbonyl compounds from flowering rape as an important source of biogenic OVOCs in the studied ecosystem. Furthermore, these relatively high levels of OVOCs, recorded during the blooming period, were also observed later during the senescence period, starting at the end of April 2017, in the study conducted by Gonzaga Gomez et al. (2019) on the same field site. However, few studies presented rapeseed as an important emitter of monoterpenes, which accounted for 60-90 % of the total VOCs identified in spring oilseed rape, whereas non-terpenoid components, including OVOCs (acetaldehyde, acetone, and 3-methyl-2-butanone) were found at low levels (McEwan and Macfarlane Smith, 1998).

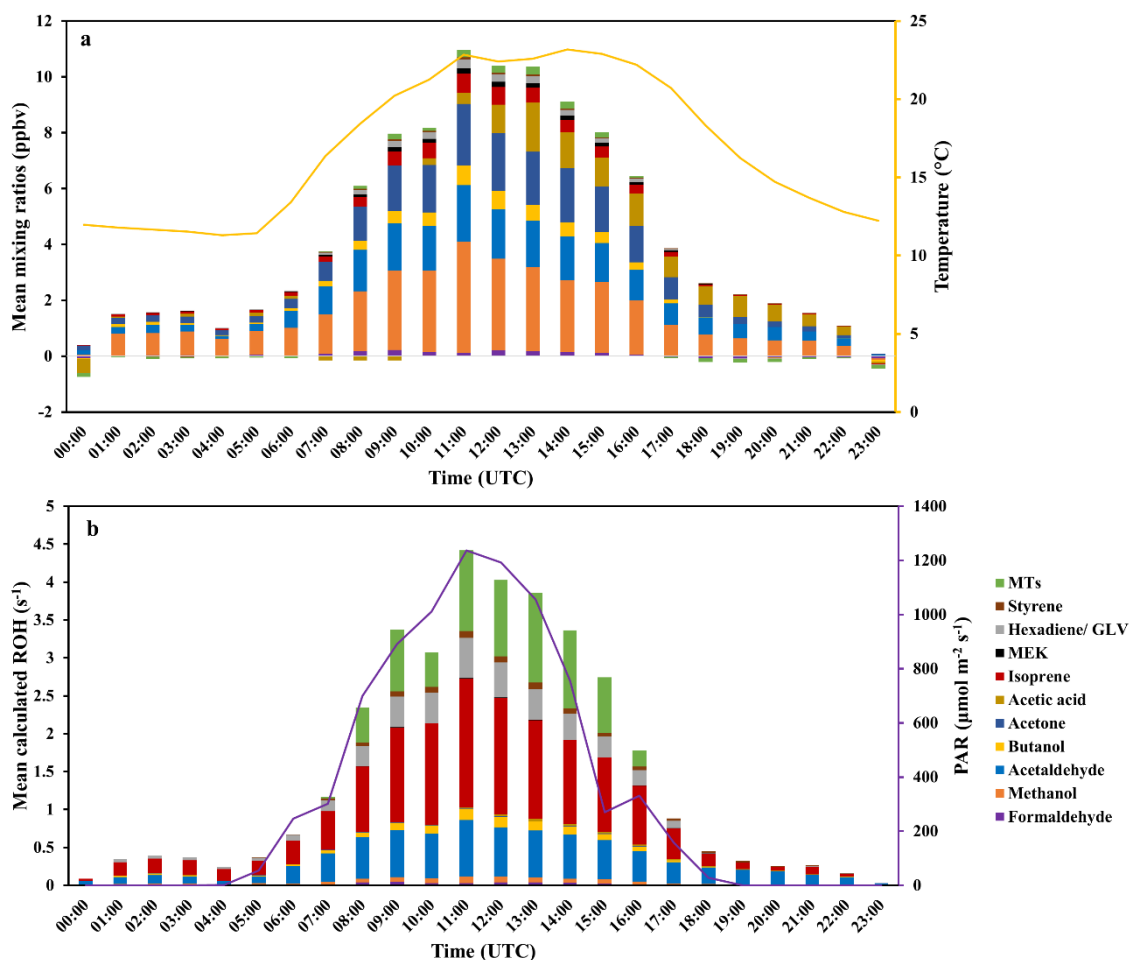


Figure 4.4 : Averaged diurnal variation of a) the mixing ratio of each BVOC measured with the PTRQI-ToFMS (ppbv) and b) their contribution to OH reactivity (s⁻¹).

When looking at individual BVOCs variability (S4.7), all compounds had a clear diurnal cycle, except for acetic acid whose variability followed neither temperature nor light. Emissions of isoprene, as well as of the rest of the OVOCs and hexadiene/Green Leaf Volatiles (GLV), were correlated to light and/or temperature, since they exhibited higher levels during day-time compared to the night-time, and for night-time levels, they showed higher levels during the 22nd night when higher night-time temperatures were recorded. Finally, monoterpenes did not show the same behavior and their emissions were close to zero during the night.

Figure 4.4.b, illustrates the mean contribution of each VOC_{rapeseed} to the mean calculated OH reactivity (cROH_{rapeseed}), that exhibited an average diurnal variation between the LOD and 4.4 s⁻¹. Interestingly, the major contributors to cROH_{rapeseed} during day-time were isoprene with 40 %, followed by acetaldehyde (21 %) and monoterpenes (18 %). Hexadiene/

GLV accounted for 12 % and the rest (formaldehyde, methanol, butanol, acetone, acetic acid, MEK and styrene), did not exceed 10 % all together. Despite that methanol was the most abundant compound in the chamber, its contribution to OH reactivity remains low, compared to less emitted but more reactive species, like isoprene and monoterpenes.

Compared to measured OH reactivity in the outgoing chamber air ($mROH_{\text{chamber}}$), all of the considered biogenic VOC_{rapeseed} explained 13 % on average of the $mROH_{\text{chamber}}$ during day-time with a maximum contribution at mid-day (11:00- 14:00 UTC) reaching 24 % on average, whereas during night-time, biogenic VOC_{rapeseed} contribution to $mROH_{\text{chamber}}$ was negligible. Contributions of ambient species and rapeseed emissions to $mROH_{\text{chamber}}$ are resumed in **Table 4.3**.

Table 4.3: Summary of the mean contribution of all the measured species (same time step) in the incoming and the outgoing chamber air to $mROH_{\text{chamber}}$ and the resulting missing OH fraction.

	Day-time Avg ± STD	Night-time Avg ± STD
cROH NO _x (s ⁻¹)	3.6 ± 2.2	3.8 ± 0.9
cROH HCs C ₂ - C ₆ (s ⁻¹)	0.4 ± 0.2	0.5 ± 0.2
cROH CO (s ⁻¹)	0.8 ± 0.1	0.9 ± 0.1
cROH CH ₄ (s ⁻¹)	0.3 ± 0.01	0.3 ± 0.07
cROH VOC _{ambient} (s ⁻¹)	0.8 ± 0.7	1.5 ± 1.0
cROH VOC _{rapeseed} (s ⁻¹)	1.9 ± 1.7	< LOD ± 0.7
Mean cROH _{chamber} (s ⁻¹)	7.8 ± 2.6	7.0 ± 1.5
Mean mROH _{chamber} (s ⁻¹)	14.4 ± 7.0	8.0 ± 2.6
Mean Missing ROH (s ⁻¹)	6.6 ± 5.0	1.0 ± 1.7
Mean relative Missing ROH (%)	46	13

4.3.2. Investigation of the missing OH reactivity

The comparison between measured OH reactivity ($mROH_{\text{chamber}}$) and the reactivity calculated by the sum of individually measured reactive compounds ($cROH_{\text{chamber}}$) enabled us to assess the known reactive carbon budget and to determine the “unaccounted for OH sink”, known as missing OH reactivity (ROH_{missing}). **Figure 4.5** shows the variability of $mROH_{\text{chamber}}$ and $cROH_{\text{chamber}}$. Little or no missing OH reactivity was observed during the night, whereas, a more important difference was seen around mid-day (mean mid-day missing OH reactivity $\approx 8 \text{ s}^{-1}$), suggesting that this missing OH reactivity was mainly related to light and/ or temperature-dependent compounds either primarily emitted or secondarily formed in the chamber.

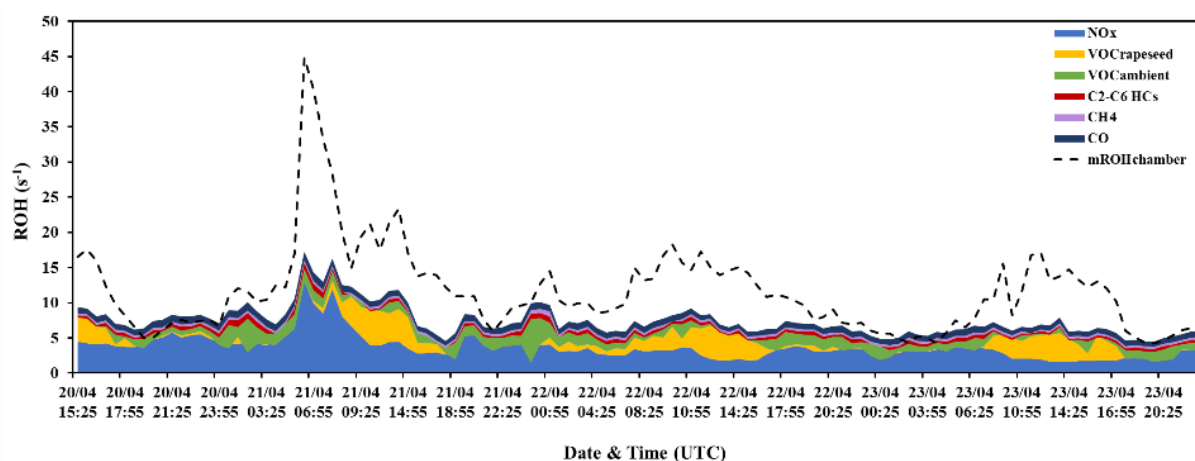


Figure 4.5: $mROH_{\text{chamber}}$ and $cROH_{\text{chamber}}$ from individual calculated ROH of VOCs (PTR-MS), VOCs (GC-FID), NO_x , CH_4 and CO summed up and the resulting missing ROH.

Among the approaches used to explore the origin of missing reactivity, one consists of correlating the missing OH reactivity with temperature (**Figure 4.6**). As such, we tried to fit the missing OH reactivity with the equation applied by Di Carlo et al. (2004), adapted from the one normally used to describe temperature-dependent emissions of monoterpenes (Guenther et al., 1993).

$$ROH_{\text{missing}}(T) = ROH_{\text{missing}}(293) \exp(\beta(T-293)) \quad (4.4)$$

with $ROH_{\text{missing}}(T)$ and $ROH_{\text{missing}}(293)$ representing the missing OH reactivity at a given temperature $T(\text{K})$ and 293 K, respectively and $\beta (\text{K}^{-1})$, the temperature sensitivity factor.

The β value obtained was around 0.14 K^{-1} with a correlation coefficient (R^2) of 0.8. In other studies, β ranged between 0.054 and 1.144 K^{-1} suggesting that in this study the day-time missing

OH reactivity may be related to temperature-dependent monoterpene-like emissions. Furthermore, missing OH reactivity moderately correlated with PAR, following an exponential relationship with a R^2 of 0.7, which suggests that the missing OH reactivity may also be due to light-dependent emissions, although it is difficult to disentangle radiation and temperature effects in field conditions, since both are correlated by the energy balance of the plant.

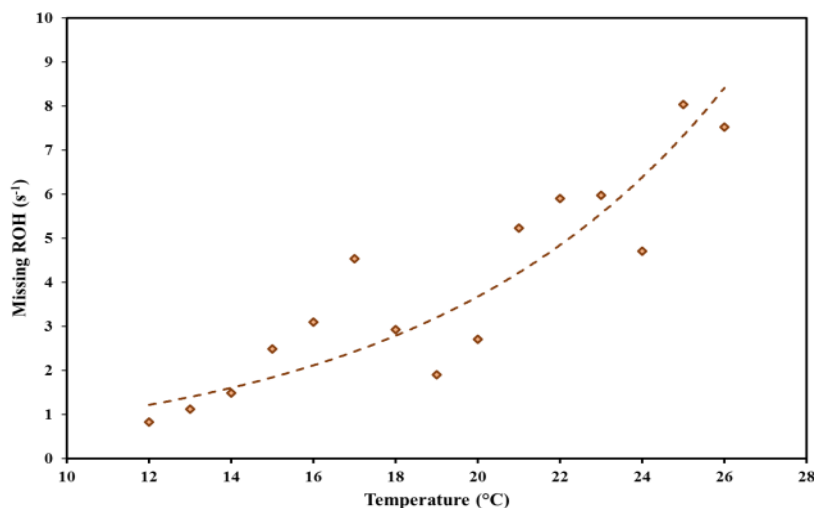


Figure 4.6 : Variability of missing OH reactivity as function of air temperature in the chamber. The regression curve equation is $ROH_{\text{missing}} = 0.23\exp(0.14(T))$ ($R^2 = 0.8$).

Figure 4.5 also demonstrates the clear diurnal co-variability between $cROH_{VOC_{\text{rapeseed}}}$ (orange) and ROH_{missing} (the difference between the dashed line of $mROH_{\text{chamber}}$ and the sum of calculated OH reactivity of the individually measured species), with higher levels around mid-day, suggesting that primary biogenic VOC_{rapeseed} , whose emissions are driven by temperature and/or light, are potential candidates for the day-time missing OH reactivity.

Mid-day missing OH reactivity: In order to investigate the potential species behind the observed mid-day missing OH reactivity, we looked at the PTRQi-ToFMS masses that correlated up to 80 % and more with isoprene. These correlations were done based on the fact that isoprene is a primary compound, which emission is known to be light and temperature dependent. As a result, 201 additional ions were investigated (See **Table S4.8**). However, when it came to estimate their contribution to total OH reactivity, this list was reduced to only 9 masses which were tentatively identified and which k_{OH} rate coefficients could be found (**Table 4.4**). Using their mixing ratios related to plant emissions (VOC_{rapeseed}), the selected 9 compounds exhibited a diurnal cycle with a maximum contribution of 1 to 1.2 s^{-1} around noon, and a negligible contribution during night hours (**Figure 4.7**). This observation is an evidence

that mid-day missing OH reactivity can be related to unaccounted primary emitted compounds, but the identified compounds only explained a part of the missing reactivity (12 % on average of mid-day missing OH reactivity). It is worth noting that, among the investigated ions (**Table S4.8**), m/z 41.038 was identified, as mentioned before (section 4.2.5), as potential fragment of isoprene. Considering its mixing ratio in the calculation of isoprene's OH reactivity, induces a maximum increase of 3 s^{-1} and an average increase of 1.9 s^{-1} around mid-day, explaining 24 % on average of mid-day missing OH reactivity. Thus, this test (**S4.9**) should be kept in mind while calculating OH reactivity and investigating the missing OH reactivity.

Considering the masses that correlated 90 % and more with m/z 69.070 (excluding the masses already investigated and mentioned in **Tables 4.2** and **4.4**), their summed mixing ratios in the chamber air out, ranged between the LOD and 0.8 ppbv. If all of them had a comparable reactivity to that of isoprene, towards the hydroxyl radical, their contribution to total OH reactivity would reach a maximum of 2.1 s^{-1} and would explain 16 % on average of mid-day missing OH reactivity. This contribution would reach a maximum of 0.02 s^{-1} only if all the investigated compounds had a reactivity comparable to that of methanol, explaining only 0.1 % on average of mid-day missing OH reactivity. Regarding the masses that correlated between 80 % and 90 % with m/z 69.070, their summed mixing ratios accounted for a maximum of 2.7 ppbv, contributing up to 6.9 s^{-1} and 0.06 s^{-1} , if all of them had a comparable reactivity to that of isoprene or methanol, respectively. These masses would explain up to 52 % and only 0.5 % on average of mid-day missing OH reactivity with a reactivity as high as that of isoprene or as low as that of methanol, respectively.

Table 4.4: List of the 9 selected masses which presented a correlation of 80% and more with isoprene (m/z 69.070).

Protonated theoretical mass	Chemical formula	Chemical compound	Rate constant ($\times 10^{-12} \text{ cm}^3 \text{ molecule}^{-1} \text{ s}^{-1}$)	Max mixing ratio (ppbv)	Max calculated ROH (s^{-1})	Ref
57.033	$\text{C}_3\text{H}_4\text{O}$	Propenal	19.6	0.23	0.11	(Atkinson, 1985)
85.064	$\text{C}_5\text{H}_8\text{O}$	Ethylvinylketone	36 ^a	0.06	0.06	(Grosjean and Williams, 1992)
85.1	C_6H_{12}	Hexene	37 ^a	0.18	0.17	(Grosjean and Williams, 1992)
87.078	$\text{C}_5\text{H}_{10}\text{O}$	2-Methylbutanal ^b	32.8 ^c	0.06	0.05	(D'Anna et al., 2001)
97.098	C_7H_{12}	Methylcyclohexene	96.1 ^d	0.3	0.66	(Darnall et al., 1976)
109.1	C_8H_{12}	4-Ethenylcyclohexene	63.9 ^a	0.23	0.36	(Grosjean and Williams, 1992)
119.082	C_9H_{10}	Indan	19.1 ^e	0.02	0.01	(Kwok et al., 1997)
133.098	$\text{C}_{10}\text{H}_{12}$	Benzene, (2-methyl-1-propenyl)-	33	0.01	0.01	(Chiorboli et al., 1983)
157.105	$\text{C}_{12}\text{H}_{12}$	Dimethylnaphtalene	74.9 ^f	0.03	0.06	(Phouongphouang and Arey, 2002)

a: Theoretical rate constant at 298 K and 1 atm

b: Other compounds may exist, 3-Methylbutanal and 2-pentanone.

c: The rate coefficient of the reaction of sec-C₄H₉CHO (2-Methylbutanal) was considered and this rate constant is higher than that of 2-pentanone ($k_{\text{OH}} = 4.56 \times 10^{-12} \text{ cm}^3 \text{ molecule}^{-1} \text{ s}^{-1}$ (Atkinson et al., 2000)

d: Rate constant at 305 K

e: Rate constant at 297 K

f: Rate constant of 1,3-dimethylnaphtalene, which is the highest among the rate coefficients of dimethylnaphtalene isomers with OH and which range between $57.9 \times 10^{-12} \text{ cm}^3 \text{ molecule}^{-1} \text{ s}^{-1}$ and $74.9 \times 10^{-12} \text{ cm}^3 \text{ molecule}^{-1} \text{ s}^{-1}$

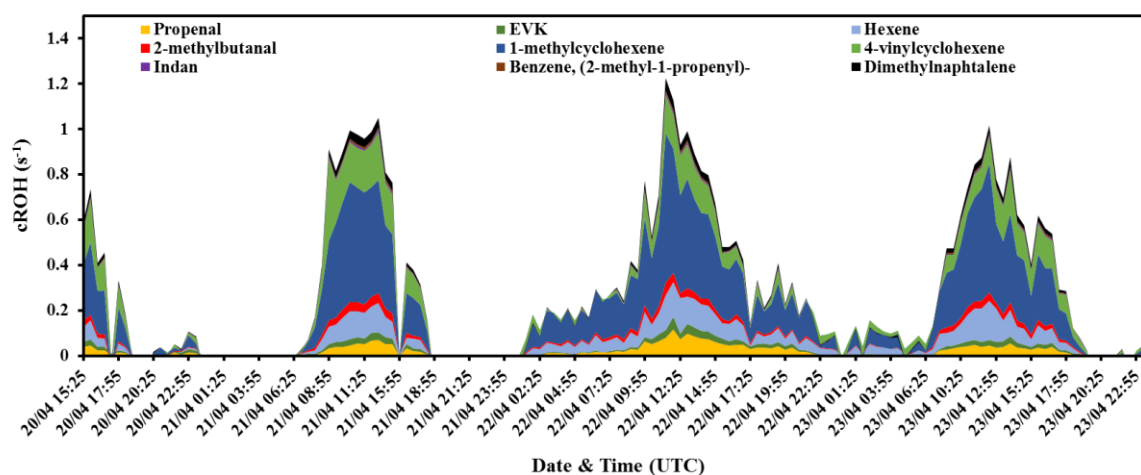


Figure 4.7: Summed calculated OH reactivity of the 9 additionally selected compounds. The mixing ratios used for the calculation correspond to the ones from the rapeseed branch ($\text{VOCs}_{\text{rapeseed}}$) and the k_{OH} are the ones mentioned in Table 4.4.

Other masses: Gonzaga Gomez et al. (2019) reported the presence of other masses which were not necessarily observed in previous studies on *Brassica napus* (König et al., 1995; Morrison et al., 2016; Müller et al., 2002; Veromann et al., 2013). Among these masses, m/z 43.018 exhibited relatively large mixing ratios, reaching 5 ppbv. This observation is not surprising, knowing that this mass represents a fragment of several oxygenated compounds. This implies that the mixing ratios of some oxygenated compounds were underestimated, leading to an underestimation of the calculated OH reactivity. Based on an intercomparison exercise (Eurochamp, Orléans, 2019), in which the deployed PTRQi-ToFMS participated along with many other PTR-MS instruments, the fragmentation rates on m/z 43.018 on the deployed PTRQi-ToFMS were as following: acetone 3.4 %, acetaldehyde 3.6 %, acetic acid 20 %, MVK 13%, MEK 1.0% (Lafouge F. personal communication). Taking these rates into account and correcting the mixing ratios of acetone, acetaldehyde, acetic acid and MEK for potential fragmentation in OH reactivity calculations, increased the calculated OH reactivity by 0.05 s⁻¹ maximum. This result highlights that, not accounting for fragmentation that can occur on some oxygenated VOCs, is not responsible of the observed missing OH reactivity.

Other missing OH reactivity events

In addition to mid-day missing OH reactivity, a higher missing OH reactivity was also observed in the early morning of the 21st April (around 07:00 UTC) and in the beginning of the evening (around 18:00 UTC) as well as on the mid-night and during the night of the 22nd April, 2017 (**Figure 4.8**). Regarding the night of the 22nd April, higher night-time mixing ratios of some BVOCs in the chamber were recorded (i.e. isoprene), meaning that this event could be explained by unknown biogenic emissions from the plant. Interestingly, acetic acid, whose emission did not follow clearly temperature or light, also exhibited larger concentration levels during this night. Studies showed that acetic acid can be primary emitted by vegetation or generated from secondary reactions (Seco et al., 2007). Gonzaga Gomez et al. (2019), reported emissions of acetic acid from rapeseed during the senescence period. Furthermore, Veromann et al. (2013), reported higher acetic acid emissions from rapeseed after nitrogen fertilization, which could be the case in our experiment, since N-treatment was applied twice before the campaign. Seen the relatively short residence time and the relatively rapid air renewal in the dynamic enclosure, chances for acetic acid formation via secondary chemistry are low. These post N-treatment emissions could also be detected under several masses (**Table S4.8**) which were identified as N-containing compounds (Kammer et al., 2019). This includes m/z 100.074,

m/z 116.074, m/z 124.117, m/z 138.059 and m/z 252.158, identified as C_5H_9NO , $C_5H_9NO_2$, $C_8H_{13}N$, $C_7H_7NO_2$ and $C_{14}H_{21}NO_3$.

No specific behavior related to BVOCs emissions from the enclosed plant could explain the higher missing OH reactivity observed in the early morning of the 21st, April (around 07:00 UTC) and in the beginning of the evening (around 18:00 UTC) as well as on the mid-night of the 22nd April (**Figure 4.8**). However, investigating known anthropogenic VOCs, such as benzene (m/z 79.053) and benzaldehyde (m/z 107.049), detected with the PTRQI-ToFMS, demonstrated the higher ambient mixing ratios of these compounds during the mentioned events. Therefore, these events of missing OH reactivity could be mainly attributed to emissions of anthropogenic origin.

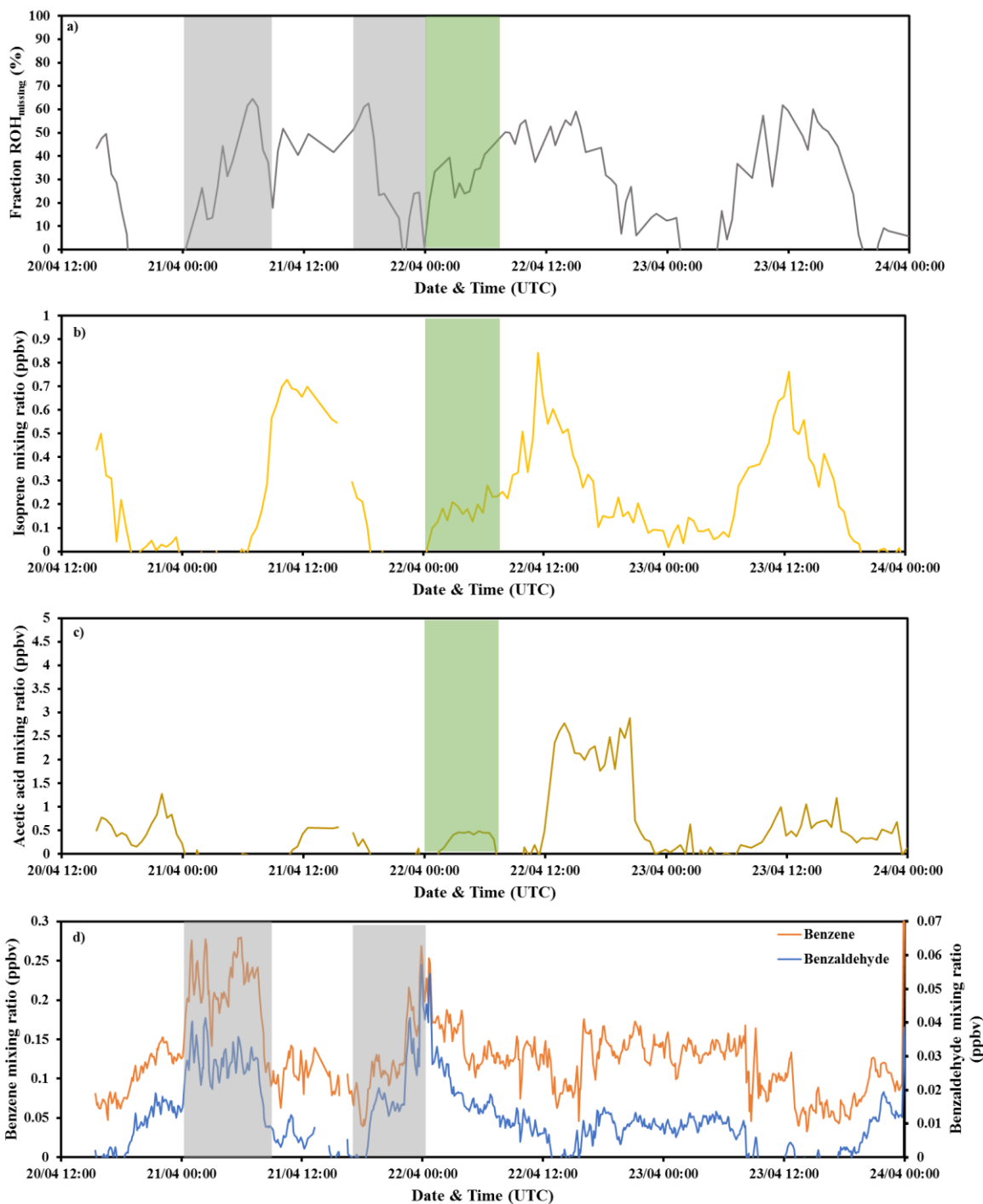


Figure 4.8: a) Variability of relative missing OH reactivity ($ROH_{\text{missing}}/mROH_{\text{chamber}}$) with b) Isoprene (rapeseed), c) Acetic acid (rapeseed) and d) Benzene (orange) and Benzaldehyde (blue) in ambient air. Green areas indicate missing OH reactivity mainly due to biogenic emissions and grey areas indicate missing OH mainly linked to anthropogenic emissions.

4.4. Conclusion

OH reactivity, defined as the total loss rate of the hydroxyl radical in the atmosphere, has showed to be an effective parameter to evaluate the loading of reactive species in ambient air. Despite that total OH reactivity measurements were performed in various environments, little was done over agricultural ecosystems. This study, presents the first characterization of total OH reactivity from rapeseed (*Brassica napus*) by means of a dynamic enclosure chamber during the blooming period in the Fr-Gri ICOS site, southwestern Paris, April 2017.

The average total OH reactivity measured from the dynamic chamber during day-time was $15 \pm 7 \text{ s}^{-1}$, against $8 \pm 3 \text{ s}^{-1}$ during night-time. OH reactivity varied diurnally in a similar manner as BVOCs emissions, which were driven by temperature and/or light. Rapeseed emissions were dominated by oxygenated compounds, which is in agreement with some previous studies. However, in terms of OH reactivity, isoprene had the largest contribution during the day, followed by acetaldehyde and monoterpenes, whereas during the night, biogenic VOCs had a negligible contribution to OH reactivity. This shows the interest to measure OH reactivity in addition to VOC abundance. No significant difference was observed between measured and calculated OH reactivity during night-time, whereas a missing fraction of up to 8 s^{-1} on average was observed around mid-day. During day-time, missing OH reactivity was exponentially correlated mainly to temperature but also to light. Further investigation of PTRQi-ToFMS masses suggested that day-time missing OH reactivity fraction is mostly related to primary emitted compounds, especially because the short residence time in the chamber (4 min) lowers the chances for secondary chemistry.

One main strength of this field experiment is to have carried out parallel measurements with the CRM and the PTRQi-ToFMS, which reflected the presence of “unaccounted for” reactive species. However, we were limited in terms of missing OH reactivity estimation, in particular due to challenges in identifying the chemical compounds behind the detected ions as well as their reaction rate coefficients for the reaction with OH. This study demonstrated the need for coupling PTR-MS and GC techniques in order to identify the compounds behind the masses detected by the PTR-MS, especially when several possible compounds are suggested for the same molecular mass. Finally, it could be of great interest to perform more laboratory work aiming to broaden our knowledge on the gas-phase chemistry and kinetics of a wider variety of atmospheric compounds with the hydroxyl radical, such as for some N-containing compounds

(C₅H₉NO, C₅H₉NO₂, C₈H₁₃N and C₇H₇NO₂), which exhibited, a diurnal cycle in the chamber air out.

Our work highlights that the studied rapeseed crop is a relatively low contributor to the amount of reactive species released in the atmosphere, and a relatively low contributor to total OH chemistry compared to forest ecosystems. If this is confirmed, this may mean that the expansion of bioenergy crops, like rapeseed, may have a limited impact on atmospheric OH chemistry. We should bear in mind, though, that bioenergy crops production has other impacts on the atmosphere and terrestrial ecosystems through ammonia and nitrous oxides emissions or nitrate leaching, and represent critical food security issues.

Supplementary Materials: The following are available online at www.mdpi.com/xxx/s1, *Figure S4.1.a*. Linear least square fit of ΔC_2 (ppbv) vs. $\Delta(m37/m19)$ for the tests conducted on the field to assess the correction for humidity differences between C2 and C3. Green dots and red dots correspond to tests performed with ambient air and outgoing chamber air, respectively, *Figure S4.1.b*. Experimental parameterization to correct for the NO interference, representing changes in C3 (ΔC_3 ppb = $C_{3\text{expected}} - C_{3\text{measured}}$) as function of NO mixing ratios (ppbv) in the reactor, *Figure S4.1.c*. Measured ROH vs. the theoretical ROH for propane and isoprene, introduced at different concentrations and under different pyrrole/OH ratios. Circles and diamonds correspond to propane and isoprene tests, respectively, *Figure S4.2*. Schematic of the CRM/PTR-MS sampling system, *Table S4.3*. Standard Ionicon transmission curve used for computing the mixing ratio, *Figure S4.4*. Rapeseed branch evolution in the dynamic enclosure. The left vertical axis represents the length of the stem, total leaves and total flowers (in cm). The right vertical axis represents the percentage of open flowers. The red line indicates the day when the chamber was re-installed after the planned fungicide application, *Figure S4.5*. Temperature recorded inside the dynamic chamber (yellow) and in ambient air (green) during the measurement period between the 20th and the 23rd, April 2017, *Figure S4.6.a*. Variability of NO_x (NO, NO₂), CO, CH₄, propane, propene, acetaldehyde and acetone in ambient air, with wind direction and wind speed, *Figure S4.6.b*. Variability of calculated OH reactivity of NO_x, CO, CH₄, total HCs C₂-C₆ and total VOC_{Sambient} (PTRQi-ToFMS), *Figure S4.7*. Variability of calculated OH reactivity of some biogenic VOCs emitted by the rapeseed plant ($\text{VOC}_{\text{rapeseed}} = \text{VOC}_{\text{chamber}} - \text{VOC}_{\text{ambient}}$), *Table S4.8*. List of the 201 masses that correlate for 80 % and more with isoprene (m/z 69.070), *Figure S9*. Variability of calculated OH reactivity using PTR-MS data with a correction of the isoprene signal (m/z 69.070) by a factor of 1.3 (blue) and by summing the m/z 69.070 with the potential fragment on m/z 41.038 (yellow).

Author Contributions: Methodology S.B., F.T. and R.S.-E. for the CRM-PTRMS, V.G. and D.B. for the GC-FID, F.L., R.C., L.G.-G. and B.L., P.B. for the NO_x measurements and meteorological data, C.B. for the dynamic chamber, F.T. for CO measurements; formal analysis, S.B., F.T. and B.L., data curation, S.B., F.T., V.G., F.L., R.C., P.B., J.K. and L.G.-G.; writing—original draft preparation, S.B.; writing—review and editing, S.B., V.G., B.L., C.B., N.Z., J.K., R.C., P.B.; supervision, V.G.; project administration, B.L.; funding acquisition, B.L.. All authors have read and agreed to the published version of the manuscript.

Funding: This research was funded by ADEME (COV3ER, n°1562C0032) project.

Acknowledgments: The authors acknowledge the European Union's Horizon 2020 research and innovation program under the Marie-Sklodowska-Curie grant agreement No 674911- IMPACT, the EU ICOS Research Infrastructure, ANAEE-FR services (ANR project n°11-INBS-0001) which provided the PTR-TOF-MS, the CNRS and the CEA. We gratefully thank Dominique Tristant and Yves Python from AgroParisTech farm for giving access to their fields. We would also like to thank S. Assan and F. Vogel for the methane data.

Conflicts of Interest: The authors declare no conflict of interest. The funders had no role in the design of the study; in the collection, analyses, or interpretation of data; in the writing of the manuscript, or in the decision to publish the results.

Conclusion chapitre 4

Les résultats obtenus durant la campagne COV³ER-2017, montrent que la réactivité en sortie de la chambre de colza (ROH_{chambre}) se situe dans la limite inférieure des réactivités préalablement mesurées dans d'autres écosystèmes. En effet, la ROH_{chambre} , variait suivant un cycle diurne, avec des maxima de jour ne dépassant pas les 20- 30 s^{-1} et des minima de nuit, ayant le même ordre de grandeur que les niveaux de réactivité en entrée de la chambre (7.5 s^{-1}). Ceci indique les faibles émissions de COVBs par la plante ou même leur absence, durant la nuit.

Les mesures en parallèle avec le PTR-ToF-MS présentait un gros avantage. Parmi les ≈ 500 masses détectées, une première liste de 12 composés a été sélectionnée, comme étant les masses les plus échangées au niveau de la chambre dynamique dont la nature chimique et la constante cinétique sont connues. Parmi ces composés, les COVs oxygénés se sont avérés majoritaires, alors que l'isoprène et les monoterpènes ont montrés des niveaux relativement faibles. Ceci est en bon accord avec les observations de Gonzaga Gomez et al. (2019), sur une chambre dynamique de colza, durant la période de senescence du même champ agricole. Malgré leurs faibles niveaux, l'isoprène et les monoterpènes se présentaient, comme les principaux contributeurs à la réactivité OH en sortie de la chambre durant le jour, alors que les oxygénés, avec leurs faibles constantes cinétiques avaient une moindre contribution. La comparaison entre la réactivité mesurée et celle calculée des données PTR-ToF-MS, GC-FID, NOx, CO, CH₄, montre une différence. Plus spécifiquement, la réactivité mesurée et celle calculée étaient généralement en bon accord durant la nuit, alors que, dès l'apparition du rayonnement solaire, la différence augmentait progressivement, pour atteindre un maximum en milieu de journée ($\approx 46\%$ en moyenne), et rediminuer dans l'après-midi. Ce comportement montre que la réactivité manquante est liée à la présence de composés réactifs, dont l'émission et par la suite la concentration dans la chambre, sont dépendants de la température et/ ou la lumière. Cependant, une réactivité manquante observée durant une nuit plus chaude, suggère plutôt une dépendance à la température.

Comme déjà mentionné, un grand nombre de masses mesurées au niveau de la chambre dynamique, étaient mis à notre disposition grâce au PTR-ToF-MS. L'idée était d'aller chercher des composés pouvant potentiellement expliquer la réactivité manquante de jour en vérifiant leur corrélation avec l'isoprène, dont l'émission est connue d'être température et lumière-dépendante. 201 masses supplémentaires ont été sélectionnées. Pour 9/201, des composés chimiques ont été proposés pour lesquels des constantes cinétiques ont été trouvées. Cependant,

ces composés, présentant un cycle diurne, n'ont pas pu expliquer plus que 1 à 1.2 s⁻¹ au maximum de la réactivité manquante de jour.

*5. Monoterpenes chemical speciation
with high time resolution using a
FastGC/PTR-MS: Results from the
experiment on Quercus ilex in
Southern France, during summer
2018*

Introduction Chapitre 5

Les deux études précédentes, effectuées l'une dans un écosystème agricole et l'autre dans un écosystème forestier, mettent en évidence le rôle important que peuvent jouer les monoterpènes, même s'ils sont faiblement émis. Ce chapitre, présente l'étude visant à caractériser la variabilité des monoterpènes spéciés, avec une résolution temporelle fine. En effet, et comme montré dans les deux premières études, les monoterpènes sont des contributeurs importants à la réactivité OH, même s'ils sont émis sous faibles quantités, comme pour le colza. En plus, leur oxydation peut conduire à la formation d'aérosols organiques secondaires et le rendement varie normalement d'un monoterpène à l'autre. Ainsi, il s'avère important d'avoir une information détaillée de ces monoterpènes, afin de mieux comprendre leur rôle dans la chimie de l'atmosphère.

Parmi les instruments utilisés pour les mesures des COVBs, la chromatographie en phase gazeuse fournit une information détaillée sur les isomères, cependant avec une résolution temporelle comprise entre 30 min et 1h 30 min. Le PTR-MS est une autre technique révolutionnaire qui trouve plusieurs types d'application dans le domaine de la qualité et chimie de l'air, vu sa sensibilité et sa sélectivité. Cependant, cet instrument demeure incapable de distinguer les isomères, ce qui risque d'être une des limitations de son utilisation. Ainsi et dans le but de combiner les avantages de ces deux instruments, un système FastGC/PTR-MS a récemment été développé. Déployé dans des études en sciences alimentaires et atmosphériques, ce système s'avère efficace dans la séparation rapide des monoterpènes avec une résolution satisfaisante. Cependant, des améliorations se sont révélées pour une meilleure séparation de certains composés qui co-éluent et pour une analyse plus rapide. De notre côté, on a travaillé sur le couplage d'une nouvelle version du prototype d'une FastGC avec le PTR-QuadMS présent dans notre laboratoire. Des expériences de laboratoire, ont permis d'optimiser au mieux les paramètres opérationnels pour une meilleure séparation des principaux monoterpènes dans un écosystème forestier. Plusieurs rampes de températures, et différents débits du gaz vecteur ont été testés ; une combinaison des deux a montré des résultats satisfaisants à appliquer sur le terrain. L'hélium a été choisi comme gaz vecteur pour une séparation de bonne qualité et rapide par rapport à l'azote. Finalement, la limite de détection du système a été déterminée, aux alentours de 500 pptv/monoterpène.

Monoterpenes chemical speciation with high time resolution using a FastGC/PTR-MS: Results from the experiment on *Quercus ilex* in Southern France, during summer 2018

Sandy Bsaibes¹, Felix Piel², V. Gros¹, F. Truong¹, F. Lafouge³, R. Ciuraru³, P. Buysse³, J. Kammer³, B. Loubet³, Michael Staudt⁴

¹ Laboratoire des Sciences du Climat et de l'Environnement, LSCE, UMR CNRS-CEA-UVSQ, IPSL, Gif-sur-Yvette, Île-de-France, 91191, France

² Ionicon Analytik GmbH, Innsbruck, Austria

³ Institut national de recherche pour l'agriculture, l'alimentation et l'environnement, INRAe, UMR INRAe-AgroPariTech, Université Paris Saclay, Route de la Ferme, 78850 Thiverval-Grignon, France

⁴ Centre d'Ecologie Fonctionnelle et Evolutive UMR 5175, 34090 Montpellier, France

Correspondence to: Sandy Bsaibes (sandy.bsaibes@gmail.com)

Valérie Gros (valerie.gros@lsce.ipsl.fr)

Abstract

Monoterpenes represent an important family of biogenic VOCs in terms of amount and chemical diversity. They can have very different lifetimes towards atmospheric oxidants with variable contributions to tropospheric ozone and secondary organic aerosols formation, which arises the attention to investigate their role in atmospheric chemistry. This family of BVOCs has been extensively studied in various environments using gas chromatography and proton-transfer-reaction mass spectrometry. The first technique provides detailed information on isomers chemical speciation, however with a time resolution higher than 30 min, and the second technique brings the advantage of real-time/ higher sensitivity measurements, without the ability of isomers differentiation. To overcome these limitations; FastGC was introduced few years ago and was commercialized with the PTR-ToF-MS, showing promising results in real-time separation of isomers, with the need of further improvements depending on the application. In this context, a new version of a FastGC prototype was coupled to a PTR-QuadMS available in our laboratory. Extensive laboratory experiments were performed, in order to test the system's performance and to optimize its operational parameters for monoterpenes separation. Several temperature ramps and carrier gas flow rates were tested, showing satisfying results. Helium was selected as carrier gas, with a flow rate of 3 sccm, and the detection limit was

determined to be around 500 pptv/monoterpene. The system was afterwards deployed in a three-weeks field campaign, taking place in the green oak forest located in Puechabon, South of France. Known for its important monoterpenes emissions, dynamic enclosures were installed at four different branches of four different oak trees. BVOCs and speciated monoterpenes were measured in the incoming and the outgoing chambers air. Results demonstrated the feasibility of the FastGC/PTR-MS system for continuous measurements in the field. It also allowed to distinguish between three types of green oak trees, having different proportions of the emitted monoterpenes: pinene-type, myrcene-type and limonene-type. The type of emissions is genetically fixed, with a diurnal variability that showed to be dependent on solar radiation.

5.1. Introduction

Terrestrial vegetation, including forests, crops, grasslands and shrubs, represents the dominant source of volatile organic compounds released in the atmosphere. With 750 - 1150 TgC yr⁻¹ estimated annual global emissions, they account for about 90% of total VOCs emissions (Guenther et al., 1995; Lathière et al., 2006). Plant-produced VOCs are of particular interest, seen their abundance and their considerable role in gas phase and heterogeneous chemistry of the troposphere. Indeed, they are subject to photochemical processes, involving atmospheric oxidants like OH, O₃ and NO, leading to the formation of harmful tropospheric ozone and secondary organic aerosols. Despite the considerable effort invested to better understand BVOCs-mediated tropospheric photochemistry, substantial uncertainties still exist, highlighted by discrepancies often found between measured total OH reactivity and the estimated OH reactivity derived from simultaneous VOCs measurements, with total OH reactivity defined as the sum of the concentration of each compound, multiplied by the respective k rate coefficient of the reaction with OH. These differences, noted as missing OH reactivity, are due to unmeasured or unidentified primary emitted and/ or secondary formed reactive species. They highlight the need of a more detailed characterization of BVOCs, especially in forest environments where higher values of OH reactivity and missing OH reactivity were reported (Hansen et al., 2014; Mao et al., 2012; Nölscher et al., 2012a, 2016; Sinha et al., 2010; Zannoni et al., 2017).

In natural ecosystems, VOCs are emitted from all plants organs, namely flowers, stems, roots and most importantly foliage, with a large chemical diversity. They serve as communication intermediates and can be released as part of the plant defense strategy against herbivores,

pathogens and abiotic stresses. Their amount as well as their chemical composition show a genotypic variation as well as a dependency on biotic (plants, animals, microorganisms) and abiotic external factors such as temperature, light and water availability (Penuelas & Llusia, 2001). The most prominent compound groups, are isoprene and monoterpenes, representing 70% and 11%, respectively of BVOCs global estimated flux (Sindelarova et al., 2014). While isoprene has a single known k rate coefficient in respect to atmospheric oxidants, monoterpenes consist of multiple structural isomers with greatly varying reactivities. Furthermore, they contribute to the formation of secondary organic aerosols (SOA), with variable yields. Indeed, limonene photooxidation showed a relatively high SOA yield (58%), compared to α -pinene and β -pinene which SOA yields are around 32 and 31%, respectively (Lee et al., 2006). As such, it is of great interest to quantify each individual monoterpenes isomer in order to achieve a better characterization of BVOCs implications in the oxidative capacity of the atmosphere. In addition, monoterpenes were reported to be dominant in some forests ecosystems, with pool emissions depending only on temperature or de novo emissions depending on light and temperature, in the same manner as isoprene emissions. Seen their variable emission rates and their relatively high reactivities, ambient air concentrations of monoterpenes can show significant short-term variabilities, which requires high-time resolution measurement techniques.

Several analytical techniques have been used to characterize monoterpenes emissions from plants. Conventional gas chromatography methods, providing detailed information regarding the chemical composition, is one of them. As such, monoterpenes isomers could be separated and quantified, however with a frequency varying between 30 min and 1 h 30 min. PTR-MS is another revolutionary technique allowing real-time determination of monoterpenes at low atmospheric levels (ppbv- pptv). However, PTR-MS is limited by its inability to distinguish compounds with the same molecular mass. In order to combine the advantages of both techniques, a FastGC/PTR-MS system was developed, tested and deployed in food (Romano et al., 2014) and atmospheric sciences (Materić et al., 2015; Pallozzi et al., 2016; Papurello et al., 2016). Indeed, PTR-MS provided real-time measurements of total monoterpenes and the GC method allowed the identification and the quantification of each one of them. While Romano et al. (2014), were the first to test a FastGC prototype coupled to a PTR-ToF-MS on wine, proving that the technique extended the analytical capabilities of the PTR-MS, Materić et al., (2015) deployed the system for plant monoterpenes research. In their study, laboratory experiments on monoterpenes standards, Scots pine, black pine and Norway spruce samples,

showed the potential of this method for the separation and the identification of low concentrations (4- 6 ppbv per individual monoterpene) of most abundant monoterpenes, through rapid chromatographic runs. However, the system was still subject to optimization, in terms of temperature ramp, injection time, flows, total run time, carrier gas and column type and length. Later on, Pallozi et al. (2016) used the built-in Fast-GC, coupled to a PTR-ToF-MS to characterize individual monoterpenes emissions from branch enclosures of young *Quercus ilex* (three-year-old) and *E. camaldulensis* (two-year-old) saplings, while changing the enclosure temperature. Their system appeared to be quite sensitive but not sufficiently selective, since sabinene and β -pinene co-eluted and p-limonene and cis- β -ocimene were partially separated. These studies showed that the FastGC/PTR-MS system is a promising technique for near real-time characterization of individual monoterpenes. They also confirmed the need for a further characterization in order to achieve a fast separation with a good resolution.

BVOCs, and more particularly monoterpenes emissions from *Quercus ilex*, have been subject to extensive studies, in the last three decades. Abundant in the Mediterranean area, *Quercus ilex* is known as a strong emitter of monoterpenes, contrary to many deciduous oak species emitting large amounts of isoprene. The short-term control of monoterpenes emissions, involved not only temperature but also light. In that manner, the usual exponential function used to describe temperature-dependent emissions of monoterpenes was not sufficient, and the model developed for isoprene showed to be more suitable. These conclusions were confirmed by other observations demonstrating that, monoterpenes from *Quercus ilex* are formed in the chloroplast from photosynthesis intermediates, and they are emitted after synthesis as response to light induction, without being accumulated inside leaves or bark (Loreto et al., 1996; Staudt and Seufert, 1995). Previous studies, used chromatographic techniques and showed that α -pinene, sabinene and β -pinene are the main emitted monoterpenes, representing about 80 % of total monoterpenes. This is the case of the dominant chemotype in Mediterranean oak forests. However, other studies highlighted the presence of other chemotypes with different genetically fixed emissions of monoterpenes, with a dominance of limonene or myrcene (Staudt et al., 2001).

Would the FastGC/PTR-MS be an adequate tool for continuous individual monoterpenes separation and detection, in a real environment? What are the challenges associated to the instrument deployment on the field? Are we able to detect all the previously reported monoterpenes with a better time resolution compared to classical chromatographic methods

used in previous studies? Do all detected monoterpenes exhibit the same variability with light, even with rapid changes in the radiation received by the branch?

This study is the first one to deploy a non-commercialized FastGC/PTR-QuadMS system in a three-weeks field experiment. It aimed to (i) optimize monoterpenes measurements with the FastGC/PTR-MS system through extensive laboratory experiments and (ii) deploy it in a field experiment to characterize speciated monoterpenes emissions, with a relatively high time resolution (10 min). Measurements were performed from different branches and stem dynamic chambers, in the Puechabon forest, a region characterized by its Mediterranean climate with hot/ dry summers. The performance of the system was tested during this field work. Levels of individual monoterpenes were monitored and BVOCs fluxes were calculated for each branch and stem chamber, in order to evaluate the branch-to-branch and stem-to-stem emissions variabilities.

5.2. Materials and methods

5.2.1. Description of the measurement site

The ADEME-COV³ER field campaign was conducted between June and July 2018 at the Puechabon experimental site. It is located 35 km northwestern Montpellier, south of France (43°44'30" N, 3°35'40" E). The forest is dominated by *Quercus ilex* which represents more than 80% of the vegetation. The average tree height is about 5.5 m and the density of stems is around 4700 stems per ha (2015). The main species composing the understory are *Buxus sempervirens*, *Phyllirea latifolia*, *Pistacia terebinthus* and *Juniperus oxycedrus*. The area is characterized by a Mediterranean climate, with rainfalls during autumn and winter and dry conditions during summer. This forest grows on a rocky soil from hard Jurassic limestone filled with clay. Because of the large fraction of rocks and stones in the soil profile available water cumulated over 4.5 m depth averages only 150 mm. As a consequence of this small soil water reserve, the vegetation undergoes very frequent drought stress during the summer (source: <http://puechabon.cefe.cnrs.fr/spip.php?article1>).

5.2.2. Branch enclosure



Figure 5.1: Photos of the branch (left) and stem chambers (right) used during the COV³ER- 2018 Puéchabon field experiment.

In order to achieve a better time resolution chemical speciation of monoterpenes and to monitor their mixing ratios variability, dynamic enclosure systems were deployed on *Quercus ilex* branches and stems (**Figure 5.1**). During the COV³ER- 2018 Puechabon field campaign, two branch dynamic chambers and two stem chambers were installed in parallel on 4 different branches and two different stems. The branches were enclosed in cylindrical shaped chambers with a 15 cm diameter. Each chamber consisted of two Plexiglas rings interconnected with 3 thin metal braces that were adjusted in length to suit the branch size. The air flow was kept around 7- 11 L min⁻¹ for a volume of approximately 3.5 L.

The stem chambers, consist of a U-shape stainless steel sheet (5 cm wide and 50 cm long) vertically fixed on the stem at a 3 cm distance to the bark, to which is clipped a coated 50 µm thin FEP film surrounding the stem. The ends of the film are pressed to the stem with bungee cords and flexible plastic rods are added to prevent the film being drawn to the stem during sampling. The estimated stem surface enclosed is between 1460 and 1760 cm². The air flow running through the stem chambers ranged between 4 and 7 L min⁻¹ and the volume of the enclosed air around the stem section was about 5.6 – 6 L.

Unfiltered ambient air was drawn through the chambers so they were operated at slight under-pressure. A small fan with Teflon blades allowed mixing of the chamber air and maintained heat exchange. Temperature and PAR were monitored continuously using a thermocouple placed inside and a quantum probe placed outside of the chamber, respectively. CO₂ and H₂O exchanges were measured with a LICOR 840 infra-red gas analyzer. Further details can be found in (Staudt et al., 2018).

5.3. FastGC/PTR-MS system

5.3.1. Description of the FastGC system and mode of operation

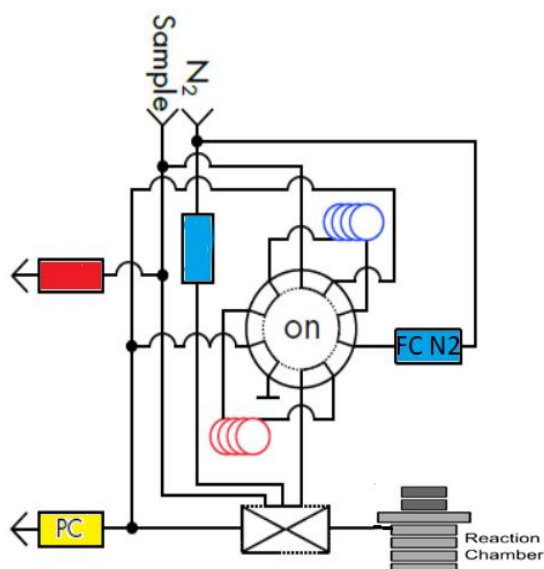


Figure 5.2: Schematic drawing of a PTR-QuadMS inlet system with a FastGC setup including a capillary column, a sample loop and a 10-port valve allowing the switching between real-time and FastGC measurements.

This study focused on determining the variability of monoterpene speciation from different compartments of the studied oak forest ecosystem. For this purpose, PTR-QuadMS (IONICON Analytik, Innsbruck, Austria) was coupled to a prototype version of the FastGC add-on (IONICON Analytik, Innsbruck, Austria) allowing a rapid chromatographic separation of isomeric compounds in fast spectral runs (tens of seconds). A detailed description of the commercial FastGC can be found in Romano et al. (2014) and Ruzsanyi et al. (2013). The

modified prototype we used is described in Malásková et al. (2019). Briefly, a 10 m nonpolar dimethyl polysiloxane column (MXT1, RESTEK, USA) with an I.D. of 0.53 mm and an active phase of 0.25 μm is resistively heated via a laboratory power supply (PSI 5000 A, EPS Stromversorgung GmbH, Germany). The laboratory power supply was controlled by a microcontroller (Arduino UNO ref3, Arduino, USA). Switching between real time measurements and spectral runs is realized by a two position 10-port diaphragm valve (VICI AG, Switzerland) combined with a 3-way solenoid valve as actuator (see **Figure 5.2**). The switching process was performed fully automated via PTR-MS Control v2.7. Make-up flow is injected into a custom made 5-port virtual valve, to ensure only sample from the carrier gas flow enters the drift tube.

During real-time measurements, the sample loop, made from passivated stainless steel ($v = 0.5$ mL) is constantly flushed. At this time, the sampling unit of the FastGC is isolated from the column which is continuously back flushed with the carrier gas. Regarding the FastGC cycle, it goes as follows: a first step consists of filling the sample loop with the air sample. Second, the valve is switched so the sample loop is connected in series with the GC column, allowing the injection of the air sample that is pushed through the column by a constant flow of the carrier gas. Finally, compounds are separated in the column and they elute at different times, heading to the PTR-MS to be analyzed. The efficiency of the separation and the quality of the resulting chromatograms can be influenced by operational parameters, such as temperature and carrier gas flow rates, which can play a role on the retention times as well as on the peaks shapes. For that reason, extensive laboratory experiments were performed prior to the campaign, in order to test the performance of the instrument under different operational parameters. The outcome of these tests is summarized in section 5.3.2.

5.3.2. Laboratory optimization phase

In order to achieve a fast and satisfying separation of monoterpenes, using the FastGC/PTR-MS system, three main parameters were tuned: the column temperature program, the nature and the flow rate of the carrier gas. Sampling was made from the headspace of individual and mixture of five available monoterpenes solutions: α -pinene, myrcene, Δ -3-carene, limonene and terpinene. A first stage of tests, aimed to evaluate the effect of the temperature program on the peak shape and the retention times. Using N_2 as the carrier gas, with an initial flow rate of 10

sccm, the application of a temperature ramp showed to be advantageous on the quality of the chromatographic separation, compared to isothermal conditions. Indeed, under a fixed temperature, some monoterpenes exhibited larger and less intense peaks, which can affect the resolution in the presence of several compounds. In a second stage, experiments were performed with different flow rates (ranging between 5 and 15 sccm) of N₂ as carrier gas. Under the same temperature program, chromatograms demonstrated a better separation with relatively lower flow rates (see **Figure 5.3**). However, lower flow rates meant longer GC runs. This said, a compromise had to be done between a good separation, a satisfying peak resolution and a fast GC run. In this perspective, around 43 different tests were performed with different combinations of temperature ramps and N₂ flow rates. Satisfying results were obtained applying temperature ramp in **Table 5.1**, with a carrier gas flow rate of 3 sccm. In a third stage, N₂ was replaced by He as carrier gas. Under the same flow rate (3 sccm) and using the temperature ramp of **Table 5.1**, a good peak shape and a faster chromatographic run were obtained. This is expected seen helium's higher velocity in the temperature range of 0- 300 °C, compared to H₂. Finally, the quantitative analysis, using a NPL (National Physical Laboratory) gas standard with six monoterpenes, allowed us to check the limit of detection of the FastGC/PTR-MS system, that was around 500 pptv/monoterpene. It should be noted that, it was chosen to monitor monoterpenes chromatographic separation under *m/z* 81 (with a dwell time of 200 ms), seen the higher sensitivity of the PTR-MS for this mass compared to *m/z* 137.

Table 5.1: The selected temperature ramp after several laboratory tests with different temperature programs.

Time (s)	0	10	100	130	160
Voltage (V)	5	35	45	50	50

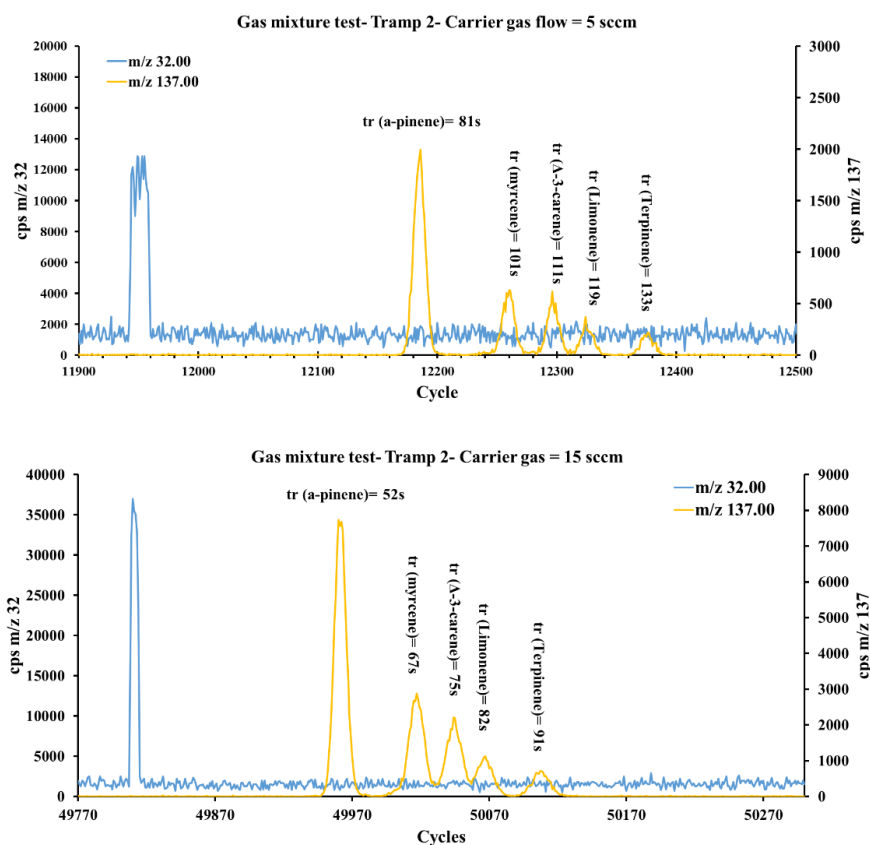


Figure 5.3: Comparison between two chromatograms of the same monoterpene gas mixture, injected in the same conditions but with two different carrier gas flows: the upper graph corresponds to the experiment with a flow of 5 sccm and the lower graph, to the experiment with a carrier gas flow of 15 sccm.

5.3.3. Operating conditions during the campaign

During the COV³ER- 2018 Puechabon field experiment, the temperature ramp was set as indicated in **Table 5.2** and operational parameters were as following: 2.2 mbar drift pressure, 600 V drift voltage and 60°C drift tube temperature, resulting in a reduced electric field (E/N) of 131 Td (1 Td = 10⁻¹⁷ V/cm²). 3 sccm of Helium and 15 sccm of N₂ were used as carrier and make-up flow, respectively. The inlet line consisted of a PEEK capillary tube heated up to 60°C and the inlet flow was around 100 sccm. Real-time mode measurement was on the following *m/z*: *m/z* 21 (100 ms), *m/z* 25 (100 ms), *m/z* 30 (100 ms), *m/z* 32 (100 ms), *m/z* 37 (100 ms), *m/z* 55 (100 ms), *m/z* 33 (100 ms), *m/z* 45 (100 ms), *m/z* 59 (100 ms), *m/z* 69 (200 ms), *m/z* 81 (200 ms), *m/z* 137 (200 ms), *m/z* 139 (100 ms), *m/z* 151 (100 ms) and *m/z* 169 (100 ms). The FastGC mode was limited to *m/z* 21 (50 ms), *m/z* 32 (10 ms) and *m/z* 81 (200 ms).

Table 5.2: Temperature ramp deployed for the measurement of monoterpenes during COV³ER- 2018 field experiment.

Time (s)	0	10	100	150	160	161
Voltage (V)	5	35	45	50	50	0

5.3.4. System calibration

During the campaign, the PTR-MS was calibrated, for real-time measurements, using a calibration gas containing 16 VOCs in the 1 ppmv range (custom made standard, Praxair NV, Belgium), and the FastGC/ PTR-MS was calibrated, for monoterpenes chromatographic separation, using a NPL standard containing 6 monoterpenes: α -pinene (2.25 ± 0.07 ppbv), β -pinene (2.13 ± 0.11 ppbv), myrcene (2.49 ± 0.12 ppbv), Δ_3 -carene (2.34 ± 0.12 ppbv), cis-ocimene (2.27 ppbv) and limonene (2.24 ± 0.11 ppbv). The NPL gas mixture was injected daily at a fixed concentration, in order to check the retention time of each monoterpenes and detect potential shifts. A complete calibration consisted of introducing different concentrations of the gas standard, which permitted to derive a sensitivity coefficient, used to covert normalized counts (ncps) into ppbv. All monoterpenes present in the standard had similar sensitivity coefficient ranging between 2.63 for myrcene and 3.40 for β -pinene. Since the NPL standard does not contain sabinene, a mean coefficient calculated from the obtained coefficients, was calculated to be around 3.01. Individual monoterpenes retention times and peaks intensities, used to identify and quantify peaks obtained from branch chambers sampled air are demonstrated in **Figure 5.4** and summarized in **Table 5.3**.

Table 5.3: Mean retention time (\pm STD) and mean peak height (\pm STD) obtained for each of the monoterpenes present in the NPL calibration mixture.

	a-pinene (2.25 ± 0.07 ppb)	b-pinene (2.13 ± 0.11 ppb)	myrcene (2.49 ± 0.12 ppb)	d-carene (2.34 ± 0.12 ppb)	limonene (2.24 ± 0.11 ppb)/ ocimene (2.27 ppb)
Mean tr (s)	94.09	108.27	111.45	120.82	127.82
STD (s)	2.39	2.72	2.66	2.82	2.82
Mean peak height (cps)	54.40	55.47	35.52	46.67	117.21
STD (cps)	8.47	9.35	6.21	6.71	23.26

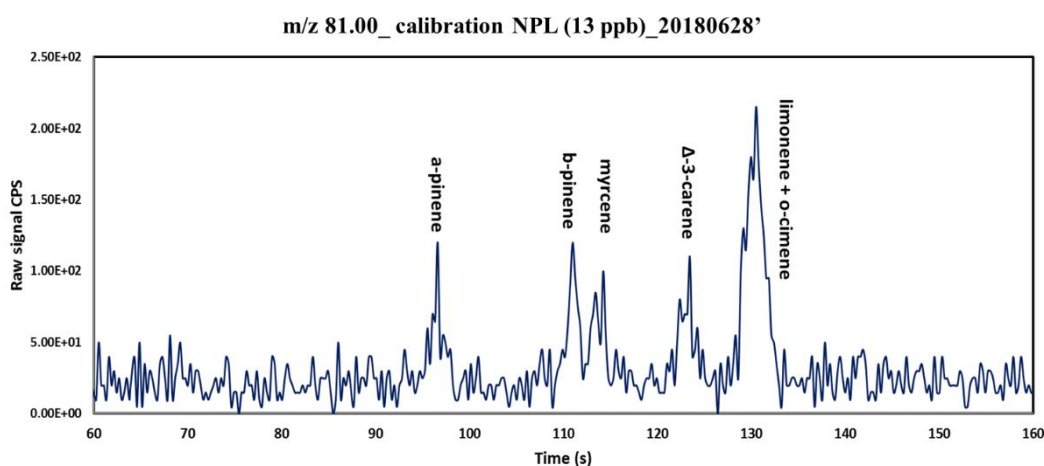


Figure 5.4: FastGC/PTR-MS chromatogram of a calibration mixture (NPL) containing: α -pinene, β -pinene, myrcene, Δ -3-carene, limonene and o-cimene. This graph represents one of the daily replicates performed with the same standard. The drawn line represents m/z 81 (monoterpene fragment).

5.3.5. FastGC/PTR-MS sampling system

The air going in and the air going out of the dynamic chambers were sampled through two 7 m long, ¼” OD Teflon lines. The inlet air was sampled from an independent line located close to the chambers and the outlet air was taken from the main line drawing air through the chambers. Both lines led to a 4 port-valve (V1 in **Figure 5.5**) allowing quick switches between inlet and outlet air samples. While measuring in one line (i.e. outlet air), the other line was continuously flushed using a pump (P1 in **Figure 5.5**) and vice versa. Background measurements were also possible using the Gas Calibration Unit (GCU, IONICON, Analytik, Austria). For each branch and stem chamber, a sequence of 10 min inlet air/ 50 min outlet air measurements was adopted. The air flow through the lines was around 1- 1.2 L min⁻¹. Continuous online monitoring of VOCs mixing ratios was made during the period from the 29th June to the 2nd July and from the 6th to the 10th July, 2018 on four different branch chambers and two stem chambers.

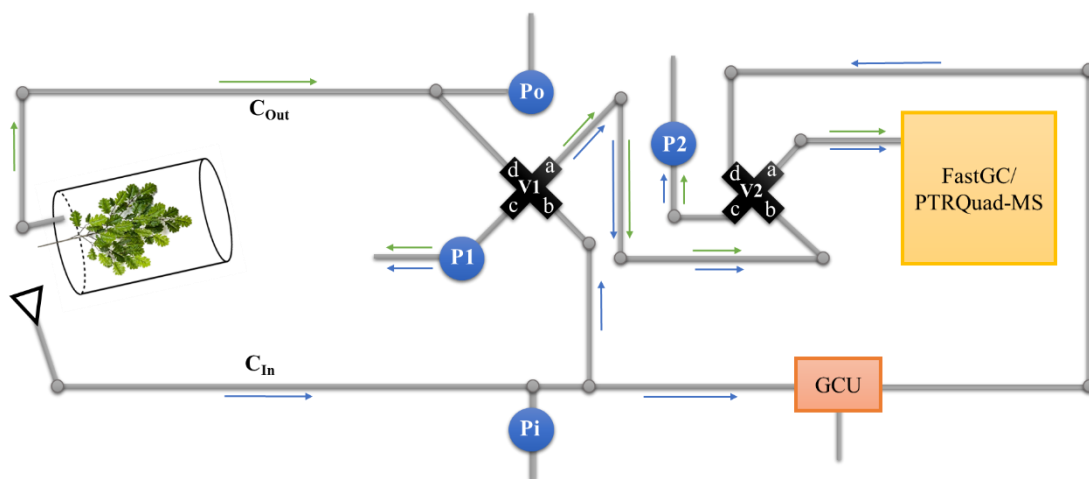


Figure 5.5: Schematic of the sampling system going from the dynamic chamber to the FastGC/PTR-MS. P_o and P_i stand for the pumps drowning outlet and inlet air, respectively. $P1$ and $P2$ represent the flushing pumps connected to VICI valve 1 and 2, respectively. C_{In} and C_{Out} represent the incoming and the outgoing chamber air, respectively.

5.3.6. Data analysis

Chromatograms were analyzed with custom written Matlab scripts (MATLAB R2019a). Since the signals recorded by the PTR-QMS are rather noisy at the short dwell times used, signals were first smoothed with a 5 point Savitzky Golay filter. To account for fluctuations in starting temperature and small delays in automated starting of the ramp, chromatograms were aligned on the O_2 Peak. O_2 traverses the column without interactions and is thus a good reference point. Signals were further baseline corrected and peaks identified with Matlab's "findpeaks" function. The threshold for peaks was set to 3-times the standard deviation plus the average obtained from the first 100 datapoints. Peaks were then fitted using the custom peakfit.m function (<https://terpconnect.umd.edu/~toh/spectrum/InteractivePeakFitter.htm>) assuming a gaussian peakshape.

5.3.7. Evaluation of the system efficiency in the separation of monoterpenes with a higher time resolution

Calibrations and tests performed prior to the campaign, as well as those done daily during the field experiment, were consistent in showing the ability to separate most of the main monoterpenes with FastGC runs. However, they also confirmed the limited resolution reached by the FastGC system. Indeed, it was not possible to separate limonene and ocimene, which co-eluted, producing one intense peak. This reduced maximum resolution is most probably due to the column short length, its high initial temperature (30- 35°C) and the absence of a cryofocusing unit, which is useful to limit the excessive spreading of the injection band (Pallozzi et al., 2016). Regarding the sensitivity, it was satisfactory, seen the relatively low injected sample volume and the relatively low resolution (compared to conventional GC instruments). The minimum detected amount of a monoterpene peak was about 500 pptv.

5.4. Results

5.4.1. BVOCs concentrations for branch enclosures

Figure 5.6 shows the variability of the sum of monoterpenes (m/z 81) mixing ratios, in respect to the photosynthetic active radiation (PAR).

For all oak branches, monoterpenes were by far, the main emitted compounds (see **Table 5.4**). This evergreen oak, widespread in the Mediterranean forest, is well-known for its monoterpenes emissions, which exhibited a clear diurnal cycle, showing maxima during day-time and minima during night-time, following temperature and light profiles. However, two day-time peaks were generally observed for each branch, similarly to the PAR variation recorded on the level of each branch. This observation is a clear evidence that, monoterpenes emissions from green oak leaves, are linked to solar radiation, which is in agreement with previous studies on *Quercus ilex*. Indeed, monoterpenes emissions from the leaves of *Quercus ilex* were described, in a satisfying way, by Guenther's algorithms used to describe light and temperature dependent emissions of isoprene (Bertin et al., 1997). This light-dependency also highlights the de novo emissions of monoterpenes, which are synthesized and directly emitted under the effect of light, and this is due to the absence of specialized structures for terpene storage, contrary to most monoterpenes emitting plants (Loreto et al., 1996). Hence, during dark hours, total MTs levels

were close to the LOD with similar values recorded in the outgoing and the ingoing air (ambient air). No emissions occurred from the leaves in the dark (**Figure 5.6**). Whereas, when the sun rose (PAR different from 0) around 04:00 UTC, light intensity as well as MTs levels started to increase, reaching a maximum at mid-day, decreasing in the afternoon and getting to a minimum starting 17:00- 18:00 UTC. Even though MTs mixing ratios recorded higher values during day-time, their maxima were observed at slightly different moments of the day, for the different branches. This is mainly due to the position of the branch chamber regarding sunlight.

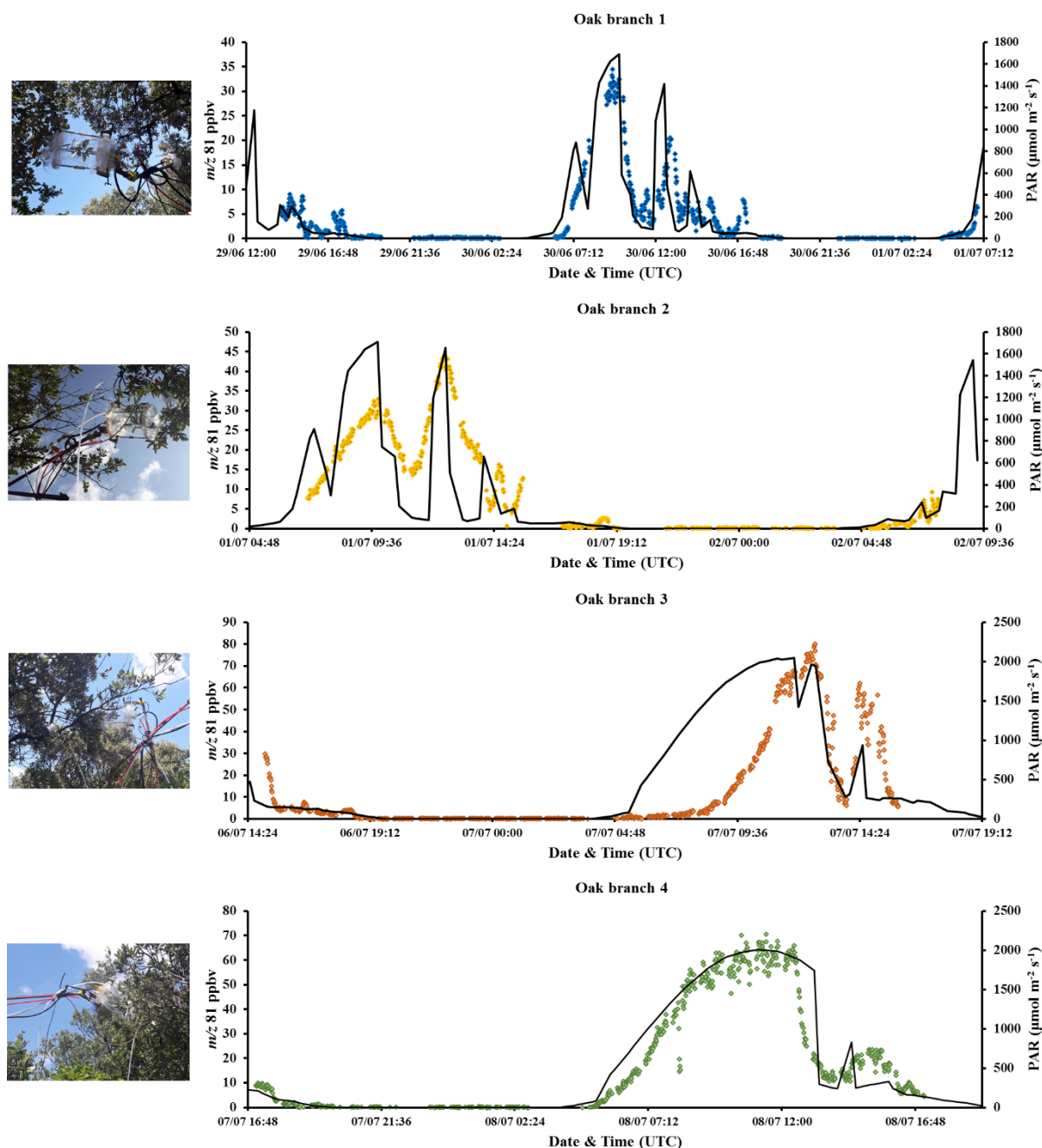


Figure 5.6: Diurnal variability of monoterpenes mixing ratios ($C_{\text{Out}} - C_{\text{In}}$) with the photosynthetic active radiation (PAR) for all four branch chambers.

5.4.2. BVOCs emission fluxes for branch enclosures

In order to compare total monoterpenes emissions between the four branches, emission fluxes of monoterpenes, as well as of other measured compounds, were calculated using eq. (5.1).

$$F = \frac{(C_{\text{out}}(\text{VOC}) - C_{\text{in}}(\text{VOC})) \times Q}{DW} \quad (5.1)$$

where F is the VOC flux expressed in $\mu\text{g} \cdot \text{g}^{-1}(\text{biomass dry weight}) \cdot \text{h}^{-1}$, $C_{\text{out}}(\text{VOC})$ and $C_{\text{in}}(\text{VOC})$ are the outlet and inlet VOC concentrations in $\mu\text{g} \cdot \text{m}^{-3}$, DW is the dry biomass (g) of plants (leaves and/or fruit organs) inside the enclosure, Q is the air flow rate in $\text{m}^3 \cdot \text{h}^{-1}$. For each one hour of measurements, C_{out} was sampled for 50 min and C_{in} for 10 min. The concentrations were therefore interpolated at common time steps prior to compute the fluxes.

Table 5.4 summarizes the operational conditions, meteorological parameters and the mixing ratios recorded for each enclosure. As mentioned before, monoterpenes were the main emitted compounds. Their emission fluxes exceeded significantly those of isoprene and the sum of OVOCs. Their average day-time emission flux ranged between 7.6 and 19.5 $\mu\text{g} \cdot \text{g}^{-1} \cdot \text{h}^{-1}$, with a maximum reaching 83.5 $\mu\text{g} \cdot \text{g}^{-1} \cdot \text{h}^{-1}$ for branch 3. Similar maxima were recorded by Staudt et al., (2002), on the same field site, between July and August (80 $\mu\text{g} \cdot \text{g}^{-1} \cdot \text{h}^{-1}$). In our study, branches 3 and 4 had the highest emission rates (18.8 and 19.5 $\mu\text{g} \cdot \text{g}^{-1} \cdot \text{h}^{-1}$) followed by branch 2 (12.3 $\mu\text{g} \cdot \text{g}^{-1} \cdot \text{h}^{-1}$) and 1 (7.6 $\mu\text{g} \cdot \text{g}^{-1} \cdot \text{h}^{-1}$). Since similar external conditions were observed for all four branches, differences in emission rates are most probably related to genotypic and physiological factors specific for each branch. One previous study reported that the emission rate from *Quercus ilex* increases as leaves become more developed (Pio et al., 1993). Thus, it suggests that leaves on branch 1 were younger than those on the other branches.

Table 5.4: Summary of the operational conditions, meteorological parameters, mean and maximum mixing ratios and emission fluxes of monoterpenes, isoprene and OVOCs (methanol, acetone, acetaldehyde) for the four branch chambers.

Branch chamber		1	2	3	4
Measurement days		29th- 30th, Juin 2018	30th, Juin- 2nd, July 2018	6th-7th, July 2018	7th-8th, July 2018
Chamber flow rate (L/min)		10	10	8.3	8.3
Dry weight (leaves + stem (g))		2.231	2.388	2.654	3.541
T (°C)		15 - 37	14 - 37	14 - 39	16 - 40
PAR		0- 1691	0- 2013	0 - 2048	—
BVOCs					
MTs	Max day-time (ppb)	34.56	43.74	80.08	70.63
	Mean day-time (ppb)	5.07	12.43	18.30	23.13
	Max day-time flux (µg.g-1.h-1)	52.10	43.42	82.57	56.01
	Mean day-time flux (µg.g-1.h-1)	7.64	12.34	18.78	19.52
Isoprene	Max day-time (ppb)	5.13	4.52	10.07	7.68
	Mean day-time (ppb)	0.23	0.76	2.15	1.62
	Max day-time flux (µg.g-1.h-1)	3.86	2.24	5.18	3.04
	Mean day-time flux (µg.g-1.h-1)	0.23	0.38	1.10	0.68
OVOCs	Max day-time (ppb)	12.95	1.97	6.54	8.93
	Mean day-time (ppb)	0.39	0.42	1.57	3.55
	Max day-time flux (µg.g-1.h-1)	6.35	0.62	1.83	1.95
	Mean day-time flux (µg.g-1.h-1)	0.28	0.10	0.53	0.77

5.4.3. Monoterpenes chemical speciation

One of the main highlights of this field campaign, was the use of a FastGC/PTR-MS system to monitor individual monoterpenes variability from different oak branches. Even though this oak species was extensively investigated in the past (Bertin et al., 1997; Loreto et al., 1996; Staudt et al., 2001; Staudt and Seufert, 1995), measurements were often based on conventional analytical techniques, where monoterpenes are trapped on adsorption tubes, followed by an offline analysis using GC-FID, with six/ seven data points per day, or online analysis by GC-MS with a data point each hour. Therefore, installing our system on this *Quercus ilex* dominated site, is a good opportunity to validate it in a well characterized environment. It provides also a near real-time monitoring of individual monoterpenes variability, helping to constraint previous observations on monoterpenes emission dependency on solar radiation.

Figure 5.7 shows four chromatograms obtained for the four studied branches, at the same hour of different days (around 12h45 UTC). In total, six different peaks could be separated. Five of them were identified, from the first eluted to the last eluted peak, as α -pinene, sabinene, β -pinene, myrcene and limonene, while the last one remained unknown. However, it should be noted that the limonene peak could also include ocimene, since limonene and ocimene could not be separated. These five identified compounds were already reported to be the main emitted monoterpenes from *Quercus ilex* leaves, where they can account for up to 90- 100% of total monoterpenes released (Bertin et al., 1997; Staudt et al., 2001). Other terpenes were also

detected in previous studies (Loreto et al., 1996; Staudt et al., 2001), including α -thujene, camphene, γ -terpinene, p-cymene and linalool. However, these compounds were not detected by FastGC/PTR-MS, most probably due to their release in trace amounts as reported in these previous studies, which are apparently lower than our instrument LOD (≈ 500 pptv).

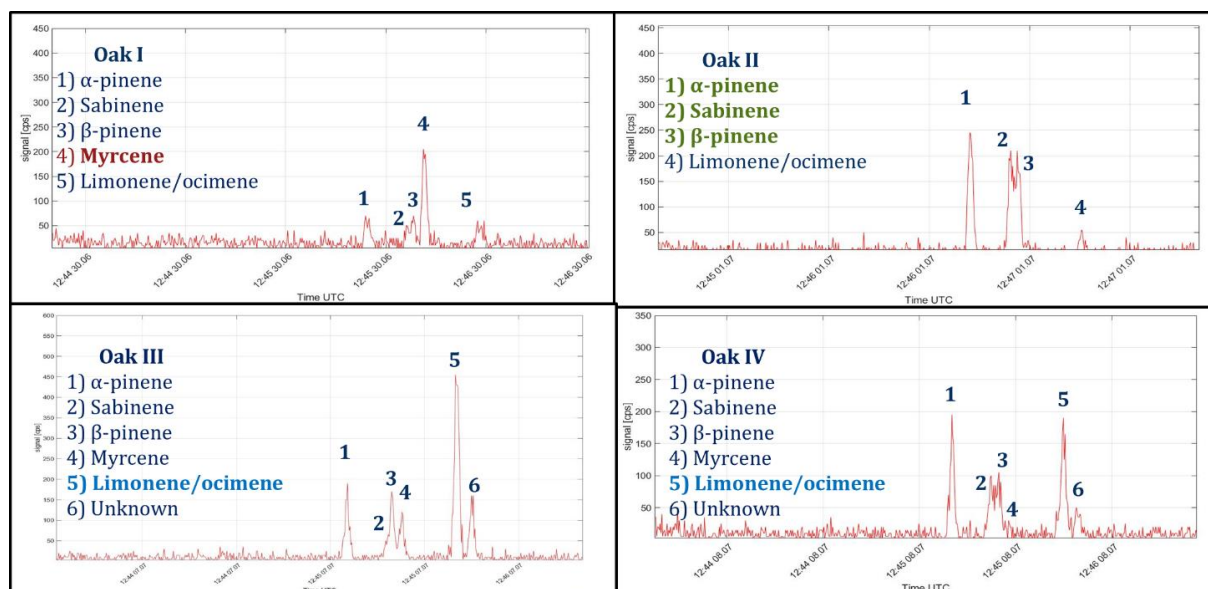


Figure 5.7: FastGC chromatograms from the four studied *Quercus ilex* branch enclosures at the same hour of different days (around 12h45 UTC).

When comparing the four chromatograms, we can clearly see that, the detected monoterpenes were emitted in distinctly different proportions. While *Q. ilex* 1 exhibited a major peak of myrcene, *Q. ilex* 2 had similar proportions of α -pinene, β -pinene and sabinene, and the last two investigated branch chambers showed important peaks of limonene (+ocimene). Indeed, these four branches represented three principal groups of holm oak trees, which are distinguished with respect to the proportions of the major compounds. *Q. ilex* 1 is a myrcene type oak, *Q. ilex* 2 is a pinene type and *Q. ilex* 3 and 4 belong to the limonene-type. The presence of three different chemotypes in *Q. ilex*, was previously reported by Staudt et al. (2001) where authors suggested that these different chemotypes are related to genotypic differences rather than to environmental influences. In this same study, a cluster analysis of 146 *Q. ilex* trees in southern France, showed that the pinene chemotype is dominant in this region with 71% of the trees emitting mainly pinenes. 21% of investigated trees had higher proportions of limonene and 8% emitted a blend containing large proportions of myrcene.

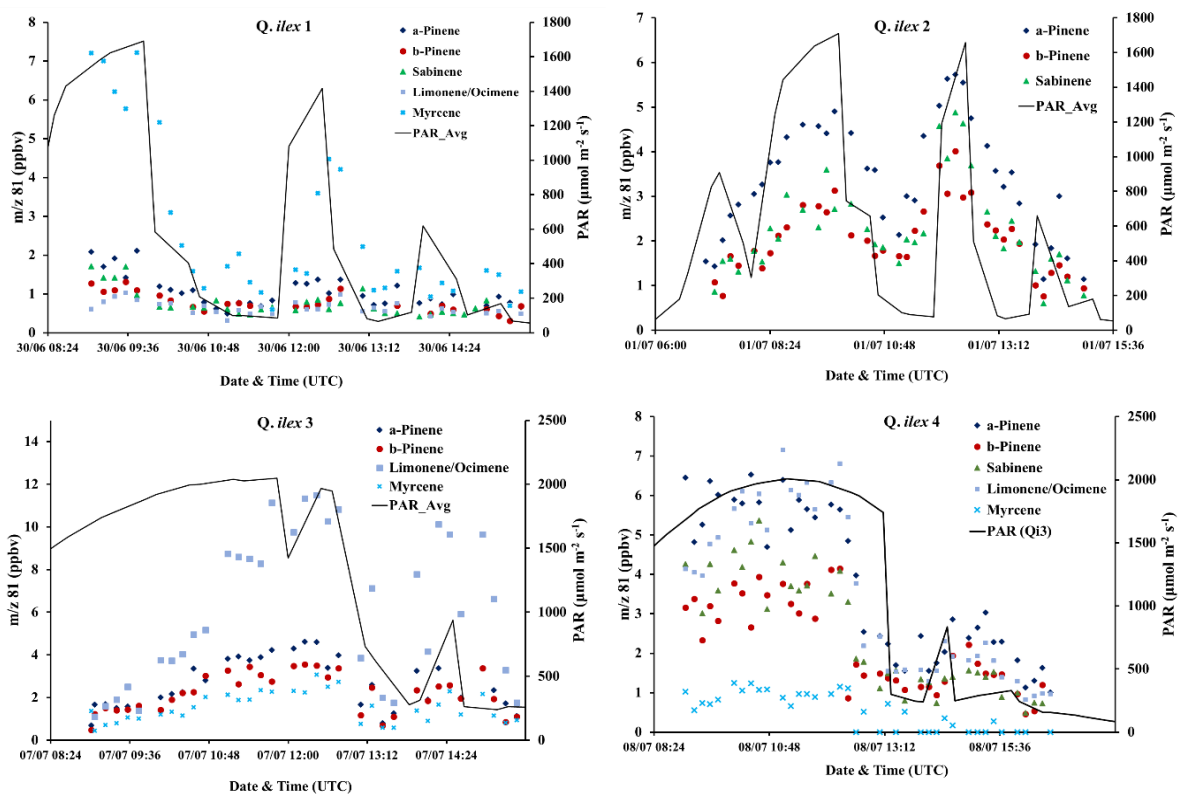


Figure 5.8: Variability of individual monoterpenes in the outgoing chambers air of the four studied branch chambers.

The integration of the resulting chromatograms (6 chromatograms/ hour among which 5 corresponded to outgoing air samples and 1 to an incoming air sample), allowed us to quantify the identified individual monoterpenes for each branch chamber. **Figure 5.8** presents the variability of individual monoterpenes mixing ratios in the outgoing chamber air. In fact, total monoterpenes levels were quite low (max ≈ 9 ppbv around noon UTC) in the incoming chamber air (ambient air), most probably due to efficient mixing and dilution in the atmosphere, that individual monoterpenes levels were also quite low and generally below the FastGC/PTR-MS detection limit. Thus, monoterpenes were hardly detected and quantified in ambient air.

Figure 5.8 shows that all speciated monoterpenes followed the solar radiation profile, and exhibited higher levels with higher photosynthetic active radiation. When the branch was in the shadow (i.e. branch chamber 2, around 11h UTC), all monoterpenes mixing ratios dropped down. These observations suggest that all detected monoterpenes have a light-dependent

emission and most probably are released from the same physiological processes. As mentioned before, *Q. ilex* 1 was characterized by a higher level of myrcene compared to pinenes. Its mixing ratio was around 3.4 times higher than that of α -pinene at the maximum PAR (8h30- 9h30 UTC). For *Q. ilex* 2, α -pinene was dominant almost all day long with similar levels of β -pinene and sabinene. At maximum PAR, α -pinene concentration in the outgoing chamber air was around 1.6 times higher than that of β -pinene. Interestingly, two different behaviors were observed for the limonene-type oak branches. For *Q. ilex* 3, limonene/ocimene was by far the dominant monoterpene. At maximum radiation, it showed a mixing ratio 2.6 times higher than that of α -pinene, whereas for *Q. ilex* 4, limonene/ocimene and α -pinene had close values, with slightly higher levels of limonene/ocimene. These compositions remained similar all day long.

5.5. Conclusion

Using the PTR-QuadMS available in our laboratory, an updated prototype of a FastGC was added, tested and optimized for monoterpenes speciation with a fine time resolution. The system was deployed during the COV³ER-2018 field campaign, conducted in the Puechabon forest, South of France. This forest is dominated by *Quercus ilex*, a green oak tree known for its important monoterpenes emissions. Enclosures were installed at four different branches. Real-time and chromatographic measurements were performed in the incoming and outgoing chambers air.

This work highlights the ability of a FastGC/PTR-QuadMS system to provide an online separation and detection of individual monoterpenes. Indeed, using helium as carrier gas and optimizing the temperature ramp, we were able to monitor the variability of 5 monoterpenes: α -pinene, sabinene, β -pinene, myrcene and limonene (+ocimene), with a data point each 10 min. However, even though our system was able to separate sabinene and β -pinene, which was an issue in a previous study (Pallozi et al., 2016), the sensitivity could be further improved, since limonene and ocimene still co-eluted. In addition, the FastGC/PTR-QuadMS used in this study, hardly detected individual monoterpenes at trace levels (< 500 pptv). Despite these limitations, near real time chromatographic separation allowed to monitor fast changes in individual monoterpenes mixing ratios and revealed the presence of 3 different green oak trees chemotypes: pinene-type for which monoterpenes emissions are dominated by α -pinene, β -pinene and sabinene, myrcene-type, for which myrcene is the major emitted monoterpene and

limonene-type, exhibiting higher levels of limonene (+ocimene). These results come to confirm previous observations, showing that the type of monoterpenes emissions from *Quercus ilex* is genetically fixed, with a variability following diurnal and fast changes in the solar radiation received by the leaves.

Acknowledgements

This study was supported by the ADEME (COV³ER, n°1562C0032) project. The authors acknowledge the European Union's Horizon 2020 research and innovation program under the Marie-Sklodowska-Curie grant agreement No 674911- IMPACT, the EU ICOS Research Infrastructure, ANAEE-FR services (ANR project n°11-INBS-0001), the CNRS and the CEA. We would also like to thank Jean-Eudes Petit for the technical assistance.

Le système FastGC/PTR-MS, optimisé au laboratoire a été utilisé dans une campagne de mesure de trois semaines dans une forêt de chênes verts située dans la forêt domaniale de Puéchabon, au sud de la France. Faisant partie de la campagne de terrain du projet ADEME-COV³ER de 2018, l'instrument a permis de mesurer les COVBs et les monoterpènes en entrée et en sortie de quatre chambres dynamiques de branches, de quatre chênes verts différents. Vu les faibles niveaux de monoterpènes en entrée des chambres (air ambiant), il n'était pas possible de distinguer les monoterpènes spéciés à ce niveau. La performance de l'instrument a bien été testée sur le terrain, montrant qu'il est capable de séparer les principaux monoterpènes avec une résolution temporelle de 10 min. Cependant, des améliorations peuvent être apportées pour séparer le limonène et l'ocimène qui sortaient toujours sous un même pic plus intense, et pour mesurer des concentrations plus faibles que 500 pptv/monoterpènes.

Les résultats de FastGC/PTR-MS ont permis de distinguer trois types de chênes verts dont la nature et les proportions des monoterpènes émis sont fixées génétiquement : le type pinène pour lequel α -pinène, β -pinène et sabinène sont les principaux monoterpènes émis. Le type myrcène, pour lequel le myrcène est majoritairement émis et le type limonène pour lequel le limonène est le principal monoterpène émis. Ces résultats viennent confirmer des observations faites précédemment sur cette espèce de chêne. Cependant, on a pu voir que tous les monoterpènes montraient une dépendance à la température et que leurs niveaux chutaient rapidement dès que la branche est à l'ombre et ne reçoit plus de lumière.

6. Conclusion and Perspectives

Aiming to characterize biogenic VOCs and their OH reactivity in agro-ecosystems, this thesis focused on: (i) improving an in-house “Comparative Reactivity Method” instrument for OH reactivity measurements, mainly for environments rich in reactive species, (ii) measuring OH reactivity in a forest and an agricultural land, in ambient air and from a dynamic chamber and (iii) optimizing as well as deploying a FastGC/PTR-MS system in a forest environment to better characterize individual monoterpenes with a high time resolution, species that showed to be important contributors to total OH reactivity in the first two studies.

Since its development, the CRM or the Comparative Reactivity Method has proved to be an advantageous technique for OH reactivity measurements, with an extensive range of applications. Indeed, several CRM instruments were built throughout the world in the past few years and deployed in urban, rural and remote environments, for ambient air and chambers/enclosures measurements. In this context, a new version of the Comparative Reactivity Method was built and optimized during the first stage of this PhD. Several technical improvements were presented, compared to the previous version, among which, continuous monitoring of pressure, temperature and relative humidity, parameters that can have an effect on the measurements, and the automated control of the gas flows going in and out of the reactor. However, this method also requires careful corrections to derive ambient OH reactivity. Indeed, previous intercomparisons (Fuchs et al., 2017; Zannoni et al., 2015) including two or more CRM instruments, demonstrated the importance of instrument-specific corrections to be applied on OH reactivity raw data. Therefore, many laboratory and field tests, including an intercomparison exercise, were performed in order to characterize these correction factors for different environments. The main conclusions were: (i) the correction factor for the deviation from pseudo-first order kinetics depends on the injected gas as well as on the pyrrole-to-OH ratio: higher the pyrrole-to-OH ratio, lower the correction, (ii) highly reactive species (i.e. isoprene and α -pinene) require pyrrole-to-OH ratios higher than 4 for a correction factor closer to unity, (iii) similar trend, however different correction factors appear for different systems, confirming the need for individual-instrument characterization.

LSCE-CRM was deployed in two field experiments targeting two different types of ecosystems.

The first field campaign was conducted in a rapeseed field located in Grignon, southwestern Paris, as part of the ADEME- COV³ER project (Biogenic Volatile Organic Compounds: Emissions by managed ecosystems). Simultaneous measurements of OH reactivity and VOCs were performed, during the blooming season (April 2017), in the incoming and the outgoing air of a single rapeseed crop dynamic chamber. These measurements were used in order to: (i)

evaluate the individual contribution of a specific agricultural source (crop) to total OH reactivity and (ii) to constrain our knowledge of the emitted species from rapeseed. We found that, total OH reactivity was in the lower range compared to other studied ecosystems, with a maximum that did not exceed 20- 30 s⁻¹ at mid-day in the outgoing chamber air (ROH_{chamber}), and a mean value of 7.5 s⁻¹ in ambient air (ROH_{ambient}). A good agreement was found between measured and calculated OH reactivity during night-time, whereas a higher difference appeared around mid-day, highlighting a missing fraction (46% on average), mostly related to primary temperature-dependent emissions. We tried to consider further masses provided by the PTR-ToF-MS measurements in order to close the OH reactivity budget. 201 more masses were selected showing more than 80% correlation with isoprene (compounds with a clear diurnal cycle). Among these masses, 9 were considered since they could be attributed to known chemical compounds with well-established rate coefficients for the reaction with OH. Finally, these compounds could not explain more than 1- 1.2 s⁻¹ of the missing OH reactivity in the outgoing chamber air during the day, showing that there are still some missing reactive species.

The second field experiment took place in a maritime Pine forest in the Landes region, as part of the ADEME-LANDEX project. Total OH reactivity and BVOCs were monitored inside (6 m) and above the canopy (12 m) between the 3rd and the 19th, July 2017. During this campaign, we had the opportunity to compare the CRM OH reactivity measurement to a FAGE (Fluorescence Assay by Gas Expansion) instrument measurement. The FAGE instrument performs direct measurements of the OH decay rate by laser-induced fluorescence (LIF). At the same location inside the canopy or at two different locations, measurements with both instruments showed a good agreement (slopes= 1.28 and R²= 0.87), within instruments uncertainties. Our results demonstrated a diurnal variability of total OH reactivity with maxima during stable nights, following higher mixing ratios of monoterpenes, due to lower mixing/dilution in the atmosphere. Levels up to 99 s⁻¹ and 70 s⁻¹ were recorded inside and above the canopy, respectively, among the highest seen in forest ecosystems. We found no substantial difference in the atmospheric chemical composition between both levels with monoterpenes being, by far, the main contributors to OH reactivity (68- 65% and 92- 89% during day-time and night-time, inside and above, respectively). When we compared the measured OH reactivity with the calculated one from available measurements at both heights, we obtained an average missing fraction of 22% inside the canopy and 33% above it. However, this missing fraction also showed a variability with the height and the time of the day. Indeed, we noticed a day-time difference that was dependent on temperature. Missing OH reactivity vs. temperature analysis

suggested that the day-time missing inside canopy was not only due to “unaccounted for” primary emissions, but also to unmeasured/unidentified secondary oxidation products. Regarding night-time, the transport of long-lived primary emissions and their oxidation products, from the widespread les Landes forests, is most probably behind the higher missing OH fraction seen for one stable/warm night. Apparently, these atmospheric conditions are favorable to their accumulation in the nocturnal boundary layer. These results highlighted that OH reactivity measurements on the branch scale could be of great interest, allowing to verify our observations on the missing OH fraction. In addition, modelling the oxidation of the biogenic precursors can add some valuable information to our measurements, helping to constrain the origin of missing OH reactivity.

As it can be noticed, monoterpenes appeared to account for a significant fraction of total OH reactivity in each of the studied ecosystems. However, they are measured with the PTR-MS, as “total monoterpenes”, with no detailed information about their chemical speciation. This can be a limitation in terms of calculated OH reactivity and the evaluation of the missing fraction. Motivated by the need of high time resolution measurements of speciated monoterpenes, we worked on coupling a new version of a FastGC prototype (IONICON), with the PTR-QuadMS available in our laboratory. Laboratory experiments showed that this in-house, non-commercialized system is promising in terms of rapid separation of the major monoterpenes (1 data point each 10 min), when optimizing the main operational parameters: the column temperature ramp and the carrier gas flow rate. Afterwards, the system was successfully deployed during a three-weeks field campaign in the Puechabon green oak forest, south of France. As part of the ADEME-COV³ER 2018 field experiment, we monitored BVOCs and individual monoterpenes in the incoming and the outgoing air of four branch chambers of four different oak trees. We could separate and identify the major five monoterpenes in the outgoing chambers air, with a high time resolution: α -pinene, sabinene, β -pinene, myrcene and limonene (+ocimene). However, limited by the instrument LOD (\approx 500 pptv), it was difficult to identify and quantify monoterpenes in ambient air. For the first chamber we could see that monoterpenes are dominated by myrcene, for the second one, monoterpenes were mainly α -pinene, β -pinene and sabinene and for the last two branches, limonene was the main emitted monoterpene. These results allowed us to distinguish between three types of green oak trees and confirm previously reported observations in this ecosystem. We could clearly see differences in monoterpenes proportions, depending on the tree type and these proportions stayed the same, independently from the time of the day. Fast changes in the luminosity received by the branch induced quick

variations in individual monoterpenes levels. Finally, the instrument performance can certainly be improved by optimizing the operational parameters, in order to achieve a better separation in a shorter time.

Perspectives for further research

The work done during this PhD underlines the importance of measuring Total OH reactivity as a global parameter allowing to evaluate the total loading of reactive species in a specific environment. Indeed, comparing the measured OH reactivity with the calculated one, demonstrated that, there are still reactive compounds, contributing to the chemistry in the atmosphere, however still missing in the set of individually measured compounds, using available analytical techniques. This work highlights also the multiple applications of this technique, from the enclosure scale to different heights in ambient air. All these points, put the accent on the importance of accurate measurement of this parameter, for a better evaluation of the missing fraction.

On the technical level, two axes can be developed in parallel: (i) seen the dependency of the correction factor for the deviation from pseudo-first order kinetics on the pyrrole-to-OH ratio and on the gas standard, it would be of great interest to perform calibration tests using a wider variety of chemical compounds with a wide range of reactivity with the hydroxyl radical and at different pyrrole-to-OH ratios. Such comprehensive characterization would require much more time, however, it will certainly bring better insight on this correction and its variability. Indeed, it will help choosing optimal conditions for a minimum correction for many slowly and highly reactive compounds. (ii) Knowing all the challenges that exist experimentally wise, the use of a model would be a valuable complement, in order to achieve a better understanding of the chemical processes taking place within the reactor. Michoud et al. (2015), followed this approach, trying to compare experimentally obtained correction factors to those resulting from a simple and more complex model.

One of the main objectives of characterizing OH reactivity, is the comparison of the total reactivity measured with the one calculated from the measured species. This approach helps evaluating the amplitude of the unmeasured fraction as well as its potential origins. So far, the Total OH reactivity tool, helped to stress that many unknowns are still associated to natural emissions (forests, crops) and their chemical transformation. However, understanding the missing reactivity is often more complicated than it seems, particularly because most of the

time, the unmeasured compounds are a mixture of primary emissions and secondary generated products. In this perspective, several tools can be combined to OH reactivity measurements to disentangle the two processes and better understand field results of OH reactivity, more specifically, at biogenic dominated sites:

(i) Branch enclosures allow to isolate one specific source, in order to distinguish its emissions from the atmospheric background. Measurements from a rapeseed dynamic enclosure system were performed during this PhD, with results demonstrating that the missing fraction was most probably related to unmeasured emitted compounds by the rapeseed crop. This approach can also be a valuable tool to constrain the conclusions made for the LANDEX campaign in terms of missing OH reactivity. Indeed, as done by Kim et al. (2011), measuring OH reactivity from a pine branch enclosure will certainly help in the understanding of the real source of the missing OH reactivity. In case the measured and the calculated OH reactivity were in good agreement, this will give confidence in the secondary nature of the unmeasured compounds contributing to the missing OH fraction.

(ii) Another interesting application, is the measurement of OH reactivity fluxes as done by Nolscher et al., (2013). In their study, fluxes of OH reactivity were measured from Norway Spruce by using a plant cuvette. Their main focus was to highlight the drivers of the missing reactivity when the primary species are the unmeasured compounds. They confirmed that heat stress induced on plants trigger the emission of unknown/unmeasured compounds, therefore explaining the missing OH reactivity. This work could have been done for the rapeseed chamber. However, due to the system perturbation by frequent switches between incoming and outgoing chamber air (1h/1h), longer measurements were performed in the outgoing air and less frequent measurements in the incoming air. This limitation prevented us from doing OH reactivity fluxes, adding to this, that the dry mass at the end of the campaign was not really representative of the mass during measurements, since the plant was during its growth season. Hence, fluxes calculations were not possible. Despite these limitations, our system showed promising results in this perspective, requiring more adapted operational conditions for this type of measurements.

(iii) Chemical models resembling the chemistry of the oxidation of BVOCs to different details would be of great benefit when combined to measurements. This would help to: (i) identify the unmeasured reactive compounds contributing to the measured reactivity in LANDEX, (ii) confirm the larger impact of local biogenic oxidation compared to long-range transported aged air masses, (ii) constrain our knowledge on the contribution of BVOCs in rural sites to the formation of ozone and SOAs.

(iv) Using the FastGC/PTRMS measurements in parallel with OH reactivity measurements in ambient air and from dynamic enclosures, would help in a more detailed calculation of the contribution of single isomers, such as monoterpenes, to total OH reactivity, reducing the uncertainties on calculated OH reactivity.

(v) The observations made during this thesis, highlight the lower BVOCs emissions and OH reactivity from a specific agricultural source, compared to forests. However, it is of great interest to extend the investigations on VOCs from croplands, seen the multitude of different sources, the expansion of agricultural lands and changes in land cover/land use. A first step, presented in this manuscript, consisted on characterizing BVOCs and their OH reactivity from a rapeseed crop. More research in this field was done, in the frame of the ADEME- Agrimultipol project, in which I also participated. Indeed, VOCs were monitored inside and near livestock buildings. This work is the subject of the paper by Kammer et al. (2019), presented in the appendix.

Finally, this thesis studied OH reactivity in "low-NO_x" environments. However, it would be interesting to carry out biogenic VOC studies close to urban areas, to better characterize their contribution to the formation of secondary pollutants (aerosols, ozone) in pollution plumes events.

Conclusion et Perspectives

Dans le but de caractériser les COVBs et leur réactivité OH dans divers agroécosystèmes, ce travail de thèse visait à : (i) améliorer le système de réactivité comparative (Comparative Réactivité Method CRM) du LSCE pour la mesure de la réactivité OH totale, surtout pour des écosystèmes riches en espèces réactives, (ii) mesurer la réactivité OH dans des écosystèmes forestier et agricole, en air ambiant ainsi qu'en sortie de chambre dynamique, (iii) mettre en place, optimiser et déployer un système de chromatographie en phase gazeuse rapide (FastGC) dans un écosystème forestier pour la caractérisation des monoterpènes avec une résolution temporelle plus fine.

Depuis son développement, la CRM s'est avérée une technique avantageuse pour la mesure de la réactivité OH. En effet, plusieurs systèmes existent à travers le monde et ont été déployés dans un nombre de sites urbains, ruraux, forestiers et côtiers (Yang et al., 2016). Ainsi, la première phase de cette thèse, consistait à mettre en place une nouvelle version de la CRM. Plusieurs améliorations techniques ont été apportées au système par rapport à la version précédente, incluant un contrôle automatique des débits d'entrée et de sortie ainsi qu'un suivi continu de la température, de la pression et de l'humidité dans le réacteur. Cependant, les mesures par CRM exigent l'application de certaines corrections, qui ont été déterminées via différents tests effectués au laboratoire et durant les campagnes de mesure. Les principales conclusions à ce niveau sont les suivantes : La correction pour la déviation du pseudo-premier ordre s'est montrée dépendante de l'espèce injectée et du rapport pyrrole/OH (C1/OH). En effet, les expériences ont montré que : (1) la correction est plus faible pour les composés relativement moins réactifs (propane) avec OH, (2) plus le rapport est élevé, plus la correction est faible pour tous les composés testés et plus la différence dans le facteur de correction entre un composé peu réactif et un autre plus réactif est faible, (3) chaque système réagit différemment concernant ces corrections, ce qui met l'accent sur l'importance d'une caractérisation complète, spécifique à chaque système CRM.

Après avoir testé la performance du système, la CRM a été déployée dans deux campagnes de mesures : une première campagne a eu lieu dans un champ de colza dans le cadre du projet ADEME-COV³ER (COV biogéniques : Emissions par les Ecosystèmes gERés) et une campagne dans la forêt des Landes dans le cadre du projet ADEME-LANDEX.

La campagne de mesure LANDEX était effectuée dans une forêt de pins maritimes au sud de la France. La réactivité OH ainsi que les COVs ont été mesurés dans et au-dessus de la

canopée. Durant cette campagne, on avait l'opportunité de comparer les mesures CRM aux mesures d'un instrument FAGE (Fluorescence Assay by Gas Expansion). Les mesures au même endroit dans la canopée, ont montré un accord satisfaisant entre les deux mesures, en prenant en compte les incertitudes sur les mesures. La réactivité OH variait suivant un cycle diurne bien marqué sur les deux hauteurs de mesures, avec des maxima durant les nuits stables. En effet, la réactivité OH montrait une variabilité similaire à celle des monoterpènes, qui s'accumulaient dans la couche limite nocturne, conduisant à des réactivités plus fortes. Des maximums de 99 s^{-1} et 70 s^{-1} ont été rapportés dans et au-dessus de la canopée, respectivement. La comparaison entre la réactivité mesurée et celle calculée révèle la présence d'une fraction manquante de 22 et 33% en moyenne, dans et au-dessus de la canopée. Cependant, la réactivité manquante montrait également une variabilité diurne sur les deux hauteurs : pour les mesures de jour, cette fraction manquante dépendait de la température. L'analyse a montré qu'il s'agit non seulement de composés primaires mais aussi d'espèces secondaires non mesurées ou non identifiées. Pour les mesures de nuit, la fraction manquante était relativement importante pour une nuit chaude et stable. Les rétro trajectoires des masses d'air ont révélé l'origine continentale des masses d'air arrivant sur site pour cette nuit, suggérant que des composés primaires et leurs produits secondaires ont été transportés sur site des forêts environnantes.

En ce qui concerne la campagne colza, elle était liée au projet ADEME-COV³ER. Le projet visait à fournir de nouvelles références de flux de COVB au niveau des grandes cultures et forêts gérées. Il avait comme objectif également de mieux caractériser les émissions liées aux pratiques agricoles, comme sources importantes de COVB (Karl et al., 2009). Des mesures simultanées de réactivité OH, de COVs et de composés inorganiques ont été effectuées en entrée et en sortie d'une chambre dynamique installée sur un jeune brin de colza en période de floraison. Les résultats obtenus mettent en évidence la réactivité relativement faible dans cet écosystème comparé aux écosystèmes forestiers. Une variabilité diurne de réactivité OH a été observée en sortie de la chambre, avec des maximums ne dépassant pas les $20\text{-}30 \text{ s}^{-1}$ en milieu de journée. Un bon accord a été trouvé entre la réactivité mesurée et celle calculée en sortie de la chambre pour les mesures de nuit, alors qu'une plus grande différence existait pour les mesures de jour. Cette variabilité de la fraction manquante suggère qu'elle est due à des composés primaires dépendants de la température et/ ou de la lumière. Parmi 201 masses du PTR-MS, examinées pour leur corrélation avec l'isoprène, l'un des principaux contributeurs à la réactivité OH, 9 masses ont été considérées dans la réactivité calculée, cependant n'expliquant qu'une fraction ($1\text{-}1.2 \text{ s}^{-1}$) au maximum de la réactivité manquante de jour.

Finally, and as observed in the two first measurement campaigns, monoterpenes, even emitted in small quantities, can contribute significantly to OH reactivity. In this context, it was motivated to set up and optimize a FastGC/PTR-MS system with the aim of achieving a rapid separation of monoterpenes species, which can be useful for a better consideration in reactivity calculations. Laboratory work allowed testing the system performance and choosing optimal parameters to measure the main monoterpenes with a measurement every 10 minutes. Subsequently, the system was deployed in a green oak forest in southern France. The objective was to test the system performance for continuous measurements in a real environment and to follow the variability of individual monoterpenes emitted by oak branches. The measurements allowed following the variability of the main monoterpenes: α -pinene, sabinene, β -pinene, myrcene and limonene. This variability proved to depend primarily on light, with drops that can be rapid, in monoterpenes levels when the branch no longer received light. These compounds showed different proportions from one branch to another, which highlighted the presence of three types of green oaks (*Quercus ilex*): pinene type, myrcene type and limonene type, confirming previous observations but with a temporal resolution never reached and which allowed showing that these proportions remained the same throughout the day.

Perspectives

The work carried out during this thesis has highlighted the importance of measuring OH reactivity as a global parameter allowing to evaluate the load of reactive species in the atmosphere. This parameter was also used to show the presence of primary and secondary compounds not measured but which also contribute to OH reactivity. However, at the technical level, it remains important to well characterize the correction factors to apply on OH reactivity measurements by CRM, especially the correction for the deviation of the pseudo-first order regime. In fact, it will be interesting to calibrate the system with a large variety of different compounds, presenting different reactivities with the OH radical and under a wide range of pyrrole/OH ratio. In addition, the use of a parallel model, perhaps a complementary approach, could help to better understand the chemical processes taking place in the reactor.

Au niveau des champs d'application :

- Vu les incertitudes sur l'origine de la réactivité manquante sur les mesures dans et au-dessus de la canopée dans la forêt de pins maritimes, il sera intéressant de déployer la CRM pour des mesures en sortie d'une chambre dynamique d'une branche, pour mieux comprendre la source de la réactivité manquante : primaire ou secondaire ?
- Il serait intéressant d'effectuer des mesures de flux comme rapportées par Nolscher et al., 2013, où l'objectif était de mettre en évidence les principaux « driver » de la réactivité manquante. Ce travail aurait pu être fait sur les mesures en sortie de la chambre dynamique de colza, cependant les mesures en ambient étaient moins fréquentes, ce qui était une limitation pour le calcul de flux. De plus, la masse sèche de la plante à la fin de la campagne n'est pas vraiment représentative de sa masse durant la période de mesure comme elle était en voie de croissance.
- Les modèles de chimie atmosphérique, peuvent être des outils utiles pour identifier les composés non mesurés contribuant à la réactivité OH et pour une meilleure compréhension de la contribution des COVB à la formation d'ozone et d'AOS en zones rurales.
- Des mesures en parallèle de FastGC et CRM peuvent aider pour un calcul plus détaillé de la réactivité OH due aux monoterpènes par exemple, réduisant l'incertitude des calculs utilisant la somme des monoterpènes totaux.
- Les mesures de réactivité OH près d'une source agricole spécifique (culture) montrent des niveaux relativement faibles. Cependant, il sera intéressant de caractériser la réactivité d'autres sources agricoles également émettrices en COV, comme les bâtiments d'élevages, constituant le sujet d'un papier de Kammer et al., 2019 (auquel j'ai contribué) en annexe.
- Finalement, cette thèse a étudié la réactivité OH dans des environnements « low-NOx ». Cependant il sera intéressant d'effectuer des études de COV biogéniques proches des zones urbaines, pour mieux caractériser leur contribution à la formation de polluants secondaires (aérosols, ozone) dans une situation de panache de pollution.

Appendix

Appendix A

Supplement of chapter 3: Variability of hydroxyl radical (OH) reactivity in the Landes maritime Pine forest: results from the LANDEX campaign 2017

Supplementary material 3.1: Data availability

Table S3.1: Timetable of the data available from each instrument measuring inside and / or above the canopy.

		June 2017								July 2017																		
		23	24	25	26	27	28	29	30	1	2	3	4	5	6	7	8	9	10	11	12	13	14	15	16	17	18	19
Above canopy (12 m)	GC-NMHC																											
	GC-OVOC																											
	GC-BVOC1 LSCE																											
	PTR-ToF-MS																											
Inside canopy (6 m)	GC-BVOC2 IMT																											
	PTR-QiToFMS																											

Supplementary material 3.2: Consistency between GC-BVOC instruments and the PTR-MS on monoterpenes measurements

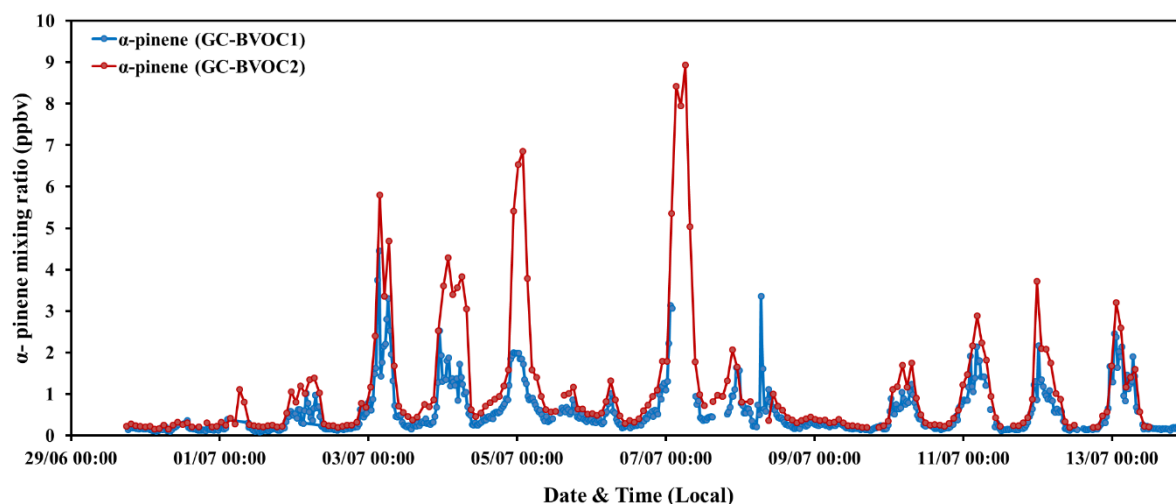


Figure S3.2.a: Variability of α -pinene mixing ratios measured at 12 m by the GC-BVOC1 (blue) and at 6 m by the GC BVOC2 (red).

Before the 13th of July, the consistency between the two GC-BVOC instruments was checked, taking into account the intercomparison of the standard cylinders used to calibrate each GC-BVOC. In addition, the profiles of the 8 species commonly measured by both GCs, were compared. Figure S3.2.a, shows the variability of α -pinene mixing ratios recorded by the GC-BVOC1 at 12 m height (blue) and by the GC-BVOC2 at 6 m height (red). The diurnal variability was demonstrated at both heights. Both instruments measured similar values during day-time when the vertical turbulence was higher and the mixing was more efficient within the canopy. However, a difference in the values recorded by the two GCs was seen during most nights, mainly related to the lower turbulence and the higher vertical stratification.

In order to verify the consistency between the GC instruments and the PTR-MS inside and above the canopy, the sum of the different monoterpenes concentrations measured by both GC-BVOCs and the sum of monoterpenes measured at $m/z=137 + m/z=81$ by the PTR-MS were compared.

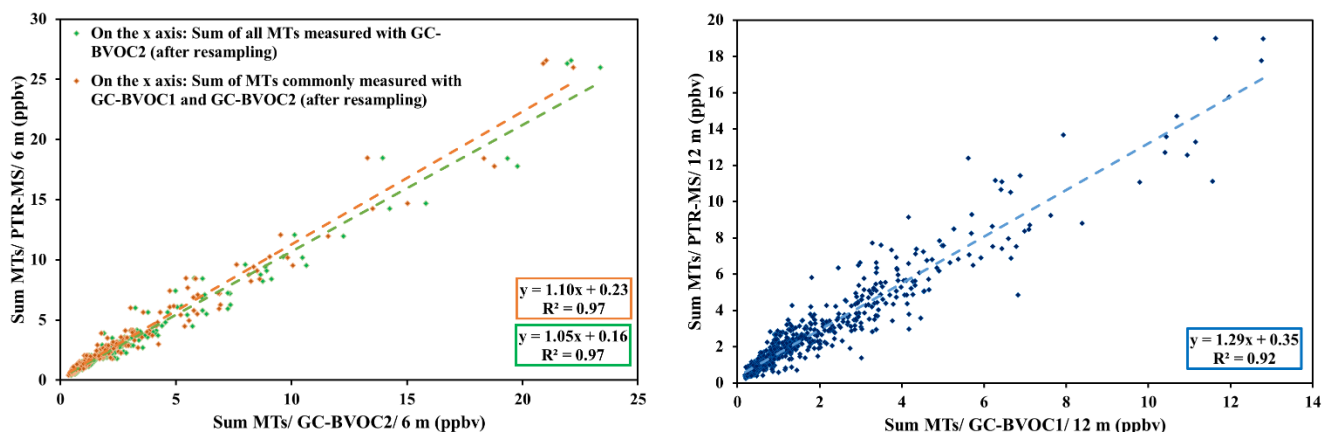


Figure S3.2. Correlation between (b) the sum of monoterpenes measured by the GC-BVOC2 and the PTR-MS at 6 m height and (c) the sum of monoterpenes measured by GC-BVOC1 and the PTR-MS at 12 m height. In Fig. S3.2.b, green dots consider the sum of all BVOCs measured by the GC-BVOC2 whereas orange dots consider the sum of the monoterpenes measured by GC-BVOC2 which are commonly measured by the GC-BVOC1.

Figures S3.2.b and c show that the concentrations are in good agreement most of the time. Higher concentrations were observed with the PTR-MS with a slope of 1.3 at 12 m. It is worth noting that a resampling of GC-BVOCs and PTR-MS datasets was made to get the same time base. As the GC-BVOC2 (6 m) has a time resolution of 90 min, the GC-BVOC1 (12 m) of 30 min and the PTR-MS of 30 min, a resampling using averaging with a time resolution of 90 min of the PTR-MS data and a linear interpolation was chosen for the comparison at 6 m height and a linear interpolation with a time resolution of 30 min at 12 m height.

The maximum difference between the sum of monoterpenes measured by the PTR-MS and all of the monoterpenes measured by the GC-BVOC2 at 6 m was 3.2 ppbv, whereas, the maximum difference between the sum of monoterpenes measured by the PTR-MS and the monoterpenes measured by the GC-BVOC1 at 12 m was 4.4 ppbv.

Supplementary material 3.3: Use of monoterpenes ratios in the weighted k rate coefficient calculation

Ratios of the different monoterpenes were calculated using GC-BVOC data at both heights. Figure S3.3.a shows the ratios at 12 m height.

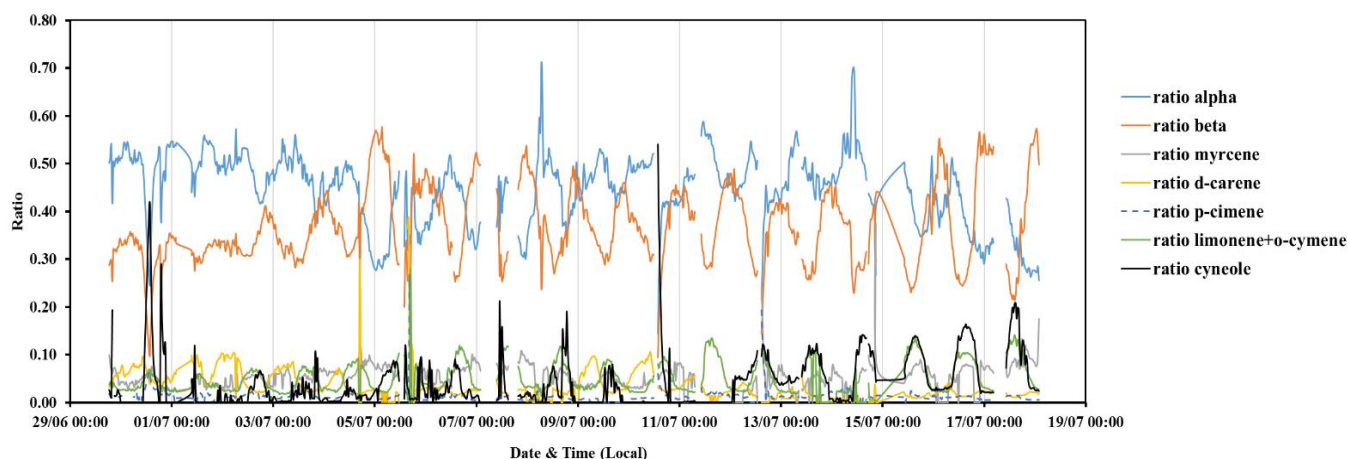


Figure S3.3.a: Ratio of all 8 monoterpenes calculated with the GC-BVOC1 data at 12 m height

Above canopy (12 m)

The comparison of the calculated OH reactivity from each monoterpene with the one obtained from the ratios for the GC-BVOC1 data and the PTR-MS data, regarding the overlapping period, is shown in Fig. S3.3.b for the measurements at 12 m height. The use of the ratios in OH reactivity calculations is in good agreement with the use of individual monoterpenes and their respective k rate constants, except for some overestimations at the peaks, observed when using the PTR-MS data. It is worth noting that, *cis*-*o*-cimene is co-eluted with limonene. Therefore, the ratio of *cis*-*o*-cimene and limonene over their sum was calculated using the GC-BVOC2 data (average: 0.15/0.85 respectively).

When plotting the calculated OH reactivity from the sum of GC-BVOC1 monoterpenes and k_{weighted} with the calculated OH reactivity using each individual monoterpene and its respective k rate constant, a slope of 0.96 was obtained, reflecting a good agreement (Fig. S3.3.c). Whereas, a higher slope of 1.30 was obtained when considering the sum of monoterpenes from the PTR-QiToFMS data with k_{weighted} (Fig. S3.3.d). This observation is in agreement with the one made in figure S3.2.c, when comparing the sum of monoterpenes

concentrations from the GC-BVOC1 and the PTR-MS, and it is probably related to the underestimation of total monoterpene concentration by the GC technique.

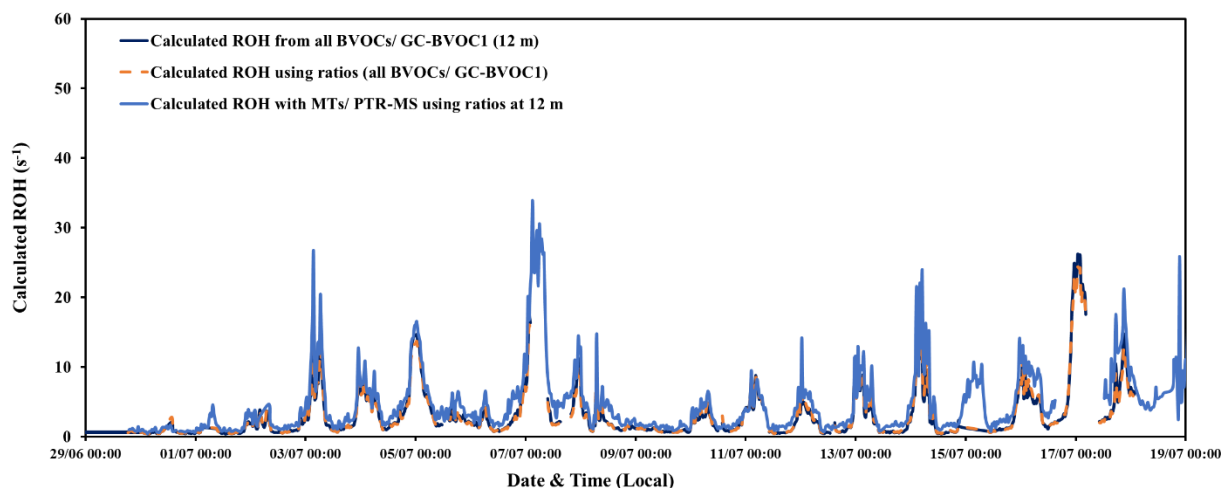


Figure S3.3.b: OH reactivity calculated for monoterpenes measured with the GC-BVOC1 at 12 m using the concentration and the k rate constant of each monoterpene (dark blue line), with the sum of the concentrations weighted by the ratio of each monoterpene multiplied by the respective rate constant (orange dots), with the sum of monoterpenes measured by the PTR-MS considering the weighted k rate constant reactivity from the monoterpenes measured by the GC-BVOC1 (light blue line).

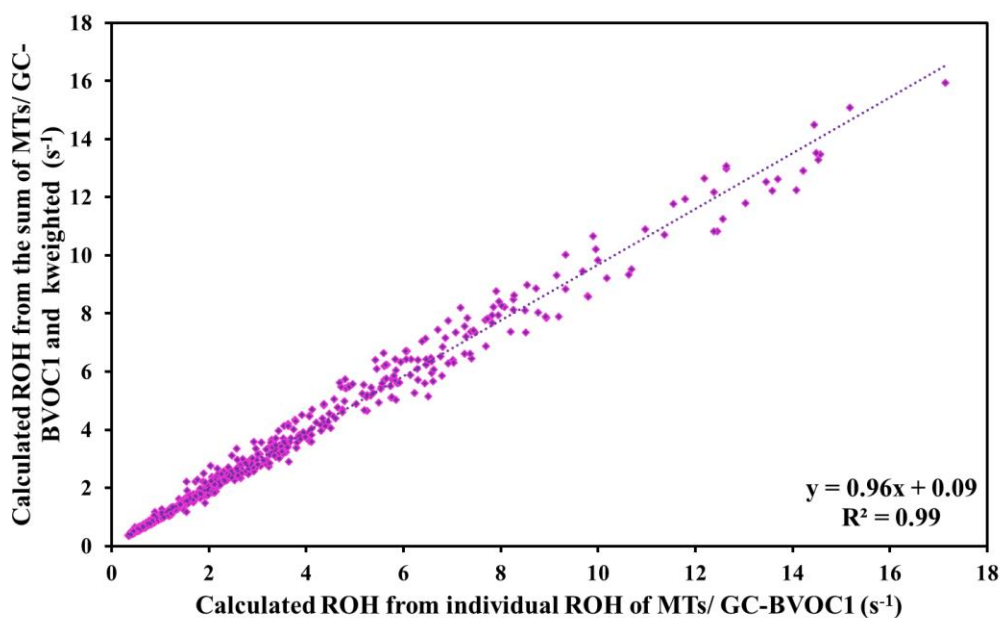


Figure S3.3.c: Correlation between the calculated OH reactivity from the sum of monoterpenes measured by the GC-BVOC1 multiplied by k_{weighted} with the calculated OH reactivity from individual monoterpenes measured by the GC-BVOC1.

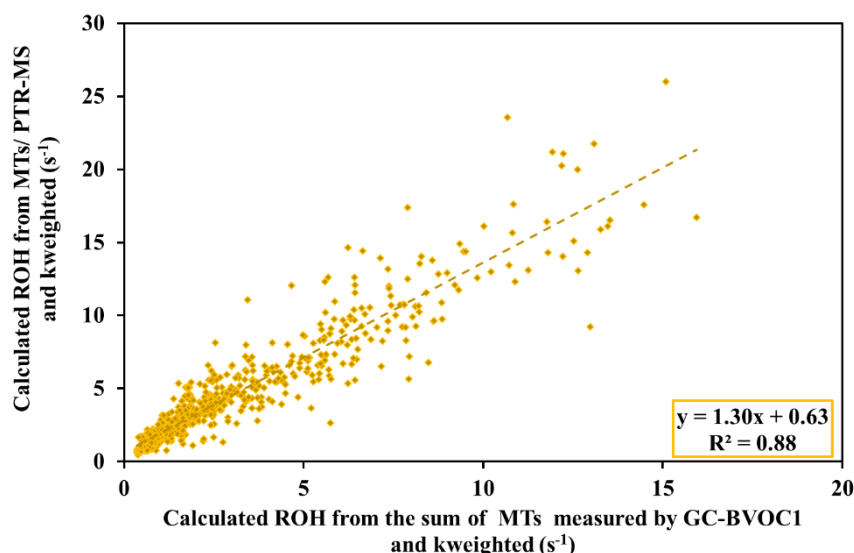


Figure S3.3.d: Correlation between the calculated OH reactivity from the sum of monoterpenes measured by the PTR-MS multiplied by k_{weighted} and the calculated OH reactivity from the sum of monoterpenes measured by GC-BVOC1 multiplied by k_{weighted} .

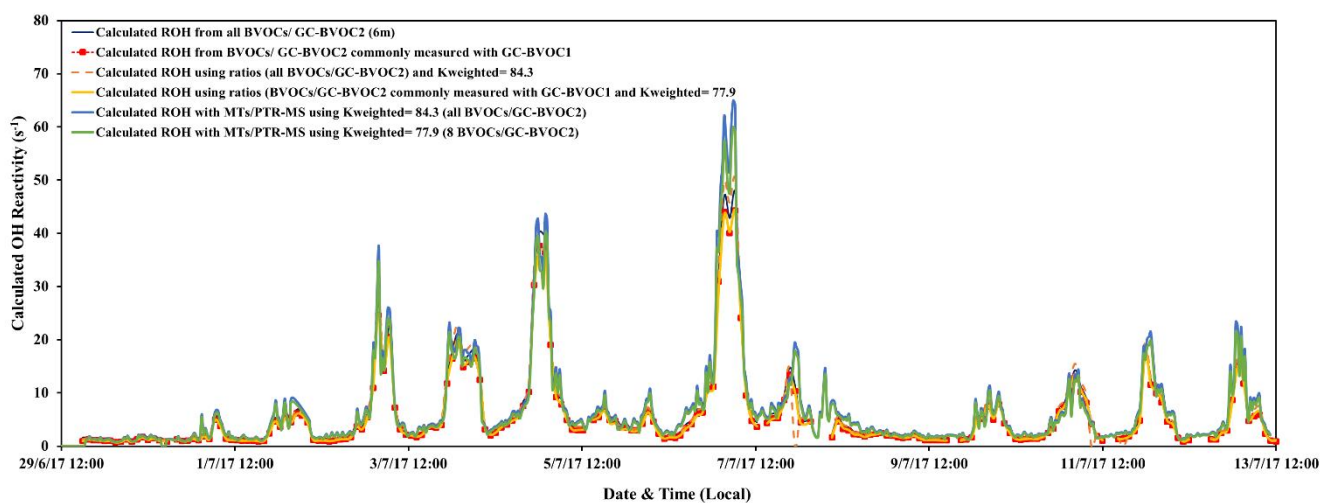


Figure S3.3.e: OH reactivity calculated from GC-BVOC2 monoterpenes measured at 6 m using the concentration and rate constant of each monoterpene (dark blue line), from GC-BVOC1 monoterpenes commonly measured by the GC-BVOC1 (LSCE) at 12m height (red dashed line), from the total monoterpenes concentration weighted by the ratio of each monoterpene multiplied by the respective rate constant (orange dashed line), from total monoterpenes measured by the PTR-MS considering the weighted reactivity from the monoterpenes measured by the GC-BVOC2 (blue) or the restricted list (corresponding to those commonly measured by the GC-BVOC1 (green)).

Inside canopy (6 m)

The calculated OH reactivity from each monoterpene was also compared at 6 m height, with the one obtained from the ratios for the GC-BVOC2 data and the PTR-MS data (fig. S3.3.e). Ratios calculations were made either by using all the monoterpenes measured by the GC-BVOC2 (14 compounds). In this case the weighted k rate constant was $84.3 \times 10^{-12} \text{ cm}^3 \text{ molecule}^{-1} \text{ s}^{-1}$. Either based on 8 monoterpenes only, which are the ones commonly measured by the GC-BVOC1. In this case, the weighted k rate constant was $77.9 \times 10^{-12} \text{ cm}^3 \text{ molecule}^{-1} \text{ s}^{-1}$. As shown in figure S3.3.e, an overall good agreement was seen. However, some overestimations are seen at the peaks when using the data from the PTR-MS data. The calculated OH reactivity at the highest peak is overestimated by approximately 17.5 s^{-1} (36.7%) at the maximum when considering $k_{\text{weighted}} = 84.3 \times 10^{-12} \text{ cm}^3 \text{ molecule}^{-1} \text{ s}^{-1}$ and by 12.5 s^{-1} (26.3%) when taking $k_{\text{weighted}} = 77.9 \times 10^{-12} \text{ cm}^3 \text{ molecule}^{-1} \text{ s}^{-1}$.

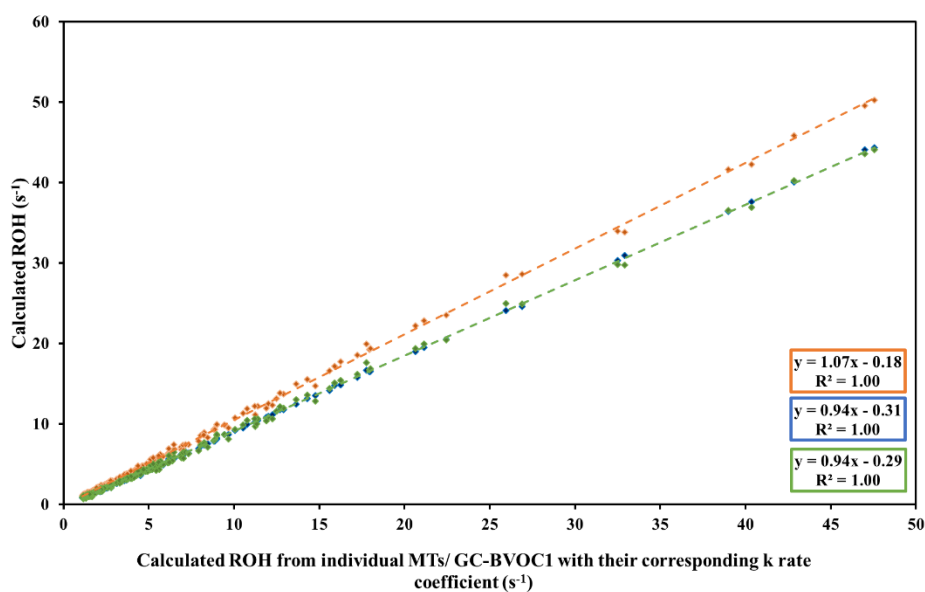


Figure S3.3.f: Correlation between the calculated OH reactivity from 8 BVOCs measured by GC-BVOC2 (the ones that are commonly measured by GC-BVOC1 (blue)), calculated OH reactivity from the sum of monoterpenes measured by the PTR-MS multiplied by $k_{\text{weighted}} = 84.3 \times 10^{-12} \text{ cm}^3 \text{ molecule}^{-1} \text{ s}^{-1}$ (based on all BVOCs/GC-BVOC2) (orange) and the calculated OH reactivity of the sum of monoterpenes measured by the PTR-MS and multiplied by the weighted $k = 77.9 \times 10^{-12} \text{ cm}^3 \text{ molecule}^{-1} \text{ s}^{-1}$ (based on the 8 common BVOCs measured by both GCs) with the calculated OH reactivity from all individual monoterpenes measured by the GC-BVOC1.

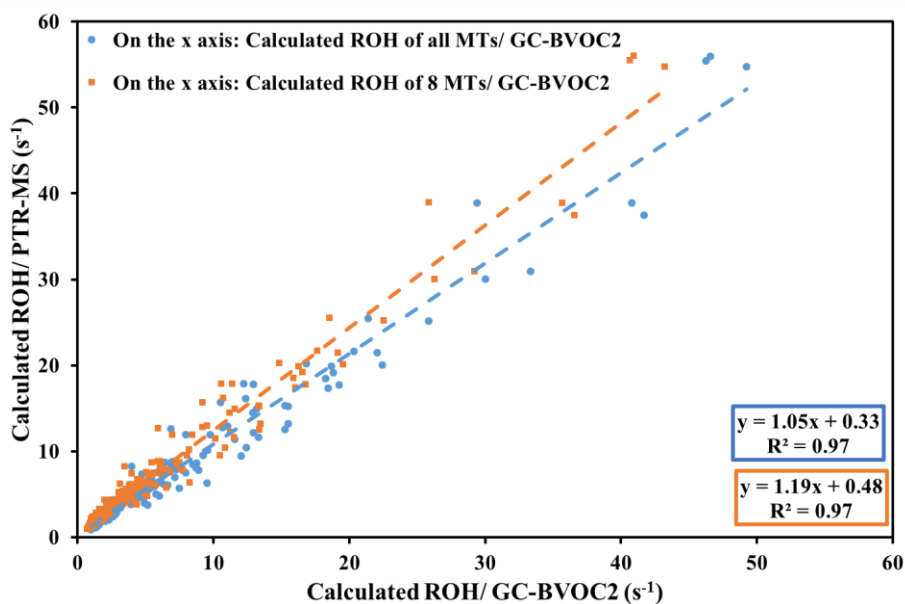


Figure S3.3.g: Comparison between the calculated OH reactivity from the sum of monoterpenes measured with the PTR-MS and the ones calculated with all the monoterpenes measured by the GC-BVOC2 (blue dots) or with only the monoterpenes commonly measured by the GC-BVOC1 and 2 (orange dots).

Regarding inside canopy measurements, a good agreement ($R^2=1$, slope of 0.94) exists between the calculated OH reactivity taking each individual monoterpene and the one with the sum of monoterpenes and k_{weighted} (from the mean ratios, $k = 77.9 \times 10^{-12} \text{ cm}^3 \text{ molecule}^{-1} \text{ s}^{-1}$). This agreement was also seen when comparing the sum of monoterpenes measured by the PTR-MS to the sum obtained by GC-BVOC2 (Fig. S3.2.b). It is worth noting that this value of k_{weighted} obtained using GC-BVOC2 compounds commonly measured with the GC-BVOC1 is used for the final calculation of the reactivity and comparisons with measured ones, in order to compare similar data sets at both heights. Finally, when comparing the OH reactivity calculated from the sum of monoterpenes measured by the PTR-MS and k_{weighted} ($84.3 \times 10^{-12} \text{ cm}^3 \text{ molecule}^{-1} \text{ s}^{-1}$) and the sum of the monoterpenes measured by the GC-BVOC2, a good agreement (Fig. S3.3.g, $R^2=0.97$, slope of 1.05) was obtained. However, a higher slope was recorded when taking into account only the 8 monoterpenes commonly measured by both GC-BVOC (Fig S3.3.g, slope of 1.19).

Supplementary material 3.4: Correction of Isoprene concentration measured with the PTR-MS

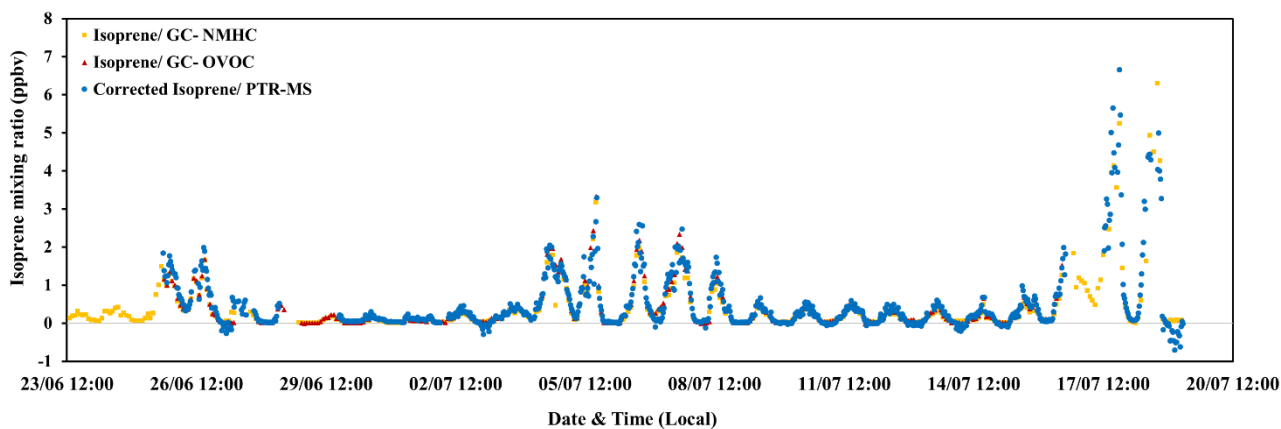


Figure S3.4.a: Comparison of isoprene concentration measured by three different instruments: corrected data from the PTR-MS (blue points), NMHC (orange points), and OVOC (red points) from 23th of June to 18th of July 2017.

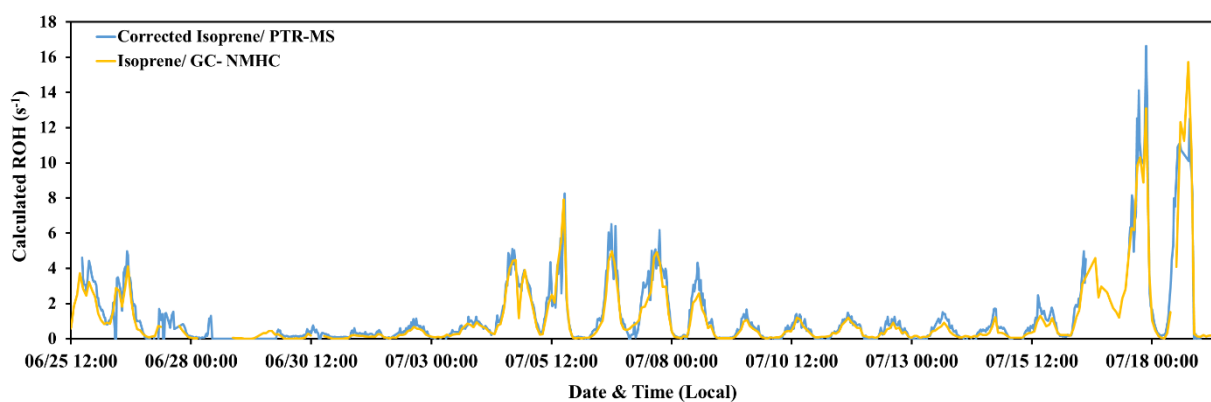


Figure S3.4.b: Calculated OH reactivity of isoprene measured with the PTR-MS (corrected/ blue) and the GC-NMHC (orange) at 12 m height.

Supplementary material 3.5: Contribution of OVOCs and NMHCs to OH reactivity above the canopy

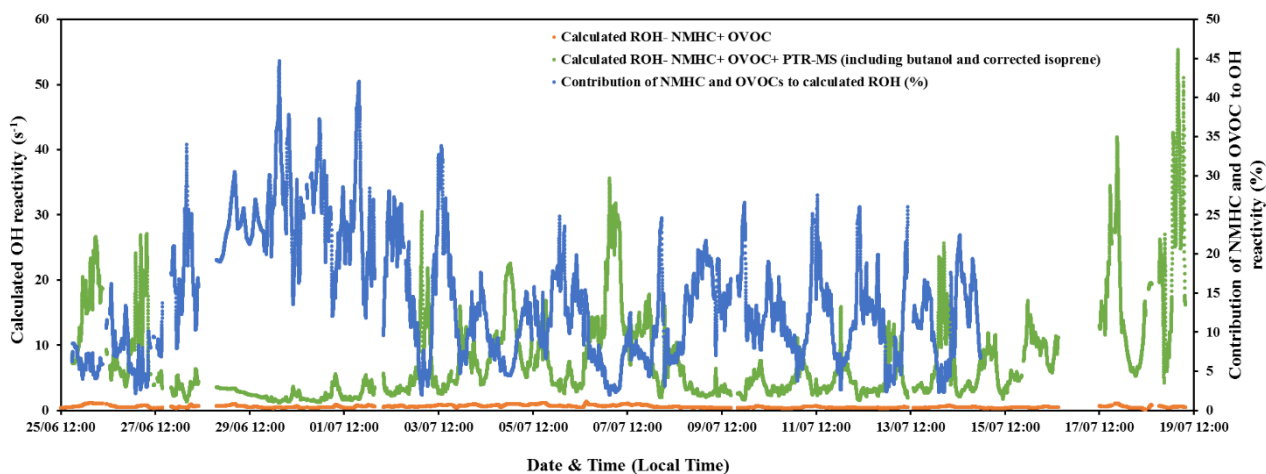


Figure S3.5: Graph representing the calculated OH reactivity from the GC-NMHC, the GC-OVOC, and the PTR-MS data (including butanol and corrected isoprene) (green dots), from the GC-NMHC and GC-OVOC data alone (orange dots), and the percentage of OH reactivity due to NMHC and OVOC (blue dots).

Supplementary material 3.6: Butanol (from SMPS exhaust) contribution to OH reactivity

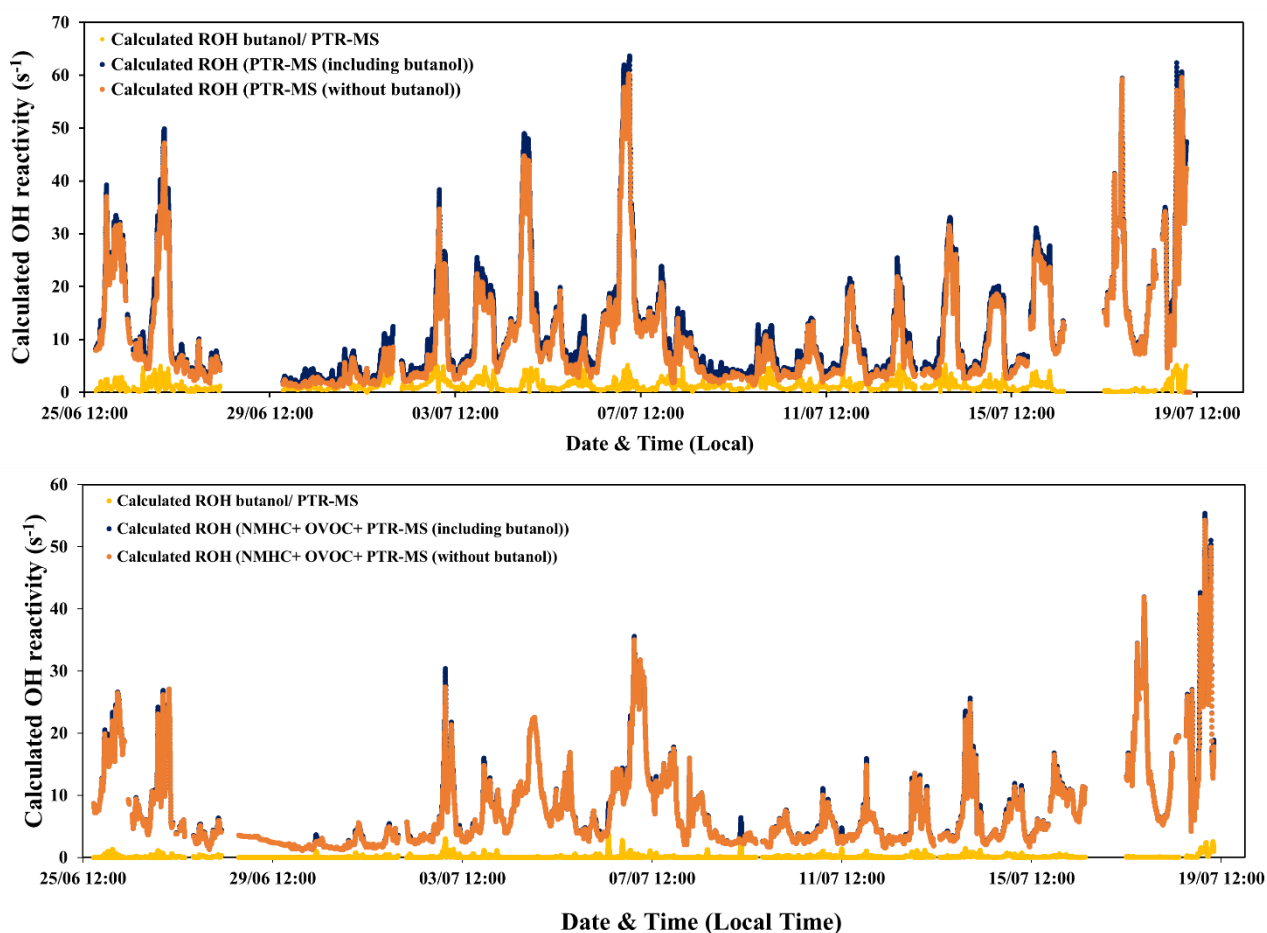


Figure S3.6: Butanol contribution to calculated OH reactivity inside (upper graph) and above (lower graph) the canopy.

Supplementary material 3.7: Assumptions made for OH reactivity calculations

Table S3.7: Summary of the assumptions taken into account for the calculation of OH reactivity and for the estimation of some compound's contribution to OH reactivity from ancillary measurements.

Problem	Assumption considered
Monoterpenes speciation	Ratios of speciated monoterpenes from GC-BVOC (1 and 2) were taken into account to calculate a weighted k rate constant of the reaction of monoterpenes with OH. The k_{weighted} was used to calculate the reactivity of monoterpenes measured by the PTR-MS.
Measured species only at 12 m	NMHC and OVOC were not taken into account in the calculation of OH reactivity at 12 m and 6 m heights. Their contribution is discussed at 12 m height where they were measured.
Interferences	Isoprene (PTR-MS): A factor of 4% is considered to correct for the contribution of monoterpenes to the isoprene signal in the PTR-MS. MACR+MVK ($m/z=71$ in PTR-MS): The ratio has been calculated from the GC-OVOC. An average ratio of 0.3 of MACR over the total concentration has been found and used to weight the rate constant for this mass.
Butanol contribution	The contribution of butanol to OH reactivity is estimated at 12 m where it was weak and at 6 m where it was more variable.

Supplementary material 3.8: Original and resampled data from the LSCE-CRM and UL-FAGE instrument

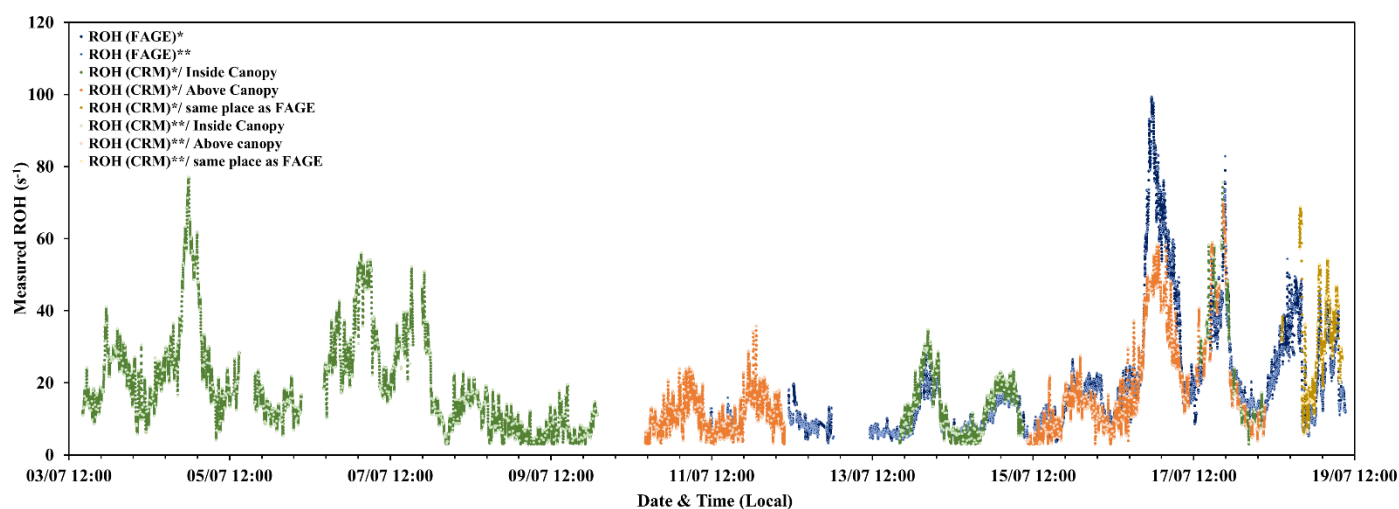


Figure S3.8: Comparison between the original data set (***) from both OH reactivity instruments and the resampled data set (*).

Supplementary material 3.9: Summary of day/ night measured, calculated and missing OH reactivity, inside and above the canopy

Table S3.9: Summary of day/ night averages of measured, calculated and missing OH reactivity, inside and above the canopy. The * indicates above canopy average values when measurements were performed at both heights.

	Day/ Night	Measured ROH/ LSCE-CRM (s ⁻¹)	Calculated ROH PTR-QiToFMS (s ⁻¹)	Calculated ROH PTR-QiToFMS + other measurements (s ⁻¹)	Missing ROH considering PTR-QiToFMS (s ⁻¹)	Missing ROH considering PTR-QiToFMS + other measurements (s ⁻¹)	Mean Temperature (°C)	Mean u* (m s ⁻¹)	Day/ Night state
Inside Canopy	3rd, July	14.5	5.3	7.8	9.2	6.8	22.9	0.4	Cool
	3rd- 4th, July	25.7	16.1	20.1	9.6	5.6	15.6	0.1	Stable/ Cool
	4th, July	20.0	9.9	12.3	10.0	7.7	26.5	0.6	Warm
	4th- 5th, July	45.6	28.1	32.6	17.5	13.1	21.7	0.2	Stable/ Warm
	5th, July	16.8	8.1	10.8	8.7	6.0	28.1	0.4	Warm
	5th- 6th, July	12.6	4.8	8.5	7.8	4.2	18.9	0.3	Unstable/ Stable/ Warm
	6th, July	22.1	11.0	13.9	11.1	8.2	24.2	0.4	Warm
	6th- 7th, July	37.5	33.6	37.3	3.9	< LOD	20.1	0.1	Stable/ Warm
	7th, July	28.1	18.6	21.6	9.5	6.5	28.3	0.4	Warm
	7th- 8th, July	17.9	9.6	13.1	8.3	4.8	21.2	0.4	Unstable/ Warm
	8th, July	13.2	7.5	10.4	5.7	< LOD	23.0	0.5	Cool
	8th- 9th, July	7.3	2.5	5.3	4.9	< LOD	19.5	0.5	Unstable/Warm
	9th, July	7.4	3.0	5.3	4.4	< LOD	20.9	0.8	Cool
Above Canopy	9th- 10th, July	7.9	3.4	7.1	4.5	< LOD	18.2	0.3	Unstable/ Stable/ Cool
	10th, July	7.7	2.6	4.3	5.1	3.4	20.6	0.5	Cool
	10th- 11th, July	13.0	5.1	6.9	8.0	6.1	17.3	0.1	Stable/ Cool
	11th, July	9.5	3.4	5.2	6.1	4.3	20.9	0.4	Cool
	11th- 12th, July	15.8	6.1	7.9	9.7	7.9	17.0	0.1	Stable/ Cool
Inside Canopy	12th, July	10.9	3.0	4.7	7.9	6.2	20.5	0.7	Cool
	12th- 13th, July						18.0	0.1	Stable/ Cool
	13th, July	6.7	3.1	6.3	3.6	< LOD	20.1	0.4	Cool
	13th- 14th, July	18.7	15.6	19.3	3.1	< LOD	18.0	0.1	Stable/ Cool
	14th, July	8.9	6.7	9.1	< LOD	< LOD	21.2	0.5	Cool
Above Canopy	14th- 15th, July	17.1	13.2	16.3	3.9	< LOD	15.2	0.1	Stable/ Cool
	15th, July a.m	13.3	12.9	15.9	< LOD	< LOD	22.0	0.4	Cool
	15th, July p.m	7.0	4.2	5.9	< LOD	< LOD			
	15th- 16th, July	15.6	10.8	12.7	4.5	< LOD	16.6	0.1	Stable/ Cool
1h Inside/ 1h Above Canopy	16th, July	10.0	8.1	9.9	< LOD	< LOD	26.7	0.5	Warm
	16th- 17th, July						21.6	0.1	Stable/ Warm
	17th, July	41.5/ 35.4*	23.3/ 20.4*	25.1/ 22.4*	18.2/ 15.1*	16.4/ 13.0*	28.9	0.4	Warm
17th- 18th, July	17th- 18th, July	20.4/ 20.5*	15.3/ 13.4*	17.3/ 15.3*	5.2/ 7.1*	3.1/ 5.2*	23.2	0.3	Unstable/ Warm
	18th, July	11.5/ 8.4*	7.9/ 6.4*	10.1/ 8.1*	3.6/ < LOD	< LOD/ < LOD	30.3	0.5	Warm

Appendix B

Supplement of chapter 4: Characterization of total OH reactivity in a rapeseed field: Results from the COV³ER experiment in April 2017

Supplementary material 4.1: CRM characterization tests

In order to test the performance and the stability of the CRM/ PTR-MS system, several experiments were performed at the beginning, the middle and the end of the campaign. These tests also aimed to determine three correction factors, for the difference in humidity between C2 and C3, for OH recycling due to high NO mixing ratios and for the deviation from pseudo-first order kinetics.

- Correction for the difference in humidity between the C2 and the C3 levels

Experiments were performed by introducing a known amount of zero air at different humidity inside the reactor while the instrument is measuring C2. The dependency of the difference in the observed C2 on the difference of m/z 37-to- m/z 19 ratio is investigated and used to correct the ambient C2 value. A linear least squares fit describes the dependency of C2 on the m/z 37-to- m/z 19 ratio. The slope of the fit obtained from the experimental tests is then used to correct the C2 value during ambient measurements in the following way: $C2_{\text{corrected}} = C2^* = C2 + p[(m/z37/m/z19)_{\text{during C3}} - (m/z37/m/z19)_{\text{during C2}}]$

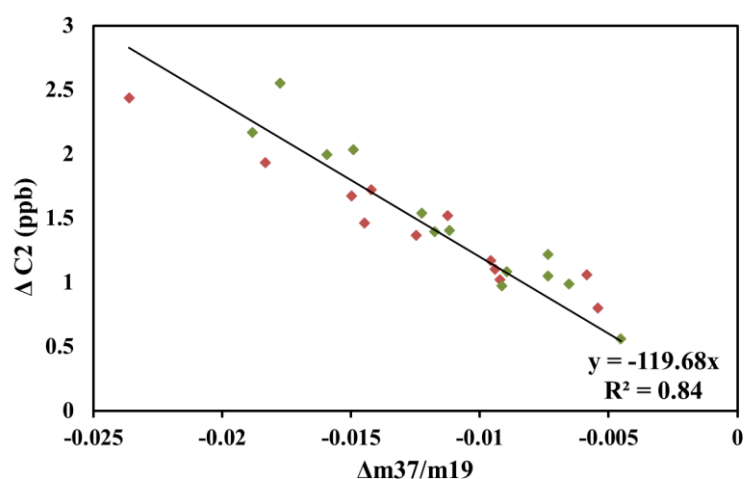


Figure S4.1.a: Linear least square fit of $\Delta C2$ (ppbv) vs. $\Delta(m37/m19)$ for the tests conducted on the field to assess the correction for humidity differences between C2 and C3. Green dots and red dots correspond to tests performed with ambient air and outgoing chamber air, respectively.

- **Correction on C3 for the spurious OH production from the reaction between HO₂ (formed from H₂O photolysis) and NO**

To assess the required correction for C3 values, different amounts of NO were introduced inside the reactor while sampling humid zero air. The difference of measured C3 (ppbv) was plotted as function of NO concentration (ppbv).

$$C3_{\text{corrected}} = C3^* = C3_{\text{measured}} + \Delta C3$$

With $\Delta C3 = a [\text{NO}]^2 + b[\text{NO}]$ as shown in figure S4.1.b.

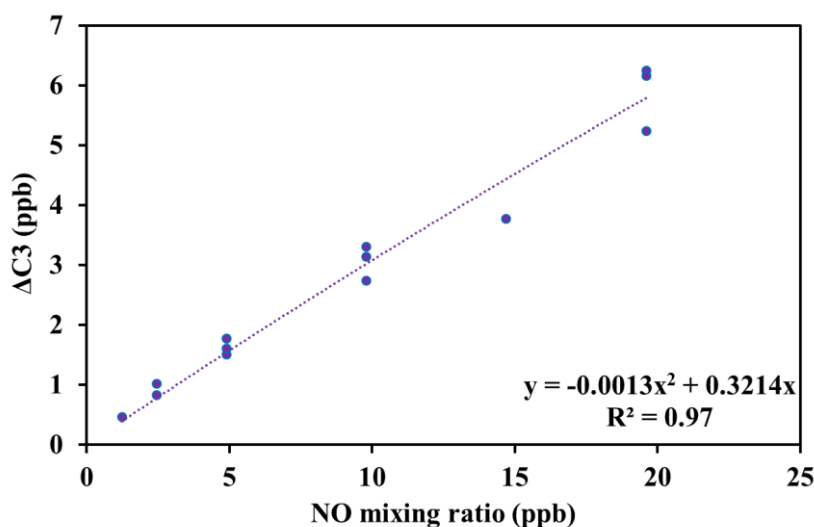


Figure S4.1.b: Experimental parameterization to correct for the NO interference, representing changes in C3 ($\Delta C3 \text{ ppb} = C3_{\text{expected}} - C3_{\text{measured}}$) as function of NO mixing ratios (ppbv) in the reactor.

- **Correction for not operating the CRM under pseudo-first-order conditions**

Tests were performed by introducing different concentrations of two gas standards: propane with a relatively low reactivity with OH and isoprene which is relatively highly reactive with OH. Different pyrrole/OH ratios were investigated ranging between 1.7 and 2.7. As shown in figure S4.1.c, measured reactivity during tests was plotted against the expected one form calculation (calculated OH reactivity is the product of the gas standard concentration and its rate constant for the reaction with OH). The inverse of the resulting slopes represents the correction factors that vary for each compound, as function of the pyrrole/OH ratio.

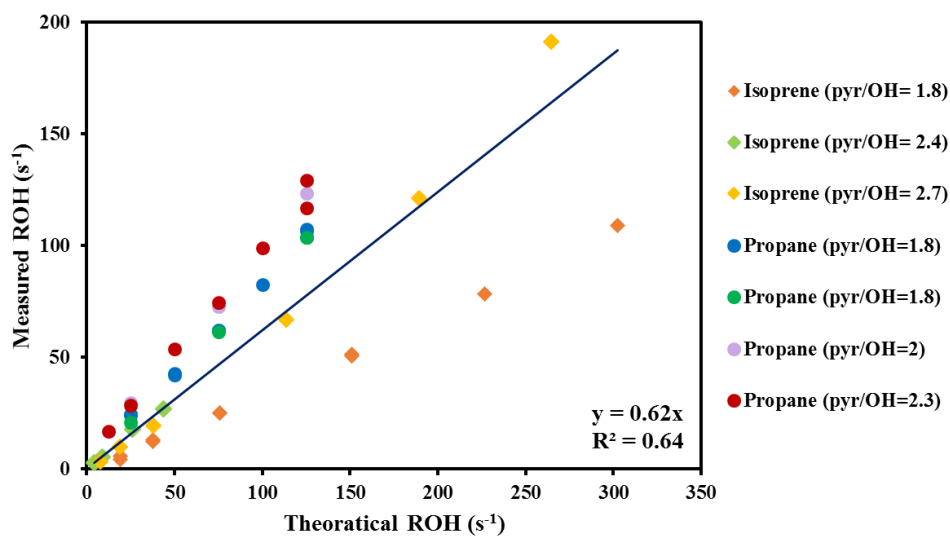


Figure S4.1.c: Measured ROH vs. the theoretical ROH for propane and isoprene, introduced at different concentrations and under different pyrrole/OH ratios. Circles and diamonds correspond to propane and isoprene tests, respectively.

Supplementary material 4.2: CRM/PTR-MS sampling system

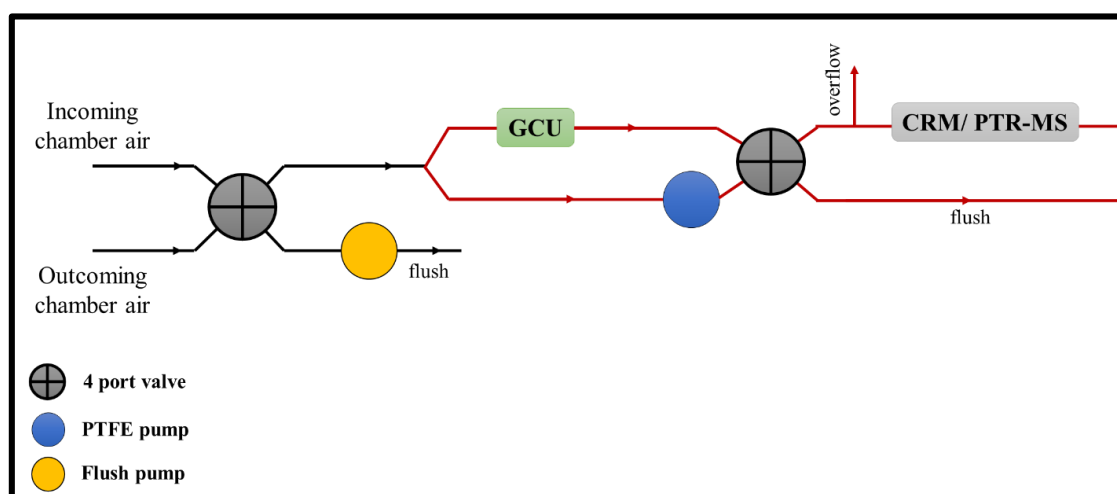


Figure S4.2: Schematic of the CRM/PTR-MS sampling system.

Supplementary material 4.3: PTRQi-ToFMS VOCs mixing ratio computation

The pre-processing steps provided averages and standard deviations cps for the ion peaks selected R_i . The mixing ratio of the compound $\chi_{i,ptr}$ (in ppbv) was calculated as in Abis et al., (2018) and Gonzaga et al. (2019):

$$\chi_{i,ptr} = 1.657 e^{-11} \times \frac{U_{drift} T_{drift}^2}{k p_{drift}^2} \times \left(\frac{cps_{R_iH^+}^{norm}}{cps_{H_3O^+}^{norm} + cps_{H_2O.H_3O^+}^{norm}} - \frac{cps_{R_iH^+}^{norm}(zeroair)}{cps_{H_3O^+}^{norm} + cps_{H_2O.H_3O^+}^{norm}(zeroair)} \right) \times S_i \quad (S4.3.1)$$

$$cps_{R_iH^+}^{norm} = \frac{TR_{H_3O^+}}{TR_{R_iH^+}} \times cps_{R_iH^+} \quad (S4.3.2)$$

where U_{drift} is the voltage of the drift tube (V), T_{drift} is the drift tube temperature in Kelvin (K), $cps_{R_iH^+}$ is the count per second (cps) of the product ion, $cps_{H_3O^+}$ and $cps_{H_2O.H_3O^+}$ are the cps of the source ion and the first water cluster, k is the protonation reaction rate assumed constant for all compounds ($2.5 \cdot 10^{-9} \text{ cm}^3 \text{ s}^{-1}$), *norm* stands for normalized, $TR_{H_3O^+}$ is the transmission factor for H_3O^+ , $TR_{R_iH^+}$ is the transmission factor for mass of protonated compound R_i , p_{drift} is the pressure in the drift tube, and S_i is the normalized sensitivity of the analyzer. Here *zeroair* stands for cps measured for zero air in the same conditions of pressure, temperature and voltage. The standard transmission curve from supplier was used to compute the normalized counts per seconds $cps_{R_iH^+}^{norm}$ (Table S4.3). $cps_{H_3O^+}^{norm}$ was computed from ion m/z 21.022 ($H_3^{18}O^+$) by multiplying by the isotopic factor 487.56, the first water cluster was taken as the ion peak m/z 37.028. In equation (S4.3.1), the number $1.657 e^{-11}$ is a constant specific to the instrument, accounting for the reaction time in the drift tube. The calibration procedures used to determine the zero and S_i are detailed in the manuscript.

Table S4.3: Standard Ionicon transmission curve used for computing the mixing ratio

m / z	TR	$\frac{\text{TR}_{\text{H}_3\text{O}^+}}{\text{TR}_{\text{R}_i\text{H}^+}}$
< 21	0.018	1.000
33	0.40	0.045
59	0.65	0.028
79	0.75	0.024
107	0.86	0.021
146	0.96	0.019
> 181	1.00	0.018

Supplementary material 4.4: The rapeseed branch physiological evolution

At the beginning of our measurements (7th till 15th, April), the rapeseed branch exhibited a rapid and more intensive growth, in terms of stem, leaves and flowers length as well as of number of open flowers, than during the last 10-day period (Figure S4.4), where the plant growth became more stable. Note that on the 15th, the chamber was uninstalled due to a planned fungicide application, and re-installed on the 17th, but on a higher part of the branch than before, including less stem, leaves and flowers.

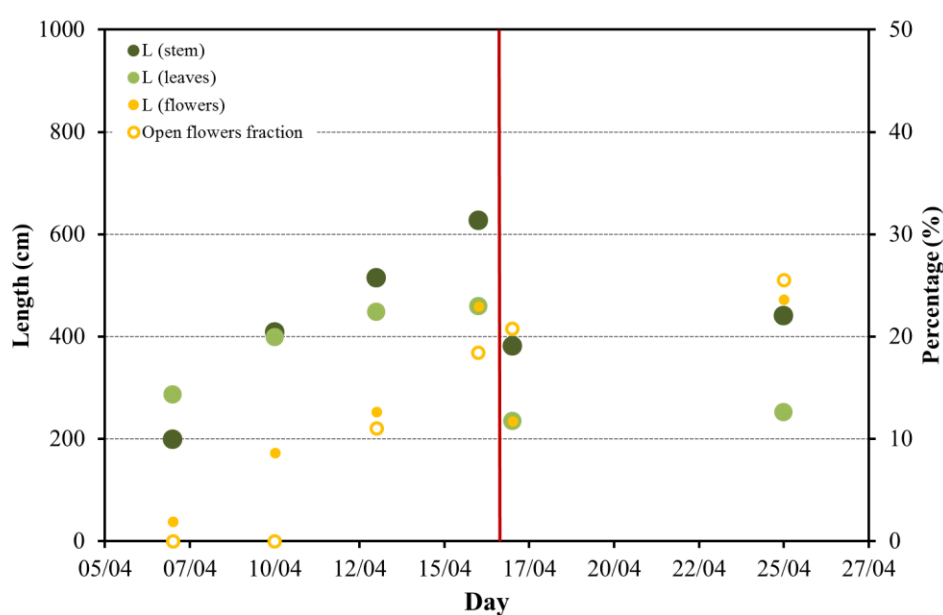


Figure S4.4: Rapeseed branch evolution in the dynamic enclosure. The left vertical axis represents the length of the stem, total leafs and total flowers (in cm). The right vertical axis represents the percentage of open flowers. The red line indicates the day when the chamber was re-installed after the planned fungicide application.

Supplementary material 4.5: Comparison between temperatures recorded inside and outside the dynamic chamber

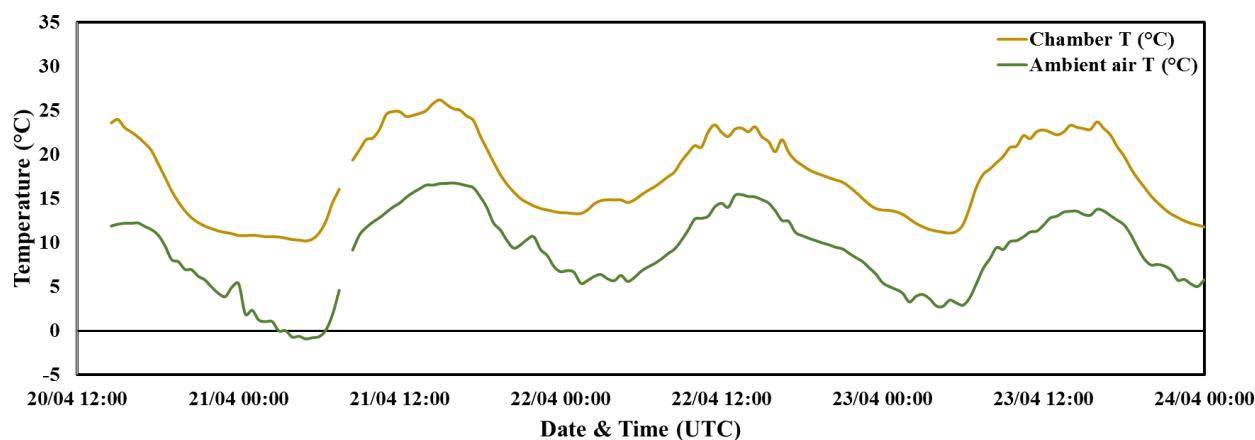


Figure S4.5: Temperature recorded inside the dynamic chamber (yellow) and in ambient air (green) during the measurement period between the 20th and the 23rd, April 2017.

Figure S4.5 shows the variability of temperatures recorded inside the chamber and in ambient air. Both temperatures had the same trend for the studied period, however a difference up to 12°C could be observed. This should be kept in mind when analyzing BVOCs and OH reactivity variability related to the enclosed rapeseed plant. Indeed, some BVOCs emissions are known to be temperature-dependent and their emissions could be enhanced under higher temperatures. However, higher concentrations of known/ detected BVOCs should result in higher $mROH_{\text{chamber}}$. Hence, these discrepancies in temperature should not affect the discussion on missing OH reactivity.

Supplementary material 4.6: Anthropogenic VOCs and inorganic compounds in ambient air

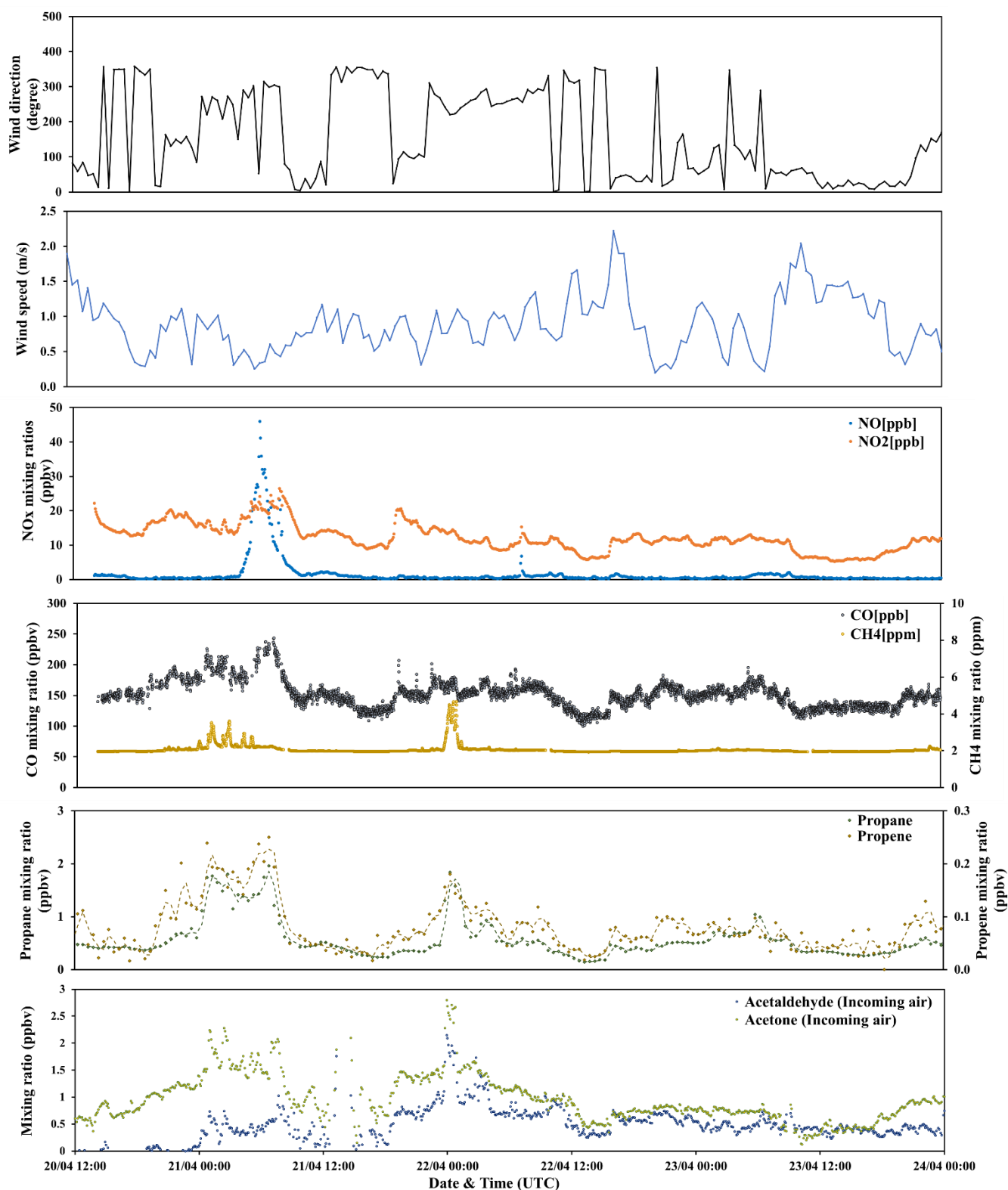


Figure S4.6.a: Variability of NO_x (NO, NO₂), CO, CH₄, propane, propene, acetaldehyde and acetone in ambient air, with wind direction and wind speed.

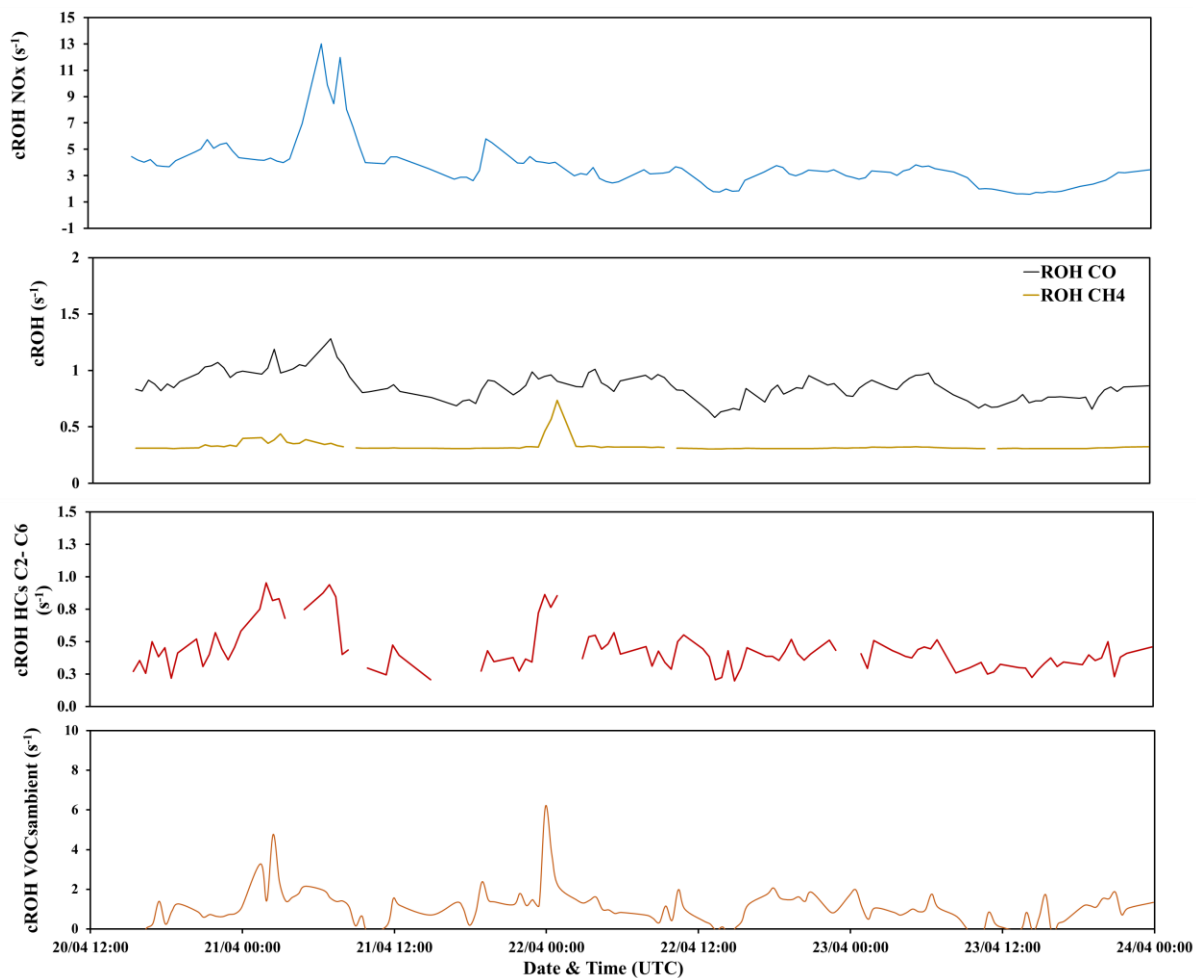


Figure S4.6.b: Variability of calculated OH reactivity of NO_x, CO, CH₄, total HCs C₂-C₆ and total VOC_{Sambient} (PTRQi-ToFMS).

Supplementary material 4.7: Biogenic VOCs inside the chamber

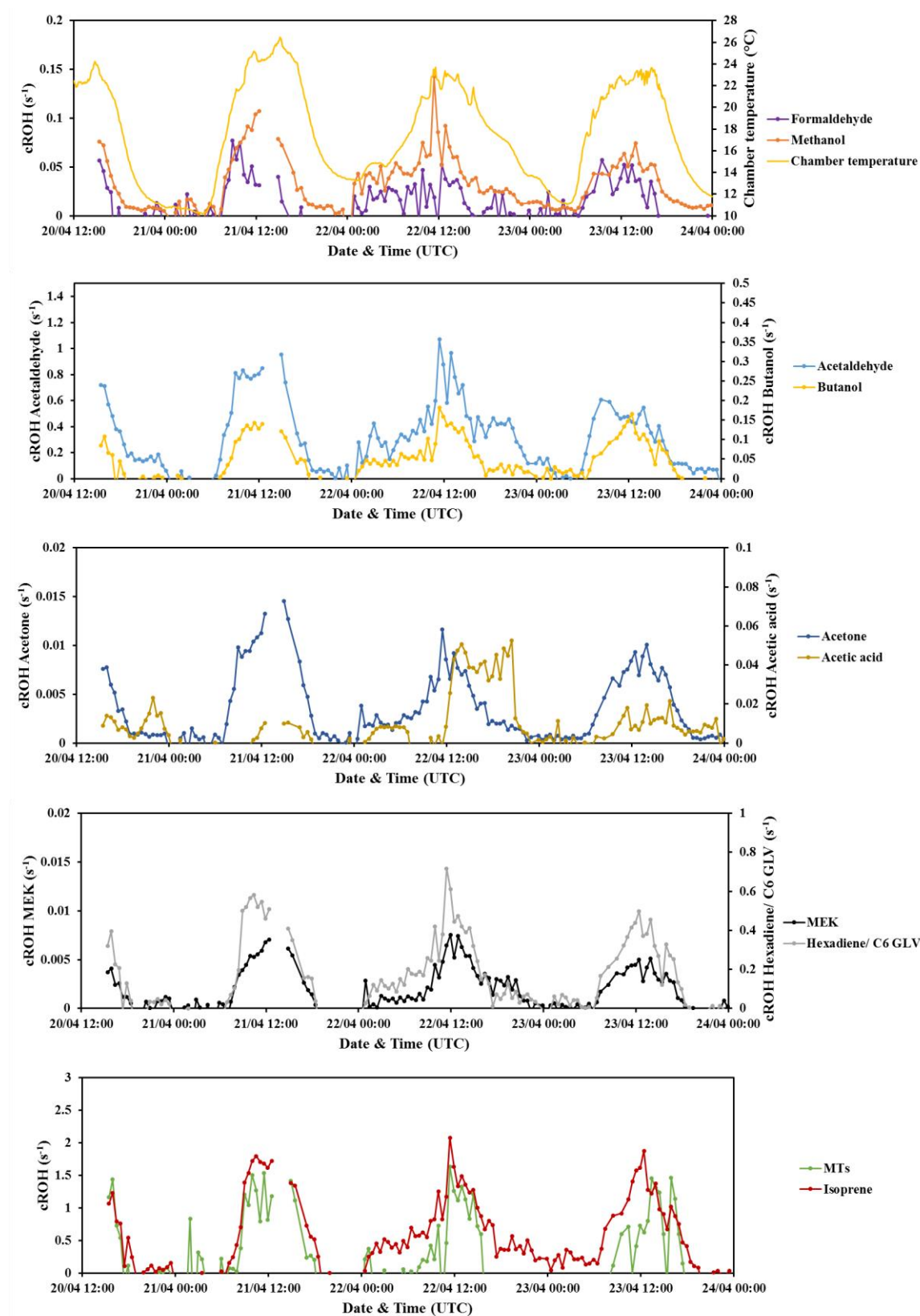


Figure S4.7: Variability of calculated OH reactivity of some biogenic VOCs emitted by the rapeseed plant ($\text{VOCs}_{\text{rapeseed}} = \text{VOCs}_{\text{chamber}} - \text{VOCs}_{\text{sambient}}$).

Supplementary material 4.8: Selection of PTRQi-ToFMS masses for missing OH reactivity investigation

Table S4.8: List of the 201 masses that correlate for 80 % and more with isoprene (m/z 69.070)

Protonated theoretical masses	R ²
228.191, 248.981, 128.068, 180.101, 197.219, 72.017, 226.255, 376.073, 153.157, 196.212, 211.235, 264.264, 108.053, 86.059, 208.206, 87.078, 375.062, 229.198, 142.08	0.8
116.074, 158.088, 236.237, 98.026, 252.158, 102.086, 207.202, 134.068, 38.963, 185.13, 144.097, 85.027, 90.061, 183.206, 194.195, 170.191, 186.093, 85.064, 248.006, 184.207, 269.248, 210.226, 101.023	0.81
212.236, 159.131, 130.147, 303.291, 116.037, 169.189, 211.14, 250.25, 290.281, 209.217, 143.097, 172.096, 157.105, 193.187, 241.195, 154.166, 249.178, 182.196, 171.108, 255.218, 232.202, 205.082, 173.145, 204.175	0.82
88.048, 209.141, 278.282, 251.168, 54.938, 250.179, 133.098, 244.212, 161.096, 155.085, 141.09, 102.06, 155.175, 247.006, 235.227, 237.245, 187.076, 230.199, 263.263, 221.217, 243.213	0.83
234.221, 80.997, 127.076, 84.044, 174.147, 98.062, 60.048, 206.192, 287.258, 168.18, 87.042, 100.074, 181.19, 138.059, 289.265, 233.218, 205.186, 101.059, 141.159, 99.008, 142.163, 150.129	0.84
160.132, 262.244, 218.19, 148.116, 126.092, 260.238, 165.089, 187.155, 190.159, 57.033, 219.202, 192.176, 277.272, 137.058, 167.174, 231.202, 259.232	0.85
162.089, 180.18, 166.163, 70.039, 248.237, 128.148, 188.147, 246.22, 195.202, 138.133, 273.251, 245.219, 152.149, 201.171, 179.173	0.86
95.083, 146.119, 216.178, 106.037, 202.171, 165.158, 276.262, 217.183, 274.245, 191.172, 139.143, 215.181	0.87
261.247, 96.088, 275.254, 140.149, 247.23, 123.042, 176.142, 147.11, 189.15, 145.118	0.88
151.143, 117.087, 124.044	0.89
175.141, 39.023, 119.082, 100.117, 127.144, 105.032, 149.127, 123.115, 56.058, 56.024	0.90
68.052, 113.129, 44.055, 125.13, 124.117, 126.135, 178.161	0.91
82.074, 164.149, 109.1	0.93
110.103, 99.116, 72.088, 69.07, 177.157, 86.103, 112.119	0.94
163.142, 111.115, 58.068, 97.098, 98.104, 85.1	0.95
84.088	0.96
70.073	0.97

Supplementary material 4.9: Sensitivity test on Isoprene's calculated OH reactivity

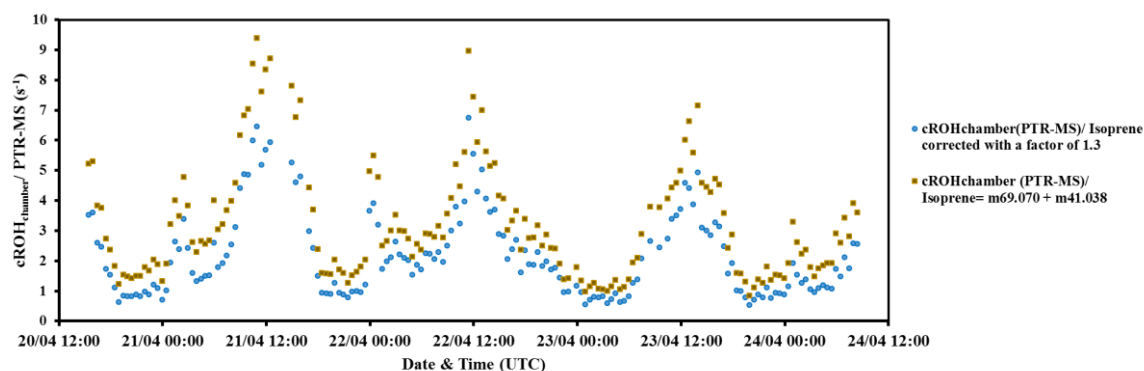


Figure S4.9: Variability of calculated OH reactivity using PTR-MS data with a correction of the isoprene signal (m/z 69.070) by a factor of 1.3 (blue) and by summing the m/z 69.070 with the potential fragment on m/z 41.038 (yellow).

m/z 41.038 was identified as potential fragment of isoprene. In order to test the impact of taking this mass, or not, into account in OH reactivity calculation, this mass was accounted for by summing its mixing ratio with that of m/z 69.070. An increase in OH reactivity was obtained with a maximum increase of 3 s^{-1} . This test explained 1.3 s^{-1} on average of day-time missing OH reactivity, meaning that the correction for potential fragmentation of isoprene would decrease the day-time missing OH reactivity by 20 % on average.

Appendix C

Characterization of particle and gaseous pollutant emissions from a French dairy and sheep farm

Authors

Julien Kammer^{1,2,*}, Céline Décuq¹, Dominique Baisnée², Raluca Ciuraru¹, Florence Lafouge¹, Pauline Buysse¹, Sandy Bsaibes², Ben Henderson³, Simona M. Cristescu³, Rachid Benabdallah¹, Varunesh Chandra¹, Brigitte Durand¹, Oliver Fanucci¹, Jean-Eudes Petit², Francois Truong², Nicolas Bonnaire², Roland Sarda-Estève², Valerie Gros² and Benjamin Loubet^{1*}

Affiliations

¹INRA, UMR ECOSYS, INRA, AgroParisTech, Université Paris-Saclay, 78850 Thiverval-Grignon, France

²Laboratoire des Sciences du Climat et de l'Environnement, CEA-CNRS-UVSQ, IPSL, Université Paris-Saclay, 91191 Gif-sur-Yvette, France

³Department of Molecular and Laser Physics, IMM, Radboud University, Nijmegen, the Netherlands

*Corresponding authors:

Julien Kammer

Laboratoire des Sciences du Climat et de l'Environnement (LSCE)

CEA-CNRS- University of Versailles Saint-Quentin-en-Yvelines (OSVQ)

Orme des merisiers, Building 714

91191 Gif/Yvette, France

Tel.: +33 1 30 81 55 41

Mail: julien.kammer@lsce.ispl.fr; julien.kammer@gmail.com

Abstract

Agricultural activities highly contribute to atmospheric pollution, but the diversity and the magnitude of their emissions are still subject to large uncertainties. A field measurement campaign was conducted to characterize pollutant emissions from an experimental farm in France. In a sheepfold and a dairy stable, more than four hundred Volatile Organic Compounds (VOCs) were characterized using an original combination of both online and off-line measurements. CO₂ and ammonia (NH₃) were the most concentrated compounds inside the buildings (above the ppm level), followed by methanol, acetic acid and acetaldehyde. A CO₂ mass balance model were used to estimate NH₃ and VOC emission rates. To our knowledge, this study constitutes the first evaluation of emission rates for most of the identified VOCs. We evidenced that the dairy stable emitted more VOCs than the sheepfold. Despite strong VOC and NH₃ emissions, the chemical composition of particles indicates the gaseous farm emissions do not affect the fine particles loading inside the farm. This could be mainly explained by the low residence time inside both buildings. The dataset with new references will help to improve emissions inventories.

Keywords: VOC emissions, Ammonia, Agriculture, Air quality, PTR-Qi-TOF-MS

Highlights

- More than 400 hundred VOCs have been identified in a dairy and sheep farm in France
- VOC emission rates have been determined for the first time for several VOCs
- VOC emissions from the dairy stable were higher than sheepfold emissions
- Aerosol chemical composition was not affected by ammonia and VOC emissions

1. Introduction

Agricultural activities are one of the major sources of pollutants in the atmosphere. Agricultural emissions can be both particulate and gaseous and affect the air quality as well as the climate. For example, at global scale, agriculture is the main source of ammonia (NH_3) in the atmosphere; a gaseous compound which plays a central role in atmospheric particles formation and chemistry (Behera et al., 2013; Massad and Loubet, 2015; Yao et al., 2018; Yu et al., 2012). Among all agricultural activities, livestock management is recognized as a significant source of NH_3 , and was estimated to contribute to around 34 to 40 % of global NH_3 emissions (Behera et al., 2013; Schmithausen et al., 2018). Livestock is also a strong emitter of greenhouse gases such as methane (CH_4) or carbon dioxide (CO_2) (Hempel et al., 2016; Huang et al., 2015; Maldaner et al., 2018; Ngwabie et al., 2014). Other studies have shown that farm buildings emitting numerous volatile organic compounds (VOCs) may be as important as traffic road contributions (Ciganek and Neca, 2008; Ngwabie et al., 2008; Shaw et al., 2007; Yuan et al., 2017). VOCs are key species for atmospheric chemistry and climate that are able to produce secondary pollutants, such as ozone or aerosols (Atkinson and Arey, 2003; Curci et al., 2009; Derognat, 2003; Hallquist et al., 2009; Seinfeld and Pandis, 2006). The chemical structure of VOCs strongly affects their ability to generate ozone and aerosols. It is therefore essential to identify the chemical structure of the VOCs emitted by farm buildings, and evaluate the magnitude of their emissions. Despite the great number of compounds that may be emitted, only a few studies have proposed a complete VOCs identification list (Blunden et al., 2005; Ciganek and Neca, 2008; Feilberg et al., 2010; Schiffman et al., 2001; Yuan et al., 2017). To achieve a complete VOCs screening, it is recommended to conduct studies combining both on-line (such as PTR-MS techniques) and off-line (using chromatographic techniques) measurements (Ni et al., 2012). However, studies combining both methodologies remain scarce, and only a limited number has provided emission factors, which are crucial parameters for evaluating environmental impacts of livestock management at various scales. For example, Feilberg et al. (2010) combined on-line and off-line techniques to estimate VOC emissions from an intensive pig production, but they were limited to few compounds due to the use of a quadrupole PTR-MS. Ciganek and Neca (2008) reported the identification of more than one hundred VOCs using gas chromatography-mass spectrometry (GC-MS) at both pig and cattle farm. The authors reported concentrations inside and outside the buildings, without estimating their emissions. Schiffman et al. (2001) identified 331 VOCs during swine operations using off-line GC-MS, but emissions were not estimated. From the few studies providing VOC emission

rates from farm buildings, there is a review focused on swine facilities where Ni et al. (2012) pointed out that there were only three studies measuring emission factors from swine facilities, with huge differences; up to three orders of magnitude for some compounds. Most of the reported studies dealt with pig, dairy or poultry farming, but little is known about other livestock. To date, there are only two studies dealing with VOCs emissions from sheep farming (Ngwabie et al., 2007; Yuan et al., 2017). Therefore, more studies about VOCs emissions from farm buildings are needed to better constrain VOC emission inventories.

For that purpose, a field campaign was carried out at an experimental farm in the western region of Paris (France). The aim of the study was first to characterize VOCs fingerprint inside a dairy stable and a sheepfold, which were both naturally ventilated buildings. On-line (Proton Transfer Reaction – Quadrupole ion guide – Time Of Flight – Mass Spectrometry, PTR-Qi-TOF-MS) and off-line (Thermal Desorption-Gas Chromatography – Mass Spectrometry, GC-MS and Gas Chromatography – Flame Ionization Detector, GC-FID) measurements were carried out outside and inside both buildings. Then, fine aerosol chemical composition (using an aerosol chemical speciation monitor, ACSM) was measured to characterize the contribution of livestock to fine aerosol loading. Finally, a CO₂ mass balance model was used to estimate NH₃ and VOC emission rates and emission factors from both buildings.

2. Materials and methods

2.1. Experimental set up

A field measurement campaign was conducted in an experimental farm located at Grignon, in the western region of Paris, France (35 km west from Paris, 48°50'28.89" N, 1°56'56.03" E, altitude: 131 m above sea level). The experimental set up consisted of a mobile laboratory van where the instruments were placed. Three different locations were investigated: inside a dairy stable, inside a sheepfold, and outdoor in the vicinity of the two former buildings (Figure S1). The PTR-Qi-TOF-MS (used to measure VOCs) and the ACSM (used to measure the fine aerosol chemical composition) were not available at the same time (only one day in common, during the outside period). As a result, the field campaign was divided in two main parts: during the first one, when only the PTR-Qi-TOFMS was available, and the second part when the ACSM was available. All the other instruments described below were available all along the field campaign. The first place investigated was the dairy stable, between the 16th and the 20th of November 2017 (with the PTR-Qi-TOF-MS), then between the 28th of November and the 1st

of December 2017 (with the ACSM). The van was located in a corner of the stable, which was naturally ventilated (Figure S1). The number of animals inside the stable along the experiment was 205 animals: 173 dairies and 32 calves, with a mean weight of about 550 kg by animal. For dairies, the milk yield was 30 kg per day by animals. The second location investigated was the sheepfold between the 20th and the 22nd of November 2017 (with the PTR-Qi-TOF-MS), then between the 24th and the 28th of November 2017 (with the ACSM). The building was also naturally ventilated, but with a priori a lower air exchange rate than the dairy stable. 1041 animals were in the building during measurement period, 488 ewes, 534 lambs (males and females) and 19 rams. The mean body weight for sheep was estimated to be about 80 kg per animal. Finally, we moved the mobile laboratory outside in the farm, directly nearby the sheepfold and close to the dairy barn between the 22th and the 24th of November 2017 (with the PTR-Qi-TOF-MS, then the ACSM). At this last location, there were some animal-feeding storages, a manure storage and a methanisor close to the mobile laboratory (Figure S1). Tractors were moving in the farm both outdoor and inside the farm buildings which would have also influenced our measurements.

2.2. Sampling and instrumentation

Wind speed and direction were measured inside the buildings and outside using a 3-dimension sonic anemometer (R3, Gill instruments). CO₂ was measured with an open path infrared gas analyser (LI-7500, LI-COR biosciences). The mobile laboratory van used in this study was designed for atmospheric studies, with air conditioning and tubing dedicated to gas and aerosols sampling. All measurements were performed at heights between 1.5 and 2 m above ground level. Nitrogen oxides (NO_x, being the sum of NO and NO₂) were monitored with a chemiluminescent gas analyser (model 42C, Thermo Fischer scientific). The NO_x analyser sampled the air through a 1.5 m Teflon non-heated inlet at 2 L min⁻¹ and was calibrated before the campaign.

NH₃ measurement were performed every 2 minutes using a commercial laser photoacoustic-based analyser (LSE Monitors B.V., the Netherlands). The inlet was 1.2 m Teflon tubing (1/8 inches diameter) heated at 40/45 °C; the inlet flow inside the analyzer was 0.040 L min⁻¹. A Teflon filter was added at the inlet of the tubing to prevent particle penetration inside the instrument. The NH₃ analyzer was calibrated before the campaign by the manufacturer, and had a detection limit of 1-2 ppb.

VOCs were measured online using a proton transfer reaction - quadrupole ion guide - time of flight - mass spectrometer (PTR-Qi-TOF-MS, Ionicon analytik GmbH), that have been fully

described by Abis et al. (2018). Air was sampled using 1.5 m long Teflon tubing with a 1/8 inches diameter. The inlet airflow was set at 0.2 L min⁻¹, and the inlet was heated at 80°C to avoid semi volatile compounds condensation inside tubing. A Teflon filter (Ø = 0.45 µm, Pall Life Sciences 4785 Ion Chromatography (IC) Acrodisc Syringe Filters) was placed at the entry of the sampling line to remove particles from the air to analyse. The PTR-Qi-TOF-MS operated in standard conditions, with a drift pressure set between 3 mbar (in the sheepfold and outside) and 3.5 mbar (in the stable), a drift temperature of 80 °C and a drift voltage close to 751 V (in the sheepfold and outside) and 878 V (in the stable). These conditions were set to ensure a constant E/N ratio (where E is the electric field strength and N the gas number density) about 133 Td (1 Td = 10⁻¹⁷ V cm⁻²). Such range of the E/N ratio limit fragmentation and sensitivity of the protonation rate to variations in relative humidity (Pang, 2015; Tani et al., 2003). Blanks were daily performed with high purity zero air (Alphagaz 1, zero air: 80% nitrogen, 20% oxygen, purity: 99.9999%, Air Liquide) to check instrument background signal, and calibrations were frequently achieved with a toluene gas standard (102±10 ppb, Messer) diluted in the zero air. During the experiment, the mass spectra up to m/z 510 were recorded every second with a TOF scan of 25 kHz.

To complete PTR-Qi-TOF-MS analysis, off-line analysis was performed. For TD-GC-MS measurements, VOCs were trapped on cartridges using two different adsorbents (Tenax TA and carbotrap 300). Before the campaign, the tubes were pre-conditioned by heating at 80 °C under a helium stream of 60 L min⁻¹ for 6 hours. Then, ambient air was sampled during 3 to 5 hours at 0.5 L min⁻¹, and regulated with a mass flow controller (Bronkhorst) (Table S3). After exposure, cartridges were stored in the dark at a temperature about 4°C until their analysis. Tubes were desorbed using a thermo-desorption unit (TDU) from Gerstel. The TDU was programmed to desorb the tubes from 50 to 260 °C for 10 min at a rate of 60 °C/min. VOCs were cryo-focused in the Programmable Temperature Vaporization (PTV) at -20 °C using a carbotrap liner. VOCs separation were carried out using an Agilent 7890B gas chromatograph on a capillary column (30 m length, 0.25 mm inner diameter, 0.25 µm df, DB624 column, Restek). The oven temperature was initially set at 40 °C for 5 min, heated at a rate of 11 °C/min to 60 °C, then heated at a rate of 20°C/min to 220°C and maintained during 2 minutes. Helium was used as carrier gas. VOCs detection was performed with an Agilent 5977A mass spectrometric detector. The Electronic Impact (EI) mode was at +70 eV; the monitoring was from m/z 36 to 300. The ion source and Quadrupole analyser temperature were respectively set at 230 and 150 °C.

Canister sampling was also performed by sampling the air during 15 minutes every 4 hours (Table S3). Air sampled by canisters was analysed by GC-FID (HP 6890) equipped with a CP-Al₂O₃ Na₂SO₄ column, providing a complementary analysis of small hydrocarbons. A pre-concentrator (Entech 7200) was placed at the inlet of the instrument to allow automatic injections. A standard cylinder with 5 non methane hydrocarbons (NMHC, Messer) was used to check the instrument functioning, and an internationally reference standard containing 32 NMHC from C2 to C10 (NPL, National Physics Laboratory, Teddington, UK) was used to calibrate.

In order to characterise the aerosol composition inside the farm buildings, an Aerosol Chemical Speciation Monitor (ACSM) was used during the field campaign, providing near real time concentrations of submicron organic matter (OM), nitrate (NO₃⁻); sulphate (SO₄²⁻), ammonium (NH₄⁺) and chloride (Cl⁻). Measurement principle of the ACSM has been extensively described elsewhere (Ng et al., 2011). Briefly, submicron particles are successively sampled at 3 L min⁻¹, sub-sampled at 85 mL min⁻¹, focused through an aerodynamic lens, and eventually flash-vaporized over a 600°C-heated tungsten vaporizer, followed by ionization by EI at 70 keV. Fragments are separated by quadrupole, and a fragmentation table is applied to retrieve the concentrations of the above-listed components. The ACSM has been calibrated from the injection of 300 nm ammonium nitrate particles, as described in Ng et al. (2011). Comparison with few filter samplings allowed to validate the obtained calibrations values (Figure S4).

3. Methodology

3.1. Identification of emitted VOCs

PTR-Qi-TOF mass spectrums were all analysed using PTR-Viewer 3.2.8.0 (Ionicon analytik GmbH). To identify the emitted VOCs, we determined a separate peak table for each location (stable, sheepfold, outdoor). For that purpose, we used 30 minutes averaged mass spectra to be statistically relevant. To exclude impurities from our analysis, the mass spectra obtained with pure zero air was subtracted to ambient mass spectra. In the case of the sheepfold dataset, we determined the peak table by scanning several 30 minutes mean mass spectra selected during different hours of the day and night. For the stable, we determined the peak table by analysing mass spectra corresponding to contrasting situations. We considered that CO₂ may be a good tracer for animal activity and NH₃ a good tracer for litter emissions. We hence kept the four following situations: high CO₂/high NH₃, high CO₂/low NH₃, low CO₂/high NH₃ and low CO₂

/ low NH₃. Mass spectra from these 4 situations were successively inspected, to cover all possible cases. For the outdoor measurements, we chose mass spectra at different time of the day and determined peak tables from these spectra. For each of the 3 locations, we excluded periods when NO and/or NO₂ mixing ratios were too high, to avoid situations where an anthropogenic combustion source (*e.g.* tractor passing by) biasing our analysis. Once the peak tables were determined, the counts per second for each peak was integrated over each one-second mass spectra using PTR-Viewer 3.2.8.0. We then averaged over 5 min the obtained data. For PTR-Qi-TOF-MS, molecular formula was proposed based on *i*) the exact m/z value, *ii*) the theoretical isotopic distribution of the associated molecular formula, and *iii*) the coherence of the atoms included in the compound, with respect to chemical rules such as valence of atoms, etc.

TD-GC-MS data were processed by MassHunter (B.07.04.5560) software (Agilent Technologies Inc.). Automatic peak detection and mass spectrum deconvolution were performed using Unknowns Analysis (B.06.00) software. Each compound was accompanied by a deconvoluted spectrum, which was compared to the NIST (National Institute of Standards and Technology, 2011) Mass Spectrum database to allow its identification. A minimum match factor of 70 % between the reference mass spectrum and the observed one was required. Each compound was then manually scrutinized to confirm the proposed formula, and its retention time was analysed regarding the compounds physico-chemical properties (*e.g.* boiling point).

3.2. Emission rates calculation

Emission rates were calculated with a mass balance model (Pedersen et al., 1998; Schmithausen et al., 2018), based on the following equation:

$$E_{(i)} = Q * (C_{\text{indoor}(i)} - C_{\text{outdoor}(i)}) \quad (1)$$

Where E (in g h⁻¹) is emission rate of the compound i, Q (in m³ h⁻¹) is the ventilation flow rate of the building, C_{indoor(i)} and C_{outdoor(i)} (in g m⁻³) are the compound i concentrations inside and outside the buildings. In equation (1), C_{indoor(i)} was averaged at half-hourly time steps, while C_{outdoor(i)} was averaged over the entire outside experimental period.

The ventilation flow rate, which was considered the same for all gases, was estimated from CO₂ as (Hassouna et al., 2015; Pedersen et al., 2008):

$$Q = \frac{CO_{2\text{HPU}} \times A_{\text{animals}} \times \text{HPU}}{(CO_{2\text{indoor}} - CO_{2\text{outdoor}}) \times 10^{-6}} \quad (2)$$

Where CO_{2HPU} (in $g\ h^{-1}\ hpu^{-1}$) is the CO_2 production rate by heat production unit, $A_{animals}$ (unitless) is the relative animal activity, HPU is the number of heat production units (1 heat production unit = 1000 W), $CO_{2indoor}$ and $CO_{2outdoor}$ (in $g\ m^3$) are the CO_2 mixing ratios inside and outside the building, respectively. As recommended in the literature, CO_{2HPU} for stable and sheepfold were set to $393\ g\ h^{-1}\ hpu^{-1}$ and $344\ g\ h^{-1}\ hpu^{-1}$, respectively (Hassouna et al., 2015; Pedersen et al., 2008; Schmithausen et al., 2018). These values are specifically recommended for farm buildings, and take into account for both animal respiration and CO_2 contribution from manure. $A_{animals}$ was here estimated using equation 3 (Pederson et al., 2002):

$$A_{animals} = 1 - a \times \sin\left(2 \times \frac{\pi}{24}\right) \times (h + 6 - h_{min}) \quad (3)$$

Where a is a constant expressing the relative amplitude of the animal activity during the day (0.2 for dairy cows), h is the hour of the day and h_{min} is the time of the day with minimal activity (02:10 for dairy cows).

The coefficients for animal activity concerning the sheepfold were not available in the literature. Thus, for sheepfold the CO_2 production was not corrected for animal activity, and ventilation flow rate equation for sheepfold was estimated with $A_{animals} = 1$.

For both buildings, HPU were calculated by normalizing by 1000 the total heat produced by each building. The latter is obtained from the heat produced (Hp , in W) by animals for a building multiplied by the total number of animals. Hp has been calculated as following (Pederson et al., 2002; Schmithausen et al., 2018):

$$Hp = \alpha \times BW^{0.75} + \beta \times Y \quad (4)$$

Where Hp is the heat produced by one cow (in W) BW is the mean body weight of animals (in kg) and Y is the milking yield of a cow or an ewe (30 and 0.25 kg per day, respectively) and represent the weight daily gain in the case of a lamb, α and β are coefficient from the literature (Pedersen et al., 2008, 1998; Pederson et al., 2002; Schmithausen et al., 2018). For a cow, α is 5.6 and β is 2. For sheep (ewe or lamb) α is 6.4 and β is 145.

Finally, VOC emission rates can be calculated using the ventilation rate estimated and equation 1.

3.3. Statistical analysis

All statistics were performed with R software (Rstudio version 1.0.153). First, the normality of each VOCs measured with the PTR-Qi-TOF-MS was tested using a Shapiro-Wilk test. Then, we computed the correlation between each VOCs for the sheepfold, the stable, and outside. As the distribution for each compound was not normal according to the Shapiro-Wilk tests, correlations were calculated using kendall correlation test. The p values lower than 0.005 were rejected and not considered as significant for correlation analysis in Figure 4. The optimal number of groups as represented on Figure 4 were determined by a k-means analysis, which allow to determine the optimum number of clusters for given dataset (number of clusters that best explain variance).

Dairy stable and sheepfold emission rates were calculated only for compounds which mixing ratios were statistically different inside the building compared to outdoor mixing ratios. In the case of compounds only measured inside the buildings (not detected outdoor), we only considered compounds with mixing ratios statistically higher than the mixing ratio of the same compound in the zero air. Differences between ambient air and the outdoor/zero air were computed using a welsh t-test, as our samples were independents with different variances. If the obtained p-values were above 0.005, we considered that the samples were not significantly different.

4. Results

4.1. Time series

Figure 1 presents, for the entire experiment (stable, sheepfold and outdoor), time series of CO₂ and NH₃ mixing ratios (measured by the LSE Monitors analyzer), and two VOCs (trimethylamine and dimethylsulfide) previously reported in the literature as emitted by farm buildings (Feilberg et al., 2010; Ngwabie et al., 2008, 2007; Shaw et al., 2007; Sun et al., 2008). NH₄⁺ concentrations (in the particle phase) inside the farm and at SIRTA station (fixed measurement station 20 km south-east from the the farm at 48°42'32.0"N, 2°08'55.5"E and belonging to the European Research Infrastructure ACTRIS) are also presented in Figure 1. First, CO₂ and NH₃ mixing ratios were much higher in both buildings than outdoor. It also seems that both compounds roughly followed similar trends in both buildings and outside. CO₂ and NH₃ mixing ratios were quite similar during the two periods in the stable (orange area at the beginning and the end of the campaign in Figure 1). A similar observation can also be made

for the sheepfold. As a result, the PTR-Qi-TOF-MS and ACSM measurement periods can be compared, and we consider that conclusions deduced from one period can apply for all the campaign. In the sheepfold (delimited by the green fonts in Figure 1), clear and reproducible diurnal cycles of compounds concentrations can be observed and easily explained by the ventilation variability. Indeed, in the evening, the large lateral doors of the sheepfold are closed, leading to pollutants accumulation in the building during the night. As soon as the door are opened in the early morning, pollutants concentration dropped due to increased dilution with external air.

Regarding VOCs, trimethylamine (C_3H_9N) was also higher in the farm buildings than outside. Its temporal evolution seems to be highly correlated to NH_3 , rather than CO_2 . This may indicate a similar origin between NH_3 and trimethylamine. Such correlations between compounds will be further investigated later in the manuscript. Two VOCs that were identified as potential tracers for the dairy stable and the sheepfold are also represented on Figure 1. Acetaldehyde was found at high mixing ratios inside the stable, regarding the sheepfold and outdoor. As a result, acetaldehyde may be used as a tracer of the dairy stable. Dimethylsulfide (DMS, C_2H_6S) mixing ratios in the dairy stable were similar to the outside. Thus, it seems that the sheepfold is the main source of DMS in the farm, and that the dairy stable does not emit DMS. The absence of DMS emissions from the dairy stable differs from previous studies about dairy farm emissions, where DMS was often reported (Filipy et al., 2006; Ngwabie et al., 2007). NH_4^+ concentration in PM_{10} (particles with an aerodynamic diameter lower than $1 \mu m$) are available during the second part of the campaign. While NH_3 was more concentrated inside the building, NH_4^+ was surprisingly around the same levels in both farm buildings as outside. We also compared NH_4^+ concentrations measured at the farm to measurements performed at the SIRTA station. Concentrations were in the same range, and followed exactly the same temporal trend. The same reasoning applied for the other components of the aerosol composition (see Figure S2). Only 3 peaks of organic matter were higher at the farm than at the SIRTA station, that could be attributed to a tractor passing close to the mobile laboratory. Thus, we can conclude that farm building emissions did not lead to significant modification to the chemical composition of fine aerosols. This will be further discussed later, in light of gaseous emissions, and residence time inside both buildings.

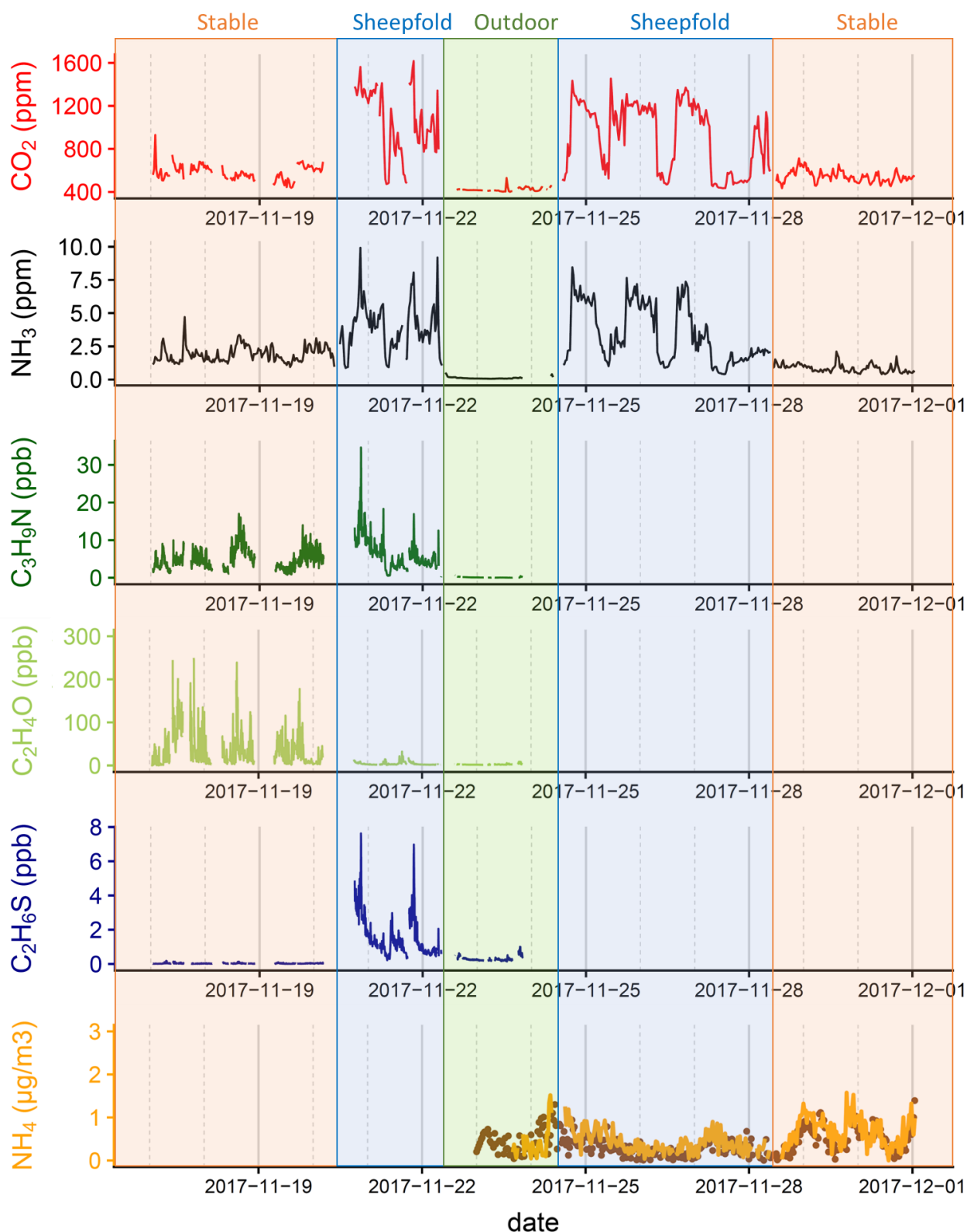


Figure 1: Time series of CO₂ (in ppm), ammonia (NH₃ in ppm), trimethylamine (C₃H₉N in ppb), acetaldehyde (C₂H₄O in ppb), dimethylsulfide (DMS, C₂H₆S in ppb), and ammonium (NH₄⁺, in μg m⁻³) for the experimental farm (light brown line) and the SIRT station (brown points) during the whole experiment. Orange fonts correspond the measurement period in the dairy stable, the blue fonts to the sheepfold and the green font to the outdoor. Each vertical bar (continue and dashed) represents a new day, at 00:00 local time.

4.2. VOCs identification

Combining the three techniques (GC-FID, TD-GC-MS and PTR-Qi-TOF-MS), more than 400 compounds were detected during the whole experiment. All the identified compounds are listed in the associated data file, and the number of identified compounds by each technique can be found in Table S1. Information about the parameters used for identification, such as PTR-Qi-TOF-MS mass resolution, or GC retention time can be found in the supplementary data file. Using the PTR-Qi-TOF-MS, 387 molecular formulas were successfully attributed. 62 molecular formulas among the 387 detected by the PTR-Qi-TOF-MS were also identified using off-line TD-GC-MS, and 8 using GC-FID (Table S1). Considering that these measurement techniques are independent, the number of common compounds underline the consistency of the identification process. Only 3 compounds were identified on all the 3 techniques: benzene, toluene and C₇H₁₄ isomers. The number of compounds identified by the 3 techniques is logically low because the range of VOCs detected by the 3 techniques were very different. The GC-FID detected C₂-C₈ hydrocarbons (alkane, alkene or alkyne), whereas the TD-GC-MS was not set up to measure small hydrocarbons (the first hydrocarbon detected by TD-GC-MS is benzene), and the PTR-Qi-TOF-MS cannot measure linear alkanes. The only alkanes detected using the PTR-Qi-TOF-MS are cyclic alkanes. For example, C₇H₁₄ and C₅H₁₀, that were cyclic alkanes based on the chromatographic analysis (see the associated data file). Nevertheless, the possibility that a corresponding alkene, isomer to the cyclic alkane, was detected by the PTR-Qi-TOF-MS and not detected by GC-FID cannot be fully excluded. A similar conclusion was drawn for TD-GC-MS and PTR-Qi-TOF-MS: only cyclic alkanes were measured by the PTR-Qi-TOF-MS (*e.g.* cyclopentane or cyclobutane). Thus, the PTR-Qi-TOF-MS did not detect any linear alkane, except methane. Methane indeed provides a significant signal at *m/z* 17.038 (corresponding to protonated methane, CH₄H⁺) despite its low proton affinity (118 kcal mol⁻¹) probably due to very high mixing ratios inside the farm buildings (Chupka and Berkowitz, 1971; Haque et al., 2017; Hempel et al., 2016; Schmithausen et al., 2018). But it cannot be considered as quantitative as methane proton affinity was lower than water proton affinity. We can hypothesize that methane is protonated in the lenses region of the PTR-Qi-TOF-M, as suggested for CO₂ by Herbig et al. (2009).

More compounds have been found in the dairy stable than in the sheepfold and outdoor (Table S1). About half of the compounds were oxygenated compounds, around a third were hydrocarbons, followed by nitrogen (N containing compounds) and sulfur containing

compounds (S containing compounds), at 13 % and 3 % respectively. Few halogenated compounds (1 % of the identified molecular formulas) were also detected.

Note that according to off-line analysis (GC-FID and/or TD-GC-MS), some of the molecular formulas identified with the PTR-Qi-TOF-MS correspond to several compounds (Table S1). For example, the protonated ion corresponding to m/z 113.1325 was identified as C_8H_{16} using PTR-Qi-TOF-MS. Behind this molecular formula, TD-GC-MS analysis identified 3 cyclic alkanes (Cyclohexane, ethyl- ; Cyclopentane, 1,2,3-trimethyl- ; Cyclohexane, 1,3-dimethyl-). Thus, there were certainly more compounds than the number of molecular formulas identified with the PTR-Qi-TOF-MS.

4.3. Investigation of VOCs in the dairy stable, the sheepfold and outdoor

Figure 2 shows the speciation of VOCs by functional groups in the stable, the sheepfold and outdoor. We first observe that the distributions of the chemical families (Figure 2) were roughly similar in the sheepfold and the dairy stable, and slightly different from outside. Thus, only a detailed VOC identification made it possible to clearly separate the chemical fingerprint of each building. This especially able by combining of techniques as performed in this study. Such identification may help to identify tracers for each building.

In the stable, 33% of the molecular formulas identified correspond to hydrocarbons. Most of them are alkenes; many aromatic hydrocarbons were detected, such as BTEX (benzene, toluene, ethylbenzene and xylenes) or some polycyclic aromatic hydrocarbons (PAHs), as naphthalene or acenaphthene derivatives for example. Typical hydrocarbons frequently attributed to biogenic origin (isoprene, monoterpenes and sesquiterpenes) are also reported in the dairy stable (Schiffman et al., 2001). It is interesting to note that many molecular formulas identified have the same carbon chain (from 3 to 20 carbon atoms), with the number of hydrogens that increase by 2 (for example, from $C_{12}H_{10}$, $C_{12}H_{12}$, $C_{12}H_{14}$, to $C_{12}H_{22}$). Another useful observation is that isopentane, 1-butene and pentane 2,2,4-trimethyl were detected only in the stable. These compounds may hence be specific tracers of the dairy stable emissions in the whole farm activities. About half of the compounds (49%) are oxygenated compounds (compounds with molecular formulas $C_xH_yO_z$). Most of them contain between one and three oxygen atoms, as shown in Figure 2. Only 6% of oxygenated compounds contain 4 or more oxygen atoms. Thus, the majority of the oxygenated compounds in the stable are not highly oxidized VOCs. As for hydrocarbons, oxygenated compounds with the same carbon chain and the same number of oxygen atoms were detected. The size of the carbon chains ranged from 3 to 16 carbon atoms.

Most of the hydrocarbons carbon chains have the same size as that of the oxygenated compounds (except for those with 17 carbon atoms). We can hypothesize that numerous oxygenated compounds may have been produced by the reaction of hydrocarbons with the atmospheric oxidants (as OH radical or ozone), in addition to the classical microbial degradation pathways. Many characteristic groups of oxygenated compounds were found in significant proportions inside the stable: alcohols or carboxylic acids, as well as ketones, ethers, aldehydes and even esters. We noticed that oxygenated VOCs with the highest masses were mostly ester compounds with a few long chain aldehydes (*e.g.* nonanal, decanal, pentadecanal). Nitrogen compounds represented 13 % of the identified molecular formulas. Most of them are small amines or amide compounds, such as dimethylamine (C₂H₇N), formamide (CH₃NO), triazine (C₃H₃N₃) or C₄H₅N. Triazine measurement is interesting as it was only measured inside the stable. We observed small-sulfured compounds, also known to be strongly odorant such as methanethiol (CH₄S), dimethyl sulfide (C₂H₆S) and dimethylsulfoxide (C₂H₆OS) (Feilberg et al., 2010; Schiffman et al., 2001). TD-GC-MS analysis confirmed the presence of benzothiazole (C₇H₅NS) in the emissions from the stable, and allowed to identify C₅H₇NS as thiazole, 2,4-dimethyl-. Two chlorinated compounds were also measured: chloramide and dichloromethane. Dichloromethane was previously reported in emissions from pig and cattle buildings (Ciganek and Neca, 2008; Schiffman et al., 2001). But, to the best of our knowledge, chloramide is reported here for the first time in dairy stable emissions.

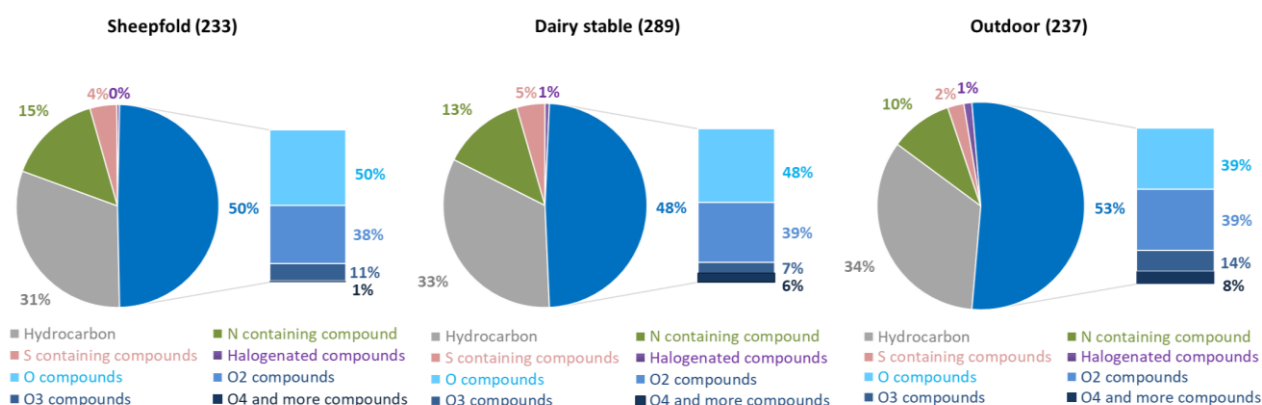


Figure 2: Percentage of functional group among the gaseous molecular formulas identified inside the sheepfold, the stable, and outside. The oxygenated compounds were detailed by number of oxygen atoms in the right part of each graph. The total number of identified molecular formulas is given between brackets.

In the sheepfold, hydrocarbons constitute 31 % of the 235 identified molecular formulas, while they represent around 33 % in the stable. Most of the hydrocarbons identified are cyclic alkanes, alkenes, and frequently aromatic compounds such as benzene and naphthalene derivatives (Table S1). The presence of several aromatic compounds was also observed and could have important implications for atmospheric chemistry, due to their reactivity and their ability to form secondary organic aerosols (Atkinson and Arey, 2007; Tomaz et al., 2017). We also noticed that isoprene was emitted inside the sheepfold, and no specific monoterpene was identified using TD-GC-MS, as in the stable. Octane, a C_8H_{18} compound, was only identified in the sheepfold, whereas the same molecular formula corresponded to pentane 2,2,4-trimethyl- in the stable. Oxygenated compounds represent 50 % of the identified molecular formulas, practically the same proportion as in the stable (Figure 2). Oxygenated compounds contain less O atoms than in the stable, as less molecular formulas contain more than three oxygen atoms (1 % in the sheepfold compared to 6 % in the stable). Our identification highlights that oxygenated VOCs are mostly carboxylic acids, ketones, or alcohols, and a few aldehydes. As in the stable, few long-chain aldehydes were identified in the sheepfold, but some of these oxygenated compounds, such as 6-methyl-1-octanol ($C_9H_{20}O$) are not reported in the sheepfold. That means that the sheepfold and stable fingerprints of oxygenated compounds are different. Exactly as in the stable, we observed that for oxygenated compounds and hydrocarbons, many molecular formulas identified have the same carbon chain. Again, it suggests that oxygenated compounds originated at least partly from reaction of hydrocarbons with the oxidants. In the sheepfold, the proportion of nitrogen compounds was slightly higher than in the stable (15 % against 13 %). Odorant compounds such trimethylamine or pyridine derivative were notably observed. Pyridine (C_5H_5N), methylpiperidine ($C_6H_{13}N$), dimethylpyridine (C_7H_9N), and benzenepropanenitrile (C_9H_9N) were specific to the sheepfold (*i.e.* not detected elsewhere), and could hence be used as sheepfold emission tracer. Seven S containing compounds were measured inside the sheepfold. Among them, methanethiol (CH_4S), dimethylsulfide (C_2H_6S), dimethylsulfoxide (C_2H_6Os) and dimethylsulfone ($C_2H_6O_2S$) were reported to be strongly odorant compounds (Hansen et al., 2016; Schiffman et al., 2001). The two other sulfur compounds were thiazole compounds. We observed one halogenated compound, dichlorobenzene ($C_6H_4Cl_2$), which was not reported in the stable nor outdoor.

237 molecular formulas were identified during the outdoor experiment. This number is very close to that of sheepfold, and lower than in the stable. This is logical considering that the location of the mobile van outside was close the sheepfold (Figure S1). Hydrocarbons

represented 34 % of the identified molecular formulas, which is a little higher than in the buildings (Figure 1). Alkenes, alkynes, cyclic alkanes were identified, and some aromatic compounds. As in the buildings, we noticed that many hydrocarbons had the same carbon chain, ranging from C₂ to C₂₂. The proportion of oxygenated compounds was slightly higher outdoor than in both buildings (53% outdoor, and 49% inside both buildings). Another difference compared to the chemical fingerprint inside the buildings is the lower proportion of oxygenated compounds that contained 1 or 2 oxygen atoms (Figure 2). This means that oxygenated compounds were more oxidized outside than inside the two buildings. This was expected considering that measurement inside the buildings were closer to the VOC sources. N containing compounds represented only 10% of the identified molecular formulas (Figure 1), which is a lower fraction than inside the buildings. The same observation applied for S containing compounds, which only represented 2%. Acetamide (C₂H₅NO) was identified outside but was not observed in the buildings, suggesting that it may come from other sources such as the feeding storage or methanisor close to the measurement place (Figure S1). Three halogenated compounds were identified outdoor. Among them chloramide and dichloromethane were also found in the stable, but not in the sheepfold.

4.4. Most concentrated compounds inside the building and outside

Figure 3 presents the mean mixing ratios and percentiles (25th and 75th percentiles) of the 20 most concentrated compounds in the stable, in the sheepfold and outdoor. In the three locations, the most concentrated compounds were CO₂ and NH₃, both exceeding the ppm level. The mixing ratios of NH₃ measured inside the buildings were in the same range as previous studies (Hensen et al., 2009; Huang and Guo, 2018; Ngwabie et al., 2008, 2007; Ni et al., 2012). For NH₃, mean mixing ratios in the sheepfold and the stable were about 48 and 21 times higher than outside, respectively. In the sheepfold and the stable, CO₂ mean levels were about 2.5 times and 1.4 times higher than the outdoor mixing ratios, respectively. Thus, NH₃ enrichment inside both buildings was higher than CO₂ enrichment, as already observed in naturally ventilated buildings (Ngwabie et al., 2014, 2007). Both CO₂ and NH₃ levels were higher in the sheepfold than in the stable, in agreement with the study of Ngwabie et al. (2007).

The most concentrated VOCs were mainly small-oxygenated compounds. Methanol (CH₄O) was the most concentrated VOC in the investigated locations. Methanol mean mixing ratios were around 46 ppb, 25 ppb and 16 ppb in the stable, the sheepfold and outdoor, respectively. These mixing ratios were in the same order of magnitude as previous studies in various farm buildings (Blunden et al., 2005; Ngwabie et al., 2008; Ni et al., 2012). However, our results are

quite different from other studies, where ethanol was more concentrated than methanol (Ngwabie et al., 2008, 2007; Shaw et al., 2007; Yuan et al., 2017). Acetic acid ($C_2H_4O_2$) mean mixing ratios were found to be similar in the sheepfold, the stable and outdoor. It was the 2nd most concentrated VOC in the sheepfold and outdoor, and the third in the dairy stable. Actually, the 2nd most concentrated VOC in the stable was acetaldehyde (C_2H_4O), with mixing ratios close to that of methanol (41 ppb, see Figure 3). Acetaldehyde was only in eighth and seventh position in the sheepfold and outside, and mean mixing ratios were one order of magnitude lower than in the stable. This was the case for most of the VOCs that were more concentrated in the stable than in the sheepfold and outside.

Only few hydrocarbons (C_xH_y) were among the most concentrated compounds listed in Table 1. Toluene was one of the most concentrated compounds only in the stable (Figure 3). For butene, the mixing ratios were comparable inside and outside the farm buildings. This means that both buildings were not strong sources of butene.

Figure 3 shows that nitrogen oxides (NO_x) mixing ratios were higher in the buildings than outside, meaning that both buildings can be considered as a source of NO_x . Both NO and NO_2 were more concentrated inside the stable than outdoor. However, in the sheepfold, only NO_2 was higher than outside (NO mixing ratios were very close in the sheepfold and outside, see Figure 3).

Trimethylamine (C_3H_9N) was the most abundant N containing compound after NH_3 , in both buildings (Figure 3). Trimethylamine was one of the few compounds listed in Figure 3 more concentrated in the sheepfold than in the stable. For both buildings, mixing ratios were in agreement with previous studies in dairy or sheep farms (Ngwabie et al., 2008, 2007). We observed that there was more N and S containing compounds among the 20 most concentrated compounds in the sheepfold than in the stable and outdoor (Figure 3). H_2S was one of the most concentrated S containing compound inside the stable, but was not detected in the sheepfold or outdoor. H_2S may hence be used as a tracer of stable emissions within the whole farm (Figure 3 and Table S1). H_2S was already reported inside farm buildings, and is known to be co-emitted with NH_3 and amines (Blunden and Aneja, 2008; Feilberg et al., 2017). H_2S levels measured in our study are close to that measured in dairy cattle stables, but at least one order of magnitude below reported values in pig farms (Feilberg et al., 2017, 2010). In the sheepfold, the two S containing compounds among the most concentrated ones were DMS (dimethylsulfide, C_2H_6S) and dimethylsulfone ($C_2H_6O_2S$), which were in the same range as reported by previous studies (Ngwabie et al., 2008, 2007; Trabue et al., 2010). For the outdoor measurement there is only one S containing compound and no N containing compounds (except NH_3).

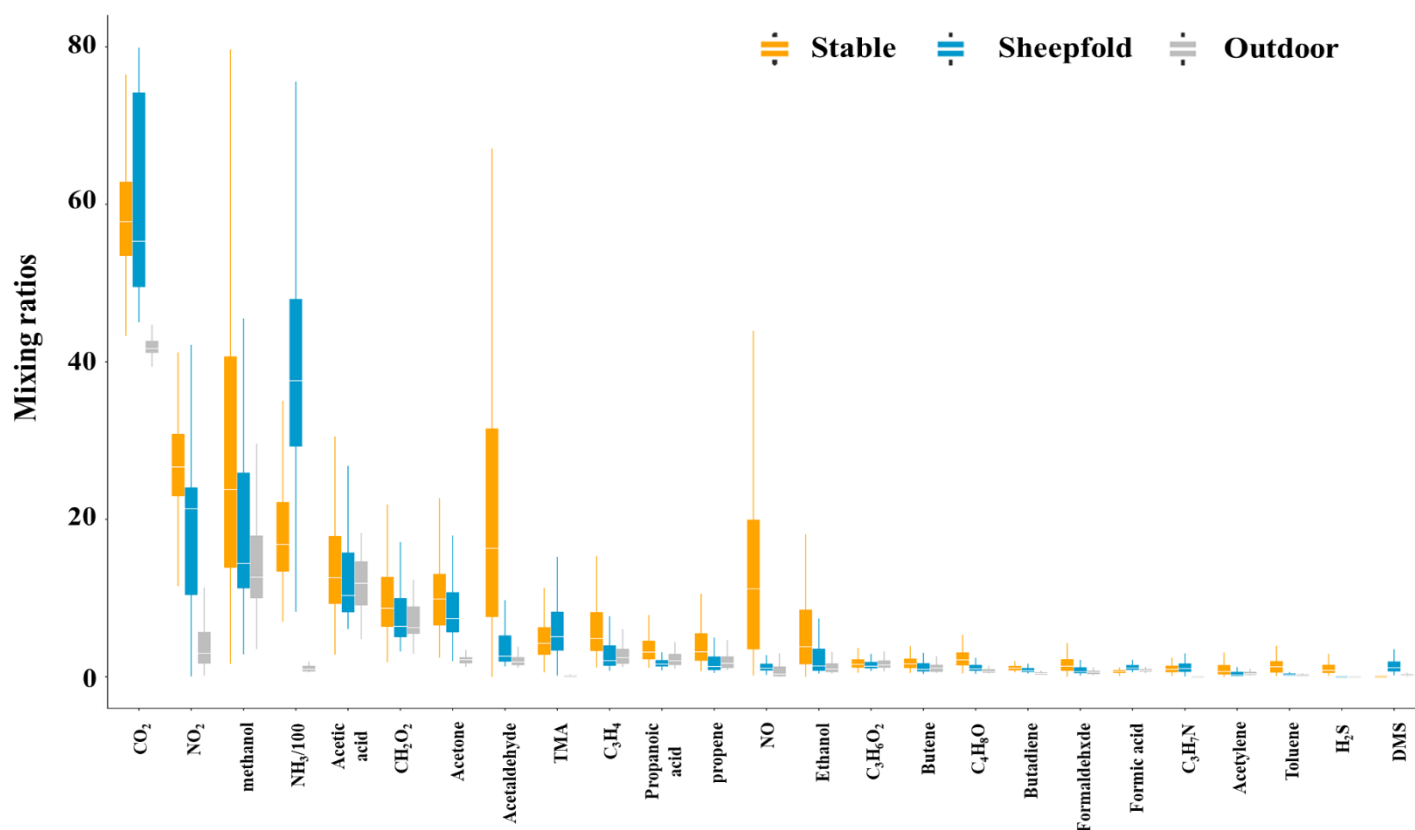


Figure 3: Median mixing ratios and percentiles (25th and 75th) of the 20 most concentrated compounds inside the dairy stable, the sheepfold, and outside. All the means and the percentiles are given in ppb, except for CO₂ in ppm. Note that NH₃ was divided by 100 for scaling reasons.

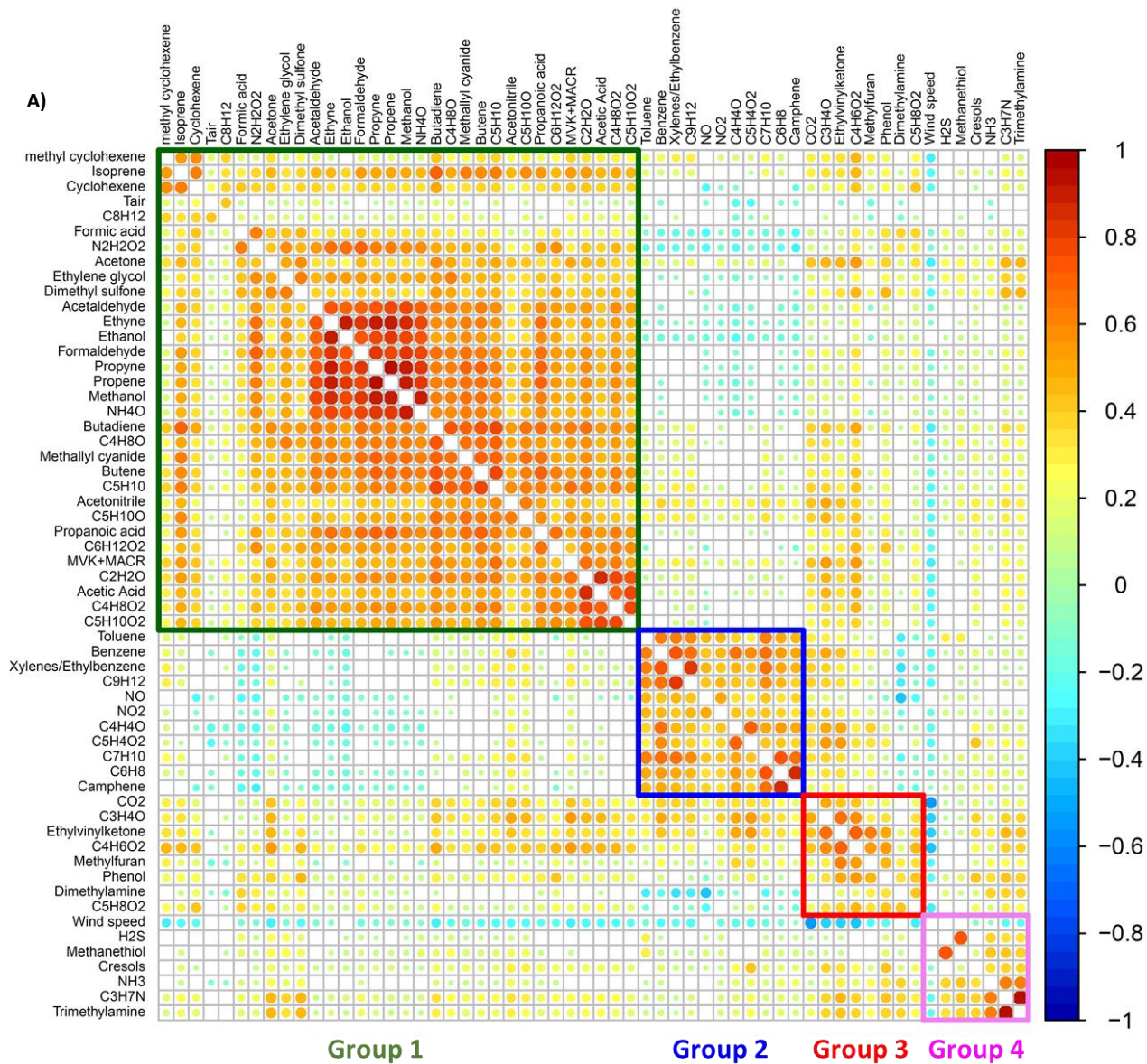
4.5. Correlation between different compounds

We performed a correlation analysis between VOCs having a mean mixing ratio above 0.1 ppb (to keep only the most significant VOCs). This criterion leads to subset 52 VOCs for the stable and 43 for the sheepfold. The correlation was based on the temporal evolution of each compound. The aim of such correlation analysis is to see which VOCs correlated to each other, and with other physico-chemical parameters such as NO_x, CO₂, NH₃, temperature and wind speed. Hence, a high temporal correlation between compounds may underline similar emission processes or species involved in a same chemical process. The aim is to determine whether all the VOCs originated from one or several sources. The obtained correlations in the sheepfold and the stable are represented on Figure 4.a, and 3.b.

The case of the stable is complex, and represented on Figure 4.a. One can first observe that almost all the VOCs were anti-correlated with wind speed. It means that VOCs were emitted by sources inside the stable, and did not come from external contamination. 4 groups can be

identified on the correlation heat-map, using the k-means analysis. A first group of 31 compounds (group 1 in Figure 4.a) is mainly composed of hydrocarbons and oxygenated compounds. There were also 4 N containing compounds, 1 S containing compound and air temperature. The air temperature was very weakly correlated with VOCs, although it was included in this first group. The 2nd group of 11 compounds only includes hydrocarbons and oxygenated compounds, in addition to NO_x (group 2 in the Figure 4.a). The third group contains 8 compounds: CO₂, dimethylamine and oxygenated compounds. Considering that CO₂ is mainly emitted by animals, we can suppose that the source of VOCs in this group is mainly related to dairy cattle breathing, known to emit several VOCs (Oertel et al., 2018; Spinhirne et al., 2004). 6 compounds and wind speed were composing the last group: 2 N-containing compounds, 2 S-containing compounds, cresols and NH₃. Most of these compounds have a strong unpleasant odor. The presence of NH₃ and small S-containing compounds suggests that the main source for this group is the dairy cattle excreta. This is strengthened by the presence of cresols in this group, well known to be emitted by urea and feces (Mackie et al., 1998; Shaw et al., 2007; Sun et al., 2008). Mackie et al. (1998) explained that cresols are produced during the microbial degradation of tyrosine and associated with the production of phenol. Logically, phenol and cresols were positively correlated, even if phenol is in another group (Figure 4.a). The source of VOCs in group 1 and group 2 are more difficult to identify. Markers of anthropogenic combustion sources, such as BTEX, trimethyl benzene, propyl benzene, and NO_x were in the group 2. As all the compounds were anti-correlated with wind speed, the anthropogenic source should be inside the stable. This suggests that farming activities implying a tractor (mulching for example) may be the source of the compounds in this group. But all the compounds in this group were also correlated to CO₂ (tracer of animal emissions) and C₁₀H₁₆, mostly known as biogenic monoterpenes. Especially, C₆H₈ was highly correlated to C₁₀H₁₆. The explanation is probably due to the fragmentation of the monoterpenes, known to highly contribute to the corresponding m/z 81.069 (Tani et al., 2003). To conclude, anthropogenic combustion sources may thus contribute at least partly to this group, in addition to animal activity (due to correlation with CO₂ group). Finally, the last group (group 1) seems to contain VOCs that were correlated to both the groups 2 (anthropogenic) and 3 (animal emissions). Some of these VOCs were also slightly anticorrelated to group 2. Identifying a source for this group of compounds is very difficult. We can thus conclude that the VOCs in this group can be emitted by sources identified in all the other groups (Figure 4.a). The VOCs inside this group are thus compounds that can be emitted both by the dairy cattle and their waste.

In the sheepfold, almost all the VOCs were positively correlated to each other, whatever the chemical group they belong to (hydrocarbons, N containing compounds or oxygenated compounds, Figure 4.b). On the contrary, none of them were correlated with the wind speed (p values < 0.005) and all the VOCs were only barely correlated to air temperature. One can note that NO was not correlated with any VOC, and NO₂ only slightly with few VOCs. BTEX and C₉H₁₂ (identified as benzene derivatives) were frequently attributed to anthropogenic sources, even though they were already reported inside farm buildings or sheep breath analysis (Ciganek and Neca, 2008; Fischer et al., 2015). In the case of the influence of a combustion source, BTEX would be strongly correlated with NO_x (NO+NO₂). But in the sheepfold, they were not correlated with NO_x. We thus can affirm that NO_x and BTEX may not arise from a combustion source, and we can therefore assume that the source of these compounds were inside the sheepfold (Figure 4.b). CO₂ can be used in the sheepfold as an animal emission tracer, whereas NH₃ could be mostly related to emissions from manure. Even if the k-mean analysis did not reveal any optimal number of groups, we can see that NH₃ was highly correlated to trimethylamine and C₃H₇N. Thus, these two amines are likely to be emitted by the animal excreta together with NH₃. It is difficult to go further in this analysis as CO₂ and NH₃ were correlated, meaning that animals and manure emissions cannot be well separated in the sheepfold. Finally, we can hypothesize that all the compounds were emitted by manure laying on the soil and the animals, and no other sources can be identified unlike to the dairy stable. The absence of groups traduces that the main driver of the concentration inside the sheepfold is probably the dynamic flow inside the building rather than the source strength.



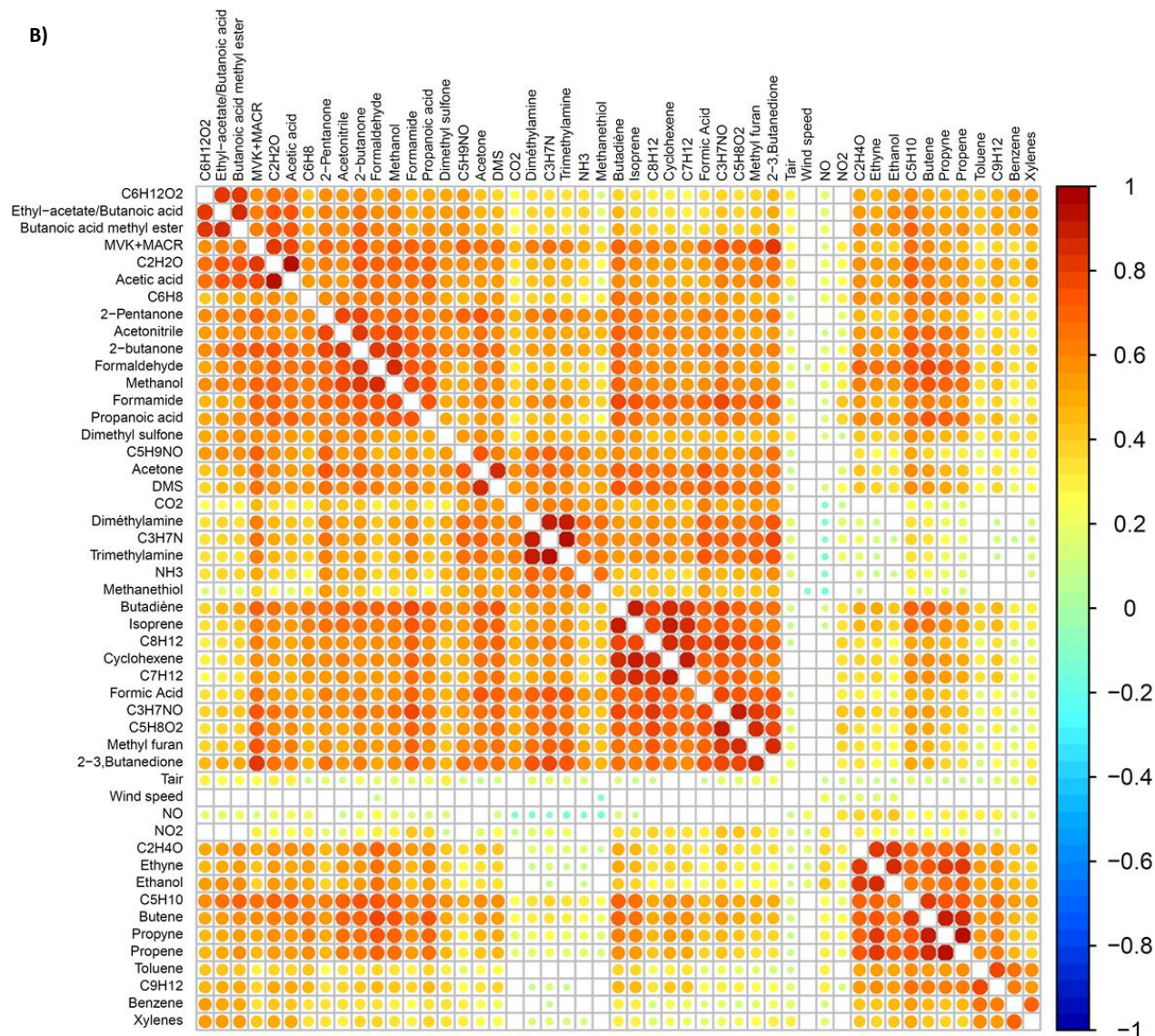


Figure 4: Correlations between compounds inside the stable (A) and the sheepfold (B). The correlation scales (on the left of each graph) range from -1 to 1 (unitless). Blue color means that two compounds are negatively correlated and red colors means that they are positively correlated. Empty boxes either correspond to the diagonal (autocorrelation), or to the cases where correlation between the compounds were not significant ($p < 0.005$). The order of the compounds is defined using a hierarchical clustering (based on the distance between the compounds). The number of groups were determined as the optimum clustering number from a k-means analysis. For the sheepfold, no optimum has been found, explaining why there is no group on Figure 4.b.

4.6. NH₃ Emission rates

Mean ventilation rates have been estimated to be around 440 000 m³ h⁻¹ and 230 000 m³ h⁻¹ in the dairy stable and the sheepfold, which is similar to previous studies in naturally ventilated buildings (Ngwabie et al., 2014; Schmithausen et al., 2018; Wang et al., 2016). The ventilation rate inside the sheepfold is therefore lower than in the stable, which was expected considering that the windows of the sheepfold are smaller than in the stable. The mean residence times inside both buildings, deduced from the mean ventilation rates, was estimated to be around 3 minutes in the stable, and around 6 minutes in the sheepfold. The residence time and the ventilation rate variability are nevertheless highly dependent on external wind speed and specific actions such as the opening of the buildings lateral doors. For example, in the sheepfold, the residence time can fall below the minute when the lateral doors of the building are open.

NH₃ emission rates for the stable and the sheepfold were estimated to be 9.73 (±7.12) kg N day⁻¹ and 8.72 (±5.54) kg N day⁻¹ (values between brackets are the standard deviation, representing the temporal variability of the emissions through the experiment) (Figure 5.a). NH₃ emissions from each building are roughly similar, although NH₃ mixing ratios were higher inside the sheepfold (Figure 3). This is due to the lower ventilation rate that led to lower dilution in the sheepfold than in the dairy stable. The NH₃ emission rates calculated here are in the same order of magnitude as the one previously reported for the same farm by Loubet et al. (2012), using inverse modelling on a crop field downwind the farm. They reported a value of 8.3 kg N day⁻¹ for the whole farm, slightly lower than the value calculated in the present study. This difference could be due to the seasonality effect, but also to an underestimation of the inversion model due to absence of deposition in the model of Loubet et al. (2012). It was shown above that animals and their excreta are the main source of VOCs inside both buildings. It thus makes sense to normalize emissions by the number of animals, or the amount of living units (LU, 1 LU = 500 kg) as usually performed in similar studies. The normalization by the number of animals shows that a dairy cow emitted more NH₃ than a sheep (Figure 5.b), which is due to the different weight of animals. We calculated that for the dairy stable and the sheepfold, emission rates by animals were 17.3 (±12.7) kg N year⁻¹ animal⁻¹ and 3.1 (±1.9) kg N year⁻¹ animal⁻¹ respectively (Figure 5.b). These emission factors are in the same order of magnitude than those frequently used in emission inventories (Aneja et al., 2012; Battye, 2003; Behera et al., 2013; Bouwman et al., 1997). For example, Bouwman et al. (1997) used an emission rate of 40-50 kg N year⁻¹ animal⁻¹ for dairy cattle and 1 kg N year⁻¹ animal⁻¹ for sheep, in a global scale estimation. A study about Indian agricultural emissions conducted by Aneja et al. (2012) referred to NH₃

emissions rates of 4.3 kg N year⁻¹ animal⁻¹ and 1.4 kg N year⁻¹ animal⁻¹ for dairy cattle and sheep, respectively. In Europe, Van der Hoek used emission rates of 28.5 kg N year⁻¹ animal⁻¹ for dairy cattle and 0.24 kg N year⁻¹ animal⁻¹ for sheep. As a conclusion, it appears that dairy cattle emission rates from our study are in good agreement with previous results whereas sheep emission rates are slightly higher. As the weight of a dairy cow and a sheep are very different, a normalization by the amount of animal weight is frequently performed. Emission rates were estimated to be 1.8 (±1.3) g N h⁻¹ LU⁻¹ and 2.2 (±1.4) g N h⁻¹ LU⁻¹ for the dairy stable and the sheepfold, respectively (Figure 5.a). These values are in agreement with previous studies conducted in naturally ventilated buildings (Koerkamp et al., 1998; Ngwabie et al., 2014, 2009; Wang et al., 2016). Our study shows that sheepfold emissions of NH₃ were higher than that of the dairy stable, for an equivalent amount of living units (Figure 5.a).

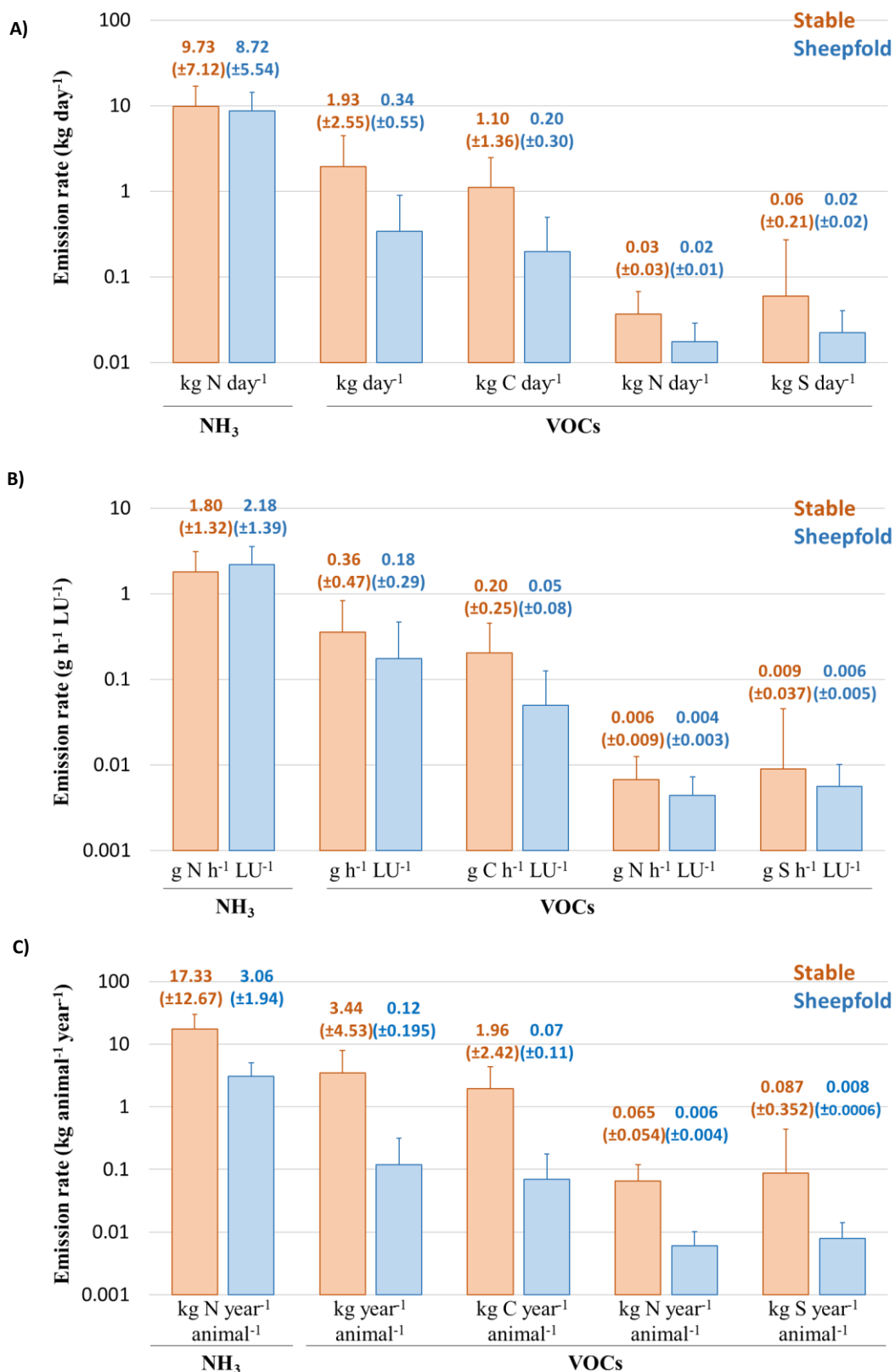


Figure 5: Mean emission rates of NH₃, the sum of VOCs, and VOCs in terms of carbon (C), nitrogen (N) and sulfur (S), for the dairy stable (orange bars) and the sheepfold (blue bars). Emission rates are given A) by building (in kg day⁻¹), B) by living unit in each building (in g h⁻¹ LU⁻¹) and C) by animals (in kg year⁻¹ animal⁻¹). Numbers above each bar plot give the corresponding mean emission rate value and its standard deviations between commas.

4.7. Most emitted VOCs

For VOCs, we calculated emission rates only for the compounds with mean mixing ratios higher inside the buildings than outside. This resulted in 230 VOCs emitted (80% of the 289 identified) for the dairy stable, and 177 for the sheepfold (76% of the 233 identified). The ratio of emitted compounds among the identified compounds is thus very close for both buildings. Table S2 listed the 10 most emitted VOCs with their corresponding mean emission rates, together with NH₃ and NO_x. Detailed emission rates for all VOCs can be found in the associated data file. Total VOC emission rates have been calculated to be 1.93 (± 2.55) kg day⁻¹ for the dairy stable and 0.34 (± 0.55) kg day⁻¹ for the sheepfold (Figure 5.b).

Conversely to NH₃, the dairy stable was found to emit about five times more VOCs than the sheepfold. VOCs represented 16.3 % of the NH₃ emissions in the stable, and 3.2 % in the sheepfold (as a mass ratio, considering ammonia emissions in kg NH₃, not only in kg N). We also evaluated that sheep emit much less VOCs than dairy cows: VOC emission rates were 0.12 (± 0.19) kg year⁻¹ sheep⁻¹ and 3.44 (± 4.53) kg year⁻¹ dairy⁻¹ (Figure 5). This is still true if the emissions rates are normalized by living units: VOCs emission rates were estimated to be 0.36 (± 0.47) g h⁻¹ LU⁻¹ and 0.18 (± 0.29) g h⁻¹ LU⁻¹ in the dairy stable and the sheepfold. The difference of emitted VOCs between dairy cows and sheep is therefore not only due to the animal weight.

In both farm buildings, the 10 most emitted VOCs contributed to more than 75% of the total VOC emissions (Figure S4). Methanol was measured as the most concentrated VOC in both buildings (Figure 3). However, it was not the most emitted VOC as it was only the 2nd most emitted VOC in the stable and the 7th most emitted VOC (Table S2). This was mainly due to *i*) the high mixing ratios of methanol outdoor and *ii*) the low molecular weight of methanol. In the dairy stable, methanol emissions were 0.59 (± 0.81) kg year⁻¹ animals⁻¹ (Table S2). Strong discrepancies can be found in the literature. For example, Shaw et al. (2007) used a chamber to measure methanol emission rates from lactating cows of 0.35 (± 0.15) kg year⁻¹ animals⁻¹, this was very close to our study. But Sun et al. (2008), in a study equivalent to that of Shaw et al. (2007), reported methanol emission rates of 61 kg year⁻¹ animals⁻¹. This point illustrates the variability of VOC emission rates between different studies. In the dairy stable, acetaldehyde was the most emitted VOC, with an emission rate of 1.08 (± 1.36) kg year⁻¹ animals⁻¹. This result differs from other studies where methanol or ethanol were frequently reported as the most emitted VOCs (Filipy et al., 2006; Ngwabie et al., 2008; Sun et al., 2008). After acetaldehyde

and methanol, acetone was the most emitted VOC, followed by trimethylamine and ethanol. As suggested above, H₂S was only emitted by the stable and could be proposed as a tracer of the dairy stable. This is also the case of NO and toluene, but they could not be proposed as tracers because several other sources (especially traffic roads) may emit these compounds in the vicinity of the farm. Emissions of compounds typical from farm buildings, such as cresols, indole and phenol, are not in the most emitted compounds. However it is essential to characterize their emissions due to their high odor activity value (Feilberg et al., 2010; Hansen et al., 2016). The detailed emission rates for such compounds is provided in the associated datafile.

The most emitted VOC in the sheepfold was C₂H₂O (ketene or ethenone, which can also be a fragment of oxygenated compounds such as ethanol or acetic acid) with an emission rate of 0.022 (±0.025) kg_C year⁻¹ animals⁻¹. Acetone was the 2nd most emitted VOC, just before trimethylamine. Methanol emission rates were 0.007 (±0.053) kg year⁻¹ animals⁻¹ in the sheepfold. These values are lower by an order of magnitude compared to the only previous study about sheep VOC emissions (Ngwabie et al., 2007). This could be due to *i*) the different methodologies to estimate the emission rates *ii*) their use of a conventional quadrupole PTR-MS not being able to separate isobar compounds (such as ¹⁷O¹⁶O⁺ and O₂.H⁺ ions) and *iii*) the difference between the two farms (agricultural practices, climate, animals, etc.). Ethanol was the most emitted VOC in the study of Ngwabie et al. (2007) in a sheepfold. But in our case, ethanol emissions were 3 order of magnitude below their study, with 0.012 (±0.025) kg_C year⁻¹ animals⁻¹ in the sheepfold. We also highlighted that the sheepfold emitted NO₂ but no NO. NO₂ emission rate was higher but close to VOC emission rates, with a mean emission rate of 0.17 (±0.33 kg day⁻¹). There are also two S-containing compounds in the 10 most emitted VOCs by the sheepfold, DMS and dimethylsulfone (Table S2). These compounds are of interest as they were not emitted by the stable. C₉H₁₂ and C₃H₇N are also only emitted by the sheepfold. These 4 VOCs could be assessed as tracers of sheepfold emissions.

These results showed that N containing compounds were a significant part of emitted VOCs, especially in the sheepfold, and quantified their emissions. NH₃ and amines (TMA-trimethylamine, DMA-dimethylamine, indole and others) could be important species regarding atmospheric chemistry, as they are able to favor new particle formation and secondary organic aerosol formation (Duporté et al., 2016; Lehtipalo et al., 2018; Yao et al., 2018; Yu et al., 2012). Especially, Yu et al. (2012) demonstrated that amines and NH₃ catalyze the formation rate of

stable clusters from sulfuric acid and water mixtures. However, aerosol measurements revealed that the fine aerosols chemical composition inside farm buildings was not different from ambient measurements performed 20 km from the farm. Thus, VOC emissions did not significantly affect the fine aerosol chemical composition close to the source (*i.e.* inside the building or outside close to them). This could be due to the very short residence time inside the buildings (in the order of minutes), which is not long enough to let the Secondary Organic Aerosols (SOA) formation affect the fine particle composition (Hallquist et al., 2009). This could also be the results of low oxidant levels inside the buildings, that do not allow strong semi-volatile production.

4.8. VOC emission rates in terms of C, N and S

Emission rates were also calculated for each VOC in terms of C, N, and S in both buildings (Figure 5). The stable emitted about five times more C through VOCs than the sheepfold; emission rates for the sum of VOCs in terms of C were $1.10 (\pm 1.36) \text{ kg day}^{-1}$ in the stable and $0.20 (\pm 0.30) \text{ kg day}^{-1}$ in the sheepfold (Figure 5.a). This is even more contrasted when emission rates were calculated by animals (Figure 3.b), with values of $1.96 (\pm 2.42) \text{ kg}_C \text{ year}^{-1} \text{ animals}^{-1}$ for the stable and $0.07 (\pm 0.11) \text{ kg}_C \text{ year}^{-1} \text{ animals}^{-1}$ for the sheepfold. The emission factors for the N contained in VOCs were $0.03 (\pm 0.03) \text{ kg day}^{-1}$ and $0.02 (\pm 0.1) \text{ kg day}^{-1}$ for the stable and the sheepfold, respectively (Figure 5.a). Contrary to what was found for NH_3 , the emission factor of N emitted through VOCs was higher in the stable than in sheepfold, even when the emission rates are expressed as function of living units or animals (Figure 5.b and 5.c). These emission factors are also very low compared to NH_3 emission factors. N emitted through VOCs only represents 0.2% and 0.3 % of the NH_3 emission factor (in amount of emitted N).

The S emission factor for the sum of VOCs was $0.06 (\pm 0.027) \text{ kg S day}^{-1}$ and $0.02 (\pm 0.002) \text{ kg S day}^{-1}$ in the dairy stable and the sheepfold. As for C and N, the amount of S emitted was higher in the stable than in the sheepfold. DMS was the most emitted S containing compound in the sheepfold, accounting for 40 % of the sheepfold S emission. Surprisingly, the dairy stable did not emit DMS (*i.e.* mixing ratios outside were higher than inside the building), while some studies reported strong emissions from dairy buildings (Filipy et al., 2006; Ngwabwe et al., 2008; Shaw et al., 2007). 67 % of S emitted in the dairy stable could be attributed to H_2S (no H_2S emissions were recorded for the sheepfold). Feilberg et al. (2017) found a ratio between H_2S and NH_3 of 0.06, whereas it was 0.004 in our study. Thus, it seems that the dairy stable was not a strong S emitter in contrast to the literature.

Figure 6 represents the chemical fingerprint of VOC emissions. The fingerprint of VOC emissions was mostly composed of C, for more than 80 % in each building. This is logical considering that most of the detected VOCs were oxygenated VOCs and hydrocarbons that contain a large number of C atoms, and that N or S containing VOCs mostly have a few atoms (Table S1). N and S were found in a greater proportion in the sheepfold, but the emission factors were greater in the stable. The chemical compounds and the magnitude of the emissions are thus different in each building. Finally, C/N/S composition of VOC emissions allow identifying differences between the buildings, contrary to what was found above for mixing ratios (Figures 2 and 6).

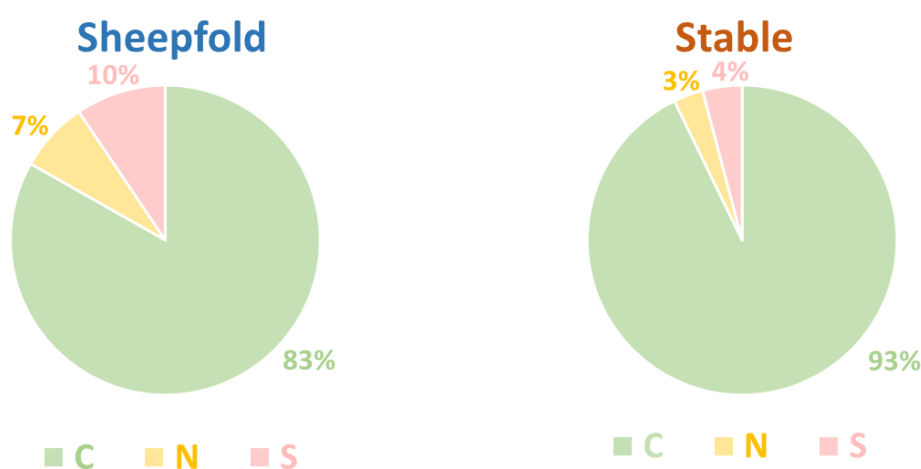


Figure 6: Speciation of VOC emissions by amount of C, N, and S in the sheepfold and the dairy stable.

4.9. Estimation of VOC emissions from livestock at national scale

The emission factors for most VOCs were estimated for the first time in a sheepfold and a dairy stable, more specially in France. To scale up VOC emissions, previous studies used NH₃ emission inventories at national scale. A ratio between VOCs and NH₃ emission rates can then be used to estimate VOC emissions at large scales (Hobbs et al., 2004). Following the French Interprofessional Technical Centre for Studies on Air Pollution (CITEPA), NH₃ emissions due to livestock were about 246.6 kt in 2016. We estimated from our results that the amount of VOCs emitted was 10% of the amount of NH₃ due to livestock (mean of the sheepfold and the dairy stable). Applying this ratio would lead to a VOC emission of 24.6 kt year⁻¹ for the year 2016 in France. CITEPA estimated that VOC emissions from livestock were one order of magnitude larger than the present one (201.6 kt year⁻¹, CITEPA, February 2019). For comparison, traffic road emissions of VOCs for the same period were estimated to be 66.2 kt

year⁻¹. Livestock VOC emissions are therefore significant regarding other anthropogenic sources, even if it is lower than expected. This estimation of VOC emissions from livestock at national scale should be interpreted very carefully, as this study covered only one farm during one short field campaign. For example, it was shown for few VOCs that emission factors may differ from one order of magnitude among the season (Filipy et al., 2006). Nevertheless, the present study highlights the meaning of livestock management as a significant source of VOCs.

5. Conclusion

This study revealed that both sheep and dairy cattle farming emit a large spectrum of VOCs. The results highlight that combining online mass spectrometric and off-line chromatographic techniques is essential to better characterize VOC emissions, especially in a VOCs enriched environment such as farm buildings. In both buildings VOCs were mostly oxygenated compounds and hydrocarbons. N containing compounds and S containing compounds were found in lower proportions but could be key compounds for odor questions as well as atmospheric chemistry. We evidenced that the difference in the fingerprint of gas phase compounds emitted by the stable and the sheepfold was tight if we only pay attention to chemical families. Tracers for each buildings of the experimental farm can now be proposed. For the stable, Triazine, H₂S, 1-butene, isopentane, pentane and acetaldehyde have been identified as potential tracers. For the sheepfold most of tracers are nitrogen containing compounds. Among them, methylpiperidine, pyridine, dimethylpyridine and benzenepropanenitrile were highlighted. DMS was also observed to be mostly emitted by the sheepfold. Our study also showed that most of the VOCs were more concentrated inside than outside the buildings, leading to a higher exposure levels for animals and farmers inside the buildings.

Our results suggest that animals and litter inside the sheepfold were the main source of VOCs based on the correlation analysis. In the dairy stable the correlation analysis highlights 3 different sources. The litter on the soil seems to be a strong emitter of N and S containing compounds, through the biodegradation of animal excreta. The farming activities seem to be important contributors of hydrocarbons. The third source identified is represented by the animals. A future study focused on VOCs emitted by dairy and sheep breath would support our findings, and help to separate animal and excreta emissions.

Emission rates have shown that a dairy cow emitted more NH₃, NO_x, and VOCs than a sheep. But at the farm level, the sheepfold was found to emit roughly as much NH₃ as the stable. The loss of N through VOCs was found to be only minor compared to NH₃. As a conclusion, it is

thus maybe not necessary to take into account the loss of N through VOCs for agronomical nitrogen budget studies at farm levels. Despite emissions of NH₃ and many VOCs, the aerosol chemical composition was not affected by farm emissions. Secondary aerosol formation may probably be most significant in the plume of the farm, rather than inside the buildings. This assumption needs to be investigated in future studies.

Based on the new emission rates provided in this study, we estimated that livestock VOC emissions could be overestimated by one order of magnitude. However, more studies in different periods and farms are thus required to reduce uncertainties about emissions, and understand their driving factors.

Acknowledgments: Yves Python and Dominique Tristant are thanked for providing the access to experimental farm. The authors acknowledge ANAEE-France for the PTR-Qi-TOF-MS funding, and the French Environment and Energy Management Agency ADEME for the funding through the AgriMultiPol program (17-03 C0012).

Competing interests: The authors declare no competing of interest.

Data and materials availability: More details about the VOCs identified with PTR-Qi-TOF-MS, GC-FID and TD-GC-MS can be found on the online associated data file. The emission factors for individual VOCs from each building are also given in the associated data file.

List of Figures

Figure 1.1: Idealized diurnal evolution of the atmospheric boundary layer over land in fair weather (after Stull, 1988).	7
Figure 1.2: Schematic summarizing anthropogenic and biogenic sources of volatile organic compounds (VOCs) (de Gouw, 2006).	7
Figure 1.3: Comparison of the number of BVOCs emissions diversity studies (1957- 2011) for major biome types and compound categories (Guenther, 2013).	13
Figure 1.4: Generalized relative emission of isoprene and monoterpenes in relation to light (PAR) under constant temperature, and temperature under constant light as described by potential algorithms (Kesselmeier and Staudt, 1999).	15
Figure 1.5: Factors controlling VOCs emissions (adopted from Penuelas & Llusia, 2001).	17
Figure 1.6: Scheme of VOCs oxidation with the hydroxyl radical OH.	21
Figure 1.7: Carbon mass balance of SOA (assuming aerosol is 60% carbon) and gas-phase oxidation products resulting from the photooxidation of isoprene, eight monoterpenes, three oxygenated monoterpenes, and four sesquiterpenes, conducted individually at the Caltech Indoor Chamber Facility (Lee et al., 2006). The “other 1” category represents the calibrated products nopinone and MACR + MVK from β -pinene and isoprene, respectively, and the uncalibrated products limononaldehyde, caronaldehyde, pinonaldehyde, β -terpinaldehyde, and α -terpinaldehyde, from limonene, 3-carene, α -pinene, β -terpinene, and α -terpinene, respectively. The “other 2” category represents limonaketone from limonene and 3-methyl furan from isoprene. Aerosol molar yields ($\text{mg aerosol m}^{-3}/\text{mg terpene m}^{-3}$) were calculated assuming an aerosol density of 1.25 g cm^{-3}	25
Figure 1.8: Total OH reactivity results from published experiments conducted worldwide at forested sites. Bars refer to the ranges observed between the minimum (often corresponding to the instrumental LOD) and the maximum values published (Adopted from Zannoni et al., 2016).	37
Figure 2.1: Simplified representation of a proton-transfer reaction mass spectrometer utilizing a quadrupole mass filter: HC = hollow cathode discharge source and SD = source drift region (Blake et al. 2009).	46
Figure 2.2: Set-up of the fastGC add-on, including the capillary column, the sample loop, the 10-port valve and the PTR-MS drift-tube.	52
Figure 2.3: FastGC/ PTR-MS chromatograms after the injection of an α -pinene sample. m/z 32 and m/z 137 refer to O_2 and α -pinene, respectively.	53
Figure 2.4: Comparison between two chromatograms of the same monoterpenes gas mixture, injected in the same conditions but with two different carrier gas flow rates: the upper graph (a) corresponds to the experiment with a flow rate of 5 sccm and the lower graph (b), to the experiment with a carrier gas flow rate of 15 sccm.	55
Figure 2.5: Chromatograms of a) in-house made mixture of monoterpenes under optimized Trapp and carrier gas flow rate, using N_2 as carrier gas and b) an α -pinene standard injected under the same optimized conditions with He as carrier gas.	57
Figure 2.6: Pyrrole concentration monitored with the PTR-MS during a typical OH reactivity measurement with the CRM. C0, C1, C2 and C3 are the mixing ratios at the different stages of the experiment (Zannoni et al., 2015).	59
Figure 2.7: Schematic of the CRM instrument built at LSCE. Flow rates of the injected and the extracted gases are shown.	61
Figure 2.8: A method validation and calibration using different standards showing a good reproducibility, with error bars representing the total calculated uncertainty (Sinha et al., 2008).	63
Figure 2.9: Changes in C2 (ppbv) depending on changes in $m/z37/m/z19$ and RH changes during four different humidity tests performed in the frame of the Dunkirk field campaign by Michoud et al. (2015).	65

Figure 2.10 : Changes in C3 as function of NO in the reactor. Three experiments conducted at different pyrrole-to-OH ratios (1.6, 2.2 and 3.9) are presented. The right axis corresponds to the absolute change in OH reactivity for the experiment conducted at pyrrole-to-OH 2.2 (Michoud et al., 2015).	67
Figure 2.11 : Correction factor of reactivity for the kinetics regime reported vs. pyrrole-to-OH ratio in the reactors of two CRM (LSCE and Mines de Douai) instruments during an intercomparison. Correction for CRM- LSCE is represented in red while correction for CRM-MD is represented in blue. Full circles refer to the experiments conducted with propane while hollow circles refer to the experiments with ethane as gas standard. Linear fits include coefficient values $\pm 1\sigma$ (Zannoni et al., 2015).....	68
Figure 2.12: Comparison of the trends of the simulated and measured correction factors with the pyrrole-to-OH ratio. The measured correction factors are presented in blues circles. The simulated correction factors stem from simulations conducted using MCM and constrained with ethane under dry conditions (green open diamonds) and wet conditions (green filled diamonds), or constrained with isoprene under dry conditions (red open squares). The colored area corresponds to the range of pyrrole-to- OH ratios observed during the Dunkirk field campaign (1.6–2.2) (Michoud et al., 2015).....	69
Figure 2.13: Photo of the online page allowing an automatic control of the gas flows and a continuous monitoring of the overflows, the pressure and the relative humidity in the exhaust flow and the temperatures at different location inside the box.....	74
Figure 2.14: LSCE-CRM new set-up. On the left the first version with a stainless-steel 4-way valve for switching between dry and wet N ₂ , with no heating of the line between the water reservoir and the reactor. On the right, the second version with a Teflon 4-way valve and a heated/covered line conducting nitrogen to the reactor, with several temperature sensors.	75
Figure 2.15 : Example of a calibration performed in dry and humid conditions, introducing different levels of pyrrole.....	75
Figure 2.16: Linear least square fit of $\Delta C2$ (ppb) vs. $\Delta(m37/m19)$ for the tests conducted during field experiments to assess the correction for humidity differences between C2 and C3. The left graph corresponds to the COV ³ ER field campaign with green dots and red dots resulting from tests performed with ambient air and outgoing chamber air, respectively. The right graph corresponds to the LANDEX field campaign.	76
Figure 2.17 : Changes in C3 ($\Delta C3 = C3_{\text{expected}} - C3_{\text{measured}}$) as function of NO concentration introduced inside the reactor during the COV ³ ER field work.....	77
Figure 2.18: Comparison of measured OH reactivity with the calculated one from the addition of gas standards at various pyrrole-to-OH ratios. Graph a) corresponds to propane tests and graph b) to isoprene tests. Graphs c and d, show isoprene and propane tests at pyrrole-to-OH ratios of 1.8 and 2.3-2.4, respectively.....	78
Figure 2.19: Variation of correction factors derived from laboratory experiments, introducing isoprene and α -pinene standards. Under different pyrrole-to-OH ratios. The left graph corresponds to LSCE-CRM correction factors and the right graph corresponds to MPIC-CRM correction factors.	79
Figure 3.1: Deployment of instruments at the measurement site. Left side (a) corresponds to the horizontal deployment, the right side (b) represents the different sampling levels with respect to the average trees' height.....	105
Figure 3.2: Time series of total OH reactivity measured by UL-FAGE (dark blue) and LSCE-CRM (light blue) instruments from the 18 th to 19 th of July 2017, at the same location inside canopy.	109
Figure 3.3: Measured reactivity by LSCE- CRM instrument as function of the measured reactivity by UL- FAGE when both instruments were measuring at the same location within the canopy (data resampled with a time resolution of 1 min). Errors bars represent the overall systematic uncertainty (1σ) that is around 15 % and 35 % for LP- LIF and the CRM, respectively.....	110
Figure 3.4: (a) Time series of total OH reactivity measured by UL-FAGE and LSCE-CRM instruments from the 13 th to 18 th of July 2017 (upper graph). Dark blue symbols represent the measured reactivity by UL-FAGE, green and yellow symbols represent the measured reactivity by LSCE-CRM inside and above the canopy, respectively. The lower graph (b) shows the sum of monoterpenes (MTs) and isoprene	

measured with the PTR-MS, in the field for the same period. Dark blue and light blue dots correspond to isoprene concentrations at 6 and 12 m height, respectively. Orange and yellow dots represent monoterpenes concentrations at 6 and 12 m height, respectively. 111

Figure 3.5: Variability of measured OH reactivity by LSCE-CRM and UL- FAGE, inside and above the canopy with (a) global radiation (black), (b) temperature (red), friction velocity (green) and with c) monoterpenes and isoprene concentrations. Yellow stripes indicate stable night-time atmospheric conditions (S nights with mean $u^* \leq 0.2 \text{ m s}^{-1}$) and blue stripes indicate unstable night-time conditions (U nights with mean $u^* \geq 0.4 \text{ m s}^{-1}$). Class SU includes nights with stable and unstable atmospheric conditions (blue + yellow stripes). Wn and Wd stand for warm nights and warm days respectively. Cn and Cd stand for cooler nights and cooler days respectively. Red dashes and black dashes indicate the temperature thresholds to distinguish warm and cool days and nights, respectively. Green dashes indicate the friction velocity threshold to distinguish stable and unstable nights. 113

Figure 3.6: Variability of measured ROH (LSCE-CRM) and calculated ROH (PTR-MS) at 6 and 12 m height. 117

Figure 3.7: The components of calculated OH reactivity within and above the canopy during day-time and night-time. The compounds measured by the PTR-MS (Table 3.3) were used to calculate their relative contributions. 118

Figure 3.8: Missing OH reactivity inside and above the canopy together with (a) temperature, (b) friction velocity (red), ozone mixing ratios inside (yellow) and above (blue) the canopy, (c) relative humidity (clear blue), MACR+ MVK+ ISOPOOH (dark blue) and acetic acid (green) inside the canopy, (d) Nopinone (yellow) and pinonaldehyde (purple) inside the canopy and (e) sesquiterpenes inside (blue) and above (green) the canopy. 120

Figure 3.9: Day-time missing OH reactivity binned by ambient temperature for the 6 m height for temperatures ranging from 292 and 308 K. Error bars represent the standard deviation on missing OH reactivity calculated for each temperature bin. 123

Figure 3.10: Air masses backward trajectories for the 4th-5th and the 6th- 7th, July nights. Red lines represent air masses arriving around mid-night UTC (around 02:00 local time), to the site. The time difference between 2 points is 6 hours. 125

Figure 4.1: Satellite image of Grignon farm, the surrounding area and the chamber used for this study. 139

Figure 4.2: Schematic representation of the system used for the measurements in the incoming and the outgoing chamber air. $mROH_{\text{ambient}}$ and $mROH_{\text{chamber}}$ stand for measured OH reactivity in the incoming and the outgoing air, respectively. $cROH_{\text{ambient}}$ and $cROH_{\text{chamber}}$ represent the calculated OH reactivity in the incoming and the outgoing chamber air, respectively. $cROH_{\text{rapeseed}}$ is calculated using VOC_{rapeseed} , determined from $VOC_{\text{chamber}} - VOC_{\text{sambient}}$ (both measured with the PTRQi-ToFMS). 148

Figure 4.3 : Variability of a) $\Delta mROH = mROH_{\text{chamber}} - mROH_{\text{ambient}}$ and b) total $mROH_{\text{chamber}}$ (blue dots represent the original OH reactivity data and black dots represent the trend obtained after smoothing the original data) and total $mROH_{\text{ambient}}$ (red dots) from the 20th to the 23rd, April 2017 with temperature ($T^{\circ}\text{C}$ - yellow), c) photosynthetic active radiation (PAR $\mu\text{mol m}^{-2} \text{ s}^{-1}$ - purple) and relative humidity (RH%- blue), all three parameters measured inside the chamber. 153

Figure 4.4 : Averaged diurnal variation of a) the mixing ratio of each BVOC measured with the PTRQi-ToFMS (ppbv) and b) their contribution to OH reactivity (s^{-1}). 156

Figure 4.5: $mROH_{\text{chamber}}$ and $cROH_{\text{chamber}}$ from individual calculated ROH of VOCs (PTR-MS), VOCs (GC-FID), NO_x , CH_4 and CO summed up and the resulting missing ROH. 158

Figure 4.6 : Variability of missing OH reactivity as function of air temperature in the chamber. The regression curve equation is $ROH_{\text{missing}} = 0.23\exp(0.14(T))$ ($R^2 = 0.8$). 159

Figure 4.7: Summed calculated OH reactivity of the 9 additionally selected compounds. The mixing ratios used for the calculation correspond to the ones from the rapeseed branch (VOC_{rapeseed}) and the k_{OH} are the ones mentioned in Table 4.4. 161

Figure 4.8: a) Variability of relative missing OH reactivity ($ROH_{\text{missing}}/mROH_{\text{chamber}}$) with b) Isoprene (rapeseed), c) Acetic acid (rapeseed) and d) Benzene (orange) and Benzaldehyde (blue) in ambient air.

Green areas indicate missing OH reactivity mainly due to biogenic emissions and grey areas indicate missing OH mainly linked to anthropogenic emissions. 164

Figure 5.1: Photos of the branch (left) and stem chambers (right) used during the COV³ER- 2018 Puéchabon field experiment. 177

Figure 5.2: Schematic drawing of a PTR-QuadMS inlet system with a FastGC setup including a capillary column, a sample loop and a 10-port valve allowing the switching between real-time and FastGC measurements. 178

Figure 5.3: Comparison between two chromatograms of the same monoterpenes gas mixture, injected in the same conditions but with two different carrier gas flows: the upper graph corresponds to the experiment with a flow of 5 sccm and the lower graph, to the experiment with a carrier gas flow of 15 sccm. 181

Figure 5.4: FastGC/PTR-MS chromatogram of a calibration mixture (NPL) containing: α -pinene, β -pinene, myrcene, Δ -3-carene, limonene and o-cimene. This graph represents one of the daily replicates performed with the same standard. The drawn line represents m/z 81 (monoterpene fragment). 183

Figure 5.5: Schematic of the sampling system going from the dynamic chamber to the FastGC/PTR-MS. Po and Pi stand for the pumps drawing outlet and inlet air, respectively. P1 and P2 represent the flushing pumps connected to VICI valve 1 and 2, respectively. C_{In} and C_{Out} represent the incoming and the outgoing chamber air, respectively. 184

Figure 5.6: Diurnal variability of monoterpenes mixing ratios (C_{Out} – C_{In}) with the photosynthetic active radiation (PAR) for all four branch chambers. 186

Figure 5.7: FastGC chromatograms from the four studied *Quercus ilex* branch enclosures at the same hour of different days (around 12h45 UTC). 189

Figure 5.8: Variability of individual monoterpenes in the outgoing chambers air of the four studied branch chambers. 190

List of Tables

Table 1.1: Chemical formulas, molecular weights, boiling points and chemical structures of selected biogenic VOCs (Fuentes et al., 2002).	10
Table 1.2 : Annual global total averaged over the period of 1980–2010 for selected BVOC species (with standard deviation σ), their relative contribution to the global total of all BVOCs expressed as emission of carbon, maximal and minimal value within the modelled period. Note that the sum of monoterpenes already includes emissions of α -pinene and β -pinene (in italics). (Adopted from Sindelarova et al., 2014).....	12
Table 1.3: Calculated atmospheric lifetimes of biogenic volatile organic compounds (Atkinson and Arey, 2003).....	23
Table 2.1: Retention times of 5 monoterpenes resulting from operating the FastGC/PTR-MS system with a temperature program (TrampI) or under a constant temperature (constant voltage of 35 V).....	54
Table 2.2: Summary of all the temperature conditions (T °C) and carrier gas (N ₂) flow rates. tested.	56
Table 2.3: Summary of the CRM operational conditions during the COV3ER and LANDEX field campaigns.	82
Table 3.1: Performance of the two OH reactivity instruments deployed during the LANDEX campaign.	94
Table 3.2 : Summary of corrections applied to raw reactivity data for LSCE-CRM. Correction coefficients are obtained from experiments performed before, during and after the field campaign....	98
Table 3.3: Summary of supporting measurements performed inside and/or above the canopy.	104
Table 3.4: Summary of the measured OH reactivity and the missing OH reactivity inside and above the canopy, during the day and the night, taking into account only PTR-MS data or all the data available at each height for OH reactivity calculations. These averages are calculated for the periods when CRM, PTR-MS and others instruments data are available.....	122
Table 4.1: Instruments deployed in the campaign and used for data analysis.....	147
Table 4.2: List of selected compounds used for OH reactivity calculations with their respective k_{i-OH} at 298 K and pressure 1 atm.	150
Table 4.3: Summary of the mean contribution of all the measured species (same time step) in the incoming and the outgoing chamber air to $mROH_{chamber}$ and the resulting missing OH fraction.	157
Table 4.4: List of the 9 selected masses which presented a correlation of 80% and more with isoprene (m/z 69.070).....	161
Table 5.1: The selected temperature ramp after several laboratory tests with different temperature programs.	180
Table 5.2: Temperature ramp deployed for the measurement of monoterpenes during COV ³ ER- 2018 field experiment.....	182
Table 5.3: Mean retention time (\pm STD) and mean peak height (\pm STD) obtained for each of the monoterpenes present in the NPL calibration mixture.	182
Table 5.4: Summary of the operational conditions, meteorological parameters, mean and maximum mixing ratios and emission fluxes of monoterpenes, isoprene and OVOCs (methanol, acetone, acetaldehyde) for the four branch chambers.	188

References

- Abis, L., Loubet, B., Ciuraru, R., Lafouge, F., Dequiedt, S., Houot, S., Maron, P. A. and Bourgeteau-Sadet, S.: Profiles of volatile organic compound emissions from soils amended with organic waste products, *Sci. Total Environ.*, 636(March), 1333–1343, doi:10.1016/j.scitotenv.2018.04.232, 2018.
- ACTRIS, 2014: - ACTRIS, 2014. WP4- NA4: Trace gases networking: Volatile organic carbon and nitrogen oxides Deliverable D4.9: Final SOPs for VOCs measurements. ACTRIS., n.d.
- Agreste: Infos rapides, Agreste Infos rapides, (015), 2–5 [online] Available from: <http://www.agreste.agriculture.gouv.fr/IMG/pdf/conjinfoleg201311toma.pdf>, 2017.
- Akritidis, D., Pozzer, A., Zanis, P., Tyrlis, E., Škerlak, B., Sprenger, M. and Lelieveld, J.: On the role of tropopause folds in summertime tropospheric ozone over the eastern Mediterranean and the Middle East, *Atmos. Chem. Phys.*, 16(21), 14025–14039, doi:10.5194/acp-16-14025-2016, 2016.
- Amedro, D., Miyazaki, K., Parker, A., Schoemaeker, C. and Fittschen, C.: Atmospheric and kinetic studies of OH and HO₂ by the FAGE technique, *Lille 1.*, 2012.
- Ashmore, M. R.: Assessing the future global impacts of ozone on vegetation, *Plant, Cell Environ.*, 28(8), 949–964, doi:10.1111/j.1365-3040.2005.01341.x, 2005.
- Asmi, E., Kivekäs, N., Kerminen, V. M., Komppula, M., Hyvärinen, A. P., Hatakka, J., Viisanen, Y. and Lihavainen, H.: Secondary new particle formation in Northern Finland Pallas site between the years 2000 and 2010, *Atmos. Chem. Phys.*, 11(24), 12959–12972, doi:10.5194/acp-11-12959-2011, 2011.
- Assan, Sabina, Baudic, Alexia, Guemri, Ali, Ciais, Philippe, Gros, Valerie, R. Vogel, F.: Characterization of interferences to in situ observations of $\delta^{13}\text{C}$ CH₄ and C₂H₆ when using a cavity ring-down spectrometer at industrial sites, *Atmos. Meas. Tech.*, 10, 2077–2091, doi:10.5194/amt-10-2077-2017, 2017.
- Atkinson, R.: Kinetics and Mechanisms of the Gas-Phase Reactions of the Hydroxyl Radical with Organic Compounds under Atmospheric Conditions, *Chem. Rev.*, 85, 69–201, doi:10.1021/cr00063a002, 1985.
- Atkinson, R. and Arey, J.: Gas-phase tropospheric chemistry of biogenic volatile organic compounds: A review, *Atmos. Environ.*, 37(SUPPL. 2), 197–219, doi:10.1016/S1352-2310(03)00391-1, 2003.
- Atkinson, R., Baulch, D. L., Cox, R. A., Crowley, J. N., Hampson, R. F., Hynes, R. G., Jenkin, M. E., Rossi, M. J. and Troe, J.: Evaluated kinetic and photochemical data for atmospheric chemistry: Part 1 – gas phase reactions of O_x, HO_x, NO_x and SO_x species, *Atmos. Chem. Phys. Discuss.*, 3(6), 6179–6699, doi:10.5194/acpd-3-6179-2003, 2003.
- Atkinson, R., Baulch, D. L., Cox, R. A., Crowley, J. N., Hampson, R. F., Hynes, R. G., Jenkin, M. E., Rossi, M. J., Troe, J. and Subcommittee, I.: Evaluated kinetic and photochemical data for atmospheric chemistry: Volume II—gas phase reactions of organic species, *Atmos. Chem. Phys.*, 6(11), 3625–4055, 2006.
- Badol, C., Borbon, A., Locoge, N., Léonardis, T. and Galloo, J. C.: An automated monitoring system for VOC ozone precursors in ambient air: Development, implementation and data

- analysis, *Anal. Bioanal. Chem.*, 378(7), 1815–1827, doi:10.1007/s00216-003-2474-0, 2004.
- Baker, B. and Sinnott, M.: Analysis of sesquiterpene emissions by plants using solid phase microextraction, , 1216, 8442–8451, doi:10.1016/j.chroma.2009.10.002, 2009.
- Berresheim, H., Elste, T., Plass-Dülmer, C., Eisele, F. L. and Tanner, D. J.: Chemical ionization mass spectrometer for long-term measurements of atmospheric OH and H₂SO₄, *Int. J. Mass Spectrom.*, 202(1–3), 91–109, doi:10.1016/S1387-3806(00)00233-5, 2000.
- Bertin, N., Staudt, M., Hansen, U., Seufert, G., Ciccioli, P., Foster, P., Fugit, J. L. and Torres, L.: Diurnal and seasonal course of monoterpene emissions from *Quercus ilex* (L.) under natural conditions - Application of light and temperature algorithms, *Atmos. Environ.*, 31(SUPPL. 1), 135–144, doi:10.1016/S1352-2310(97)00080-0, 1997.
- Bignozzi, C. A., Maldotti, A., Chiorboll, C., Bartocci, C. and Carassiti, V.: Kinetics and mechanism of reactions between aromatic olefins and hydroxyl radicals, *Int. J. Chem. Kinet.*, 13(12), 1235–1242, doi:10.1002/kin.550131204, 1981.
- Blake, R. S., Monks, P. S. and Ellis, A. M.: Proton-transfer reaction mass spectrometry, *Chem. Rev.*, 109(3), 861–896, doi:10.1021/cr800364q, 2009.
- De Bouille, P., Sotta, B., Miginiac, E. and Merrien, A.: Hormones and Pod Development in Oilseed Rape (*Brassica napus*), *Plant Physiol.*, 90(3), 876–880, doi:10.1104/pp.90.3.876, 1989.
- Bsaibes, S., Ajami, M. Al, Mermet, K., Truong, F., Batut, S., Hecquet, C., Dusanter, S., Léornadis, T., Sauvage, S., Kammer, J., Flaud, P., Perraudin, E., Villenave, E., Locoge, N. and Gros, V.: Variability of OH reactivity in the Landes maritime Pine forest: Results from the LANDEX campaign 2017, , 1–35, 2019.
- Di Carlo, P., Brune, W. H., Martinez, M., Harder, H., Leshner, R., Ren, X., Thornberry, T., Carroll, M. A., Young, V., Shepson, P. B., Riemer, D., Apel, E. and Campbell, C.: Missing OH Reactivity in a Forest: Evidence for Unknown Reactive Biogenic VOCs, *Science* (80-.), 304(5671), 722–725, doi:10.1126/science.1094392, 2004.
- Chameides, W.: Diagnostic studies of the H_xO_y-N_xO_y-O₃ Photochemical system, Using data from NASA GTE Field Expeditions, , 1–38, 1988.
- Chiorboll, C., Bignozzi, C. A., Maldotti, A., Giardini, P. F., Rossi, A. and Carassiti, V.: Rate constants for the gas-phase reactions of OH radicals with β -dimethylstyrene and acetone. Mechanism of β -dimethylstyrene NO_x-air photooxidation, *Int. J. Chem. Kinet.*, 15, 1983.
- Ciccioli, P., Brancaleoni, E., Frattoni, M., Di Palo, V., Valentini, R., Tirone, G., Seufert, G., Bertin, N., Hansen, U., Csiky, O., Lenz, R. and Sharma, M.: Emission of reactive terpene compounds from orange orchards and their removal by within-canopy processes, *J. Geophys. Res. Atmos.*, 104(D7), 8077–8094, doi:10.1029/1998JD100026, 1999.
- D’Anna, B., Andresen, Gefen, Z. and Nielsen, C. J.: Kinetic study of OH and NO₃ radical reactions with 14 aliphatic aldehydes, *Phys. Chem. Chem. Phys.*, 3(15), 3057–3063, doi:10.1039/b103623h, 2001.
- Darnall, K. R., Winer, A. M., Lloyd, A. C. and Pitts, J. N.: Relative rate constants for the reaction of OH radicals with selected C₆ and C₇ alkanes and alkenes at 305 ± 2 K, *Chem. Phys. Lett.*, 44(3), 415–418, doi:10.1016/0009-2614(76)80695-1, 1976.
- Dolgorouky, C., Gros, V., Sarda-Estève, R., Sinha, V., Williams, J., Marchand, N., Sauvage, S., Poulain, L., Sciare, J. and Bonsang, B.: Total OH reactivity measurements in Paris during

the 2010 MEGAPOLI winter campaign, *Atmos. Chem. Phys.*, 12(20), 9593–9612, doi:10.5194/acp-12-9593-2012, 2012.

Driscoll, J.: Gas chromatography in environmental analysis - Aims and challenges, in *Environmental Instrumentation Handbook*, edited by Wiley, pp. 1–17., 2004.

Dusanter, S. and Stevens, P.: Recent Advances in the Chemistry of OH and HO₂ Radicals in the Atmosphere: Field and Laboratory Measurements, in *Advances in Atmospheric Chemistry*, pp. 493–579, World Scientific., 2017.

Edwards, P. M., Evans, M. J., Furneaux, K. L., Hopkins, J., Ingham, T., Jones, C., Lee, J. D., Lewis, A. C., Moller, S. J., Stone, D., Whalley, L. K. and Heard, D. E.: OH reactivity in a South East Asian tropical rainforest during the oxidant and particle photochemical processes (OP3) project, *Atmos. Chem. Phys.*, 13(18), 9497–9514, doi:10.5194/acp-13-9497-2013, 2013.

Ellis, A. M. and Mayhew, C. A.: *Proton Transfer Reaction Mass Spectrometry: Principles and Applications*, Wiley., 2014.

FAOSTAT: World 1995-2016., 2016.

Felzer, B. S., Cronin, T., Reilly, J. M., Melillo, J. M. and Wang, X.: Impacts of ozone on trees and crops, *Comptes Rendus - Geosci.*, 339(11–12), 784–798, doi:10.1016/j.crte.2007.08.008, 2007.

Finnigan, J. J.: Boundary layer (atmospheric) and air pollution, complex terrain, *Earth Syst. Environ. Sci.*, 242–249, 2014.

Fischer, E. V., Jacob, D. J., Millet, D. B., Yantosca, R. M. and Mao, J.: The role of the ocean in the global atmospheric budget of acetone, *Geophys. Res. Lett.*, 39(1), doi:10.1029/2011GL050086, 2012.

Font, X., Artola, A. and Sánchez, A.: Detection, composition and treatment of volatile organic compounds from waste treatment plants, *Sensors*, 11(4), 4043–4059, doi:10.3390/s110404043, 2011.

Fuchs, H., Novelli, A., Rolletter, M., Hofzumahaus, A., Pfannerstill, E. Y., Kessel, S., Edtbauer, A., Williams, J., Michoud, V., Dusanter, S., Locoge, N., Zannoni, N., Gros, V., Truong, F., Sarda-Estève, R., Cryer, D. R., Brumby, C. A., Whalley, L. K., Stone, D., Seakins, P. W., Heard, D. E., Schoemaeker, C., Blocquet, M., Coudert, S., Batut, S., Fittschen, C., Thames, A. B., Brune, W. H., Ernest, C., Harder, H., Müller, J. B. A., Elste, T., Kubistin, D., Andres, S., Bohn, B., Hohaus, T., Holland, F., Li, X., Rohrer, F., Kiendler-Scharr, A., Tillmann, R., Wegener, R., Yu, Z., Zou, Q. and Wahner, A.: Comparison of OH reactivity measurements in the atmospheric simulation chamber SAPHIR, *Atmos. Meas. Tech.*, 10(10), 4023–4053, doi:10.5194/amt-10-4023-2017, 2017.

Fuentes, J. D., Lerdau, M., Atkinson, R., Baldocchi, D., Bottenheim, J. W., Ciccioli, P., Lamb, B., Geron, C., Gu, L., Guenther, A., Sharkey, D. and Stockwell, W.: Biogenic Hydrocarbons in the Atmospheric Boundary Layer: A Review, *Bull. Am. Meteorol. Soc.*, 81(7), 1537–1575, doi:10.1175/1520-0477(2000)081<1537:bhitab>2.3.co;2, 2002.

Genard-Zielinski, A. C., Boissard, C., Fernandez, C., Kalogridis, C., Lathière, J., Gros, V., Bonnaire, N. and Ormeño, E.: Variability of BVOC emissions from a Mediterranean mixed forest in southern France with a focus on *Quercus pubescens*, *Atmos. Chem. Phys.*, 15(1), 431–446, doi:10.5194/acp-15-431-2015, 2015.

Goldstein, A. H. and Galbally, I. E.: Known and unexplored organic constituents in the earth's

- atmosphere, *Environ. Sci. Technol.*, 41(5), 1514–1521, doi:10.1021/es072476p, 2007.
- Gonzaga Gomez, L., Loubet, B., Lafouge, F., Ciuraru, R., Buysse, P., Durand, B., Gueudet, J.-C., Fanucci, O., Fortineau, A., Zurfluh, O., Decuq, C., Kammer, J., Duprix, P., Bsaibes, S., Truong, F., Gros, V. and Boissard, C.: Comparative study of biogenic volatile organic compounds fluxes by wheat, maize and rapeseed with dynamic chambers over a short period in northern France, *Atmos. Environ.*, 214, 116855, doi:10.1016/j.atmosenv.2019.116855, 2019.
- de Gouw, Joost & Warneke, C.: Measurements of Volatile Organic Compounds in the earth's atmosphere using Proton- Transfer- reaction Mass Spectrometry, *Mass Spectrom. Rev.*, 26, 223–257, doi:10.1002/mas, 2007.
- De Gouw, J. and Warneke, C.: MEASUREMENTS OF VOLATILE ORGANIC COMPOUNDS IN THE EARTH'S ATMOSPHERE USING PROTON-TRANSFER-REACTION MASS SPECTROMETRY Joost, *Reprod. Hum. Horm.*, 26, 223–257, doi:10.1002/mas, 2007.
- Griffin, J., Cocker, D. R. and Seinfeld, H.: biogenic hydrocarbons $Y = Mo \bullet$, , 26(17), 2721–2724, 1999.
- Gros, V., Gaimoz, C., Herrmann, F., Custer, T., Williams, J., Bonsang, B., Sauvage, S., Locoge, N., d'Argouges, O., Sarda-Estève, R. and Sciare, J.: Volatile organic compounds sources in Paris in spring 2007. Part I: qualitative analysis, *Environ. Chem.*, 8(1), 74, doi:10.1071/en10068, 2011.
- Grosjean, D. and Williams, E. L.: Environmental persistence of organic compounds estimated from structure-reactivity and linear free-energy relationships. Unsaturated aliphatics, *Atmos. Environ. Part A, Gen. Top.*, 26(8), 1395–1405, doi:10.1016/0960-1686(92)90124-4, 1992.
- Guenther, A.: A global model of natural volatile organic compound emissions, *J. Geophys. Res.*, 100(D5), 8873–8892, doi:10.1029/94JD02950, 1995.
- Guenther, A.: Biological and Chemical Diversity of Biogenic Volatile Organic Emissions into the Atmosphere, *ISRN Atmos. Sci.*, 2013, 1–27, doi:10.1155/2013/786290, 2013.
- Guenther, A., Hewitt, C., Erickson, D., Fall, R., Geron, C., Graedel, T., Harley, P., Klinger, L., Lerdau, M., Mckay, W., Pierce, T., Scholes, B., Steinbrecher, R., Tallamraju, R., Taylor, J. and Zimmerman, P.: A global model of natural volatile organic compound emissions, *J. Geophys. Res. Atmos.*, 100(D5), 8873–8892, doi:10.1029/94JD02950/abstract, 1995.
- Guenther, A., Karl, T., Harley, P., Wiedinmyer, C., Palmer, P. I. and Geron, C.: Estimates of global terrestrial isoprene emissions using MEGAN (Model of Emissions of Gases and Aerosols from Nature), *Atmos. Chem. Phys.*, 6(11), 3181–3210, doi:10.5194/acp-6-3181-2006, 2006.
- Guenther, A. B., Zimmerman, P. R., Harley, P. C., Monson, R. K. and Fall, R.: Isoprene and monoterpene emission rate variability: model evaluations and sensitivity analyses, *J. Geophys. Res.*, 98(D7), 12609, doi:10.1029/93jd00527, 1993.
- Hallquist, M., Wenger, J. C., Baltensperger, U., Rudich, Y., Simpson, D., Claeys, M. and Dommen, J.: and Physics The formation , properties and impact of secondary organic aerosol : current and emerging issues, , (June), 5155–5236, 2009.
- Hansen, R. F., Griffith, S. M., Dusanter, S., Rickly, P. S., Stevens, P. S., Bertman, S. B., Carroll, M. A., Erickson, M. H., Flynn, J. H., Grossberg, N., Jobson, B. T., Lefer, B. L. and Wallace, H. W.: Measurements of total hydroxyl radical reactivity during CABINEX 2009 – Part

1: Field measurements, *Atmos. Chem. Phys.*, 14(6), 2923–2937, doi:10.5194/acp-14-2923-2014, 2014.

Hansen, R. F., Blocquet, M., Schoemaeker, C., Léonardis, T., Locoge, N., Fittschen, C., Hanoune, B., Stevens, P. S., Sinha, V. and Dusanter, S.: Intercomparison of the comparative reactivity method (CRM) and pump-probe technique for measuring total OH reactivity in an urban environment, *Atmos. Meas. Tech.*, doi:10.5194/amt-8-4243-2015, 2015.

Helmig, D., Bottenheim, J., Galbally, I. E., Lewis, A., Milton, M. J. T., Penkett, S., Plass-Duelmer, C., Reimann, S., Tans, P. and Thiel, S.: Volatile Organic Compounds in the Global Atmosphere, *Eos, Trans. Am. Geophys. Union*, 90(52), 513–514, doi:10.1029/2009EO520001, 2009.

Hoffmann, T., Odum, J. R., Bowman, F., Collins, D., Klockow, D., Flagan, R. C. and Seinfeld, J. H.: Formation of organic aerosols from the oxidation of biogenic hydrocarbons, *J. Atmos. Chem.*, 26(2), 189–222, doi:10.1023/A:1005734301837, 1997.

Holtslag, A. A. M.: Modeling and Parameterization, in *Atmospheric Boundary Layers*, pp. 265–273., 2015.

Holzinger, R., Lee, A., Goldstein, A. H., Program, A. S. and Resources, W.: Holzinger05: Observations of oxidation products above a forest imply biogenic emissions of very reactive compounds, *Atmos. Chem. Phys.*, 67–75, 2005.

Holzinger, R., Williams, J., Herrmann, F., Lelieveld, J., Donahue, N. M. and Röckmann, T.: Aerosol analysis using a Thermal-Desorption Proton-Transfer-Reaction Mass Spectrometer (TD-PTR-MS): A new approach to study processing of organic aerosols, *Atmos. Chem. Phys.*, 10(5), 2257–2267, doi:10.5194/acp-10-2257-2010, 2010.

Holzinger, R., Acton, W. J. F., Bloss, W. J., Breitenlechner, M., Crilley, L. R., Dusanter, S., Gonin, M., Gros, V., Keutsch, F. N., Kiendler-Scharr, A., Kramer, L. J., Krechmer, J. E., Languille, B., Locoge, N., Lopez-Hilfiker, F., Materić, D., Moreno, S., Nemitz, E., Quéléver, L. L. J., Sarda Esteve, R., Sauvage, S., Schallhart, S., Sommariva, R., Tillmann, R., Wedel, S., Worton, D. R., Xu, K. and Zaytsev, A.: Validity and limitations of simple reaction kinetics to calculate concentrations of organic compounds from ion counts in PTR-MS, *Atmos. Meas. Tech. Discuss.*, (January), 1–29, doi:10.5194/amt-2018-446, 2019.

Hu, X.-M.: Boundary Layer (atmospheric) and air pollution, *Air pollution Meteorology, Earth Syst. Environ. Sci.*, 227–236, 2015.

Ingham, T., Goddard, A., Whalley, L. K., Furneaux, K. L., Edwards, P. M., Seal, C. P., Self, D. E., Johnson, G. P., Read, K. A., Lee, J. D. and Heard, D. E.: A flow-tube based laser-induced fluorescence instrument to measure OH reactivity in the troposphere, *Atmos. Meas. Tech.*, 2(2), 465–477, doi:10.5194/amt-2-465-2009, 2009.

Jacob, D. J., Field, B. D., Li, Q., Blake, D. R., de Gouw, J., Warneke, C., Hansel, A., Wisthaler, A., Singh, H. B. and Guenther, A.: Global budget of methanol: Constraints from atmospheric observations, *J. Geophys. Res. D Atmos.*, 110(8), 1–17, doi:10.1029/2004JD005172, 2005.

Jones, C. E., Kato, S., Nakashima, Y. and Kajii, Y.: A novel fast gas chromatography method for higher time resolution measurements of speciated monoterpenes in air, *Atmos. Meas. Tech.*, 7(5), 1259–1275, doi:10.5194/amt-7-1259-2014, 2014.

Juuti, S.: Monoterpene Emission Rate Measurements From a Monterey Pine, , 95, 7515–7519, 1990.

Kaiser, J., Skog, K. M., Baumann, K., Bertman, S. B., Brown, S. B., Brune, W. H., Crouse, J. D., De Gouw, J. A., Edgerton, E. S., Feiner, P. A., Goldstein, A. H., Koss, A., Miszta, P. K., Nguyen, T. B., Olson, K. F., St Clair, J. M., Teng, A. P., Toma, S., Wennberg, P. O., Wild, R. J., Zhang, L. and Keutsch, F. N.: Speciation of OH reactivity above the canopy of an isoprene-dominated forest, *Atmos. Chem. Phys.*, 16(14), 9349–9359, doi:10.5194/acp-16-9349-2016, 2016.

Kammer, J., Perraudin, E., Flaud, P. M., Lamaud, E., Bonnefond, J. M. and Villenave, E.: Observation of nighttime new particle formation over the French Landes forest, *Sci. Total Environ.*, 621, 1084–1092, doi:10.1016/j.scitotenv.2017.10.118, 2018.

Kammer, J., Décuq, C., Baisnée, D., Ciuraru, R., Lafouge, F., Buysse, P., Bsaibes, S., Henderson, B., Cristescu, S. M., Benabdallah, R., Chandra, V., Durand, B., Fanucci, O., Petit, J.-E., Truong, F., Bonnaire, N., Sarda-Estève, R., Gros, V. and Loubet, B.: Characterization of the particle and gaseous pollutants emissions from a French dairy and sheep farm, *Sci. Total Environ.*, 2019.

Kanakidou, M., Seinfeld, J. H., Pandis, S. N., Barnes, I., Dentener, F. J., Facchini, M. C., Van Dingenen, R., Ervens, B., Nenes, A., Nielsen, C. J., Swietlicki, E., Putaud, J. P., Balkanski, Y., Fuzzi, S., Horth, J., Moortgat, G. K., Winterhalter, R., Myhre, C. E. L., Tsigaridis, K., Vignati, E., Stephanou, E. G. and Wilson, J.: Organic aerosol and global climate modelling: a review, *Atmos. Chem. Phys.*, 5(4), 1053–1123, doi:10.5194/acp-5-1053-2005, 2005.

Kari, E., Miettinen, P., Yli-Pirilä, P., Virtanen, A. and Faiola, C. L.: PTR-ToF-MS product ion distributions and humidity-dependence of biogenic volatile organic compounds, *Int. J. Mass Spectrom.*, 430, 87–97, doi:10.1016/j.ijms.2018.05.003, 2018.

Karl, M., Guenther, A., Köble, R., Seufert, G., Leip, A. and Seufert, G.: A new European plant-specific emission inventory of biogenic volatile organic compounds for use in atmospheric transport models, *Biogeosciences Discuss.*, 5(6), 4993–5059, doi:10.5194/bg-6-1059-2009, 2009.

Karl, T., Yeretjian, C., Jordan, A. and Lindinger, W.: Dynamic measurements of partition coefficients using proton-transfer-reaction mass spectrometry (PTR-MS), *Int. J. Mass Spectrom.*, 223–224, 383–395, doi:10.1016/S1387-3806(02)00927-2, 2003.

Karl, T., Guenther, A., Yokelson, R. J., Greenberg, J., Potosnak, M., Blake, D. R. and Artaxo, P.: The tropical forest and fire emissions experiment: Emission, chemistry, and transport of biogenic volatile organic compounds in the lower atmosphere over Amazonia, *J. Geophys. Res. Atmos.*, 112(18), 1–17, doi:10.1029/2006JD008539, 2007.

Kerminen, V. M., Paramonov, M., Anttila, T., Riipinen, I., Fountoukis, C., Korhonen, H., Asmi, E., Laakso, L., Lihavainen, H., Swietlicki, E., Svenningsson, B., Asmi, A., Pandis, S. N., Kulmala, M. and Petäjä, T.: Cloud condensation nuclei production associated with atmospheric nucleation: A synthesis based on existing literature and new results, *Atmos. Chem. Phys.*, 12(24), 12037–12059, doi:10.5194/acp-12-12037-2012, 2012.

Kesselmeier, J. and Staudt, M.: Biogenic volatile organic compounds (VOC): An overview on emission, physiology and ecology, *J. Atmos. Chem.*, 33(1), 23–88, doi:10.1023/A:1006127516791, 1999.

Kim, S., Karl, T., Helmig, D., Daly, R., Rasmussen, R. and Guenther, A.: Measurement of atmospheric sesquiterpenes by proton transfer reaction-mass spectrometry (PTR-MS), *Atmos. Meas. Tech.*, 2(1), 99–112, doi:10.5194/amt-2-99-2009, 2009.

- Kim, S., Guenther, A., Karl, T. and Greenberg, J.: Contributions of primary and secondary biogenic VOC to total OH reactivity during the CABINEX (Community Atmosphere-Biosphere Interactions Experiments)-09 field campaign, *Atmos. Chem. Phys.*, 11(16), 8613–8623, doi:10.5194/acp-11-8613-2011, 2011.
- König, G., Brunda, M., Puxbaum, H., Hewitt, C. N., Duckham, S. C. and Rudolph, J.: Relative contribution of oxygenated hydrocarbons to the total biogenic VOC emissions of selected mid-European agricultural and natural plant species, *Atmos. Environ.*, 29(8), 861–874, doi:10.1016/1352-2310(95)00026-U, 1995.
- Kovacs, T. A. and Brune, W. H.: Total OH loss rate measurement, *J. Atmos. Chem.*, 39(2), 105–122, doi:10.1023/A:1010614113786, 2001.
- Kulmala, M. and Kerminen, V. M.: On the formation and growth of atmospheric nanoparticles, *Atmos. Res.*, 90(2–4), 132–150, doi:10.1016/j.atmosres.2008.01.005, 2008.
- Kumar, V. and Sinha, V.: VOC-OHM: A new technique for rapid measurements of ambient total OH reactivity and volatile organic compounds using a single proton transfer reaction mass spectrometer, *Int. J. Mass Spectrom.*, 374, 55–63, doi:10.1016/j.ijms.2014.10.012, 2014.
- Kwok, E. S. C., Atkinson, R. and Arey, J.: Kinetics of the gas-phase reactions of indan, indene, fluorene, and 9, 10-dihydroanthracene with OH radicals, NO₃ radicals, and O₃, *Int. J. Chem. Kinet.*, 299–308, 1997.
- Laothawornkitkul, J., Taylor, J. E., Paul, N. D. and Hewitt, C. N.: Biogenic volatile organic compounds in the Earth system: Tansley review, *New Phytol.*, 183(1), 27–51, doi:10.1111/j.1469-8137.2009.02859.x, 2009.
- Lathière, J., Hauglustaine, D. A., Friend, A. D., Noblet-Ducoudré, N. De, Viovy, N. and Folberth, G. A.: Impact of climate variability and land use changes on global biogenic volatile organic compound emissions, *Atmos. Environ.*, 40(6), 2129–2146, 2006.
- Laufs, S., Cazaunau, M., Stella, P., Kurtenbach, R., Cellier, P., Mellouki, A., Loubet, B. and Kleffmann, J.: Diurnal fluxes of HONO above a crop rotation, *Atmos. Chem. Phys.*, 17(11), 6907–6923, doi:10.5194/acp-17-6907-2017, 2017.
- Lee, A., Goldstein, A. H., Kroll, J. H., Ng, N. L., Varutbangkul, V., Flagan, R. C. and Seinfeld, J. H.: Gas-phase products and secondary aerosol yields from the photooxidation of 16 different terpenes, *J. Geophys. Res. Atmos.*, 111(17), 1–25, doi:10.1029/2006JD007050, 2006.
- Lindinger, W., Hansel, A. and Jordan, A.: On-line monitoring of volatile organic compounds at pptv levels by means of Proton-Transfer-Reaction Mass Spectrometry (PTR-MS) Medical applications, food control and environmental research, *Int. J. Mass Spectrom. Ion Process.*, 173(3), 191–241, 1998.
- Loreto, F., Ciccioli, P., Brancajleoni, E., Cecinato, A., Frattoni, M. and Sharkey, T. D.: Different sources of reduced carbon contribute to form three classes of terpenoid emitted by *Quercus ilex* L. leaves, *Proc. Natl. Acad. Sci. U. S. A.*, 93(18), 9966–9969, doi:10.1073/pnas.93.18.9966, 1996.
- Lou, S., Holland, F., Rohrer, F., Lu, K., Bohn, B., Brauers, T., Chang, C. C., Fuchs, H., Häsel, R., Kita, K., Kondo, Y., Li, X., Shao, M., Zeng, L., Wahner, A., Zhang, Y., Wang, W. and Hofzumahaus, A.: Atmospheric OH reactivities in the Pearl River Delta - China in summer 2006: Measurement and model results, *Atmos. Chem. Phys.*, 10(22), 11243–11260, doi:10.5194/acp-10-11243-2010, 2010.

- Loubet, B., Decuq, C., Personne, E., Massad, R. S., Flechard, C., Fanucci, O., Mascher, N., Gueudet, J. C., Masson, S., Durand, B., Genermont, S., Fauvel, Y. and Cellier, P.: Investigating the stomatal, cuticular and soil ammonia fluxes over a growing tritical crop under high acidic loads, *Biogeosciences*, 9(4), 1537–1552, doi:10.5194/bg-9-1537-2012, 2012.
- Malásková, M., Olivenza-León, D., Piel, F., Mochalski, P., Sulzer, P., Jürschik, S., Mayhew, C. A. and Märk, T. D.: Compendium of the reactions of H₃O⁺ with selected ketones of relevance to breath analysis using proton transfer reaction mass spectrometry, *Front. Chem.*, 7(June), 1–14, doi:10.3389/fchem.2019.00401, 2019.
- Mao, J., Ren, X., Brune, W. H., Olson, J. R., Crawford, J. H., Fried, A., Huey, L. G., Cohen, R. C., Heikes, B., Singh, H. B., Blake, D. R., Sachse, G. W., Diskin, G. S., Hall, S. R. and Shetter, R. E.: Airborne measurement of OH reactivity during INTEX-B, *Atmos. Chem. Phys.*, 9(1), 163–173, doi:10.5194/acp-9-163-2009, 2009.
- Mao, J., Ren, X., Zhang, L., Van Duin, D. M., Cohen, R. C., Park, J. H., Goldstein, A. H., Paulot, F., Beaver, M. R., Crouse, J. D., Wennberg, P. O., Digangi, J. P., Henry, S. B., Keutsch, F. N., Park, C., Schade, G. W., Wolfe, G. M., Thornton, J. A. and Brune, W. H.: Insights into hydroxyl measurements and atmospheric oxidation in a California forest, *Atmos. Chem. Phys.*, 12(17), 8009–8020, doi:10.5194/acp-12-8009-2012, 2012.
- Materić, D., Lanza, M., Sulzer, P., Herbig, J., Bruhn, D., Turner, C., Mason, N. and Gauci, V.: Monoterpene separation by coupling proton transfer reaction time-of-flight mass spectrometry with fastGC, *Anal. Bioanal. Chem.*, 407(25), 7757–7763, doi:10.1007/s00216-015-8942-5, 2015.
- McEwan, M. and Macfarlane Smith, W. H.: Identification of volatile organic compounds emitted in the field by oilseed rape (*Brassica napus* ssp. *oleifera*) over the growing season, *Clin. Exp. Allergy*, 28(3), 332–338, doi:10.1046/j.1365-2222.1998.00234.x, 1998.
- Mermet, K., Sauvage, S., Dusanter, S., Salameh, T., Léonardis, T., Flaud, P., Perraudin, É., Villenave, É. and Locoge, N.: Optimization of a gas chromatographic unit for measuring BVOCs in ambient air, *Atmos. Meas. Tech. Discuss.*, (July), 1–32, 2019.
- Michoud, V., Hansen, R. F., Locoge, N., Stevens, P. S. and Dusanter, S.: Detailed characterizations of the new Mines Douai comparative reactivity method instrument via laboratory experiments and modeling, *Atmos. Meas. Tech.*, doi:10.5194/amt-8-3537-2015, 2015.
- Mogensen, D., Smolander, S., Sogachev, A., Zhou, L., Sinha, V., Guenther, A., Williams, J., Nieminen, T., Kajos, M. K., Rinne, J., Kulmala, M. and Boy, M.: Modelling atmospheric OH-reactivity in a boreal forest ecosystem, *Atmos. Chem. Phys.*, 11(18), 9709–9719, doi:10.5194/acp-11-9709-2011, 2011.
- Monks, P. S., Granier, C., Fuzzi, S., Stohl, A., Williams, M. L., Akimoto, H., Amann, M., Baklanov, A., Baltensperger, U., Bey, I., Blake, N., Blake, R. S., Carslaw, K., Cooper, O. R., Dentener, F., Fowler, D., Fragkou, E., Frost, G. J., Generoso, S., Ginoux, P., Grewe, V., Guenther, A., Hansson, H. C., Henne, S., Hjorth, J., Hofzumahaus, A., Huntrieser, H., Isaksen, I. S. A., Jenkin, M. E., Kaiser, J., Kanakidou, M., Klimont, Z., Kulmala, M., Laj, P., Lawrence, M. G., Lee, J. D., Lioussé, C., Maione, M., McFiggans, G., Metzger, A., Mieville, A., Moussiopoulos, N., Orlando, J. J., O'Dowd, C. D., Palmer, P. I., Parrish, D. D., Petzold, A., Platt, U., Pöschl, U., Prévôt, A. S. H., Reeves, C. E., Reimann, S., Rudich, Y., Sellegri, K., Steinbrecher, R., Simpson, D., ten Brink, H., Theloke, J., van der Werf, G. R., Vautard, R., Vestreng, V., Vlachokostas, C. and von Glasow, R.: Atmospheric composition change - global

and regional air quality, *Atmos. Environ.*, 43(33), 5268–5350, doi:10.1016/j.atmosenv.2009.08.021, 2009.

Monson, R. K., Harley, P. C., Litvak, M. E., Wildermuth, M., Guenther, A. B., Zimmerman, P. R. and Fall, R.: Environmental and developmental controls over the seasonal pattern of isoprene emission from aspen leaves, *Oecologia*, 99, 260–270, 1994.

Moreaux, V., Lamaud, É., Bosc, A., Bonnefond, J. M., Medlyn, B. E. and Loustau, D.: Paired comparison of water, energy and carbon exchanges over two young maritime pine stands (*Pinus pinaster* Ait.): Effects of thinning and weeding in the early stage of tree growth, *Tree Physiol.*, 31(9), 903–921, doi:10.1093/treephys/tpr048, 2011.

Morrison, E. C., Drewer, J. and Heal, M. R.: A comparison of isoprene and monoterpene emission rates from the perennial bioenergy crops short-rotation coppice willow and *Miscanthus* and the annual arable crops wheat and oilseed rape, *GCB Bioenergy*, 8(1), 211–225, doi:10.1111/gcbb.12257, 2016.

Muller, J. B. A., Elste, T., Plass-Dülmer, C., Stange, G., Holla, R., Claude, A., Englert, J., Gilge, S. and Kubistin, D.: A novel semi-direct method to measure OH reactivity by chemical ionization mass spectrometry (CIMS), *Atmos. Meas. Tech.*, 11(7), 4413–4433, doi:10.5194/amt-11-4413-2018, 2018.

Müller, K., Pelzing, M., Gnauk, T., Kappe, A., Teichmann, U., Spindler, G., Haferkorn, S., Jahn, Y. and Herrmann, H.: Monoterpene emissions and carbonyl compound air concentrations during the blooming period of rape (*Brassica napus*), *Chemosphere*, 49(10), 1247–1256, doi:10.1016/S0045-6535(02)00610-0, 2002.

Nakashima, Y., Kato, S., Greenberg, J., Harley, P., Karl, T., Turnipseed, A., Apel, E., Guenther, A., Smith, J. and Kajii, Y.: Total OH reactivity measurements in ambient air in a southern Rocky mountain ponderosa pine forest during BEACHON-SRM08 summer campaign, *Atmos. Environ.*, 85, 1–8, doi:10.1016/j.atmosenv.2013.11.042, 2013.

Ng, N. L., Brown, S. S., Archibald, A. T., Atlas, E., Cohen, R. C., Crowley, J. N., Day, D. A., Donahue, N. M., Fry, J. L., Fuchs, H., Griffin, R. J. and Guzman, M. I.: Nitrate radicals and biogenic volatile organic compounds : oxidation , mechanisms , and organic aerosol , , 2103–2162, doi:10.5194/acp-17-2103-2017, 2017.

Nölscher, A. C., Williams, J., Sinha, V., Custer, T., Song, W., Johnson, A. M., Axinte, R., Bozem, H., Fischer, H., Pouvesle, N., Phillips, G., Crowley, J. N., Rantala, P., Rinne, J., Kulmala, M., Gonzales, D., Valverde-Canossa, J., Vogel, A., Hoffmann, T., Ouwersloot, H. G., Vilà-Guerau De Arellano, J. and Lelieveld, J.: Summertime total OH reactivity measurements from boreal forest during HUMPPA-COPEC 2010, *Atmos. Chem. Phys.*, 12(17), 8257–8270, doi:10.5194/acp-12-8257-2012, 2012a.

Nölscher, A. C., Sinha, V., Bockisch, S., Klüpfel, T. and Williams, J.: Total OH reactivity measurements using a new fast gas chromatographic photo-ionization detector (GC-PID), *Atmos. Meas. Tech.*, 5(12), 2981–2992, doi:10.5194/amt-5-2981-2012, 2012b.

Nölscher, A. C., Bourtsoukidis, E., Bonn, B., Kesselmeier, J., Lelieveld, J. and Williams, J.: Seasonal measurements of total OH reactivity emission rates from Norway spruce in 2011, *Biogeosciences*, 10(6), 4241–4257, doi:10.5194/bg-10-4241-2013, 2013.

Nölscher, A. C., Yañez-Serrano, A. M., Wolff, S., De Araujo, A. C., Lavrič, J. V., Kesselmeier, J. and Williams, J.: Unexpected seasonality in quantity and composition of Amazon rainforest air reactivity, *Nat. Commun.*, 7(1), doi:10.1038/ncomms10383, 2016.

- Palozzi, E., Guidolotti, G., Ciccioli, P., Brilli, F., Feil, S. and Calfapietra, C.: Does the novel fast-GC coupled with PTR-TOF-MS allow a significant advancement in detecting VOC emissions from plants?, *Agric. For. Meteorol.*, 216, 232–240, doi:10.1016/j.agrformet.2015.10.016, 2016.
- Pang, X.: Biogenic volatile organic compound analyses by PTR-TOF-MS: Calibration, humidity effect and reduced electric field dependency, *J. Environ. Sci. (China)*, 32, 196–206, doi:10.1016/j.jes.2015.01.013, 2015.
- Papurello, D., Silvestri, S., Tomasi, L., Belcari, I., Biasioli, F. and Santarelli, M.: Natural Gas Trace Compounds Analysis with Innovative Systems: PTR-ToF-MS and FASTGC, *Energy Procedia*, 101(September), 536–541, doi:10.1016/j.egypro.2016.11.068, 2016.
- Parker, A. E., Amédro, D., Schoemaeker, C. and Fittschen, C.: OH radical reactivity measurements by FAGE, *Environ. Eng. Manag. J.*, 10(1), 107–114, 2011.
- Parratt, D., Macfarlane Smith, W.H., Thomson, G., Cameron, L.A. and Butcher, R. D.: Evidence That Oilseed Rape (*Brassica Napus* SSP. *Oleifera*) Causes Respiratory Illness in Rural Dwellers, *Scottish Med. J.*, 40(3), 74–76, doi:doi.org/10.1177/003693309504000305, 1995.
- Paulot, F., Wunch, D., Crouse, J. D., Toon, G. C., Millet, D. B., Decarlo, P. F., Vigouroux, C., Deutscher, N. M., Abad, G. G., Notholt, J., Warneke, T., Hannigan, J. W., Warneke, C., De Gouw, J. A., Dunlea, E. J., De Mazière, M., Griffith, D. W. T., Bernath, P., Jimenez, J. L. and Wennberg, P. O.: Importance of secondary sources in the atmospheric budgets of formic and acetic acids, *Atmos. Chem. Phys.*, 11(5), 1989–2013, doi:10.5194/acp-11-1989-2011, 2011.
- Peeters, J., Boullart, W., Pultau, V., Vandenberg, S. and Vereecken, L.: Structure-activity relationship for the addition of OH to (poly)alkenes: Site-specific and total rate constants, *J. Phys. Chem. A*, 111(9), 1618–1631, doi:10.1021/jp066973o, 2007.
- Penuelas, Josep & Llusia, J.: The complexity of factors driving volatile organic compound emissions by plants, *Biol. Plant.*, 4, 481–487, 2001.
- Penuelas, J. and Llusia, J.: The Complexity of Factors Driving Volatile Organic Compound Emissions by Plants, *Biol. Plant.*, 44(4), 481–487, doi:10.1023/A, 2001.
- Phouongphouang, P. T. and Arey, J.: Rate constants for the gas-phase reactions of a series of alkyl naphthalenes with the OH radical, *Environ. Sci. Technol.*, 36(9), 1947–1952, doi:10.1021/es011434c, 2002.
- Pinto, D. M., Blande, J. D. and Souza, S. R.: Plant Volatile Organic Compounds (VOCs) in Ozone (O₃) Polluted Atmospheres : The Ecological Effects Plant Volatile Organic Compounds (VOCs) in Ozone (O₃) Polluted Atmospheres : The Ecological Effects, , (May 2014), doi:10.1007/s10886-009-9732-3, 2010.
- Pio, C. A., Nunes, T. and Brito, S.: VOLATILE HYDROCARBON EMISSIONS FROM COMMON AND NATIVE SPECIES., 1993.
- Portillo-estrada, M.: Advantages of PTR-MS and PTR-TOF-MS techniques for measuring volatile organic compounds (VOCs) Advantages of PTR-MS and PTR-TOF-MS techniques for measuring volatile organic compounds (VOCs), , (December 2013), 2014.
- Praplan, A. P., Pfannerstill, E. Y., Williams, J. and Hellén, H.: OH reactivity of the urban air in Helsinki, Finland, during winter, *Atmos. Environ.*, 169, 150–161, doi:10.1016/j.atmosenv.2017.09.013, 2017.

- Praplan, A. P., Tykkä, T., Chen, D., Boy, M., Taipale, D., Vakkari, V., Zhou, P., Petäjä, T. and Hellén, H.: Long-term total OH reactivity measurements in a boreal forest, , (February), 2019.
- Ramasamy, S., Ida, A., Jones, C., Kato, S., Tsurumaru, H., Kishimoto, I., Kawasaki, S., Sadanaga, Y., Nakashima, Y., Nakayama, T., Matsumi, Y., Mochida, M., Kagami, S., Deng, Y., Ogawa, S., Kawana, K. and Kajii, Y.: Total OH reactivity measurement in a BVOC dominated temperate forest during a summer campaign, 2014, *Atmos. Environ.*, 131, 41–54, doi:10.1016/j.atmosenv.2016.01.039, 2016.
- Ren, X., Brune, W. H., Cantrell, C. A., Edwards, G. D., Shirley, T., Metcalf, A. R. and Lesher, R. L.: Hydroxyl and peroxy radical chemistry in a rural area of central Pennsylvania: Observations and model comparisons, *J. Atmos. Chem.*, 52(3), 231–257, doi:10.1007/s10874-005-3651-7, 2005.
- Ren, X., Brune, W. H., Oliger, A., Metcalf, A. R., Simpas, J. B., Shirley, T., Schwab, J. J., Bai, C., Roychowdhury, U., Li, Y., Cai, C., Demerjian, K. L., He, Y., Zhou, X., Gao, H. and Hou, J.: OH, HO₂, and OH reactivity during the PMTACS-NY Whiteface Mountain 2002 campaign: Observations and model comparison, *J. Geophys. Res. Atmos.*, 111(10), 1–12, doi:10.1029/2005JD006126, 2006.
- Roberts, G. C., Day, D. A., Russell, L. M., Dunlea, E. J., Jimenez, J. L., Tomlinson, J. M., Collins, D. R., Shinozuka, Y. and Clarke, A. D.: Characterization of particle cloud droplet activity and composition in the free troposphere and the boundary layer during INTEX-B, *Atmos. Chem. Phys.*, 10(14), 6627–6644, doi:10.5194/acp-10-6627-2010, 2010.
- Rodionova, M. V., Poudyal, R. S., Tiwari, I., Voloshin, R. A., Zharmukhamedov, S. K., Nam, H. G., Zayadan, B. K., Bruce, B. D., Hou, H. J. M. and Allakhverdiev, S. I.: Biofuel production: Challenges and opportunities, *Int. J. Hydrogen Energy*, 42(12), 8450–8461, doi:10.1016/j.ijhydene.2016.11.125, 2017.
- Romano, A., Fischer, L., Herbig, J., Campbell-Sills, H., Coulon, J., Lucas, P., Cappellin, L. and Biasioli, F.: Wine analysis by FastGC proton-transfer reaction-time-of-flight-mass spectrometry, *Int. J. Mass Spectrom.*, 369, 81–86, doi:10.1016/j.ijms.2014.06.006, 2014.
- Rose, C., Sellegri, K., Moreno, I., Velarde, F., Ramonet, M., Weinhold, K., Krejci, R., Andrade, M., Wiedensohler, A., Ginot, P. and Laj, P.: CCN production by new particle formation in the free troposphere, *Atmos. Chem. Phys.*, 17(2), 1529–1541, doi:10.5194/acp-17-1529-2017, 2017.
- Roukos, J., Plaisance, H., Leonardis, T., Bates, M. and Locoge, N.: Development and validation of an automated monitoring system for oxygenated volatile organic compounds and nitrile compounds in ambient air, *J. Chromatogr. A*, 1216(49), 8642–8651, doi:10.1016/j.chroma.2009.10.018, 2009.
- Ruzsanyi, V., Fischer, L., Herbig, J., Ager, C. and Amann, A.: Multi-capillary-column proton-transfer-reaction time-of-flight mass spectrometry, *J. Chromatogr. A*, 1316, 112–118, doi:10.1016/j.chroma.2013.09.072, 2013.
- Sadanaga, Y., Yoshino, A., Watanabe, K., Yoshioka, A., Wakazono, Y., Kanaya, Y. and Kajii, Y.: Development of a measurement system of OH reactivity in the atmosphere by using a laser-induced pump and probe technique, *Rev. Sci. Instrum.*, 75(8), 2648–2655, doi:10.1063/1.1775311, 2004a.
- Sadanaga, Y., Yoshino, A., Kato, S., Yoshioka, A., Watanabe, K., Miyakawa, Y., Hayashi, I., Ichikawa, M., Matsumoto, J., Nishiyama, A., Akiyama, N., Kanaya, Y. and Kajii, Y.: The

importance of NO₂ and volatile organic compounds in the urban air from the viewpoint of the OH reactivity, *Geophys. Res. Lett.*, 31(8), 3–6, doi:10.1029/2004GL019661, 2004b.

Sahu, L. K.: Volatile organic compounds and their measurements in the troposphere, , 102(12), 2012.

Sanchez, D., Jeong, D., Seco, R., Wrangham, I., Park, J. H., Brune, W. H., Koss, A., Gilman, J., de Gouw, J., Misztal, P., Goldstein, A., Baumann, K., Wennberg, P. O., Keutsch, F. N., Guenther, A. and Kim, S.: Intercomparison of OH and OH reactivity measurements in a high isoprene and low NO environment during the Southern Oxidant and Aerosol Study (SOAS), *Atmos. Environ.*, doi:10.1016/j.atmosenv.2017.10.056, 2018.

Saraiva, L. and Krusche, N.: Estimation of the Boundary Layer Height in the Southern Region of Brazil, *Am. J. Environ. Eng.*, 3(1), 63–70, doi:10.5923/j.ajee.20130301.09, 2013.

Schade, G. W.: Are Monoterpene Emissions influenced by Humidity?, , (July), doi:10.1029/1999GL900444, 1999.

Seco, R., Peñuelas, J. and Filella, I.: Short-chain oxygenated VOCs: Emission and uptake by plants and atmospheric sources, sinks, and concentrations, *Atmos. Environ.*, 41(12), 2477–2499, doi:10.1016/j.atmosenv.2006.11.029, 2007.

Sharkey, T., Wiberlet, A. and Donohue, A.: Isoprene Emission from Plants : Why and How, *Ann. Bot.*, 101, 5–18, doi:10.1093/aob/mcm240, 2007.

Simon, V., Clement, B., Riba, M.-L. and Torres, L.: The Landes experiment: Monoterpenes emitted from the maritime pine, *J. Geophys. Res.*, 99(D8), 16501, doi:10.1029/94jd00785, 1994.

Sindelarova, K., Granier, C., Bouarar, I., Guenther, A., Tilmes, S., Stavrou, T., Müller, J. and Kuhn, U.: Global data set of biogenic VOC emissions calculated by the MEGAN model over the last 30 years, , 9317–9341, doi:10.5194/acp-14-9317-2014, 2014.

Sinha V., Williams J., C. J. N. and L. L.: The Comparative Reactivity Method – a new tool to measure total OH Reactivity in ambient air, *Atmos. Chem. Phys.*, 8, 2213–2227, 2008.

Sinha, V., Williams, J., Crowley, J. N. and Lelieveld, J.: The Comparative Reactivity Method – a new tool to measure total OH reactivity in ambient air, *Atmos. Chem. Phys. Discuss.*, 8, 2213–2227, doi:10.5194/acpd-7-18179-2007, 2008.

Sinha, V., Custer, T. G., Kluepfel, T. and Williams, J.: The effect of relative humidity on the detection of pyrrole by PTR-MS for OH reactivity measurements, *Int. J. Mass Spectrom.*, 282(3), 108–111, doi:10.1016/j.ijms.2009.02.019, 2009.

Sinha, V., Williams, J., Lelieveld, J., Ruuskanen, T. M., Kajos, M. K., Patokoski, J., Hellen, H., Hakola, H., Mogensen, D., Boy, M., Rinne, J. and Kulmala, M.: OH reactivity measurements within a boreal forest: Evidence for unknown reactive emissions, *Environ. Sci. Technol.*, 44(17), 6614–6620, doi:10.1021/es101780b, 2010.

Sivaramakrishnan, R. and Michael, J. V.: Rate constants for OH with selected large alkanes: Shock-tube measurements and an improved group scheme, *J. Phys. Chem. A*, 113(17), 5047–5060, doi:10.1021/jp810987u, 2009.

Smith, D. and Španěl, P.: Selected ion flow tube mass spectrometry (SIFT-MS) for on-line trace gas analysis, *Mass Spectrom. Rev.*, 24(5), 661–700, doi:10.1002/mas.20033, 2005.

Speight, J.: *Environmental Organic Chemistry for Engineers.*, 2016.

Srivastava, A. and Majumdar, D.: We are IntechOpen , the world ' s leading publisher of Open Access books Built by scientists , for scientists TOP 1 % , Intech, i, doi:http://dx.doi.org/10.5772/57353, 2011.

Staudt, M. and Seufert, G.: Light-Dependent Emission of Monoterpenes by Holm Oak (*Quercus ilex* L .) Light-dependent Emission of Monoterpenes by Holm Oak (*Quercus ilex* L .), , (January), doi:10.1007/BF01140148, 1995.

Staudt, M., Bertin, N., Hansen, U., Seufert, G., Ciccioli, P., Foster, P., Frenzel, B. and Fugit, J. L.: Seasonal and diurnal patterns of monoterpene emissions from *Pinus pinea* (L.) under field conditions, *Atmos. Environ.*, 31(SUPPL. 1), 145–156, doi:10.1016/S1352-2310(97)00081-2, 1997.

Staudt, M., Joffre, R., Rambal, S., Staudt, M., Mandl, N., Joffre, R. and Rambal, S.: Intraspecific variability of monoterpene composition emitted by *Quercus ilex* leaves Scaling-up WUE from leaf to canopy View project VOC emission diversity in oaks View project Intraspecific variability of monoterpene composition emitted by *Quercus ilex* le, , (January), doi:10.1139/x00-153, 2001.

Staudt, M., Rambal, S., Joffre, R. and Kesselmeier, J.: Impact of drought on seasonal monoterpene emissions from *Quercus ilex* in southern France, *J. Geophys. Res. Atmos.*, 107(21), doi:10.1029/2001JD002043, 2002.

Staudt, M., Byron, J., Piquemal, K. and Williams, J.: Compartment specific chiral pinene emissions identified in a Maritime pine forest, *Sci. Total Environ.*, 2018.

Stavrakou, T., Guenther, A., Razavi, A., Clarisse, L., Clerbaux, C., Coheur, P. F., Hurtmans, D., Karagulian, F., De Mazière, M., Vigouroux, C., Amelynck, C., Schoon, N., Laffineur, Q., Heinesch, B., Aubinet, M., Rinsland, C. and Müller, J. F.: First space-based derivation of the global atmospheric methanol emission fluxes, *Atmos. Chem. Phys.*, 11(10), 4873–4898, doi:10.5194/acp-11-4873-2011, 2011.

Stone, D., Whalley, L. K., Heard, D. E. and Stone, D.: Chem Soc Rev Tropospheric OH and HO₂ radicals : field measurements and model comparisons w American plumes over the , 6348–6404, doi:10.1039/c2cs35140d, 2012.

Stone, D., Whalley, L. K., Ingham, T., Edwards, P. M., Cryer, D. R., Brumby, C. A., Seakins, P. W. and Heard, D. E.: Measurement of OH reactivity by laser flash photolysis coupled with laser-induced fluorescence spectroscopy, *Atmos. Meas. Tech.*, 9(7), 2827–2844, doi:10.5194/amt-9-2827-2016, 2016.

Stull, R. B.: *An Introduction to Boundary Layer Meteorology*, Kluwer Academic Publishers., 1988.

Sulzer, P., Hartungen, E., Hanel, G., Feil, S., Winkler, K., Mutschlechner, P., Haidacher, S., Schottkowsky, R., Gansch, D., Seehauser, H., Striednig, M., Jürschik, S., Breiev, K., Lanza, M., Herbig, J., Märk, L., Märk, T. D. and Jordan, A.: A proton transfer reaction-quadrupole interface time-of-flight mass spectrometer (PTR-QiTOF): High speed due to extreme sensitivity, *Int. J. Mass Spectrom.*, 368, 1–5, doi:10.1016/j.ijms.2014.05.004, 2014.

Taipale, R., Ruuskanen, T. M., Rinne, J., Kajos, M. K., Hakola, H., Pohja, T. and Kulmala, M.: Technical note: Quantitative long-term measurements of VOC concentrations by PTR-MS - Measurement, calibration, and volume mixing ratio calculation methods, *Atmos. Chem. Phys.*, 8(22), 6681–6698, doi:10.5194/acp-8-6681-2008, 2008.

Tani, A.: Fragmentation and Reaction Rate Constants of Terpenoids Determined by Proton Transfer Reaction-mass Spectrometry, *Environ. Control Biol.*, 51(1), 23–29, doi:10.2525/ecb.51.23, 2013.

Tani, A., Hayward, S. and Hewitt, C. N.: Measurement of monoterpenes and related compounds by proton transfer reaction-mass spectrometry (PTR-MS), *Int. J. Mass Spectrom.*, 223–224, 561–578, doi:10.1016/S1387-3806(02)00880-1, 2003.

Tilman, D., Balzer, C., Hill, J. and Befort, B. L.: Global food demand and the sustainable intensification of agriculture, *Proc. Natl. Acad. Sci.*, 108(50), 20260–20264, doi:10.1073/pnas.1116437108, 2011.

Tingey, D. T., Manning, M., Grothaus, L. C. and Burns, W. F.: Influence of Light and Temperature on Monoterpene Emission Rates from Slash Pine, *Plant Physiol.*, 65(5), 797–801, doi:10.1104/pp.65.5.797, 1980.

Veromann, E., Toome, M., Kännaste, A., Kaasik, R., Copolovici, L., Flink, J., Kovács, G., Narits, L., Luik, A. and Niinemets, Ü.: Effects of nitrogen fertilization on insect pests, their parasitoids, plant diseases and volatile organic compounds in *Brassica napus*, *Crop Prot.*, 43, 79–88, doi:10.1016/j.cropro.2012.09.001, 2013.

Vuolo, R. M., Loubet, B., Mascher, N., Gueudet, J. C., Durand, B., Laville, P., Zurfluh, O., Ciuraru, R., Stella, P. and Trebs, I.: Nitrogen oxides and ozone fluxes from an oilseed-rape management cycle: The influence of cattle slurry application, *Biogeosciences*, 14(8), 2225–2244, doi:10.5194/bg-14-2225-2017, 2017.

Wallace, J. M. and Hobbs, P. V.: *Atmospheric Science: An Introductory Survey: Second Edition.*, 2006.

Warneke, C., Veres, P., Holloway, J. S., Stutz, J., Tsai, C., Alvarez, S., Rappenglueck, B. and Fehsenfeld, F. C.: Airborne formaldehyde measurements using PTR-MS: calibration, humidity dependence, inter-comparison and initial results, , 2345–2358, doi:10.5194/amt-4-2345-2011, 2011.

Watts, S. F.: The mass budgets of carbonyl sulfide, dimethyl sulfide, carbon disulfide and hydrogen sulfide, *Atmos. Environ.*, 34(5), 761–779, doi:10.1016/S1352-2310(99)00342-8, 2000.

Williams, J. and Brune, W.: A roadmap for OH reactivity research, *Atmos. Environ.*, 106, 371–372, doi:10.1016/j.atmosenv.2015.02.017, 2015.

Wilson, E. W., Hamilton, W. A., Kennington, H. R., Evans, B., Scott, N. W. and Demore, W. B.: Measurement and estimation of rate constants for the reactions of hydroxyl radical with several alkanes and cycloalkanes, *J. Phys. Chem. A*, 110(10), 3593–3604, doi:10.1021/jp055841c, 2006.

Winterhalter, R., Herrmann, F., Kanawati, B., Nguyen, T. L., Peeters, J., Vereecken, L. and Moortgat, G. K.: The gas-phase ozonolysis of β -caryophyllene (C₁₅H₂₄). Part I: An experimental study, *Phys. Chem. Chem. Phys.*, 11(21), 4152–4172, doi:10.1039/b817824k, 2009.

Yang, Y., Shao, M., Wang, X., Nölscher, A. C., Kessel, S., Guenther, A. and Williams, J.: Towards a quantitative understanding of total OH reactivity: A review, *Atmos. Environ.*, 134(2), 147–161, doi:10.1016/j.atmosenv.2016.03.010, 2016.

Yuan, B., Koss, A. R., Warneke, C., Coggon, M., Sekimoto, K. and De Gouw, J. A.: Proton-

Transfer-Reaction Mass Spectrometry: Applications in Atmospheric Sciences, *Chem. Rev.*, 117(21), 13187–13229, doi:10.1021/acs.chemrev.7b00325, 2017.

Zannoni, N.: OH reactivity measurements in the Mediterranean region, PhD Thesis, Université Paris-Saclay., 2015.

Zannoni, N., Dusanter, S., Gros, V., Sarda Esteve, R., Michoud, V., Sinha, V., Locoge, N. and Bonsang, B.: Intercomparison of two comparative reactivity method instruments in the Mediterranean basin during summer 2013, *Atmos. Meas. Tech.*, 8(9), 3851–3865, doi:10.5194/amt-8-3851-2015, 2015.

Zannoni, N., Gros, V., Lanza, M., Sarda, R., Bonsang, B., Kalogridis, C., Preunkert, S., Legrand, M., Jambert, C., Boissard, C. and Lathiere, J.: OH reactivity and concentrations of biogenic volatile organic compounds in a Mediterranean forest of downy oak trees, *Atmos. Chem. Phys.*, 16(3), 1619–1636, doi:10.5194/acp-16-1619-2016, 2016.

Zannoni, N., Gros, V., Sarda Esteve, R., Kalogridis, C., Michoud, V., Dusanter, S., Sauvage, S., Locoge, N., Colomb, A. and Bonsang, B.: Summertime OH reactivity from a receptor coastal site in the Mediterranean Basin, *Atmos. Chem. Phys.*, 17(20), 12645–12658, doi:10.5194/acp-17-12645-2017, 2017.

Titre : Caractérisation des composés organiques volatils biogéniques (COVB) et leur réactivité OH dans divers agro-écosystèmes.

Mots clés : COVB, Monoterpènes, Réactivité OH, FastGC/PTR-MS, Forêt, Agriculture

Résumé : Le radical hydroxyle OH est le principal oxydant dans la troposphère, mais ses puits restent encore difficiles à quantifier. L'un de ses principaux puits, est l'oxydation des Composés Organiques Volatils (COVs), composés provenant principalement de sources naturelles, à l'échelle du globe. Ils comprennent une grande variété d'espèces chimiques avec des réactivités très variables vis-à-vis des radicaux OH. Mesurer la réactivité OH totale, permet d'évaluer la charge en espèces réactives et d'estimer l'importance des espèces non mesurées/ non connues. Dans ce contexte, ce travail de thèse a d'abord visé d'optimiser la CRM ou « Comparative Reactivity Method », pour la mesure de la réactivité OH. Une fois les performances vérifiées, la CRM a été déployée dans deux écosystèmes : forestier et agricole. Les mesures de réactivité OH dans une forêt de pins maritimes ont montré des maxima de nuit arrivant jusqu'à 99 s^{-1} dans la canopée ; des

niveaux se situant dans la limite supérieure de ce qui a été précédemment vu en sites forestiers. Des réactivités plus faibles, ne dépassant pas les $20\text{-}30 \text{ s}^{-1}$ en milieu de journée, ont été observées dans un champ agricole, en sortie d'une chambre dynamique de colza, en milieu de floraison. Dans ces deux écosystèmes, une différence a été trouvée entre la réactivité mesurée et celle calculée à partir des composés gazeux mesurés individuellement. Elle indique la présence d'une fraction manquante de composés primaires et secondaires non mesurés/ non identifiés. Ces travaux ont également mis en évidence l'importance de déterminer la spéciation des monoterpènes. Ceci nous a motivé à, optimiser et déployer un système de FastGC/ PTR-MS dans une forêt de chênes verts, ce qui nous a permis de suivre avec une haute résolution temporelle le cycle diurne des principaux monoterpènes, dont l'émission dépend du type de chêne ainsi que de la lumière.

Title: Characterization of biogenic volatile organic compounds (BVOCs) and their OH reactivity in various (agro)ecosystems.

Keywords: BVOCs, Monoterpenes, OH reactivity, FastGC/PTR-MS, Forest, Agriculture

Abstract: The hydroxyl radical OH is the most powerful oxidant in the troposphere, however, characterizing its sinks remains a challenge. One important OH sink, is the oxidation of volatile organic compounds (VOCs), mainly released from biogenic sources, on the global scale. VOCs include a wide variety of chemical species with different lifetimes towards OH. Measuring OH reactivity is a useful tool to evaluate the loading in reactive species and to estimate the amplitude of unmeasured/unidentified compounds. In this context, this PhD work aimed to build and optimize a CRM or Comparative Reactivity method instrument for OH reactivity measurements. Afterwards the CRM was deployed in a forest and an agricultural ecosystem. OH reactivity in a maritime pine forest showed maxima during night, reaching

99 s^{-1} inside the canopy, among the highest in forest environments. Relatively lower levels (max $20\text{-}30 \text{ s}^{-1}$ at mid-day), were recorded from a dynamic chamber, during the blooming season of a rapeseed field. In these ecosystems, a difference was obtained between measured and calculated OH reactivity from measured compounds. It highlights the presence of a missing fraction of unmeasured primary and secondary compounds. These experiments demonstrate the importance of a detailed information on monoterpene chemical speciation. In this perspective, a FastGC/PTR-MS system was optimized and deployed in a green oak forest. It allowed to monitor, with a fine time resolution, diurnal cycles of the main monoterpene, which emissions are dependent on the tree type and on solar radiation.

